Development of a Selective Weakening Approach for the Seismic Retrofit of Reinforced Concrete Structural Walls

A Thesis
submitted in partial fulfilment
of the requirements for the Degree
of
Master of Engineering
at the
University of Canterbury
by
Matthew Ireland

University of Canterbury
Christchurch, New Zealand
2007

Abstract

Recent earthquakes have highlighted the vulnerability of existing structure to seismic loading. Current seismic retrofit strategies generally focus on increasing the strength/stiffness in order to upgrade the seismic performance of a structure or element. A typical drawback of this approach is that the demand on the structural and sub-structural elements can be increased. This is of particular importance when considering the foundation capacity, which may already be insufficient to allow the full capacity of the existing wall to develop (due to early codes being gravity load orientated). In this thesis a counter-intuitive but rational seismic retrofit strategy, termed "selective weakening" is introduced and investigated. This is the first stage of an ongoing research project underway at the University of Canterbury which is focusing on developing selective weakening techniques for the seismic retrofit of reinforced concrete structures. In this initial stage the focus is on developing selective weakening for the seismic retrofit of structural walls. This is performed using a series of experimental, analytical and numerical investigations. A procedure for the assessment of existing structural walls is also compiled, based on the suggestions of currently available code provisions.

A selective weakening intervention is performed within an overall performance-based retrofit approach with the aim of improving the inelastic behaviour by first reducing the strength/stiffness of specific members within the structural system. This will be performed with the intention of modifying a shear-type behaviour towards a flexural-type behaviour. As a result the demand on the structural member will be reduced. Once weakening has been implemented the designer can use the wide range of techniques and materials available (e.g. use of FRP, jacketing or shotcrete) to ensure that adequate characteristics are achieved. Whilst performing this it has to be assured that the structure meets specific performance criteria and the principles of capacity design. A target of the retrofit technique is the ability to introduce the characteristics of recently developed high performance seismic resisting systems, consisting of a self-centring and dissipative behaviour (commonly referred to as a hybrid system).

In this thesis, results of experimental investigations performed on benchmark and selectively weakened walls are discussed. The investigations consisted of quasi-static cyclic uni-directional tests on two benchmark and two retrofitted cantilever walls. The first benchmark wall is detailed as typical of pre-1970's construction practice. An equivalent wall is retrofitted using a selective weakening approach involving a horizontal cut at foundation level to allow for a rocking response. The second benchmark wall represents a more severe scenario where the inelastic behaviour is dominated by shear. A retrofit solution involving vertically segmenting the wall to improve the ductility and retain gravity carrying capacity by inducing a flexural response is implemented.

Numerical investigations on a multi-storey wall system are performed using non-linear time-history analysis on SDOF and MDOF lumped plasticity models, representing an as-built and retrofitted prototype structure. Calibration of the hysteretic response to experimental results is carried out (accounting for pinching and strength degradation). The sensitivity of maximum and residual drifts to p-delta and strength degradation is monitored, along with the sensitivity of the peak base shear to higher mode affects.

The results of the experimental and analytical investigations confirmed the feasibility and viability of the proposed retrofit technique, towards improving the seismic performance of structural walls.

Acknowledgements

This research was undertaken at the University of Canterbury under the supervision of Dr Stefano Pampanin and Professor Des Bull.

The financial support provided by the NZ Foundation of Science and Technology through the FRST- Research Program "Retrofit Solutions for NZ" is gratefully acknowledged. Without this support the project would not have been possible.

I would like to thank the technical staff of the Civil Engineering Department for their help, experience and advice. Particularly the support provided by Russell McConchie and Tim Perigo is greatly acknowledged.

I would also like to acknowledge the BBR Contech for the supply and application of the FRP composites used in the experimental investigations. I would particularly like to thank Rob Green for his assistance and technical advice.

I would also like to thank the fellow postgraduate students I had the opportunity to work with. Particular thanks would have to go to Jimmy and Dion for their help, guidance and advice.

Finally a special thanks to my friends and family for their support and understanding throughout my time at University.

Table of Contents:

1 Introduction 1-1

1.1 General 1-1

1.2 Objectives of this Research 1-1

1.3 Thesis Outline 1-2

2 Review of Relevant Literature 2-1

2.1 Introduction 2-1

2.2 Behaviour of Existing Structural Walls 2-2

2.3 Characteristics of Existing Buildings in New Zealand 2-3

2.3.1 Historic Development of Seismic Provisions in New Zealand 2-3

2.3.2 Deficiencies in Existing Structural Walls 2-7

2.3.3 Material Properties in Existing Buildings 2-7

2.4 Performance Based Design 2-8

2.5 Traditional Seismic Retrofit Techniques 2-10

2.5.1 Reinforced Concrete Jacketing 2-10

2.5.2 Shotcrete Overlay 2-11

2.5.3 Steel Jacketing 2-12

2.5.4 Fibre Reinforced Polymers (FRP) 2-13

2.5.5 Retrofit of Structural Walls by Selective Upgrading Techniques 2-14

2.6 Seismic Retrofit and Rehabilitation Guidelines 2-16

2.6.1 FEMA-356 (2000) Prestandard & Commentary for the Seismic Rehabilitation of Buildings 2-17

2.6.2 fib Bulletin 24 (2003) – Seismic Assessment and Retrofit of R.C. Buildings 2-17

2.6.3 NZSEE (2005) – Assessment & Improvement of the Structural Performance of Buildings in Earthquake 2-18

2.6.4 EC8 – Part 3: Strengthening and Repair of Buildings (2005) 2-19

2.7 Recent Developments in High Performance Seismic Resisting Systems 2-20

3 The Concept & Implementation of Selective Weakening 3-1

3.1 Introduction to Selective Weakening 3-1

3.2 Modification of the Inelastic Response 3-2

3.3 Modification of the Demand-capacity Balance 3-4

3.4 Advantages and Disadvantages of a Selective Weakening Approach 3-8

3.5 Selective Weakening for Other Structural Systems 3-9
3.6 Prototype Structure 3-9
3.6.1 Typical Reinforcing Details of Pre-1970's New Zealand Structural Walls 3-9
3.6.2 Development of Prototype 3-11
3.7 Experimental Program 3-13

4 W1 – Pre-1970's Construction Practice 4-1
4.1 Introduction 4-1
4.2 Development of W1 4-1
4.2.1 Experimental Specimen Geometry 4-1
4.2.2 W1 - Reinforcement Detailing 4-2
4.2.3 W1 – Material Properties 4-3
4.3 Experimental Se-tup 4-4
4.4 Instrumentation Layout 4-5
4.5 Load Regime 4-7
4.6 Construction & Material Testing 4-8
4.7 Force versus Displacement Predictions – W1 4-10
4.8 Damage Observations – W1 4-11
4.8.1 Test Observations 4-11
4.8.2 Post Testing Damage Observations 4-14
4.9 Results & Analyses 4-16
4.9.1 Force versus Displacement Response 4-16
4.9.2 Axial Load 4-16
4.9.3 Vertical Displacement at base of Wall & Base Rotation 4-17
4.9.4 Equivalent Viscous Damping 4-19
4.10 Predicted versus Experimental Response 4-20

5 W2 – Shear Dominated Wall 5-1
5.1 Introduction 5-1
5.2 Development of W2 5-1
5.2.1 Experimental Specimen Geometry 5-1
5.2.2 Reinforcement Detailing 5-2
5.2.3 Material Properties 5-3
5.3 Experimental Set-up 5-3
5.4 Instrumentation Layout 5-5

5.5 Load Regime 5-7
5.6 Construction & Material Testing 5-8
5.7 Force versus Displacement Predictions 5-9
5.8 Damage Observations 5-11
5.9 Results & Analyses 5-13
5.9.1 Force versus Displacement Response 5-14
5.9.2 Axial Load 5-15
5.9.3 Equivalent Viscous Damping 5-16
5.9.4 Strain Profile in Transverse Reinforcement 5-16
5.10 Comparison of Experimental and Predicted Response 5-17

6 W1R – Selective Weakening Retrofit of a W1 Equivalent 6-1
6.1 Introduction 6-1
6.2 Benchmark Specimen Summary – W1 6-1
6.2.1 Retrofit Objectives 6-1
6.3 Retrofit Configuration and Components 6-2
6.3.1 Horizontal Saw Cut 6-2
6.3.2 Un-bonded Post-tensioning 6-3
6.3.3 Energy Dissipaters 6-5
6.3.4 Protection of Corner Regions 6-7
6.3.5 Shear Keys 6-8
6.4 Experimental Set-up 6-8
6.5 Instrumentation Layout 6-9
6.6 Load Regime 6-11
6.7 Force versus Displacement Predictions – W1R 6-11
6.8 Sample Testing of Dissipater 6-12
6.9 Observations 6-15
6.9.1 Test #1 Observations – 1st Hybrid Test 6-15
6.9.2 Test #2 – Test #4 Observations 6-17
6.9.3 Post Test Observations 6-18
6.10 Results & Analyses – Test #1 (1st hybrid test) 6-20
6.10.1 Force versus Displacement Response, test #1 6-21
6.10.2 Un-bonded Post-tensioning Forces 6-22
6.10.3 Dissipater Displacement Demand 6-24

6.10.4 Vertical Displacement at Base of Wall & Base Rotation 6-25
6.10.5 Equivalent Viscous Damping 6-28
6.11 Results and Analyses - Test #2 (1st Post-tensioned only test) 6-29
6.11.1 Force versus Displacement Response 6-29
6.11.2 Post-tensioning Forces 6-30
6.12 Results and Analyses – Test #3 (2nd hybrid test) 6-32
6.12.1 Force versus Displacement Response 6-32
6.12.2 Post-tensioning Forces 6-33
6.12.3 Dissipater Displacement Demand 6-35
6.12.4 c/d versus Lateral Drift 6-35
6.12.5 Equivalent Viscous Damping 6-36
6.13 Results and Analyses – Test #4 (2nd Post-tensioned only Test) 6-37
6.13.1 Force versus Displacement Response 6-37
6.13.2 Post-tensioning Forces 6-39
6.14 Analytical Experimental Comparison 6-40

7 W2R - Selective Weakening Retrofit of a W2 Equivalent 7-1

7.1 Introduction 7-1
7.2 Benchmark Specimen Summary – W2 7-1
7.2.1 Retrofit Objectives 7-1
7.3 Retrofit Configuration and Components 7-1
7.3.1 Saw Cuts 7-3
7.3.2 Fibre Reinforced Polymers (FRP) 7-4
7.3.3 Steel Confinement Armour 7-5
7.3.4 Un-bonded Post-tensioning 7-6
7.3.5 Material Properties 7-7
7.4 Experimental Set-up 7-7
7.5 Instrumentation Layout 7-8
7.6 Load Regime 7-9
7.7 Damage Observations 7-10
7.7.1 W2Ra Observations 7-10
7.7.2 W2Rb Observations 7-12
7.8 Results and Analyses – W2Ra 7-14
7.8.1 Force versus Displacement Response 7-14

7.8.2 Post-tensioning 7-16
7.9 Results and Analyses – W2Rb 7-18
7.9.1 Force versus Displacement Response 7-18
7.9.2 Post-tensioning 7-19
7.10 Results and Analyses - W2R (W2Ra & W2Rb Combined) 7-21
7.10.1 Equivalent Viscous Damping 7-22
7.11 Force versus Displacement Predictions 7-23

8 Experimental Findings and Comparisons 8-1
8.1 Introduction 8-1
8.2 W1 – Pre-1970's Detailing 8-2
8.3 W2 – Shear Dominated 8-4
8.4 W1R – Selective Weakening Retrofit of W1 Equivalent 8-6
8.5 W2R – Selective Weakening Retrofit of W2 Equivalent 8-8
8.6 W1 versus W1R Comparison 8-11
8.6.1 Observed Behaviour – Benchmark and Retrofitted 8-11
8.6.2 Force versus Displacement Response – Benchmark and Retrofitted 8-12
8.6.3 Possible Improvements to the Retrofit Solution 8-13
8.6.4 Other Possible Retrofit Scenarios for W1R 8-13
8.7 W2 versus W2R Comparison 8-16
8.7.1 Observed Behaviour- Benchmark and Retrofitted 8-16
8.7.2 Force versus Displacement Response – Benchmark and Retrofitted 8-17
8.7.3 Possible Improvements to the Retrofit Solution 8-17
8.7.4 Other Possible Selective weakening Retrofit Solutions for W2R 8-18
8.8 Summary 8-19

9 Numerical Modeling of Prototype Wall & Sensitivity Analysis 9-1
9.1 Introduction 9-1
9.2 Hysteretic Calibration to Experimental Results 9-1
9.2.1 Hysteresis Rules – W1 9-2
9.2.2 Strength Degradation 9-4
9.2.3 Hysteresis Rules – W1R 9-5
9.3 W1 – Hysteretic Calibration 9-6
9.3.1 Modified Takeda 9-6
9.3.2 Modified Takeda – Max Ductility Strength Degradation 9-7

9.3.3 Modified Takeda – Number of Inelastic Cycles Based Strength Degradation ...9-8
9.3.4 Pampanin Calibration ...9-9
9.3.5 Pampanin Calibration – Max Ductility Based Strength Degradation ...9-10
9.3.6 Pampanin Calibration – Number of Cycles Based Strength Degradation ...9-11
9.4 W1R – Hysteretic Calibration ...9-12
9.5 Selection and Scaling of Earthquake Records ...9-14
9.6 SDOF Time History Analysis ...9-17
9.6.1 SDOF Results – With & Without Strength Degradation ...9-18
9.6.2 SDOF Results – With and Without P-delta ...9-19
9.6.3 SDOF Results – As-built Prototype versus Retrofitted Prototype ...9-20
9.6.4 Example – As-built versus Retrofitted Prototype ...9-22
9.7 MDOF Time History Analysis ...9-23
9.7.1 MDOF Results – Sensitivity to Strength Degradation and P-delta ...9-24
9.7.2 MDOF Results – As-built Prototype versus Retrofitted Prototype ...9-26
9.8 SDOF versus MDOF Time History Results ...9-27
9.9 Summary of Time History Results ...9-29

10 Assessment of Structural Walls ...10-1
10.1 Introduction ...10-1
10.2 Displacement Based Assessment ...10-1
10.2.1 Steps to Displacement Based Assessment ...10-1
10.2.2 Creation of a SDOF Substitute Structure ...10-3
10.2.3 Assessment of Multiple Structural Walls ...10-5
10.2.4 Consideration of Performance Based Design ...10-7
10.3 Structural Wall Assessment Parameters and Procedures ...10-7
10.3.1 Nominal Flexural Capacity ...10-8
10.3.2 Ductility Capacity ...10-12
10.3.3 Base Shear Distribution ...10-13
10.3.4 Alternative Failure Mechanisms ...10-16
10.3.5 Equivalent Viscous Damping ...10-19
10.4 Displacement Based Retrofit Design ...10-20
10.5 Summary ...10-21

11 Conclusions and Recommendations 11-1

11.1 General Overview 11-1

11.2 Conclusions 11-2

11.2.1 Experimental Investigations 11-2

11.2.2 Numerical Investigations 11-3

11.2.3 Assessment of Structural Walls 11-4

11.3 Recommended Future Research 11-5

11.4 Closing Remarks 11-6

Appendix A Worked Examples A-1

A.1 Displacement Based Assessment and Retrofit of a Structural Wall A-1

A.2 Displacement Based Assessment and Retrofit of Prototype Wall A-13

Appendix B Photo Report B-1

B.1 Photos at each Drift Cycle B-1

B.1.1 W1 – Photo Report B-1

B.1.2 W2 – Photo Report B-4

B.1.3 W3 – Photo Report B-7

B.1.4 W2R– Photo Report B-10

B.2 Construction Photos B-13

B.2.1 W1 and W1R- Construction B-13

B.2.2 W2 and W2R- Construction B-14

B.3 Miscellaneous Photos B-15

B.3.1 W1 - Miscellaneous B-15

B.3.2 W2 - Miscellaneous B-16

B.3.3 W1R- Miscellaneous B-17

B.3.4 W2R- Miscellaneous B-19

Appendix C Calculations and Construction Drawings C-1

C.1 Prototype Development C-1

C.2 Similitude Scaling C-3

C.3 Design Calculations W1 ..... C-4

C.4 Design Calculations W2 ..... C-5

C.5 Stress in un-bonded post-tensioning tendons at nominal flexural capacity C-6

C.6 Calculation of Equivalent Viscous Damping C-6

C.7 FRP Design for W2R C-8
C.8 Calculating Plastic Hinge Length from Experimental Results C-12
C.9 Construction Drawings C-13
C.9.1 W1 ..... C-13
C.9.2 W2 ..... C-16
C.9.3 W1R C-19
C.9.4 W2R C-22

Appendix D Numerical Analysis Information D-1
D.1 Scaled Earthquake Record Spectra D-1
D.2 Example Ruaumoko Input Files D-3
D.2.1 W1 Takeda Calibration – No Strength Degradation D-3
D.2.2 W1 Takeda Calibration – Cyclic Strength Degradation D-4
D.2.3 W1 Pampanin Calibration – No Strength Degradation D-5
D.2.4 W1 Pampanin Calibration – Max Ductility Strength Degradation D-6
D.2.5 W1R – Bilinear Elastic and Elasto-plastic Calibration D-7
D.2.6 SDOF As-built Prototype – Time History Analysis D-8
D.2.7 SDOF Retrofitted Prototype – Time History Analysis D-9
D.2.8 MDOF As-built Prototype – Time History Analysis D-10
D.2.9 MDOF Retrofitted Prototype – Time History Analysis D-11

List of Figures:

Figure 2-1: Shear failure of a R.C. wall due to insufficient transverse reinforcement; a) Bolu (Turkey, 1999), b) Bingol (Turkey, 2003). 2-2
Figure 2-2: Common failure modes exhibited in structural walls (Paulay and Priestley, 1992) 2-2
Figure 2-3: Seismic coefficients for public and private buildings and different seismic zones from NZSS 1900 (NZSS 1900, 1964a). 2-5
Figure 2-4: Seismic zoning of New Zealand as of NZSS 1900 (NZSS 1900, 1964a). 2-5
Figure 2-5: Summary of different distributions of lateral force with height from historic design standards (Brunsdon, 1984) 2-6
Figure 2-6: Comparison of live loads and seismic live loads for NZSS 95, NZSS 1900 & NZS 4203 (Brunsdon, 1984)....2-6
Figure 2-7: Performance objective matrix (SEAOC, 1998)....2-9
Figure 2-8: Performance objective matrix, also accounting for residual displacements (Pampanin et al. 2002). 2-9
Figure 2-9: Concrete jacketing of a column (fib, 2003a)....2-11
Figure 2-10: Shotcrete being applied to a wall (Sabnis, Shroff et al., 1996) 2-12
Figure 2-11: Steel jacketing solution for a reinforced concrete column (fib, 2003a) 2-12
Figure 2-12: FRP rehabilitation and retrofit solution for a structural wall (Antoniades et al., 2003) 2-14
Figure 2-13: Selective intervention retrofit techniques, a) strength intervention, b) stiffness intervention, c) ductility intervention. (modified; Elanshai, 1992; Elanashai and Pinho, 1998; Pinho, 2000a) 2-15
Figure 2-14: Hybrid system for a beam-column connection (NZS3101:2006) 2-21
Figure 2-15: Hybrid wall systems (fib, 2003b)....2-22
Figure 3-1: Expected damage and hysteretic response before and after intermediate phases of selective weakening retrofit: (a) as-built; (b) partial selective weakening; (c) full selective weakening 3-3
Figure 3-2: The effect of a partial selective weakening technique on spectral acceleration & displacement demand 3-5
Figure 3-3: Selective weakening capacity design & performance based retrofit....3-7
Figure 3-4: Typical reinforcement detailing for a pre-1970's reinforced concrete wall in New Zealand 3-10
Figure 3-5: Wall reinforcing details, Whakatane Hospital (1961)....3-11
Figure 3-6: Idealised prototype building layout....3-12

Figure 3-7: Prototype wall details 3-13
Figure 3-8: Benchmark and retrofitted experimental wall behaviour 3-15
Figure 4-1: Portion of prototype wall represented by the experimental wall 4-2
Figure 4-2: W1 reinforcement details 4-3
Figure 4-3: W1 experimental set-up 4-5
Figure 4-4: Potentiometer layout for W1 4-6
Figure 4-5: Strain gauge locations for W1 4-6
Figure 4-6: W1 Loading regime 4-8
Figure 4-7: W1 under construction 4-9
Figure 4-8: Force versus Displacement prediction for W1 4-11
Figure 4-9: W1 at peak drift of 3.0% 4-12
Figure 4-10: Crushing in the toe region and longitudinal reinforcement buckling in W1 4-14
Figure 4-11: (a) Longitudinal reinforcement failure in tension; (b) Longitudinal reinforcement failure due to low cycle fatigue. 4-14
Figure 4-12: Starter bars left protruding from W1 foundation block once the wall had been removed 4-15
Figure 4-13: W1 force versus displacement response 4-16
Figure 4-14: W1 post-tensioning load versus lateral displacement 4-17
Figure 4-15: Elongation of potentiometers crossing the critical plane for the negative drift cycles. 4-18
Figure 4-16: Elongation of potentiometers crossing the critical plane for the positive drift cycles 4-18
Figure 4-17: Average c/d versus lateral drift for W1 4-19
Figure 4-18: Equivalent viscous damping versus drift for W1 4-20
Figure 4-19: Predicted and experimental force versus displacement response, W1 4-21
Figure 5-1: W2 reinforcement detailing and geometry 5-2
Figure 5-2: W2 experimental set-up 5-4
Figure 5-3: W2 potentiometer layout 5-6
Figure 5-4: W2 strain gauge locations 5-7
Figure 5-5: W2 loading regime 5-8
Figure 5-6: W2 under construction 5-8
Figure 5-7: Predicted strength envelopes for W2 5-10
Figure 5-8: First shear cracking at 0.2% drift 5-12
Figure 5-9: Major diagonal tension crack at 1.0% drift 5-13

Figure 5-10: W2 exhibiting a shear dominated failure mode, after experiencing a peak drift of 2.5% 5-13
Figure 5-11: W2 force versus displacement response 5-14
Figure 5-12: W2 foundation block sliding relative to strong floor 5-15
Figure 5-13: W2 axial load versus lateral displacement 5-15
Figure 5-14: Equivalent viscous damping versus drift for W2 5-16
Figure 5-15: Example of the measured strain profile up the height of W2 5-17
Figure 5-16: W2 Predicted response 5-18
Figure 6-1: Selective weakening retrofit configuration for W1R 6-2
Figure 6-2: Implementation of horizontal foundation cut 6-3
Figure 6-3: W1R post-tensioning tendon locations 6-4
Figure 6-4: Elongation of post-tensioning tendons due to wall rocking 6-4
Figure 6-5: Details and dimensions of the energy dissipaters used on W1R 6-5
Figure 6-6: W1R dissipater locations 6-6
Figure 6-7: W1R corner armour 6-7
Figure 6-8: W1R test set-up 6-9
Figure 6-9: W1R instrumentation set-up 6-10
Figure 6-10: W1R Load History 6-11
Figure 6-11: Force versus Displacement predictions, W1R 6-12
Figure 6-12: Dissipater tensile test, stress versus strain 6-13
Figure 6-13: Dissipater test displacement loading regime 6-14
Figure 6-14: Dissipater test, force versus displacement response 6-15
Figure 6-15: W1R at peak drift of 2.5% 6-16
Figure 6-16: Gap opening at drift of 2.5% 6-17
Figure 6-17: Dissipater elongation at 2.5% drift 6-17
Figure 6-18: W1R peak response during the second, third & fourth tests 6-18
Figure 6-19: Horizontal cut foundation interface, post testing 6-19
Figure 6-20: Underside of wall, post testing 6-19
Figure 6-21: Dissipaters after testing for the first and second hybrid test 6-20
Figure 6-22: Force versus Displacement response, W1R, test #1 6-21
Figure 6-23: Foundation block sliding relative to strong floor, test#1 6-22
Figure 6-24: Example of the Change in post-tension force due to cyclic displacement, test #1 6-23
Figure 6-25: Post-tension force versus wall lateral displacement, test #1 6-24

Figure 6-26: Displacement demand on dissipater, test #1 6-25
Figure 6-27: Elongation of potentiometers crossing the critical plane for negative drift cycles, test #1 6-26
Figure 6-28: Elongation of potentiometers crossing the critical plane for the positive drift cycles, test #1 6-27
Figure 6-29: c/d versus lateral drift for W1R- 1st hybrid test 6-27
Figure 6-30: Equivalent Viscous damping versus drift, hybrid test #1 6-28
Figure 6-31: Force versus displacement response, test #2 (post-tensioned only) 6-29
Figure 6-32: Foundation block sliding relative to strong floor, test #2 6-30
Figure 6-33: Change in post-tensioning force due to cyclic loading, test #2 6-31
Figure 6-34: Post-tensioning force versus lateral displacement, test #2 6-31
Figure 6-35: Force versus displacement response, test #3 6-32
Figure 6-36: Foundation sliding relative to strong floor, test #3 6-33
Figure 6-37: Cyclic change in post-tension force, test #3 6-34
Figure 6-38: Post-tensioning load versus lateral displacement, test #3 6-34
Figure 6-39: Dissipater displacement demand, test #3 6-35
Figure 6-40: Average c/d versus lateral drift for the 2nd hybrid test on W1R 6-36
Figure 6-41: Equivalent viscous damping versus drift, test #3 (2^{nd} hybrid test) 6-37
Figure 6-42: Force versus Displacement response, test #4 6-38
Figure 6-43: Foundation sliding relative to strong floor, test #4 6-38
Figure 6-44: Post-tensioning force change due to lateral loading, test #4 6-39
Figure 6-45: Change in post-tensioning load with wall lateral displacement, test #4 6-39
Figure 6-46: Predicted versus Experimental response; (a) Test #1, (b) Test #3 6-40
Figure 6-47: Predicted versus Experimental response; (a) Test #2, (b) Test #4 6-41
Figure 7-1: W2R selective weakening retrofit configuration 7-3
Figure 7-2: (a) W2R vertical saw cutting in progress; (b) W2R segmented 7-4
Figure 7-3: FRP application in progress 7-5
Figure 7-4: W2R Test set-up 7-8
Figure 7-5: Instrumentation layout for W2R 7-9
Figure 7-6: W2R load history 7-9
Figure 7-7: W2R response at peak drift cycle of 2.5% 7-11
Figure 7-8: Crushing of concrete on W2Ra between confinement armour and FRP 7-12
Figure 7-9: Spalling of concrete on W2Rb 7-14
Figure 7-10: Force displacement response for W2Ra 7-15

Figure 7-11: Foundation block sliding relative to strong floor 7-16
Figure 7-12: Change in post-tension force in W2Ra as test progresses 7-17
Figure 7-13: Post-tensioning force versus lateral drift, W2Ra 7-18
Figure 7-14: Force versus displacement response W2Rb 7-19
Figure 7-15: Change in post-tensioning force as wall progresses for W2Rb 7-20
Figure 7-16: Post-tensioning force versus lateral displacement, W2Rb 7-21
Figure 7-17: Force versus displacement response for W2R 7-22
Figure 7-18: W2R equivalent viscous damping 7-23
Figure 7-19: Experimental and analytical force versus displacement comparison 7-24
Figure 8-1: Summary of the behaviour of the benchmark walls (W1 and W2) 8-1
Figure 8-2: Summary of the behaviour of the retrofitted walls (W1R and W2R) 8-2
Figure 8-3: W1 at a peak drift of 3.0% 8-3
Figure 8-4: Force versus displacement response, W1 8-4
Figure 8-5: Observed behaviour of W2 at test completion 8-5
Figure 8-6: Force versus displacement response, W2 8-6
Figure 8-7: Retrofit configuration and components, W1R 8-7
Figure 8-8: Force versus displacement response, W1R (test #3) 8-8
Figure 8-9: Retrofit configuration and components, W2R 8-9
Figure 8-10: Force versus displacement, W2R 8-10
Figure 8-11: (a) W1 at peak response, (b) W1R at peak response 8-11
Figure 8-12: (a) W1 force versus displacement response, (b) W1R force versus displacement response 8-12
Figure 8-13: (a) W1 Force versus Displacement response (experimental); (b) Alternative retrofit solution for W1R, force versus displacement response (numerical), axial load only solution 8-14
Figure 8-14: (a) W1 Force versus Displacement response (experimental); (b) Alternative retrofit solution for W1R, force versus displacement response (numerical), two central PT-tendons & 4-10mm dissipaters 8-15
Figure 8-15: (a) W2 at end of test, (b) W2R at 2.5% drift 8-16
Figure 8-16: (a) W2 force versus displacement, (b) W2R force versus displacement 8-17
Figure 9-1: Lumped plasticity calibration model 9-2
Figure 9-2: Modified Takeda reinforced concrete hysteresis rule, with Drain-2D unloading (as per Carr, 2005) 9-3
Figure 9-3: Pampanin, beam-column joint hysteresis rule, IOP=2 (as per Carr, 2005) 9-4

Figure 9-4: Definition of strength degradation envelope (as per Carr, 2005).....9-5
Figure 9-5: (a) Bilinear elastic rule (as per Carr, 2005), (b) Elasto-plastic rule (as per Carr, 2005) 9-6
Figure 9-6: (a) W1, Takeda hysteresis calibration with no strength degradation; (b) equivalent viscous damping of experimental and calibrated hysteresis loops.....9-7
Figure 9-7: (a) W1, Takeda hysteresis calibration with max ductility strength degradation; (b) equivalent viscous damping of experimental and calibrated hysteresis loops.....9-8
Figure 9-8: (a) W1, Takeda hysteresis calibration with cyclic strength degradation; (b) equivalent viscous damping of experimental and calibrated hysteresis loops 9-9
Figure 9-9: (a) W1, Pampanin hysteresis calibration with no strength degradation; (b) equivalent viscous damping of experimental and calibrated hysteresis loops.....9-10
Figure 9-10: (a) W1, Pampanin hysteresis calibration with max ductility strength degradation; (b) equivalent viscous damping of experimental and calibrated hysteresis loops 9-11
Figure 9-11: (a) W1, Pampanin hysteresis calibration with cyclic strength degradation; (b) equivalent viscous damping of experimental and calibrated hysteresis loops 9-12
Figure 9-12: (a) W1R, hysteresis calibration for the 1st hybrid test; (b) equivalent viscous damping of experimental and calibrated hysteresis loops.....9-14
Figure 9-13: Comparison of target spectrum to mean of 16 scaled records, for PGA of 0.21g (CHCH).....9-16
Figure 9-14: SDOF model used to represent prototype wall 9-17
Figure 9-15: Peak displacement versus time for as-built and retrofitted prototype for Nor9 earthquake record (0.45g (PGA) intensity).....9-22
Figure 9-16: Force versus displacement response for Nor9 earthquake record (0.45g (PGA) intensity); (a) As-built prototype wall, (b) Retrofitted prototype wall.....9-23
Figure 9-17: MDOF lumped plasticity model used to represent prototype wall 9-24
Figure 10-1: Displacement based assessment of a structural wall (modified after Priestley, 2003) 10-2
Figure 10-2: Representation of a MDOF system as an equivalent SDOF substitute structure according to Shiata and Sozen approach (1997). 10-3
Figure 10-3: Strength versus displacement response for multiple walls (wall system) and the corresponding effective stiffness as per NZSEE (2005) (modified after Paulay, 1998)...10-6
Figure 10-4: Typical detailing requirements for confinement at the end of a structural wall and for anchoring shear reinforcement as per NZS 3101:2006 10-11

Figure 10-5: Base shear capacity and resulting bending moment and shear envelopes (modified after Priestley, 1995) 10-14
Figure 10-6: Tension shift of the bending moment envelope (modified after Priestley, 1995)… 10-15
Figure 10-7: Typical failure modes observed in structural walls, (a) flexural; (b) Shear; (c) Sliding shear 10-16
Figure 10-8: Incorporation of a reduction in stiffness due to shear cracking, in the force versus displacement response (Miranda et al., 2005). 10-18
Figure 10-9: Equivalent viscous damping versus ductility for a well detailed reinforced concrete wall. 10-20
Figure 10-10: Displacement Based Retrofit Design (modified after Priestley, 2003). 10-21

List of Tables:

Table 4-1: W1, average reinforcement stress versus strain properties....4-9
Table 4-2: W1, average concrete cylinder strengths....4-10
Table 5-1: Stress versus Strain properties of the reinforcement used in W2....5-9
Table 6-1: Dissipater tensile test, steel stress-strain characteristics....6-13
Table 7-1: W2R reinforcement stress strain characteristics....7-7
Table 9-1: Modified Takeda hysteresis parameters....9-3
Table 9-2: Description of Pampanin hysteresis parameters (as per Carr, 2005)....9-4
Table 9-3: Strength degradation parameters (as per Carr, 2005)....9-5
Table 9-4: Calibrated Takeda hysteresis parameters for W1....9-7
Table 9-5: W1 modified Takeda calibration, max ductility base strength degradation parameters....9-8
Table 9-6: W1 modified Takeda Calibration with strength degradation based on the number of cycles....9-9
Table 9-7: Calibrated Pampanin hysteresis parameters....9-10
Table 9-8: Max ductility based strength degradation parameters for Pampainin hysteresis, W1....9-11
Table 9-9: Cyclic based strength degradation parameters for Pampanin hysteresis....9-12
Table 9-10: Earthquake Record Information (Pampanin et.al, 2002)....9-15
Table 9-11: PGA of scaled earthquake records and the scale factors used....9-16
Table 9-12: Comparison of maximum drifts for SDOF systems, with & without strength degradation....9-18
Table 9-13: Comparison of residual drifts for SDOF systems with & without strength degradation....9-19
Table 9-14: Comparison of maximum drifts of SDOF systems, with and without p-delta....9-19
Table 9-15: Comparison of residual displacements of SDOF system, with and without p-delta…....9-20
Table 9-16: Comparison of maximum drifts for as-built and retrofitted prototype....9-21
Table 9-17: Comparison of residual drifts for as-built and retrofitted prototype....9-22
Table 9-18: Comparison of maximum drifts of MDOF systems, with and without p-delta....9-24
Table 9-19: Comparison of residual drifts of MDOF systems, with and without p-delta....9-25
Table 9-20: Comparison of base shear of MDOF systems, with and without p-delta....9-26
Table 9-21: Comparison of maximum drifts for as-built and retrofitted prototype wall....9-26

Table 9-22: Comparison of residual drifts for as-built and retrofitted prototype wall.....9-27
Table 9-23: Comparison of maximum base shear for as-built and retrofitted prototype wall..9-27
Table 9-24: SDOF versus MDOF maximum drift comparisons.....9-28
Table 9-25: SDOF versus MDOF residual drift comparisons 9-28
Table 9-26: SDOF versus MDOF maximum base shear comparisons 9-29

1 Introduction

1.1 General

Recent earthquakes (Turkey 1999, 2003, Taiwan 1999 and Pakistan 2005) have highlighted the insufficient seismic performance of some existing reinforced concrete structures and the need for appropriate retrofit solutions. Recently introduced legislation in New Zealand (the Building Act 2004) results in more buildings being classified as "earthquake risk buildings", a term previously used to describe un-reinforced masonry structures (NZSEE, 2005). This will substantially increase the number of buildings requiring retrofit and the need for suitable retrofit solutions.

Currently available and commonly used retrofit techniques (i.e. concrete jacketing) generally focus on increasing the strength/stiffness of the existing structure or elements to improve the seismic performance. A drawback of this approach is that the demand on the structural and sub-structural (i.e. foundations) elements can be increased. In some situations it may be suitable to strategically weaken structural elements to improve the seismic performance.

This thesis introduces and develops an alterative retrofit solution, which has been termed "selective weakening" and focuses on intentionally weakening structural elements to avoid undesirable failure modes and is used to protect other elements within the structure (i.e. foundations). After the initial weakening, currently available retrofit techniques will be incorporated in the full retrofit solution to ensure that the principles of capacity design are met, as well as target performance objectives. Selective weakening techniques will also be used to introduce to an existing structure, recent developments in high performance seismic resisting systems which exhibit a self-centring and dissipative response (commonly referred to as the hybrid system (Priestley, 1991; Priestley et al., 1999)).

1.2 Objectives of this Research

The research presented in this thesis is the first stage of an ongoing project at the University of Canterbury which will focus of developing "Selective weakening" for the seismic retrofit of reinforced concrete buildings. For this first stage the focus will be to introduce, investigate and develop selective weakening for the seismic retrofit of reinforced concrete structural walls. The main objectives of this research are discussed below:

- Conceptually investigate the use of selective weakening for the seismic retrofit of structural walls. This will involve discussing the retrofit aim, possible retrofit options and the advantages and disadvantages of using selective weakening techniques;
- Verify the use of selective weakening through a series of experimental investigations performed on benchmark and retrofitted wall specimens;
- Numerically investigate the performance of the selectively weakened experimental walls. For consideration of appropriate assumptions to make in assessment procedures the sensitivity of peak and residual displacements to p-delta and strength degradation were monitored;
- Compile a detailed assessment procedure for structural walls.

1.3 Thesis Outline

This thesis is comprised of eleven Chapters, which provide a review of literature relevant to this research, an introduction and conceptual investigation of selective weakening, a procedure for the displacement based assessment of structural walls, experimental investigation/verification of selective weakening, numerical investigations and finally a summary of the conclusions drawn from this research.

A review of previous research which is relevant to this research project is provided in Chapter 2. Included in the review is a discussion of the common failure modes observed in structural walls, a discussion of common characteristics of pre-1970's structural walls, an introduction to performance based design, a review of conventional and recently developed seismic retrofit strategies, a brief review of current seismic retrofit and rehabilitation guidelines from around the world, and an overview of the characteristic of new high performance seismic performing systems.

Chapter 3 provides an introduction to the concept of "selective weakening" for seismic retrofit, which has been developed in this thesis. Included is a conceptual investigation of selective weakening, which discusses the targeted modifications to the inelastic response, the modification to the demand-capacity balance and the advantages and disadvantages related to the use of selective weakening techniques. Also included is the selection of a prototype structure for use in the experimental and analytical investigations to be performed in later sections.

The experimental investigations performed as part of this thesis are discussed in Chapters 4 to 8. Two benchmark and two retrofitted, 2/3 scale, experimental specimens representing the base portion of a structural wall were constructed. The experimental walls were tested as cantilevers using quasi-static cyclic uni-directional testing. W1 acted as a bench mark specimen and was designed to represent a pre-1970's New Zealand structural wall, the design, construction and testing are discussed in Chapter 4. W2 (Chapter 5) also acted as a benchmark specimen and was designed to be dominated by shear. W1R (Chapter 6) was equivalent to W1 but was retrofitted using selective weakening. W2R (Chapter 7) was equivalent to W2 and was retrofitted using a selective weakening technique. A summary of the findings from the testing on the four experimental walls and relevant comparisons between the benchmark and retrofitted walls are made in Chapter 8.

Chapter 9 discusses the time-history analysis on SDOF and MDOF models representing a prototype wall using a lumped plasticity approach. Hysteretic calibration was performed to the experimental results of W1 and W1R, with and without the incorporation of strength degradation. The analyses were used to assess the sensitivity of peak and residual displacements to strength degradation. Comparison of the SDOF and MDOF systems was used to assess the effect of higher modes on the peak base shear experienced. The modelling was also used to compare the performance of the benchmark and retrofitted walls.

A displacement based assessment procedure for structural walls is presented and discussed in Chapter 10. A review and extension of the displacement base assessment procedure for structural walls provided in the NZSEE guidelines "Assessment and Improvement of the Structural Performance of Building in Earthquake" (NZSEE, 2005) is performed. This involved compiling procedures and relevant information suitable for checking the assumptions made during the assessment procedure. Particular emphasis is given to providing appropriate parameters and values to use in the assessment in pre-1970's New Zealand structural walls. A displacement based design procedure to use for the design of selective weakening retrofit solutions is also discussed.

Conclusions drawn from the analytical and experimental investigations performed in this thesis are discussed in Chapter 11. Areas that require future research, as highlighted during this research project are also discussed.

Included at the end of this thesis are a series of appendices that supplement the information provided in the Chapters. The information provided in the appendices is discussed below:

- Appendix A – Worked examples of the displacement based assessment procedure that was discussed in Chapter 10 are provided. An example of a retrofit solution using selective weakening and the corresponding displacement based design is also provided.

- Appendix B – A photographic log of the testing performed on each of the four experimental walls is provided. A selection of construction, instrumentation, test setup and post-testing photos are also provided for each of the experimental walls.

- Appendix C – Relevant design calculations and construction drawings are provided.

- Appendix D – Information relevant to the analytical investigations performed in this thesis are provided in this section. This includes scaled earthquake spectra and example Ruaumoko (Carr, 2005) input files.

References:

Carr, A.J. [2005] "Ruaumoko – A program for Inelastic Time-History Analysis". Department of Civil Engineering , University of Canterbury, New Zealand.

NZSEE. [2005]. Assessment and Improvement of the Structural Performance of Buildings in Earthquake – Study Group Draft, New Zealand Society of Earthquake Engineering, Prepared for the Department of Building and Housing, October.

Priestley, M.J.N., [1991], "Overview of the PRESSS research program", PCI Journal, 36(4), pp. 50-57.

Priestley, M.J.N., Sritharan, S., Conley, J.R. and Pampanin, S., [1999], "Preliminary Results and Conclusions from the PRESSS five-story Precast Concrete Test-building", PCI Journal, Vol. 44, No.6, pp. 42-67.

2 Review of Relevant Literature

2.1 Introduction

In order to develop a suitable and appropriate seismic retrofit strategy, the first important step is to understand the behaviour characteristics and deficiencies of the existing structure or element in question. Secondly, when developing a retrofit solution it is important to define a retrofit objective and to understand the positive and negative characteristics associated with the available retrofit techniques. New developments in seismic design technology can also be used to help define the positive behavioural characteristics that the retrofit solution should aim for.

The common failure modes observed in structural walls were investigated to determine the possible behaviour and deficiencies. The typical material properties and deficiencies of existing pre-1970's New Zealand structural walls were also investigated to obtain a realistic view of the likely performance of walls requiring retrofit. Historic New Zealand design codes were reviewed to determine how and to what level seismic effects were considered when these structures were designed.

The common available retrofit solutions for structural walls and new innovative retrofit solutions developed in recent research were reviewed. The positive and negative characteristics of each of the retrofit solutions were discussed. A brief review of current seismic retrofit and rehabilitation guidelines was performed to determine the typically suggested seismic retrofit solutions for structural walls. Performance based design principles were also reviewed to highlight typical performance objectives that should be considered when designing as retrofit solution.

A brief review of emerging high performance seismic resisting systems (hybrid) is given to understand the general behaviour characteristics and the advantages of using these systems. An attempt to incorporate the positive behavioural characteristics of these systems, in the retrofit solution being developed will be made.

2.2 Behaviour of Existing Structural Walls

Previous earthquakes have highlighted the poor performance of existing reinforced concrete structures and the need for appropriate retrofit solutions. **Figure 2-1** shows two examples of a highly undesirable shear dominated failure in structural walls, as the result of recent earthquakes in Turkey. A shear dominated inelastic mechanism is undesirable as it results in low ductility response typically with severe strength degradation and a low level of energy dissipation.

Figure 2-1: Shear failure of a R.C. wall due to insufficient transverse reinforcement; a) Bolu (Turkey, 1999), b) Bingol (Turkey, 2003).

Modern seismic provisions (such as NZS3101:2006) aim to ensure that a flexure dominated inelastic mechanism is formed within a structure. A flexure dominated inelastic mechanism is the most desirable, as a ductile behaviour with significant energy dissipation can be achieved (assuming appropriate detailing is adopted). **Figure 2-2** summarises the lateral loading and common failure modes exhibited by structural walls (Paulay and Priestley, 1992):

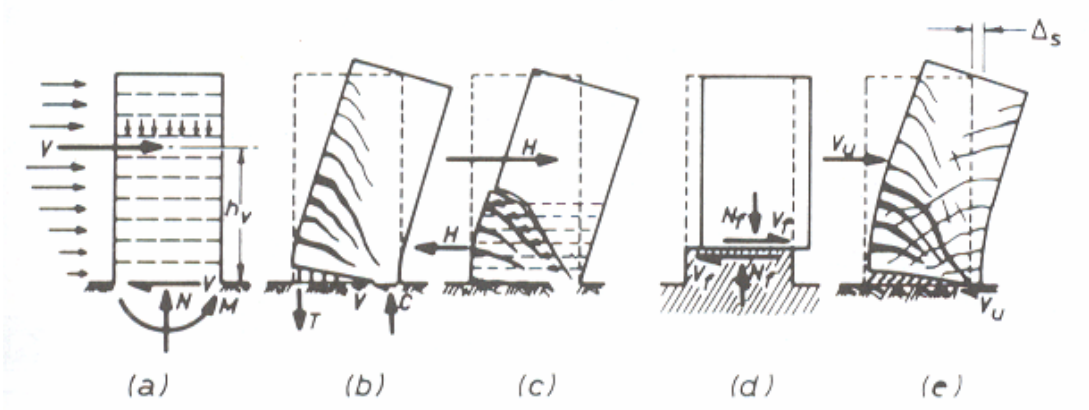

Figure 2-2: Common failure modes exhibited in structural walls (Paulay and Priestley, 1992)

a) Free body diagram of a structural wall under lateral loading;
b) Flexural plastic hinge formed at the base of the wall;
c) Shear failure due to diagonal tension or compression failure;
d) Sliding shear failure along the foundation or construction joints;
e) Serviceability failure, due to excessive deflection under service loading.

The desirable flexure dominated inelastic mechanism is not always achieved as a result of walls being designed/constructed before the implementation of appropriate seismic provisions, designed/constructed in countries without appropriate seismic provisions or inadequate design/construction. As a result, many existing buildings and structural walls might require seismic retrofit in order to achieve desirable local behaviour of individual structural walls and the overall global response of the building.

2.3 Characteristics of Existing Buildings in New Zealand

A review of historic seismic design provisions (NZS 95, 1955; NZSS 1900, 1964) from New Zealand and previous investigations into the behaviour and properties of existing New Zealand buildings (Brunsdon, 1984; NZSEE, 2005) was performed. The review was used to determine how and to what magnitude seismically induced forces were accounted for and to establish typical material properties and expected deficiencies in existing New Zealand buildings that require retrofit.

2.3.1 Historic Development of Seismic Provisions in New Zealand

A review of early seismic provisions and previous research was performed to determine the chronological development of seismic provisions in New Zealand (NZSS 95, 1955; NZSS 1900, 1964a; Brunsdon, 1984). It was found that there were three changes in the considered magnitude and distribution of seismically induced forces with height between 1936 and 1964.

Over the period of 1936-1955 a seismic coefficient of 0.08 of the assumed weight of the structure was used, with a constant distribution up the height of the structure. For public buildings the seismic coefficient was to be increased to 0.1 of the assumed weight. In 1953, NZSS 95 provided an alternative option for the considered magnitude and distribution of seismic induced forces. The alternative involved using a seismic coefficient of 0.12 at the top of the structure, with an inverted triangular distribution of force up the height of the structure

to be assumed. It was still acceptable to use a seismic coefficient of 0.08 with a constant distribution up the height of the structure at this time. Over the period of 1936-1964 the level of seismic intensity considered in the design codes did not take into account regional seismicity or the natural period of the structure.

With the introduction of NZSS 1900 Chapter 8 (NZSS 1900a, 1964) there was a revision to the magnitude and distribution of seismically induced forces. The magnitude of the seismically induced forces now accounted for regional seismicity and the natural period of the structure, whilst the distribution of seismically induced forces was now a function of the distribution of mass within a structure. **Figure 2-3** shows the variation in the magnitude of the seismic coefficient, with an increasing natural period and accounting for regional seismicity, for both private and public buildings. The magnitude of the seismic coefficient ranges between 0.04-0.12 of the assumed weight for private buildings and 0.04-0.16 of the assumed weight for public buildings. **Figure 2-4** shows the considered regions of different seismic intensity as defined by NZSS 1900 Chapter 8.

The chronological variation in the assumed distribution of seismically induced forces up the height of the structure is shown in **Figure 2-5**. **Figure 2-5** (a) show the lateral force distribution from NZSS 95 (NZSS 95, 1955), for a constant distribution with a seismic coefficient of 0.08 of the assumed weight and was used over the period of 1936-1955 (Brunsdon, 1984). **Figure 2-5** (b) shows the inverted triangular distribution of seismically induced forces that was introduced by NZSS 95 in 1953 and used up until 1964. **Figure 2-5** (c) shows the assumed distribution of seismically induced forces that was introduced in NZSS 1900 Chapter 8. The force distribution now accounted for the distribution of mass within the structure.

The chronological development of seismic live load requirements, from NZSS 95 (NZSS 95, 1955), NZSS 1900 (NZSS 1900, 1964) and NZS 4203 (NZS 4203, 1976) is shown in **Figure 2-6**.

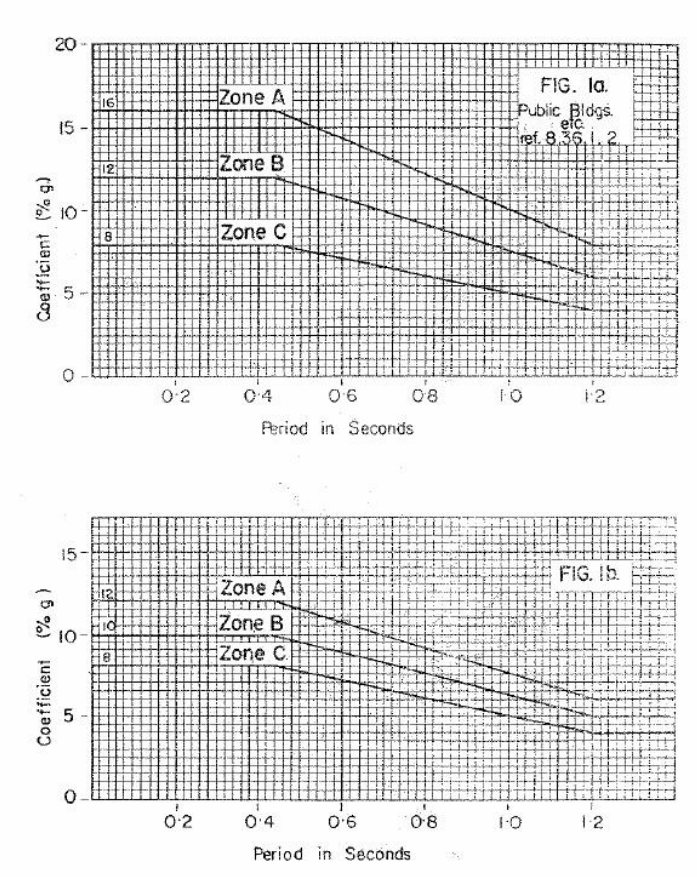

Figure 2-3: Seismic coefficients for public and private buildings and different seismic zones from NZSS 1900 (NZSS 1900, 1964a).

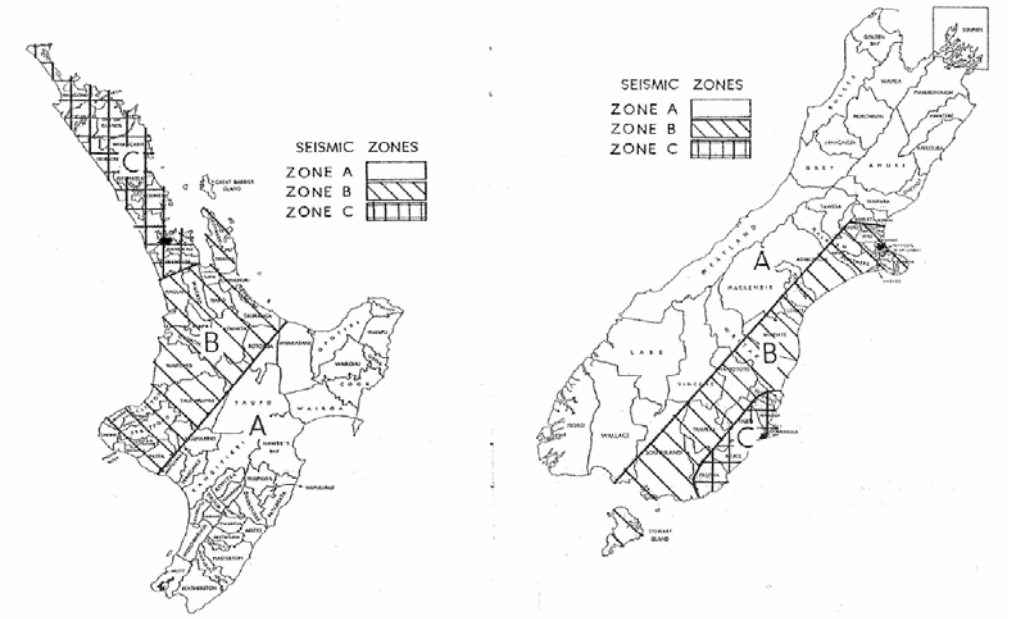

Figure 2-4: Seismic zoning of New Zealand as of NZSS 1900 (NZSS 1900, 1964a).

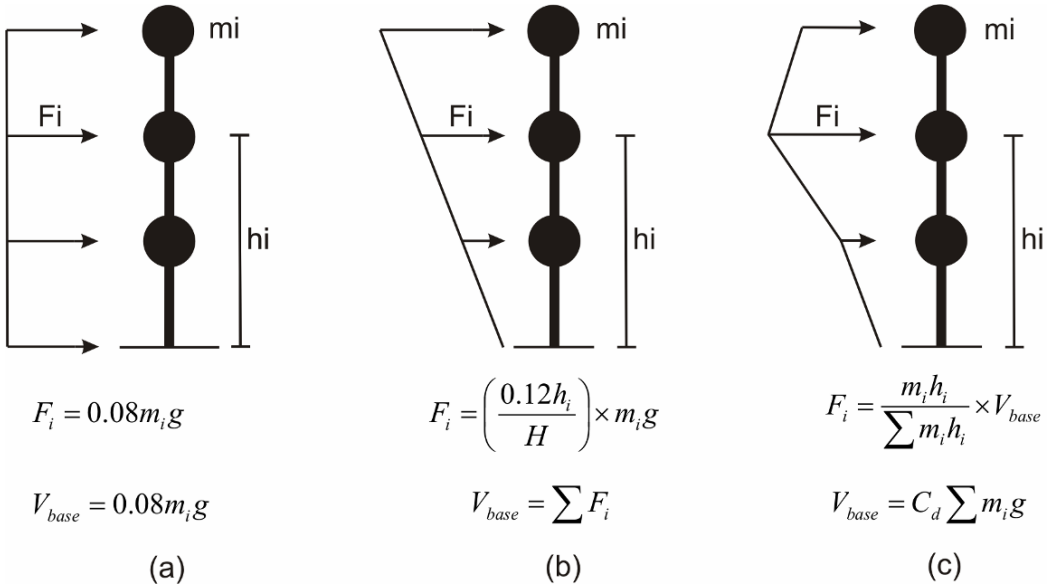

Figure 2-5: Summary of different distributions of lateral force with height from historic design standards (Brunsdon, 1984)

Usage Designation	NZSS 95		NZSS 1900		NZS 4203	
	L (kPa)	S.L. (kPa)	L (kPa)	S.L. (kPa)	L (kPa)	S.L. (kPa)
Hospitals - wards	2.88	0.96	1.44	0.48	3.0	1.0
- corridors	4.80	2.40	2.88	0.96	5.0	3.33
Offices - general	2.88	0.96	2.88	0.96	2.5	0.83
- public	4.80	1.63	3.84	1.30	4.0	1.34
Industrial - corridors	7.20	2.40	7.20	4.80	5.0	3.33
- heavy machinery	9.60	6.43	9.60	6.43	≥5.0	≥3.33
- light storage	9.60	6.43	9.60	6.43	4.0	1.34
Car Parking Buildings	7.20	4.80	2.40	0.82	2.5	0.84

Notation: L = Live Load. SL = Seismic Live Load.

Figure 2-6: Comparison of live loads and seismic live loads for NZSS 95, NZSS 1900 & NZS 4203 (Brunsdon, 1984)

2.3.2 Deficiencies in Existing Structural Walls

A review of existing New Zealand buildings from the 1936-1975 period (Brunsdon, 1984), highlighted typical expected deficiencies in the detailing and behaviour of existing structural walls. The behaviour of flexurally hinging walls from the 1936-1975 period is expected to be impaired due to inadequate detailing characteristics in the compression zones. Rectangular shaped walls typically only have transverse reinforcement for shear, therefore they are lacking appropriate reinforcement for confinement and anti-buckling.

According to previous investigations another characteristic of structural walls from this period is that they often have columns that act as boundary elements. The longitudinal reinforcement within the columns would substantially increase the flexural capacity of the wall. It was suggested that designers may have neglected the contribution to the flexural capacity from the boundary elements reinforcement, as they may have considered this to provide a conservative estimate of the flexural capacity (Brunsdon, 1984). If this was the case the principles of capacity design may not be present and a shear dominated failure mode may be observed.

2.3.3 Material Properties in Existing Buildings

A review of previous research, assessment guidelines and historic design codes was performed to determine the likely properties of the reinforcing steel and concrete used in buildings from 1936-1975.

Plain round reinforcing bars were used in New Zealand until the mid 1960's, after which deformed reinforcing bars were introduced (Liu and Park, 2001). Structural grade reinforcement with a minimum yield stress of 227MPa was used, this was later increased to 275MPa (NZSEE, 2005). Sampling of reinforcement, taken from structures built between 1930-1970 has been performed. It was determined that the 5^{th} percentile yield stress was typically 15-20% higher than the specified yield stress (Chapman, 1991). In 1964 a high yield strength reinforcement was introduced, which had a specified minimum yield stress of 414MPa (NZSEE, 2005).

When assessing a structural wall it needs to be considered that the likely concrete compressive strength might be considerably higher than the specified value. The increase in concrete compressive strength will be due to conservative mix designs and due to the concrete

increasing in strength with age. Substantial strength gain with age occurs as the cement particles were less finely ground than they are today. Tests on concrete from existing structures have shown compressive strengths of 1.8 – 2.3 times the originally specified value. The NZSEE guidelines (NZSEE, 2005), suggest that a value of 1.5 times the originally specified compressive strength should be used in the absence of specific information. Typical specified compressive strength values were investigated from historic design codes (NZSS 1900, 1964b). An ordinary grade concrete was defined to have a minimum specified compressive strength of 2000-2500psi (13.8-17.2MPa) whilst a high grade concrete was specified to have a compressive strength of up to 3500psi (24MPa).

2.4 Performance Based Design

Over recent years more emphasis has been focused on performance based seismic engineering, where structures are designed (or retrofitted) to meet defined performance objectives. A performance objective can be defined as target performance levels which are to be reached at specified seismic intensity levels (SEAOC, 1998).

The SEAOC blue book (SEAOC, 1998) specifies four seismic hazard levels, frequent, occasional, rare and maximum considered, they are termed as EQ-I, EQ-II, EQ-III and EQ-IV respectively. Performance levels can be defined in terms of expected structural and non-structural performance. Four performance levels are defined in the SEAOC blue book:

- SP1 - Fully Operational – No repairs required;
- SP2 - Operational – Requires minor repairs;
- SP3 - Life Safety – The building may be extensively damaged often beyond reparability limit;
- SP4 - Near Collapse – Life safety at risk, severe damage.

The performance levels and seismic hazards can be combined into a performance objective matrix, shown in **Figure 2-7**. The performance matrix shows the Basic Objective (to be used for most structures), which for increasing seismic hazard levels has increasing performance levels (seismic hazard levels EQ-I, EQ-II, EQ-III and EQ-IV corresponding to performance levels SP1, SP2, SP3 and SP4 respectively). For the Basic Objective, a life safety performance level is expected for a rare seismic hazard (typically 1/500 year return period). Enhanced objectives are also shown, which may be suitable for buildings that require a higher

level of performance, such as hospitals. Enhanced Objective 1 specifies a performance level of operational for a rare seismic hazard.

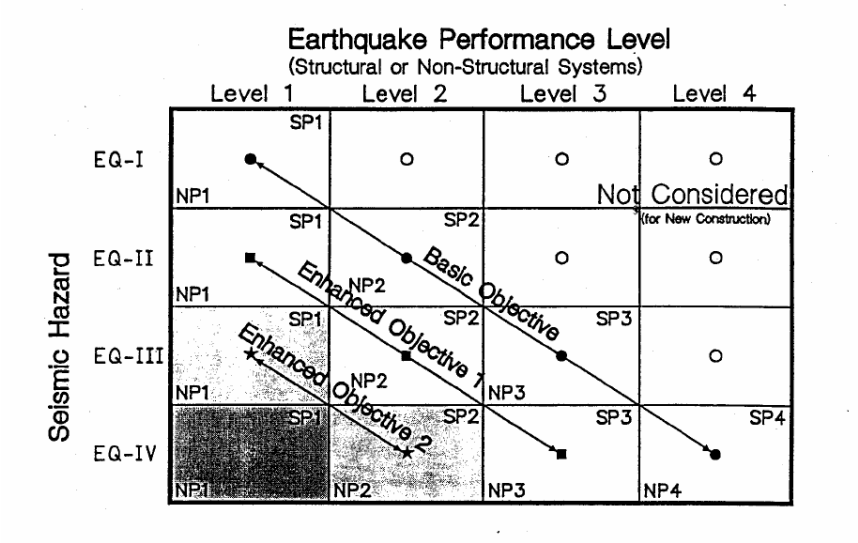

Figure 2-7: Performance objective matrix (SEAOC, 1998)

The need to incorporate residual deformations into structural performance levels was observed form the behaviour of buildings during the Kobe earthquake (1995) (Priestley, 2000). Residual displacements as a performance objective have been recently proposed because residual displacements can lead to a structure being uneconomical to repair after a seismic event (Kawashima, 1997; Priestley, 2003; Pampanin et al. 2002). A three dimensional performance objective matrix which incorporates both maximum drift and residual deformations as performance levels has been proposed and is shown in **Figure 2-8** (Pampanin et al. 2002).

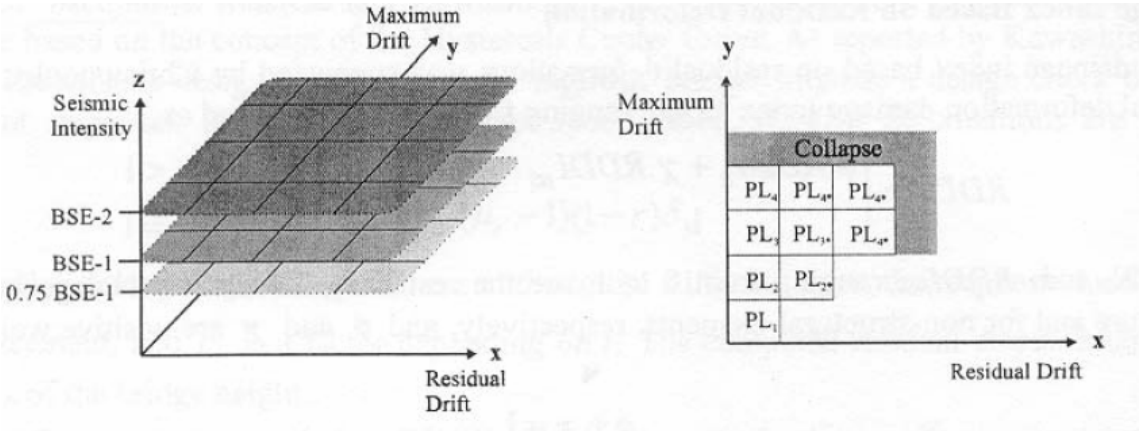

Figure 2-8: Performance objective matrix, also accounting for residual displacements (Pampanin et al. 2002).

2.5 Traditional Seismic Retrofit Techniques

Existing structural walls may require retrofitting for a number of different reasons which include poor reinforcement detailing (typical of pre-1970's design and construction), increased loading, revision of design codes or inadequate design philosophy (i.e. lack of capacity design principles). Currently, two alternative approaches for seismic retrofit are conceptually adopted and implemented: the first focuses on reducing earthquake induced forces/displacements (i.e. modifying the demand), the second approach focuses on upgrading the structure to resist earthquake induced forces/displacements (i.e. modifying the capacity). In order to reduce earthquake induced forces/displacements, base isolation or damping devices are commonly added to the structure, whilst upgrading of the structural capacity is usually achieved by intervening on specific elements or by changing the load paths within a structure.

A wide variety of different seismic retrofit techniques have been developed and implemented for existing buildings. Discussion on the available and suitability of a wide variety of seismic retrofit solutions can be found in seismic retrofit and rehabilitation guidelines (FEMA, 2000; fib, 2001; fib, 2003a; NZSEE, 2005). A brief overview of available seismic retrofit and rehabilitation guidelines will be performed in a later section. Suitable seismic retrofit techniques for structural walls, such as jacketing, shotcrete, FRP wrapping and more recently proposed selective intervention techniques will be discussed in the following sections.

2.5.1 Reinforced Concrete Jacketing

Concrete jacketing is one of the most commonly used seismic retrofit and rehabilitation techniques that has been used for reinforced concrete elements over the last few decades (fib, 2003a). Concrete jacketing involves the placement of a new jacket of concrete around an existing element to increase the thickness or length. New longitudinal, transverse, or diagonal reinforcement may also be included (Rodriguez and Park, 1991). Concrete jacketing provides an effective means of increasing the strength, stiffness and ductility of walls but there are also several drawbacks (Ghobarah and Khalil, 2004):

1) Costly upgrades of the existing foundation may be required due to the strength increase;
2) Stiffness increase will attract higher forces;
3) Uncertainty between bond of new and existing concrete;
4) Labour intensive, time consuming and disruptive to building use.

Concrete jacketing is one of the most popular retrofit techniques as it requires little specialist knowledge for design and construction. An example of a column being prepared for concrete jacketing is shown in **Figure 2-9**. Appropriate assumptions and considerations to make when designing a concrete jacket retrofit solution can be found in EC8-Part 3 (CEN, 2005) and fib bulletin 24 (fib, 2003a).

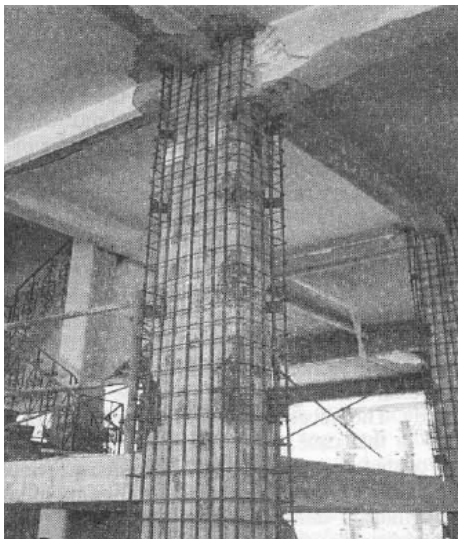

Figure 2-9: Concrete jacketing of a column (fib, 2003a)

2.5.2 Shotcrete Overlay

Shotcrete is used for the seismic retrofit of reinforced concrete walls with the same aims as concrete jacketing. The only difference is that the additional concrete is added by spraying a high cement content and fine aggregate concrete or mortar. It generally consists of a layer of Shotcrete ranging in thickness from 70-150mm, with reinforcement embedded along with a steel mesh, to restrain shrinkage cracking. Shotcrete offers similar advantages and disadvantages as concrete jacketing, with the additional disadvantage of specialist knowledge being required for placement. A significant advantage over concrete jacketing is that formwork will not be required which will particularly advantageous in confined spaces. **Figure 2-10** shows shotcrete being applied to a wall.

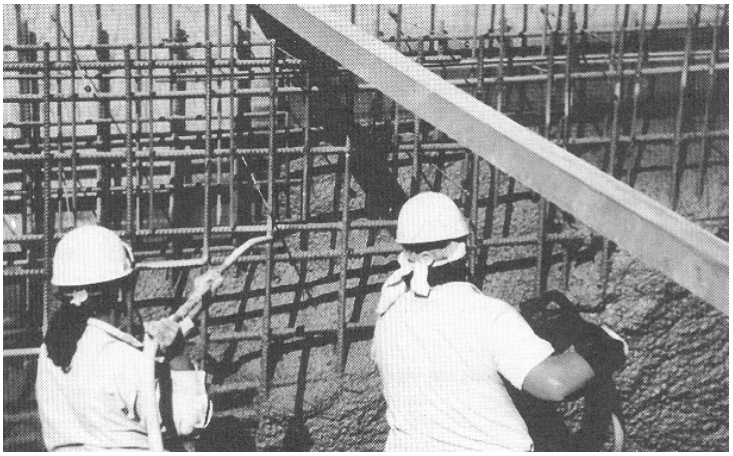

Figure 2-10: Shotcrete being applied to a wall (Sabnis, Shroff et al., 1996)

2.5.3 Steel Jacketing

Steel jacketing is a retrofit technique that is often suggested for reinforced concrete columns to increase the shear strength, provide confinement to improve the deformation capacity and to clamp deficient lap splices to allow the full section capacity to develop. Suggestions for the use and appropriate design assumptions to make can be found in fib bulletin 24 (fib, 2003a) and EC8-Part 3 (CEN, 2005). Steel jacketing is typically discussed in terms of columns (see **Figure 2-11**). A foreseen difficulty for the application to structural walls is that they typically have long cross sections. Therefore bolts passing through the wall will be required to improve the level of confinement provided. If steel jacketing is being used to increase the shear strength it will have to be provided over the full height of the column. For the clamping of lap splices EC8-Part 3 suggests that the jacket should be provided over a length of at least 50% greater than the lap splice length.

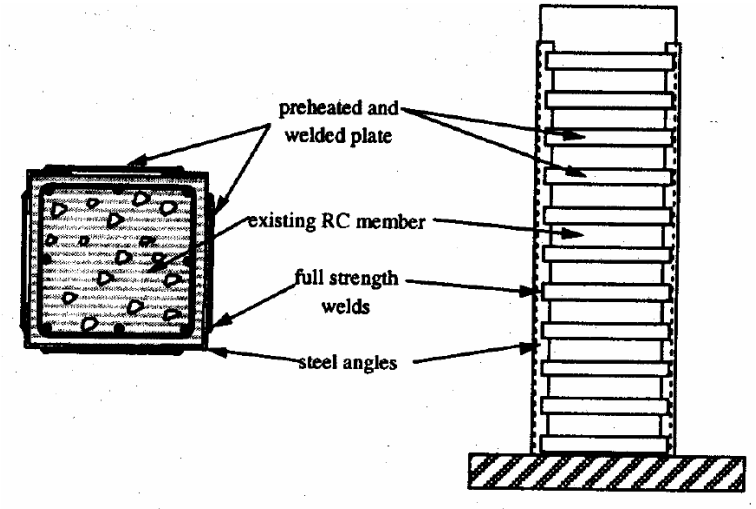

Figure 2-11: Steel jacketing solution for a reinforced concrete column (fib, 2003a)

2.5.4 Fibre Reinforced Polymers (FRP)

Fibre reinforced polymers (FRP) composites in the form of uni-directional strips and flexible sheets are often used to strengthen reinforced concrete elements (fib, 2001, 2006). FRP composites for structural applications consist of glass, carbon or aramid fibres in a resin matrix. Retrofit or rehabilitation solutions using FRP composites can be used to improve the flexural or shear strength and to provide confinement.

Advantages that the FRP composites offer over conventional retrofit options include (fib, 2001, and 2006):

- Corrosion resistant;
- Light weight;
- Very high tensile strength;
- Non-invasive retrofit solutions.

Potential problems that can result from using FRP composites for seismic retrofit include:

- Linear elastic behaviour, results in brittle failure;
- Relatively expensive;
- Susceptible to high temperatures.

FRP composites can be used in many different configurations for the seismic retrofit of reinforced concrete walls, depending on the behavioural upgrade required, information regarding the use of FRP to retrofit structural walls is very limited (fib, 2006). Testing of structural walls retrofitted or rehabilitated using FRP have highlighted the following issues (Ghobarah and Khalil, 2004; Antoniades, and Salonikios, et al, 2003):

1) Concentration of inelastic deformation at a critical flexural crack outside of the FRP jacket. This can lead to rupturing of the reinforcement;
2) Linear elastic response of FRP composites means that it can not contribute to the energy dissipation of the system. Therefore for the repair of damaged walls the original level of energy dissipation will not be regained;
3) FRP wrapping proves inefficient to provide proper confinement of long cross sections (typical of structural walls);

4) Brittle failure mechanisms can result due to bond failure between the FRP and concrete.

A retrofit solution for a structural wall, using FRP with the aim of increasing the flexural strength is shown in **Figure 2-12**. The solution consists of vertical strips of FRP extending up the edges of the wall to provide additional flexural capacity. Confinement is provided at the base of the wall by a FRP bandage and a FRP jacket is provided around the entire wall element to increase the shear capacity.

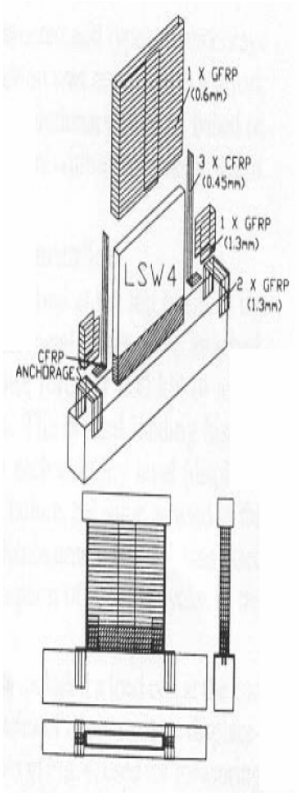

Figure 2-12: FRP rehabilitation and retrofit solution for a structural wall
(Antoniades et al., 2003)

2.5.5 Retrofit of Structural Walls by Selective Upgrading Techniques

The concept of selective intervention involves targeting independent upgrades of the characteristics of a structural member (Elanshai, 1992; Elanashai and Pinho, 1998; Pinho, 2000a; Pinho, 2000b). The characteristics of concern for structural walls are generally stiffness, shear strength, flexural strength and ductility. By using selective intervention techniques more appropriate and efficient retrofit solutions can be achieved, as the solutions directly target specific characteristics which require improvement. Selective intervention techniques are useful as advanced seismic repair and retrofitting strategies require full control

over the individual members and the global behaviour of the structure. Selective intervention used with the principles of capacity design enables a high level of control of the behaviour and failure mode.

A series of selective intervention retrofit solutions to upgrade stiffness-only, flexural strength-only, shear strength-only and ductility-only have been developed, analysed and tested (Elanshai, 1992; Elanashai and Pinho, 1998; Pinho, 2000a; Pinho, 2000b). The solutions are simple and consist of strategically located and mounted steel plates, brackets or reinforcement. **Figure 2-13** shows a series of examples of how different selective interventions can be implemented and the corresponding effect on the force versus displacement response. Full scale experimental testing on a poorly detailed frame structure, retrofitted using selective techniques has also been carried out (Pinto et al., 2002).

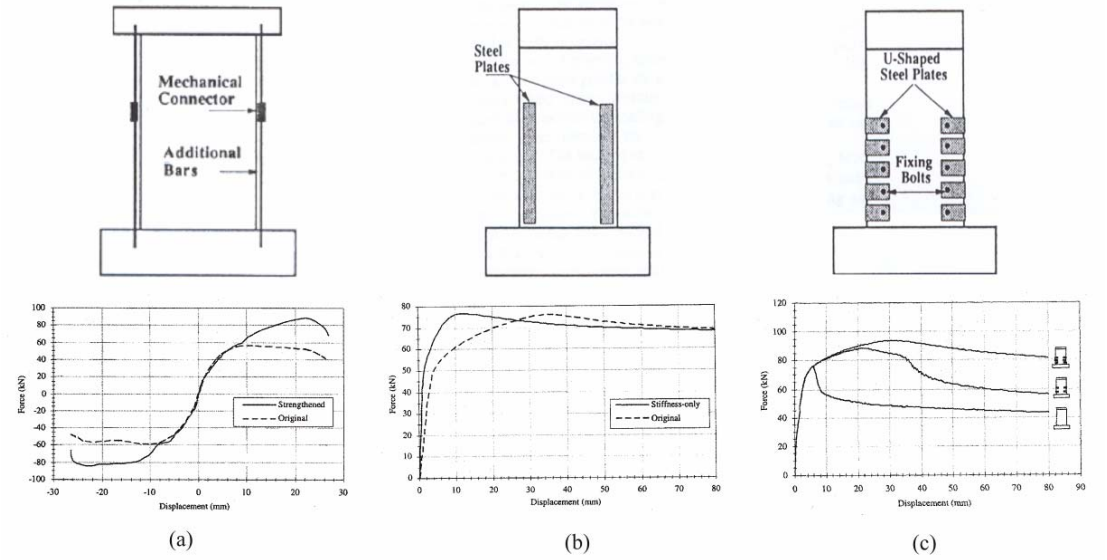

Figure 2-13: Selective intervention retrofit techniques, a) strength intervention, b) stiffness intervention, c) ductility intervention. (modified; Elanshai, 1992; Elanashai and Pinho, 1998; Pinho, 2000a)

Figure 2-13 (a) shows a flexural strength-only intervention which aims to upgrade the flexural strength of a wall, while negligibly affecting the stiffness, shear strength or ductility. This intervention may be useful in situations where capacity re-design is required or when a strength eccentricity in a structure needs to be corrected. A flexural strength-only intervention can be achieved by adding external reinforcement or plates to a member which cross the

critical plane (i.e. wall to foundation interface). A key aspect to achieve this intervention is the need to incorporate a delay mechanism to ensure that the steel plates or reinforcement do not affect the pre-yield behaviour. This delay mechanism can be as simple as a slotted connection.

A shear strength-only intervention is achieved by bonding horizontal steel plates (or FRP) at pre-determined spacings up the height of the wall section. This intervention could be performed on walls that exhibit a shear dominated inelastic mechanism. The intervention aims to increases the shear strength so that a flexural mechanism forms.

Figure 2-13 (b) shows a stiffness-only intervention which aims to upgrade the stiffness of a wall, while not significantly altering the strength or ductility. This could be useful in situations such as the repair of moderately damaged elements. A stiffness-only intervention can be achieved by bonding steel plates or FRP to the surface of the wall. An important factor in achieving a stiffness-only intervention is to ensure that the steel plates or FRP does not cross the critical sections (i.e. interface between wall and foundation), otherwise the flexural strength will be affected.

Figure 2-13 (c) shows a ductility-only intervention which aims to improve the ductility without effecting the strength or stiffness. This intervention could be useful for improving the hysteretic response by removing or lessening the effects of strength degradation. A selective ductility-only intervention can be achieved by attaching U-shaped steel plates to the edges of the wall section to improve confinement. The U-shaped plates are closed by a bolt passing through the wall, to further improve confinement. It is important to note that this intervention will only improve the ductility if the wall possesses low ductility due to poor confinement. The intervention will not work if the low ductility is due to a shear dominated inelastic mechanism.

2.6 Seismic Retrofit and Rehabilitation Guidelines

A brief review of current seismic assessment, retrofit and rehabilitation guidelines was performed to determine the most commonly suggested retrofit techniques for structural walls and assessment procedures. The documents reviewed were FEMA-356, “Prestandard and Commentary for the Seismic Rehabilitation of Buildings” (FEMA, 2000), fib bulletin,

"Seismic Assessment and Retrofit of Reinforced Concrete Buildings" (fib, 2003a) and the NZSEE Draft "Assessment and Improvement of the Structural Performance of Buildings in Earthquake" (NZSEE, 2005).

2.6.1 FEMA-356 (2000) Prestandard & Commentary for the Seismic Rehabilitation of Buildings

FEMA-356 was compiled to provide a reference document for engineers to use to make buildings more resistant to earthquakes. Included are detailed explanations of possible assessment procedures and retrofit options, for the main structural types (wall & frame structures) and materials (concrete, steel and Masonry). FEMA-356 (FEMA, 2000) is a revised version of the NEHRP "Guidelines for the Seismic Rehabilitation of Buildings" (FEMA-273) (FEMA, 1997).

Seismic retrofit options discussed in FEMA-356 (FEMA, 2000), for reinforced concrete structural walls include:

- Addition of wall boundary members – used to strengthen walls with insufficient flexural strength;
- Concrete jacketing – can be used to improve the flexural deformation capacity and to increase the shear strength;
- Carbon fibre sheets – can be epoxy bonded to the concrete surface to increase the shear capacity;
- Selective material removal – removal of concrete or severing of longitudinal reinforcement to change from a non-ductile failure mode, to a mode ductile one.

The suggestion of selective material removal is of particular interest to this research project. Suggested scenarios where selective material removal may be useful include, weakening beams to ensure a strong column, weak beam system (i.e. Capacity design) or to vertically segment walls to change the strength and stiffness.

2.6.2 fib Bulletin 24 (2003) – Seismic Assessment and Retrofit of R.C. Buildings

The fib bulletin on the "Seismic Assessment and Retrofit of Reinforced Concrete Buildings" (fib, 2003a) provides a comprehensive review of performance objectives, assessment procedures, retrofit techniques and also case studies of buildings requiring retrofit and the

retrofit solutions implemented. Suggested retrofit techniques that are discussed in fib bulletin 24 include:

- Concrete jacketing;
- Steel jacketing;
- FRP composite wrapping;
- Selective intervention techniques (as discussed in Section 2.3.4).

A detailed review and summary of force-based and displacement-based assessment procedures from assessment and retrofit guidelines from around the world is provided. The documents reviewed include the NZSEE guidelines (NZSEE, 2005), NEHRP guidelines (FEMA, 1997), FEMA 356 (FEMA, 2000) and others. A summary of typical member and building level performance vulnerabilities as observed from post earthquake reconnaissance are discussed.

2.6.3 NZSEE (2005) – Assessment & Improvement of the Structural Performance of Buildings in Earthquake

The introduction of new legislation in New Zealand (The Building Act 2004) has led to a higher proportion of existing buildings to have their seismic performance assessed. Prior to this new legislation the term "earthquake risk building" related to only un-reinforced masonry buildings (NZSEE, 2005). Now the term "earthquake risk building" is used to describe any building that does not satisfy the requirements of the New Zealand Building Code (NZBC, 1992). The NZSEE guidelines for the "Assessment & Improvement of the Structural Performance of Building in Earthquake" provide a helpful document that can be used to perform a consistent assessment of existing buildings. Provided within this document are detailed assessment procedures and suggestions for appropriate retrofit techniques.

A number of seismic retrofit options for structural walls are suggested in the NZSEE guidelines (NZSEE, 2005), which include:

- Concrete skin walls – Apply a concrete skin to an existing wall to increase the flexural or shear strength and to improve ductility. Essentially the same as concrete jacketing;
- Post-tensioning – Increase the in-plane flexural strength by applying bonded or un-bonded post-tensioning. Can be applied externally or in internal cores;

- FRP composite overlays – Apply FRP overlays to increase the stiffness or strength of the wall.

Preliminary suggestions, that in some situations it may be appropriate to deliberately weakening specific structural elements within a building, to improve the performance are made in the NZSEE guidelines. A suggested scenario where this may be applicable is the case of a highly torsional shear wall building. In this case selected shear walls may be split vertically to lower the flexural strength and to reduce the shear demand on the wall.

The assessment procedures suggested in the NZSEE guidelines were also reviewed. An initial evaluation procedure is described and it is intended that it will be used to perform a first screening of existing buildings. If buildings are determined to be earthquake prone from the initial screening process, a more detailed assessment will be required. The initial evaluation procedure is largely qualitative and requires an experienced seismic engineer, to make a judgement on the likely building behaviour and to identify critical structural weaknesses.

Methods for detailed assessment are also discussed, which include force-based assessment, displacement-based assessment, non-linear pushover and advice on using inelastic time history analysis. The displacement based assessment procedure for structural walls, outlined in the NZSEE guidelines will be discussed in more detail in Chapter 10. Detailed information regarding appropriate material properties and element level assessment procedures for reinforced concrete, steel and masonry buildings is also supplied.

2.6.4 EC8 – Part 3: Strengthening and Repair of Buildings (2005)

The scope of EC8-Part 3 "Strengthening and Repair of Buildings" (CEN, 2005) is to provide criteria for the evaluation of the seismic performance of existing buildings and to offer criteria for the selection and design of appropriate repair and strengthening techniques. Appropriate assessment procedures are discussed and detailed information regarding design assumptions and calculation procedures for the suggested retrofit solutions is provided. The retrofit techniques suggested for reinforced concrete structural walls include:

- Concrete Jacketing – Can be used to increase bearing capacity, increase flexural and/or shear strength, increase deformation capacity and improve the strength of deficient lap splices;
- Steel Jacketing – Can be used to increase shear strength, improve strength of deficient lap splices and to increase ductility through improved confinement;
- FRP Plating and Wrapping – Can be used to enhance shear capacity, provide confinement and clamp deficient lap splices.

2.7 Recent Developments in High Performance Seismic Resisting Systems

Recent developments in new building technology for high performance seismic resisting systems have focussed on using a rocking response, to ensure minimal damage and a self-centring behaviour (no residual displacements). The main disadvantage with rocking systems is that they typically result in increased lateral displacements during seismic response, due to a low level of energy dissipation. As part of the PREcast Seismic Structural Systems (PRESSS) research project, the seismic performance of un-bonded post-tensioned precast walls and "hybrid" walls was investigated (Priestley et al., 1999; Kurama et al., 1999).

The hybrid system for a beam-column connection is shown in **Figure 2-14**. The connection is formed from pre-cast concrete elements, which introduces a rocking plane at the beam-column interface. The connection shown consists of centrally located un-bonded post-tensioning and mild steel reinforcement at the top and bottom of the beam. An important characteristic is the use of un-bonded post-tensioning and an un-bonded length in the mild steel reinforcement at the beam-column interface. This allows for strain distribution in the post-tensioning and mild steel, as a gap opens when the beam rocks relative to the column. Both the un-bonded post-tensioning and the mild steel reinforcement contribute to the moment capacity of the connections. The un-bonded post-tensioning also serves to provide a re-centring capability (no residual displacements) and the mild steel reinforcement provides energy dissipation. The hybrid system is not just for beam-column connections and has been investigated for the use in structural walls at the wall-foundation connection (Kurama, 2002). An example of a hybrid wall system is shown in **Figure 2-15**.

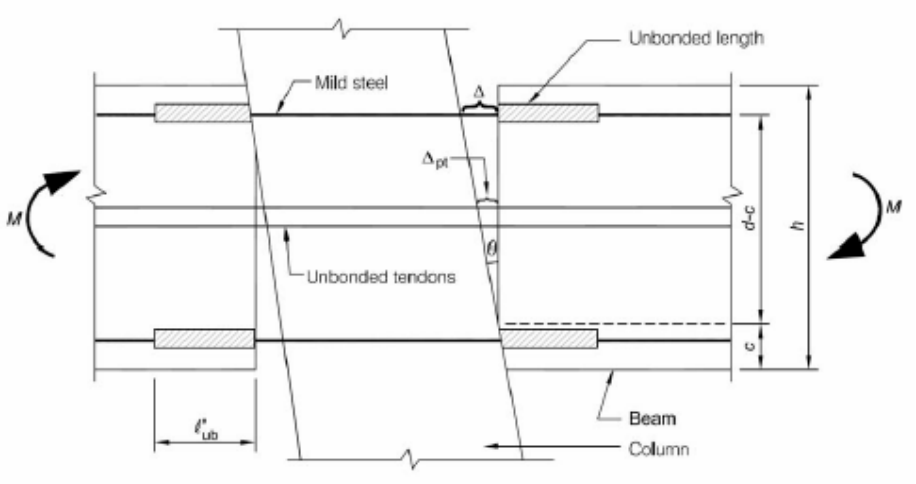

Figure 2-14: Hybrid system for a beam-column connection (NZS3101:2006)

It has been shown that un-bonded post-tensioned walls can be used to achieve a strength and initial stiffness equal to that of monolithic reinforced concrete walls, but that a moderate increase in peak lateral drift is experienced (Kurama et al., 1999). The behaviour of hybrid walls was also investigated (Kurama, 2002) and it was shown that a reduction in the peak drift experienced can be achieved (when compared to un-bonded post-tensioned walls), but it will still higher than that of an equivalent monolithic wall. A positive characteristic of these walls is a softening state, which results in a substantial reduction in stiffness (Kurama et al., 1999). This allows for large lateral displacements whilst resulting in minimal damage. The softening state is due to a geometric non-linearity as a gap opens at the rocking plane and also to non-linear behaviour of the concrete in compression.

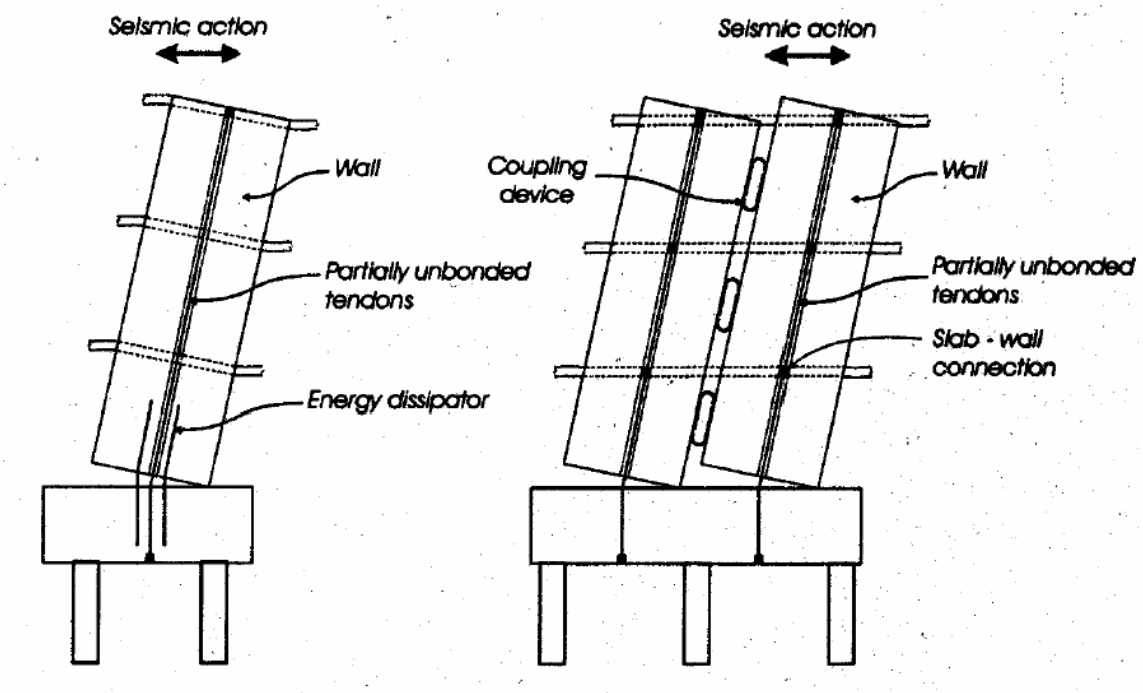

Figure 2-15: Hybrid wall systems (fib, 2003b)

The positive and negative behavioural characteristics associated with rocking wall systems are summarised in the following bullet points (Toranzo-Dianderas et al., 2004):

Positive characteristics:

1) The base shear is almost independent of the displacement once rocking has occurred (if only rely on axial load to provide re-centring, i.e. no post-tensioning);
2) Large lateral displacements can be achieved with little damage occurring as inelastic deformation is concentrated to the gap opening due to rocking;
3) Self centring behaviour resulting in no residual deformations; if appropriate restoring force is provided (by axial load or post-tensioning);
4) A bilinear behaviour with a high initial stiffness ensures that deflections can be controlled under a service level loading, but that under a larger loading rocking can occur without a major increase in force.

Negative characteristics:

1) Low energy dissipation, approximately bi-linear elastic;
2) Impact actions can be large due to wall slamming onto foundation;
3) Estimation of the seismic response requires more work to predict.

References:

Antoniades, K. K., T. N. Salonikios, et al., [2003]. "Cyclic Tests on Seismically Damaged Reinforced Concrete Walls Strengthened using Fiber-reinforced Polymer Reinforcement.", ACI Structural Journal, 100(4): 510-518.

Brunsdon, R.D., [1984]. "Seismic Performance Characteristics of Buildings Constructed Between 1936 & 1975". Research Report 84-14, Department of Civil Engineering, University of Canterbury, Christchurch, New Zealand.

CEN – Comite Europeen de Normalisation [2005] "Eurocode 8, Design of Structures for Earthquake Resistance – Part 3: Assessment and Retrofit of Buildings", EN 1998-3:2005.

Chapman, H.E., [1991], "Seismic Retrofitting of Highway Bridges", Bulletin of New Zealand Society for Earthquake Engineering, 24(2): 186-201.

Elnashai, A. S., [1992], "Effect of Member Characteristics on the Response of RC Structures", Proceedings of the Tenth World Conference on Earthquake Engineering. 10 vols, Jul 19-24 1992, Madrid, Spain, Publ by A.A. Balkema, Rotterdam, Neth.

Elnashai, A. S. and R. Pinho, [1998]. "Repair and Retrofitting of RC Walls using Selective Techniques." Journal of Earthquake Engineering 2(4): 525-568.

FEMA-273. [1997]. "NEHRP Guidelines for the Seismic Rehabilitation of Buildings". Building Seismic Safety Council (U.S.), Federal Emergency Management Agency

FEMA-356. [2000]. "Pre-Standard and Commentary for the Seismic Rehabilitation of Buildings", Federal Emergency Management Agency. Washington D.C.

fib [2001], "Externally bonded FRP reinforcement for RC structures : technical report on the design and use of externally bonded fibre reinforced polymer reinforcement (FRP EBR) for reinforced concrete structures".

fib [2003a], "Seismic Assessment and Retrofit of Reinforced Concrete Buildings", fib bulletin 24.

fib [2003b], “Seismic Design of Precast Concrete Building Structures”.

fib [2006], “Retrofitting of Concrete Structures by Externally Bonded FRPs with Emphasis on Seismic Applications”, fib Bulletin 35.

Ghobarah, A. and A. A. Khalil, [2004]. “Seismic Rehabilitation of Reinforced Concrete Walls using Fibre Composites”. 13th World Conference on Earthquake Engineering, Vancouver, B.C., Canada.

Kawashima, K. [1997]. “The 1996 Japanese Seismic Design Specifications of Highway Bridges and the Performance Based Design, Proceedings, Seismic Design Methodologies for the Next Generation of Codes”, Fajfar & Krawinkler (eds), Balkema, Rotterdam, pp. 371-382.

Kurama, Y.C., [2002], “Hybrid Post-tensioned Precast Concrete Walls for use in Seismic Regions”, PCI journal, September-October, 2002.

Kurama, Y., Sause, R., Pessiki, S. and L., [1999], “Lateral Load Behaviour and Seismic Design of Unbonded Post-tensioned Precast Concrete Walls”, ACI Structural Journal, July-August 1999.

Liu, A. and R. Park [2001]. “Seismic Behaviour and Retrofit of Pre-1970's As-built Exterior Beam-column Joints Reinforced by Plain Round Bars”. Bulletin of the New Zealand Society for Earthquake Engineering 34(1): 68-81.

New Zealand Standard, NZSS 95, Part IV, [1955], “Basic Loads to be used in Design and their Methods of Application”, New Zealand Standards Institute.

New Zealand Standard, NZSS 1900**,** Chapter 8, [1964a], “New Zealand Standard Model Building Bylaw, Basic Design Loads”, New Zealand Standards Institute.

New Zealand Standard, NZSS 1900**,** Chapter 9.3, [1964b], “New Zealand Standard Model Building Bylaw, Design and Construction, Concrete”, New Zealand Standards Institute, 60p.

NZBC [1992], “New Zealand Building Code”

NZS 4203, [1976], “Code of Practice for General Structural Design and Design Loadings for Buildings”, Standards Association of New Zealand, 80 pp.

NZSEE. [2005]. “Assessment and Improvement of the Structural Performance of Buildings in Earthquake – Study Group Draft”, New Zealand Society of Earthquake Engineering, Prepared for the Department of Building and Housing

Pampanin, S., Christopoulos, C., and Priestley, M.J.N. [2002] “Residual Deformations in the Performance-Based Seismic Assessment of Frame Structures”. Research Report No. ROSE 2002/02, IUSS Press, Pavia, Italy, August 2002, 203pp.

Paulay, T., and Priestley, M.J.N., [1992], “Seismic Design of Reinforced Concrete and Masonry Buildings” John Wiley and Sons, New York, 1992, 744pp.

Pinho, R., [2000a]. “Selective Retrofitting of RC Structures in Seismic Areas.” PhD thesis, Department of Civil and Environmental Engineering, Imperial College, London.

Pinho, R. [2000b]. “Shaking Table Testing of RC Walls.” ISET Journal of Earthquake Technology 37(4): 119-142.

Pinto, A., Varum, H., Molina, J., [2002] “Experimental Assessment and Retrofit of Full-scale Models of Existing RC Frames”, Proceedings of the Twelfth European Conference on Earthquake Engineering.

Priestley, M.J.N., [2000], “Performance Based Seismic Design”, Proc. 12 WCEE, Auckland, New Zealand, Paper No. 2381.

Rodriguez, M. and R. Park [1991]. “Repair and Strengthening of Reinforced Concrete Buildings for Seismic Resistance.” Earthquake Spectra 7(3): 439-459**.**

Sabnis, G. M., A. C. Shroff, et al. [1996]. “Seismic Rehabilitation of Concrete Structures”. Farmington Hills, Mich., American Concrete Institute. SP-160

SEAOC [1998] “Guidelines for Performance Based Seismic Engineering”. SEAOC Blue Book – Draft of Appendix G-Part 2.

SNZ. [2006] “Concrete Structures Standard NZS 3101:2006, Volume 1 Code of Practice and Volume 2 Commentary”. Standards New Zealand, Wellington.

Toranzo-Dianderas, L.A., Restrepo, J.I., Carr, A.J. and Mander J.B., [2004], “Rocking Confined Masonry Walls with Hysteretic Energy Dissipaters and Shake-table Validation”, 13th world conference on earthquake engineering, Vancouver, Canada, paper No.248.

Turkey [1999]. “Preliminary Report, Turkey-US Geotechnical Earthquake Engineering Reconnaissance Team”, University of Southern California, http://gees.usc.edu/GEES/RecentEQ/Turkey_Duzce/Reports/Bolu/bolu.htm.

Turkey [2003]. “Reconnaissance Report”, Bogazici University, http://www.koeri.boun.edu.tr/depremmuh/eqspecials/bingol/bingol_eq.htm.

3 The Concept & Implementation of Selective Weakening

3.1 Introduction to Selective Weakening

Current seismic retrofit strategies generally focus on increasing the strength/stiffness or upgrading the mechanical properties of a structure. A typical drawback of this is that an upgraded behaviour might result in an increased demand on the structural and sub-structural elements i.e. foundations. Herein proposed is a counter-intuitive but rational seismic retrofit strategy consisting of selectively weakening a structural system. Such a retrofit strategy will be applicable to alternative seismic resisting systems and components, including structural walls, beams, columns and diaphragm connections.

A selective weakening approach to seismic retrofit is performed within an overall performance based retrofit approach with the aim of improving the inelastic behaviour by first reducing the strength /stiffness of specific members within the structural system. As a result of reducing the strength and stiffness the force demand on the structure will be reduced. Once weakening has been achieved, a wide range of materials and techniques (e.g. fibre reinforced polymers, steel plates, jacketing or shotcrete) can be used to ensure that the structure has adequate strength and displacement capacity. Whilst performing a selective weakening retrofit it has to be assured that the structure meets specific performance characteristic and the principles of capacity design.

Acceptance of a selective weakening approach for seismic retrofit can be found in the NERHP guidelines (FEMA, 1997) and FEMA-356 (FEMA, 2000) documents and more recently in the NZSEE guidelines (NZSEE, 2005). Within these documents preliminary suggestions regarding the severing of longitudinal reinforcement to improve ductility or modify the inelastic mechanism and to segment walls to modify strength and stiffness are made. In this contribution an investigation is being performed to determine the feasibility of using a selective weakening approach for seismic retrofit, with a focus on reinforced concrete structural walls.

3.2 Modification of the Inelastic Response

The initial aim of using a selective weakening approach to seismic retrofit is to modify or improve the inelastic mechanism of the structure and/or its components. **Figure 3-1** (a) shows an as-built monolithic wall exhibiting some undesirable characteristics which are typical of walls requiring retrofit. These characteristics include low ductility, which can result from a shear dominated inelastic mechanism. This can lead to significant strength degradation during a cyclic response. Also shown in the hysteretic response of the as-built wall is significant pinching which is typical of concrete sections that are poorly detailed or reinforced with plain round bars. This is undesirable as it can result in lower energy dissipation and therefore increased displacement demand.

Figure 3-1 (b) shows the expected behaviour of the as-built wall after the first phase of the selective weakening approach, which has been herein termed "Partial selective weakening". Two options are shown for possibly implementing the partial selective weakening. Firstly wall (b') shows the as-built wall split vertically into two parallel walls. This will have the effect of reducing the moment capacity and therefore the shear demand on the wall. By using this technique the inelastic mechanism could be changed from shear dominated to flexure dominated with a reduced overall capacity. This application of a selective weakening approach will essentially result in two monolithic walls in series, therefore material damage will occur in the plastic hinge region depending on the type of reinforcement and bond conditions (i.e. deformed or plain reinforcement, lap splices). As the as-built wall exhibited poor reinforcement details, the two partially selectively weakened walls will still exhibit undesirable characteristics such as pinching of the hysteretic response but low ductility capacity and strength degradation could be overcome. The second option for a partial selective weakening retrofit is shown in **Figure 3-1**, as wall (b''). In this approach the wall has been cut horizontally at foundation level to induce a rocking type response. This will result in a significant reduction in the moment capacity of the wall and will change the hysteretic response to bi-linear elastic. Therefore the wall will exhibit minimal damping which will increase displacements but the majority of the inelastic behaviour will be concentrated in the gap opening as the wall rocks. It is therefore expected that there would be little or no damage after a cyclic response.

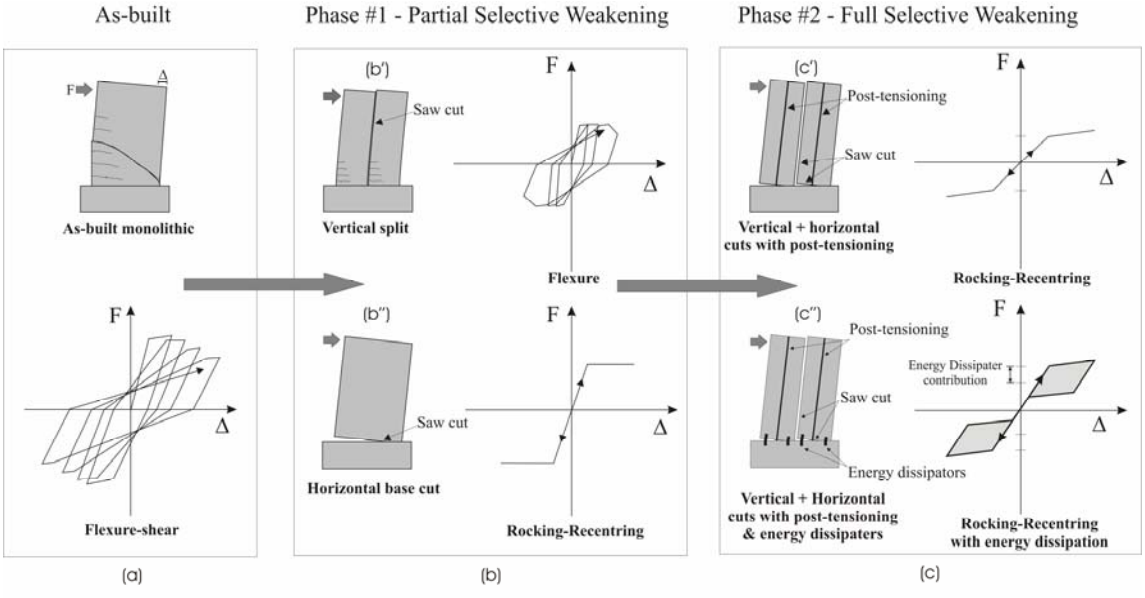

Figure 3-1: Expected damage and hysteretic response before and after intermediate phases of selective weakening retrofit: (a) as-built; (b) partial selective weakening; (c) full selective weakening

Figure 3-1 (c) shows the second phase of the process which has been termed "Full selective weakening" and relates to a complete retrofit solution being implemented that targets a specific level of strength/stiffness after an initial weakening intervention. A full selective weakening retrofit approach involves an initial strategic weakening, but then the use of currently available retrofit techniques or structural solutions, such as post-tensioning, fibre reinforced polymers and energy dissipation devices to achieve the targeted performance. This may result in a retrofitted wall of equal or greater stiffness/strength/ductility than the original. Similarly, when elements require protection from excessive seismic demand (i.e. foundations) the target level of the full selective weakening retrofit may be lower than the original. Wall (c'') has been retrofitted using a full selective weakening technique using an initial weakening involving splitting the wall vertically and cutting it horizontally at foundation level. The second phase involved the addition of un-bonded post-tensioning to increase the moment capacity and to control the rocking response. Energy dissipaters have also been added to increase the moment capacity and to provide supplemental energy dissipation. By implementing an appropriate balance of initial weakening, post-tensioning and damping a "flag shaped" hysteresis can be achieved, typical of recently developed high performance seismic resisting systems based on ductile jointed (hybrid) connections (Priestley et al., 1999; fib 2003; Pampanin 2005).

3.3 Modification of the Demand-capacity Balance

It is counter intuitive to think that by weakening a structure the seismic performance can be improved but this can result from changing/improving the inelastic mechanism and/or from reducing the demand as a result of the weakening. Selective weakening focuses on strategically altering the structural properties, which will involve an initial weakening but then a target performance level will be aimed for which could be weaker, equal or stronger that the original wall.

The design demand on a structure can be reduced by using a selective weakening retrofit intervention as the demand is usually determined by design code acceleration spectra. A common property of acceleration spectra is that the spectral acceleration reduces significantly as the natural period increases, except for small periods (typically less than 0.4 seconds). In addition to the decrease in spectral acceleration due to the natural period increase, an improved inelastic mechanism can lead to a more ductile response dissipative response. As the level of equivalent viscous damping increases the acceleration spectrum can be decreased. An example of the effects of selective weakening on the spectral demand is shown in **Figure 3-2**. As a side effect of the increased natural period due to selective weakening, the spectral displacement will be increased. To help partially mitigate the increased spectral displacement the increase in damping associated with a more ductile response will reduce the spectral displacement.

A selective weakening approach will not necessarily result in an overall weakening of the structural system. When a "full selective weakening" retrofit solution is used a target performance level can be set to ensure that there is no demand increase or that the level of demand increase is controlled. Wall designs are often governed by temperature and shrinkage effects so they can be conservative for flexural or shear demands. This can help account for a reduction in strength/stiffness due to selective weakening.

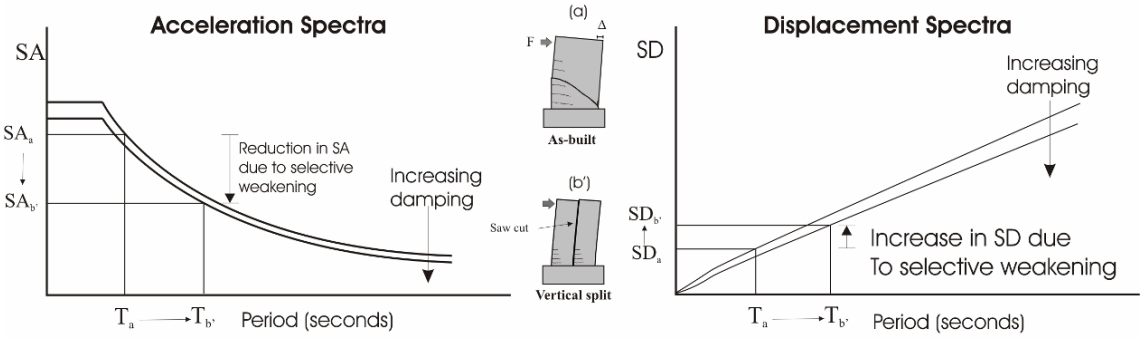

Figure 3-2: The effect of a partial selective weakening technique on spectral acceleration & displacement demand

Figure 3-3 show how selective weakening can be used as part of a performance based retrofit to ensuring capacity design of the wall system that not only includes enforcing a flexural dominated inelastic mechanism occurs (instead of a shear dominated one) but also that the capacity of the foundations are not exceeded. **Figure 3-3** (a) shows an example of force versus displacement response of an as-built wall which is governed by a shear dominated inelastic mechanism and the expected behaviour using a conventional retrofit technique and a partial selective weakening technique. The conventional technique can be for example based on concrete jacketing. When using this approach the capacity of the foundation may be exceeded. It is highly undesirable that the foundation capacity is exceeded as any repairs required after a seismic response would be difficult and expensive. If a partial selective weakening approach is used the foundation capacity will not be exceeded and a ductile response can be achieved. The contribution to the lateral load resisting system will however be reduced.

Figure 3-3 (b) show the force versus displacement response for the as-built wall and two walls using a full selective weakening retrofit approach. In the first solution (wall (c')), selective weakening has been performed by using a vertical cut to increase the aspect ratio (height to length) and a horizontal cut has been used to allow for a rocking response. In addition vertical un-bonded post-tensioning has been introduced, to add additional moment capacity and to control the rocking response. In the second solution (wall (c'')), the as-built wall that has been cut vertically down the centre of the wall and horizontally at foundation level. In addition to the initial weakening, un-bonded post-tensioning and a source of energy dissipation has been added to control the rocking response and to increase the moment

capacity to a target set in a performance based retrofit approach to ensure that the foundation capacity is not exceeded.

Figure 3-3 (c) shows a selective weakening retrofit solution for a situation where the lateral resistance needs to be increased and foundation capacity is not critical. The as-built wall (wall (a)) may require retrofitting to increase the lateral load carrying capacity and to improve the ductility of the system. A selective weakening retrofit solution, aimed at increasing the lateral load carrying capacity and increasing the ductility is shown in wall (e). The retrofit solution involves a horizontal cut at foundation level, to induce a rocking response and a combination of un-bonded post-tensioning and energy dissipaters. The retrofitted strength of the wall is higher than that of the as-built wall, but also lower than that of the foundation. A conventional retrofit technique could be used to increase the lateral resistance capacity, but a selective weakening retrofit solution offers the advantages of a self-centring behaviour and minimal damage after a cyclic response.

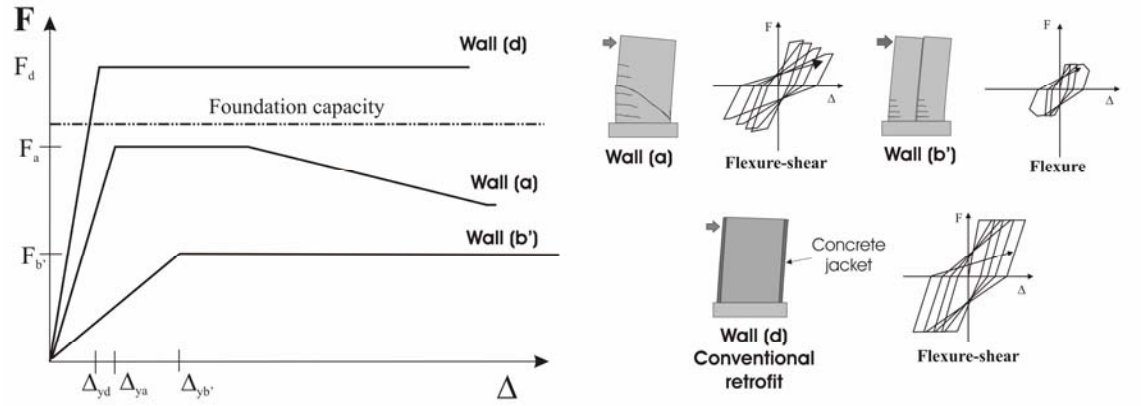

(a)

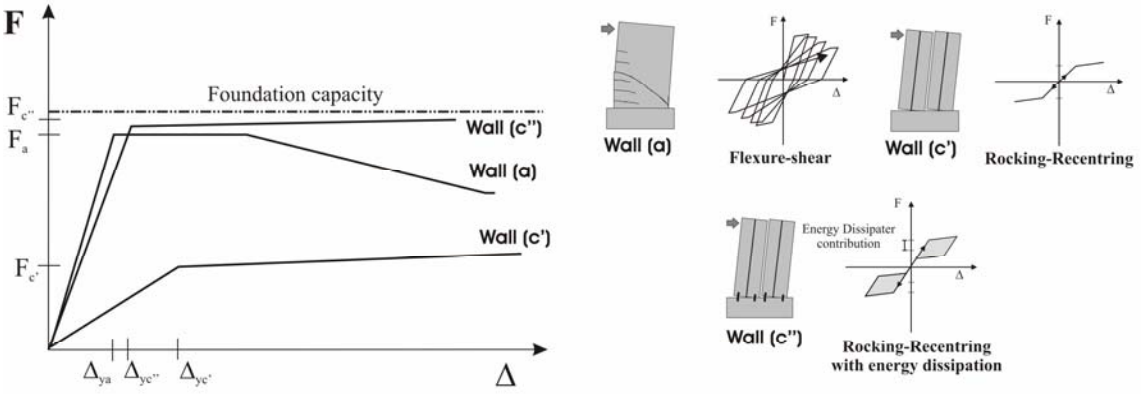

(b)

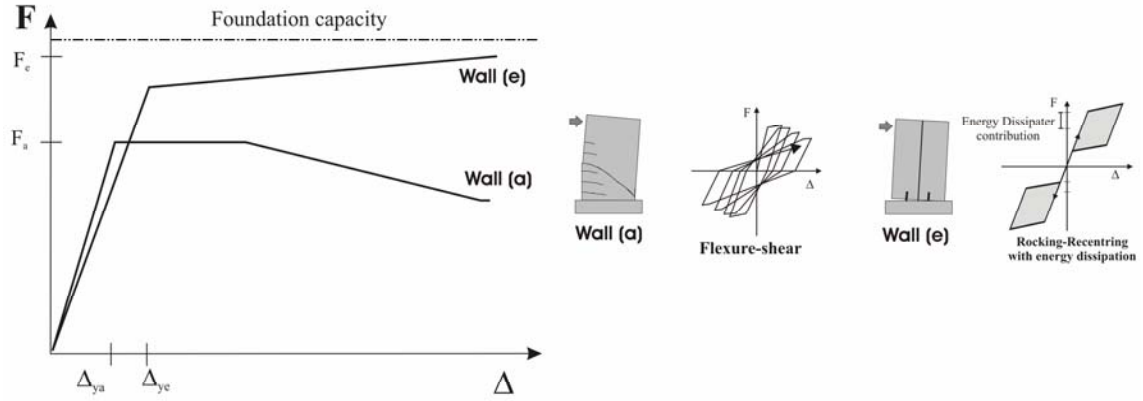

(c)

Figure 3-3: Selective weakening capacity design & performance based retrofit

3.4 Advantages and Disadvantages of a Selective Weakening Approach

A selective weakening approach for the seismic retrofit of structural walls offers many advantages over existing retrofit techniques including:

- Reduce or control the demand on the foundations by controlling the capacity of the wall/s.
- Introduce capacity design to improve the inelastic mechanism (e.g. shear to flexure).
- Reduce or eliminate damage due to plastic hinge development by introducing a rocking behaviour.
- Avoid the potential for buckling of longitudinal reinforcement due to the large spacing of transverse reinforcement in older buildings.
- Further enhance the response of the system by introducing a self-centring behaviour (i.e. no residual displacements) through vertical post-tensioning tendons as well as additional energy dissipation capacity.

Disadvantages of using a selective weakening approach are mainly related to problems in implementing the retrofit solution or new problems arising from using it. Some problems that have been considered are:

- Segmenting a wall by a vertical cut may involve severing the transverse reinforcement; a solution to re-introduce confinement and shear capacity such as FRP wrapping may be required, depending on the flexure/shear hierarchy of strength.
- A horizontal cut at foundation level will sever longitudinal reinforcement, therefore a solution to increase the moment capacity and energy dissipation will be needed, this could include a combination of post-tensioning and energy dissipation devices.
- A horizontal cut could result in the wall sliding on the cut region, therefore a shear key mechanism will be required.
- The interaction between the wall and floor diaphragm need to be considered.
- Compatibility issues with the existing structural system (i.e. rocking wall may activate other parts of the structure as the wall lifts).

3.5 Selective Weakening for Other Structural Systems

In this contribution selective weakening will only be considered for structural walls. Selective weakening however is suitable for the application to other structural elements such as frames or diaphragm connections (Pampanin, 2006).

Suggestions of a selective weakening approach applicable for frame structures are introduced in FEMA-356 (FEMA, 2000). It is suggested that by severing longitudinal reinforcement in the beams, the principles of capacity design could be introduced. This would involve modifying the strength hierarchy to ensure that a strong column weak beam system is achieved.

Selective weakening has been incorporated as part of a retrofit solution for hollowcore floor diaphragms in existing frame buildings (Jensen, 2006). The selective weakening intervention aimed to reduce the flexural capacity of the end seating connection, to minimise the demand transferred to the hollowcore floor units. Weakening was provided by a series of drill holes to provide a perforated plane of weakness.

3.6 Prototype Structure

A prototype wall specimen to represent a pre-1970's New Zealand structural wall was developed by investigating typical reinforcement detailing characteristics and historic seismic provisions.

3.6.1 Typical Reinforcing Details of Pre-1970's New Zealand Structural Walls

An investigation was performed to determine typical reinforcement details for pre-1970's walls in New Zealand, by reviewing existing building plans and historic building codes. The investigation focused on determining typical bar sizes, spacing, grade and typical detailing characteristics.

From reviewing the existing building plans it was seen that the reinforcement layout was generally quite consistent between different buildings, and independent of the wall geometry. **Figure 3-4** shows the typical bar layout that can be found in a pre-1970's reinforced concrete wall in New Zealand. The typical bar diameter for longitudinal reinforcement was ½" (12.7mm) and the transverse reinforcement diameter was typically ⅜"-½" (9.5mm-12.7mm).

The spacing of the reinforcement was also generally consistent between buildings, with the typical spacing being 1' (304mm) for both the longitudinal and transverse reinforcement. NZSS 1900 chapter 9.3 (NZS, 1964b), states that a minimum reinforcement ratio of 0.25%, should be used (in both directions), when using mild steel reinforcement. Two layers of ⅜" bars at 1' (304mm) spacing for the transverse reinforcement is just below this minimum reinforcement ratio, at 0.23%. Two layers of ½" bars at 1' spacings in an 8" wall results in a reinforcement ration of 0.47%. Two layers of reinforcement were generally used for walls over 8" (203mm) thick, but was only required for walls over 10" thick (NZS, 1964b). The transverse reinforcement is generally anchored by a 90 degree bend that hooked around the longitudinal reinforcement at the ends of the wall and was anchored in the cover concrete (Priestley, 1995). The 90 degree bend should have been followed by a length of bar of at least 16 bar diameters (NZS, 1964b). Plain round reinforcement was used in New Zealand until about the mid 1960's (Liu and Park, 2001). Discussion of typical reinforcement and concrete properties for pre-1970's structural walls in New Zealand can be found in Chapter 10.

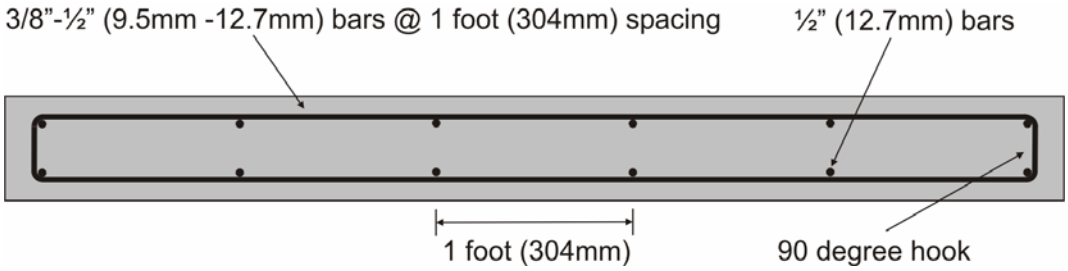

Figure 3-4: Typical reinforcement detailing for a pre-1970's reinforced concrete wall in New Zealand

Particular attention was focused on the lap detail in existing walls, as it was thought that this could govern the overall performance. It was found that typically a straight lap (without any hook) was most commonly used, with a lap length of 40 bar diameters. This equates to a lap length of 20" (504mm) for a ½" bar (typical of wall longitudinal reinforcement). This meets the requirements of NZSS 1900 (NZS, 1964b), which states that where a bar is required to develop its full working stress in tension, the minimum lap length shall be 40 bar diameters or 24 bar diameters if a 180 degree hook is used.

Figure 3-5 shows the typical detailing characteristics for a pre-1970's New Zealand structural wall that were discussed above (from Whakatane hospital, designed in 1961).

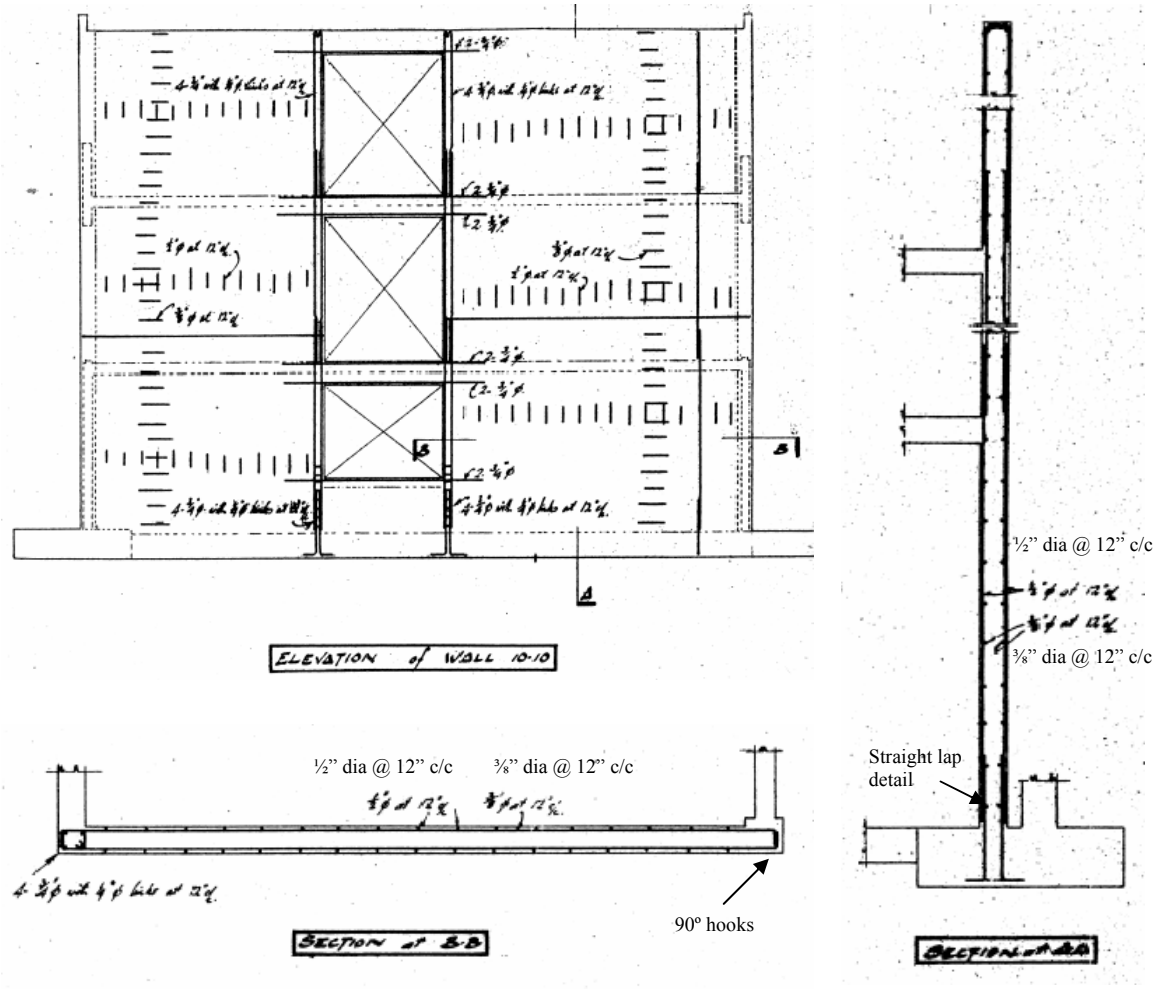

Figure 3-5: Wall reinforcing details, Whakatane Hospital (1961)
(Courtesy of Holmes Consulting Group)

3.6.2 Development of Prototype

A prototype building to represent a pre-1970's building was developed based off historic seismic provisions and typical axial load ratios. A review of historic seismic provisions from past New Zealand codes can be found in Chapter 2. A simplified structural layout was developed, which was dominated by structural walls. The prototype building, which was a three storey structure, is shown in **Figure 3-6**. The associated seismic and axial tributary areas acting on the prototype wall are highlighted.

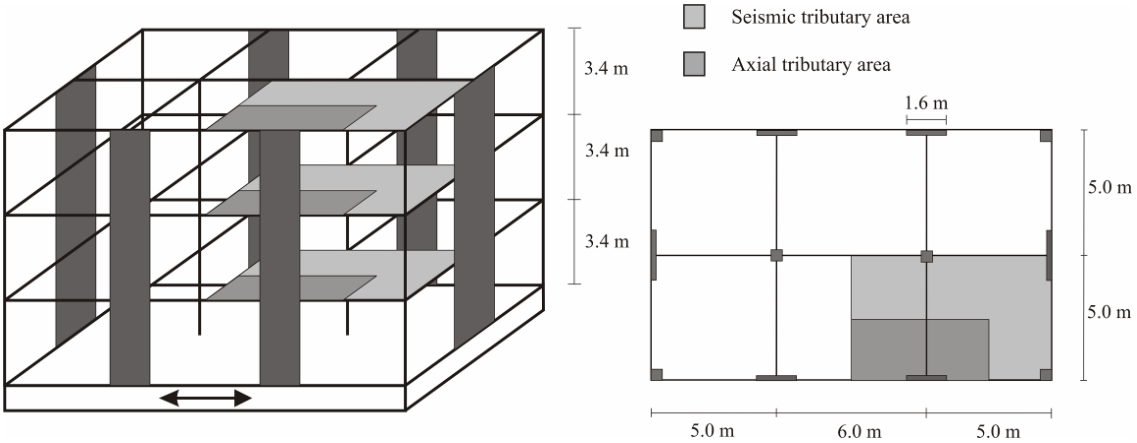

Figure 3-6: Idealised prototype building layout

Once the structural layout was determined the associated seismic and axial masses were determined by assuming a 7.5kPa floor load. This includes 0.96kPa (20lb/ft^2) for a seismic live loading which was determined from NZSS 95 (NZSS, 1955), for a general office building. Once the associated seismic massed were determined, an inverted triangular lateral force distribution with a 0.12 seismic coefficient at the top of the wall was used. The assumed lateral force distribution was consistent with NZSS 95 (NZSS, 1955). The wall reinforcement details were designed to be representative of a pre-1970's wall, and are consistent with those discussed in 3.6.1. The required prototype wall length was determined using the typically reinforcement layout and the moment demand resulting from the lateral force distribution. The axial load ratio was calculated and compared with what could typically be expected. The axial load ratio was determined to be 0.035 or 3.5% which is reasonable for a structural wall of this height. The details of the prototype wall specimen are summarised in **Figure 3-7**, calculations can be found in Appendix C.

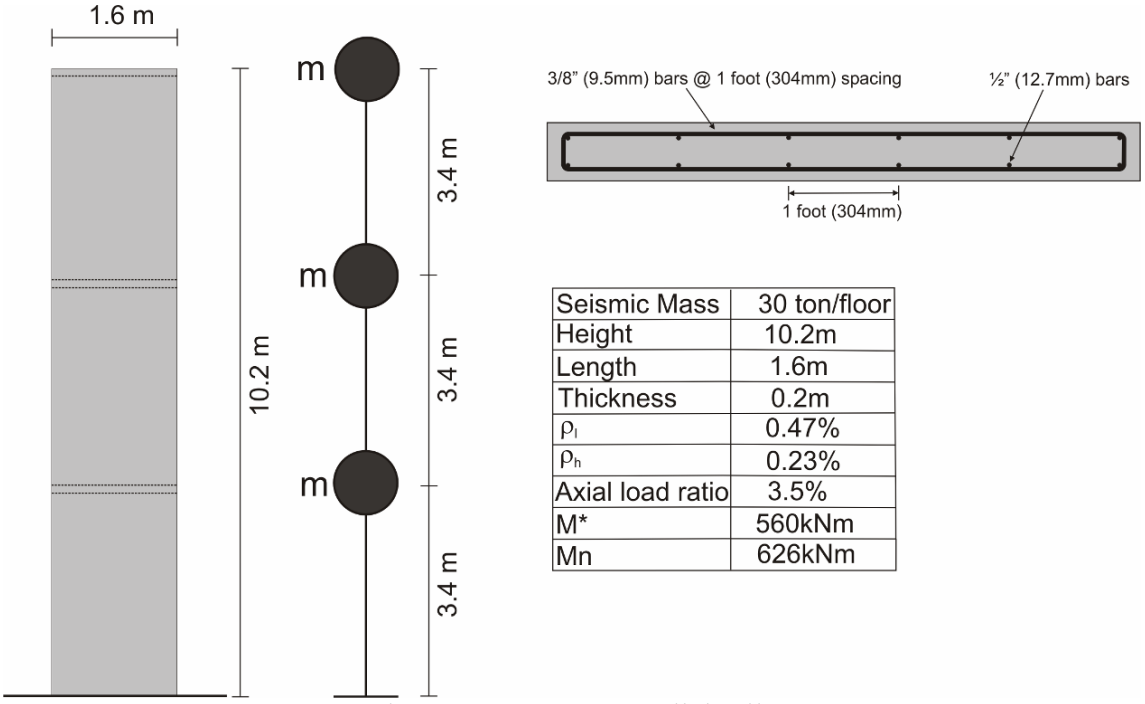

Figure 3-7: Prototype wall details

3.7 Experimental Program

A series of experimental investigations were performed as part of this research project to validate the feasibility and possibility of using selective weakening techniques for the seismic retrofit of reinforced concrete structural walls. A total of four tests were performed on two benchmark (W1 & W2) and two retrofitted structural wall specimens (W1R & W2R). Quasi-static uni-directional in-plane testing was performed on the cantilever wall specimens, which were 2/3 scale and represented the base portion of a structural wall. The experimental investigations were used for proof of concept purposes and the development, set-up, testing and results of each wall will be discussed in Chapters 4-7. A summary of the findings from the experimental tests will be provided in Chapter 8. A brief description of each of the experimental walls is provided below:

- W1 - Benchmark specimen with reinforcement details typical of pre-1970's construction in New Zealand. Plain round reinforcement was used with a lap slice in the longitudinal reinforcement at the base of the wall.

- W2 - Benchmark specimen designed to be governed by a shear failure. To achieve a high flexural strength a large quantity of boundary element reinforcement was used within the rectangular cross section.

- W1R – W1R is a W1 equivalent which has been retrofitted using a selective weakening technique that involves a horizontal cut at foundation level to induce a rocking re-centring response. The retrofit solution represents a scenario similar to that outlined in **Figure 3-3** (c), where the foundation capacity is not critical and the retrofit solution aims to reduce the peak displacements experienced during a seismic response.

- W2R – W2R is a W2 equivalent which has been retrofitted using a selective weakening solution similar to wall (b') in **Figure 3-3** (a). The retrofit solution involved vertically segmenting the wall, to improve the displacement capacity by inducing a flexural response. This ensured that the gravity carrying capacity was maintained after a cyclic response.

Figure 3-8 provides a graphical description of the expected performance of the benchmark and retrofitted experimental specimens. The expected general hysteretic shape and force verses displacement backbone curves for the benchmark and retrofitted walls are provided.

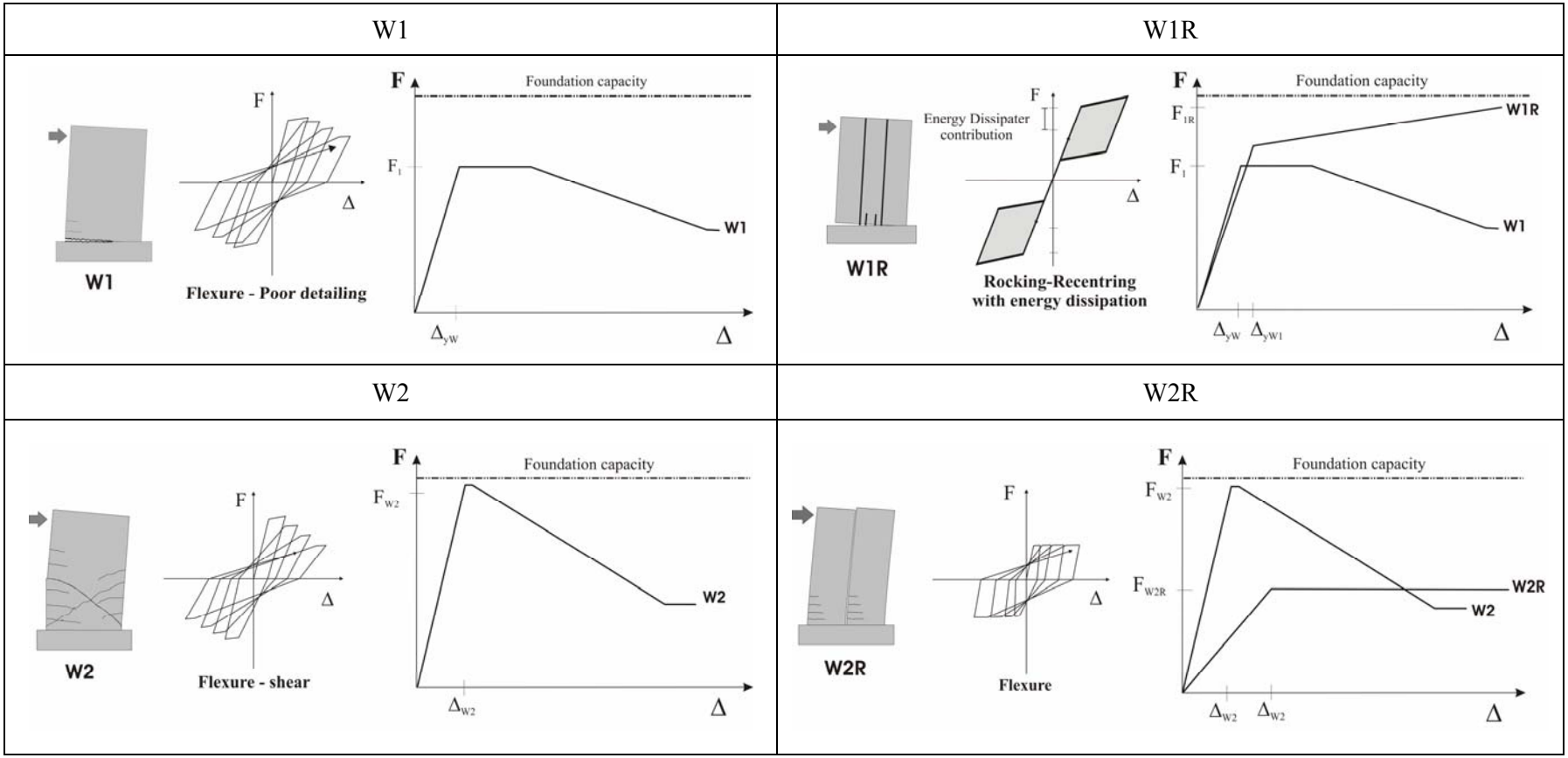

Figure 3-8: Benchmark and retrofitted experimental wall behaviour

References:

FEMA-273. [1997]. "NEHRP Guidelines for the Seismic Rehabilitation of Buildings". Building Seismic Safety Council (U.S.), Federal Emergency Management Agency

FEMA-356. [2000]. "Pre-Standard and Commentary for the Seismic Rehabilitation of Buildings". Federal Emergency Management Agency. Washington D.C.

fib [2003], "Seismic Design of Precast Concrete Building Structures"

Jensen, J.P., Bull D.K., Pampanin S. [2006], "Conceptual Retrofit Strategy for Existing Hollowcore Seating Connections", in 2006 New Zealand Society of Earthquake Engineering Conference.

Liu, A. and R. Park [2001]. "Seismic Behaviour and Retrofit of Pre-1970's As-built Exterior Beam-Column Joints Reinforced by Plain Round Bars". Bulletin of the New Zealand Society for Earthquake Engineering, 34(1): 68-81.

New Zealand Standard, NZSS 1900**,** Chapter 8, [1964a], "New Zealand Standard Model Building Bylaw, Basic Design Loads", New Zealand Standards Institute.

New Zealand Standard, NZSS 1900**,** Chapter 9.3, [1964b], "New Zealand Standard Model Building Bylaw, Design and Construction, Concrete", New Zealand Standards Institute.

New Zealand Standard, NZSS 95, Part IV, [1955], "Basic Loads to be used in Design and their Methods of Application", New Zealand Standards Institute.

Pampanin, S**.**, [2005], "Emerging Solutions for High Seismic Performance of Precast/Prestressed Concrete Buildings", Journal of Advanced Concrete Technology (ACT), *invited paper* for Special Issue on "High performance systems", Vol. 3 (2), pp. 202-223

Pampanin, S., [2006], “Controversial Aspects in Seismic Assessment and Retrofit of Structures in Modern Times: Understanding and Implementing Lessons from Ancient Heritage”, Bulletin for the New Zealand Society for Earthquake Engineering, Vol. 39, No. 2, June 2006.

Priestley, M.J.N. [1995] “Displacement-based Seismic Assessment of Existing Reinforced Concrete Buildings” Proceedings of Pacific Conference on Earthquake Engineering 2:225-44, 1995, Melbourne.

Priestley, M.J.N., Sritharan, S., Conley, J.R. and Pampanin, S., [1999] “ Preliminary Results and Conclusions From the PRESSS Five-Storey Precast Concrete Test Building, PCI Journal, Nov-Dec 1999.

4 W1 – Pre-1970's Construction Practice

4.1 Introduction

This Chapter presents the objectives, development, predictions, testing and results for W1. W1 was designed to represent as-built pre-1970's construction practice and was used as provide a benchmark specimen to aid in developing a selective weakening retrofit technique.

4.2 Development of W1

W1 adopted reinforcement details typical of pre-1970's construction practice. This wall was to be used to assess the likely behaviour of walls in New Zealand from this period and to provide a benchmark specimen for a selective weakening retrofit technique which was to be developed and tested later in the experimental program.

Important considerations regarding specimen geometry, reinforcement detailing and material properties had to be made in the development of W1. Specific aspects regarding these points are discussed in detail in the following sections.

4.2.1 Experimental Specimen Geometry

An extensive variation in wall geometry throughout existing building stock was observed. It was therefore impractical to attempt to represent all situations. Decisions regarding the geometry of W1 had to be based upon a balance of observations made from existing building plans and laboratory constraints.

A rectangular wall cross section (i.e. no boundary elements) was used as it was representative of common pre-1970's construction practice and it was also best suited for the selective weakening retrofit technique being developed. The cross sectional geometry of W1 is based off the prototype building with a structural wall seismic resisting system which was developed in Chapter 3. The cross sectional dimensions of the specimen W1 were scaled to 63% of the prototype wall geometry (using a constant density scaling approach, see Appendix C). The scale factor was governed by available reinforcing bar sizes, which will be discussed in more detail in the following section. This resulted in an experimental wall with a length of 1020mm (1600mm prototype) and a thickness of 125mm (200mm prototype).

The height of existing walls provides a constraint for laboratory testing, therefore for this experimental program it was decided that it would be suitable to create only the base portion of a wall (see **Figure 4-1**). The base portion represents the potential plastic hinge region and is typically where all inelastic action will occur. By constructing and testing only the base portion of a wall, the shear demand is significantly increased. This was not a major problem for W1 as the inelastic response was flexurally dominated. This experimental testing approach has been used in previous studies on structural walls (Pinho, 2000). A height of 1.5m was chosen for W1, this was sufficiently high enough to represent the potential plastic hinge region and was a convenient height for the testing apparatus. The experimental wall specimen was loaded as a cantilever at this height of 1.5m.

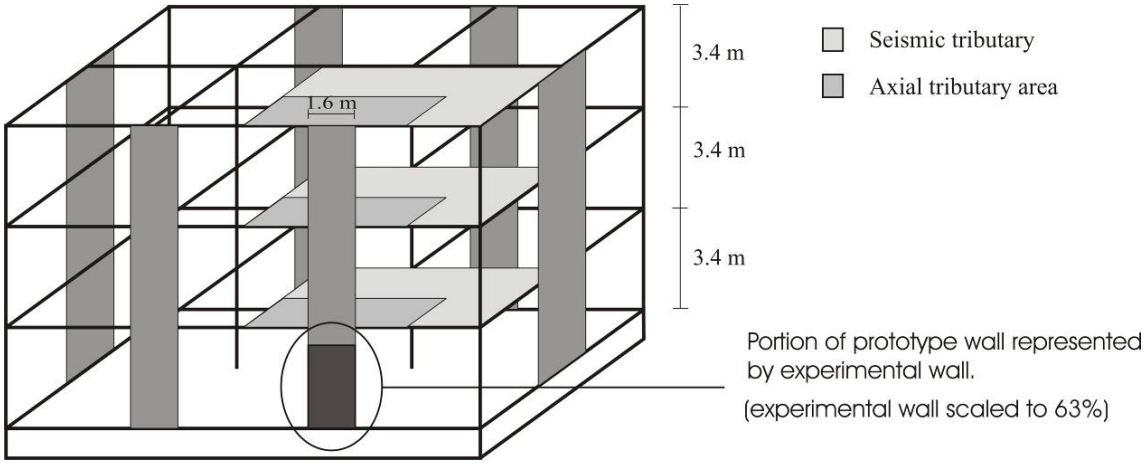

Figure 4-1: Portion of prototype wall represented by the experimental wall

4.2.2 W1 - Reinforcement Detailing

The reinforcement details for W1 were based on those developed for the prototype wall in Chapter 3. An investigation was performed to determine typical reinforcement details typical of construction practice from the pre-1970's period in New Zealand. The investigation consisted of reviewing plans of existing building from the pre-1970's period and previous research on existing building in New Zealand (Brunsdon, 1984). As for the wall cross sectional geometry the reinforcing details were scaled to 63% of the prototype dimensions. The prototype wall consisted of plain round bars of ½" (12.7mm) diameter for the longitudinal reinforcement at 12" (304mm) centres and ⅜" (9.5mm) diameter bars at 12" (304mm) centres for the transverse reinforcement. The 63% scale factor was convenient as it allowed the longitudinal reinforcement for the experimental wall to be represented by 8.0mm

plain round bars and the transverse reinforcement by 6.0mm bars, both of which are common and readily available sizes of plain round reinforcement. The reinforcement spacing was scaled accordingly to 190mm for both the longitudinal and transverse reinforcement in the experimental specimen. Two layers of longitudinal and transverse reinforcement were used within the wall. The layout of the reinforcement in W1 is shown in **Figure 4-2**.

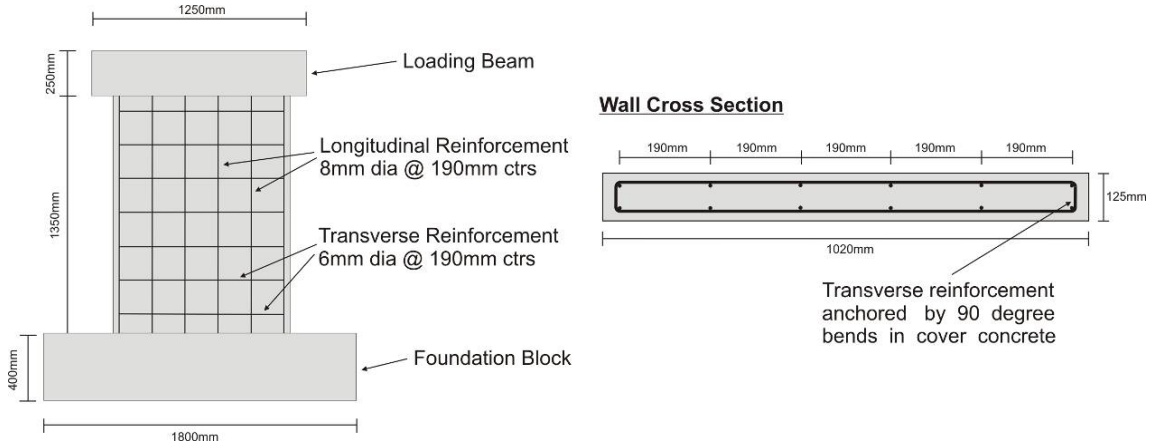

Figure 4-2: W1 reinforcement details

The use of a lap splice in the longitudinal reinforcement was considered as an important detail which could potentially govern the overall behaviour of the wall. There was a high possibility that the plain round reinforcement would provide insufficient bond capacity, which would lead to the lap splice failing before the nominal flexural strength was achieved. For this reason, the longitudinal reinforcement was lapped at foundation level with a straight lap detail of 40 bar diameters, which was based on details observed in existing buildings. This equated to 320mm for the 8.0mm in diameter longitudinal reinforcement used in W1. The lap detail was formed by leaving starter bars (40 bar diameters in length) protruding from the foundation block. The wall reinforcing cage was spliced to the starter bars left protruding from the foundation block. The wall longitudinal reinforcement was cranked to allow for the lap splice. The transverse reinforcement detailing also represented construction practice typical of the pre-1970's period. For transverse reinforcement in walls this typically consisted of plain round reinforcing bars on each face anchored by 90 degree bend in the cover concrete at the end of the wall.

4.2.3 W1 – Material Properties

The concrete material properties and reinforcement used for W1 were chosen to best represent the materials available in the pre-1970's period. An investigation into the typical concrete

compressive strength from this period was carried out in Chapter 10 and it was determined that the specified 28 day strength typically ranged from 2000-2500 p.s.i. which corresponds to 13.8-17.2 MPa. Concrete from this period can be expected to significantly increase in strength with age, due to cement from this period being relatively coarsely ground. The NZSEE draft guidelines (NZSEE, 2005) recommend that a conservative estimate of 1.5 times the specified concrete strength be used to account for this strength increase. For this reason the concrete compressive strength for W1 was specified at 25 MPa. The typical aggregate size used in pre-1970's construction was ¾" (19mm), for W1 a 13mm aggregate size was used. The actual scaled aggregate size equates to 11mm, however 13mm aggregate was the closest available size.

Structural grade reinforcement from the 1930-1970's period typically had a specified yield stress ranging from 227-275MPa. Site sampling of reinforcement from this period determined that a 5^{th} percentile value of 15-20% higher than the specified value can be expected (Chapman, 1991). Currently plain round reinforcement is available with a 300MPa specified yield stress, this is expected to provide a reasonable representation of the reinforcement used in the pre-1970's period.

4.3 Experimental Set-up

Quasi-static uni-directional in-plane testing was performed on W1, with the wall acting as a cantilever and a constant axial load applied. The experimental set-up for W1 is shown in **Figure 4-3**. This shows the configuration and set-up of reaction frames, hydraulic actuators and the post-tensioning system used to apply a constant axial load throughout the test.

Lateral loading was applied by a horizontal actuator with a capacity of 250kN. The applied lateral loading was displacement controlled, with the applied load measured by a load cell attached to the actuator and the displacement measured by a rotary potentiometer. As this was a uni-directional test any out of plane movement of the wall was restricted by steel channels which spanned between two reaction towers and passed down the sides of the loading beam of W1 (see **Figure 4-3**). The steel channels provided a low friction surface for the loading beam to slide against should they come into contact.

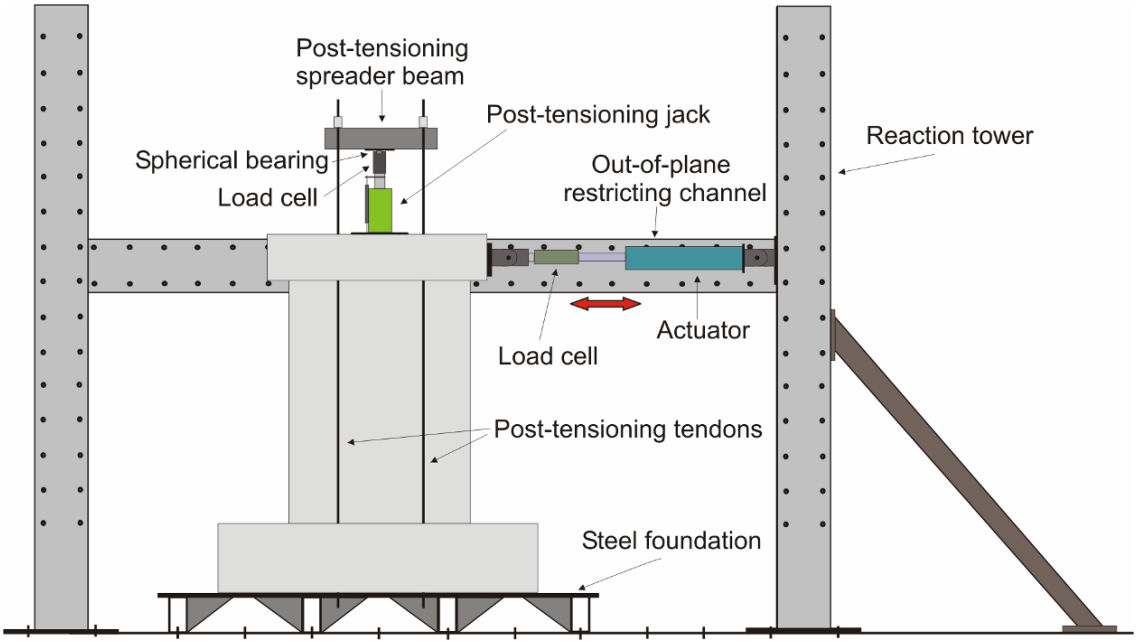

Figure 4-3: W1 experimental set-up

A constant 150kN axial load (axial load ratio = 0.047) was applied to W1 throughout the test. The axial load was applied by four 7-wire strand post-tensioning tendons (f_y=1560MPa), two on each side of the wall. The tendons passed through ducts cast into the foundation and loading beams and externally down the sides of the wall panel. To allow access to the tendons on the underside of the wall foundation the wall was placed on a raised steel foundation. At the top of the wall the tendons were attached to a spreader beam which allowed the four tendons to be loaded simultaneously by a centrally located computer controlled post-tensioning jack. A spherical bearing was used to connect the spreader beam to the post-tensioning jack to ensure that each of the tendons was equally loaded. The use of a controllable post-tensioning jack allowed the post-tensioning (axial) force to remain constant even as the wall was laterally loaded, by cancelling out any elongation of the tendons. Details of the post-tensioning system are shown in **Figure 4-3**.

4.4 Instrumentation Layout

A combination of linear and rotary potentiometers, load cells and strain gauges were used to monitor the behaviour of W1. Linear potentiometers with 30mm travel (±15mm) were used to monitor shear and flexural deformations, determine the neutral axis position, and sliding of the wall at the foundation interface. Three rotary potentiometers were distributed evenly up

the height of the wall to determine the displacement profile of the wall. **Figure 4-4** shows the potentiometers configuration on W1.

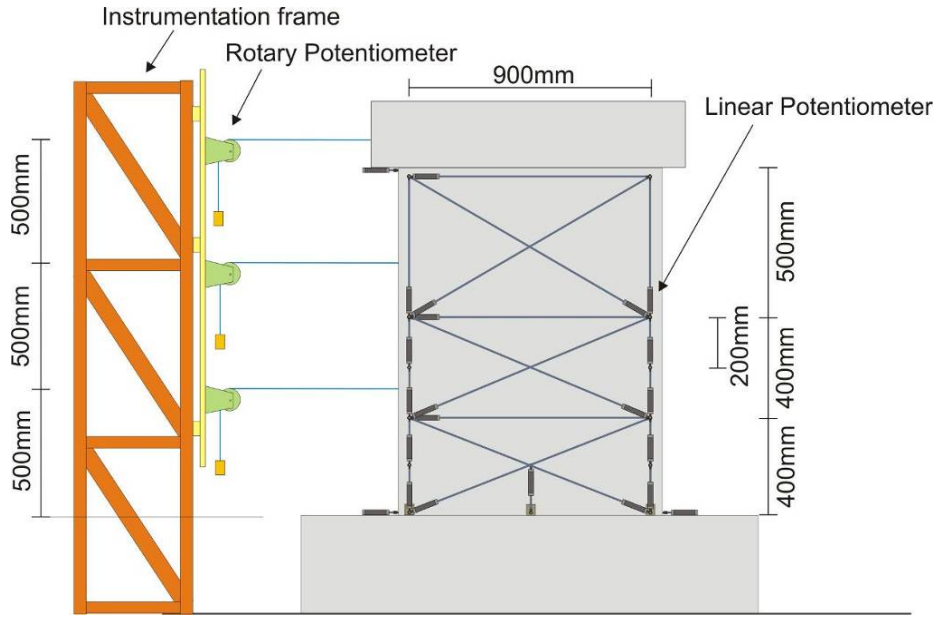

Figure 4-4: Potentiometer layout for W1

Strain gauges were used on selected longitudinal reinforcing bars to monitor the performance of the lap splice and the strain profile across the wall. Selected transverse reinforcing bars were also strain gauged. **Figure 4-5** shows the position of the strain gauges on the longitudinal and transverse reinforcement for W1.

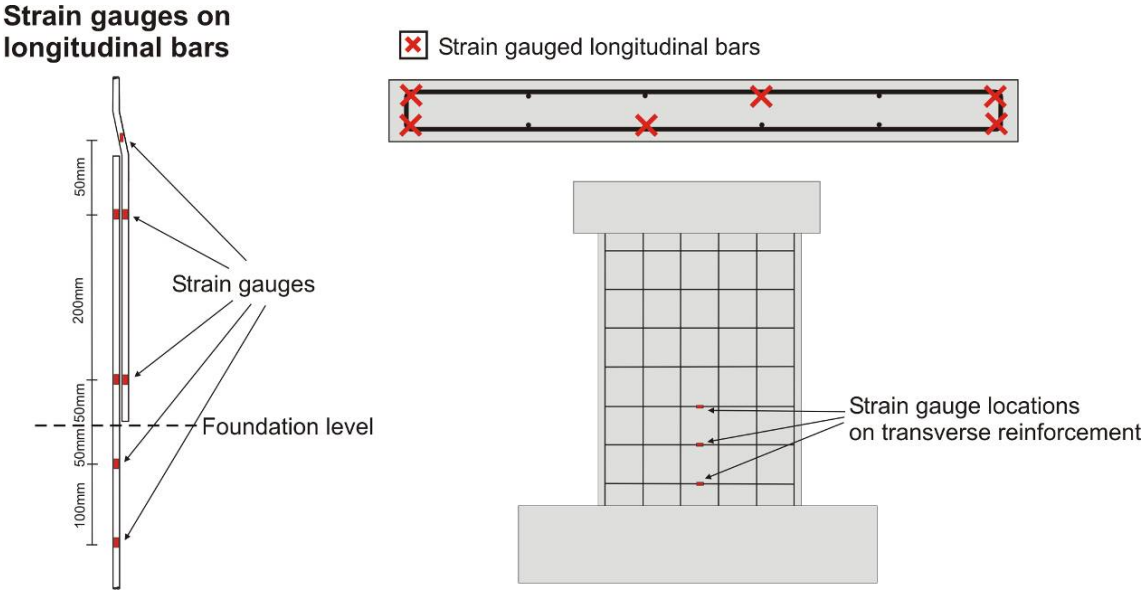

Figure 4-5: Strain gauge locations for W1

Strain gauges were placed at equal heights on the foundation starter bars and the wall longitudinal reinforcement to monitor the performance of the lap splice. The strains at corresponding locations on the foundation and wall reinforcement could be compared to see if the strain was being transferred across the lap slice. The majority of the strain gauges were located on the longitudinal reinforcement at the ends of the wall. However selected centrally located longitudinal bars were also strain gauged. This allowed the strain profile across the wall length to be monitored. Three strain gauges were also located on the transverse reinforcement to monitor any strain development due to potential shear deformation of the wall.

4.5 Load Regime

A displacement based lateral loading history was used for W1 and it is shown in **Figure 4-6**. The loading history was used to control the displacement applied by the horizontal actuator to the top of the wall. The load history consisted of cyclically increasing displacements which corresponded to drift limits which could be expected for structural walls buildings. The loading was based on drift limits instead of ductility limits to allow easy comparison of the behaviour with future tests and the incorporation with a performance based design approach. Two complete cycles were used at each drift level, this was reduced from the ACI recommended three cycle loading regime (ACI T1.1-01, 2001) which is typically for assessing the performance of "new" structures. As this was an assessment and retrofit project it was thought that the three cycle regime was too demanding for the assessment of existing structures. A peak drift of 3.0% was used for the load history of W1.

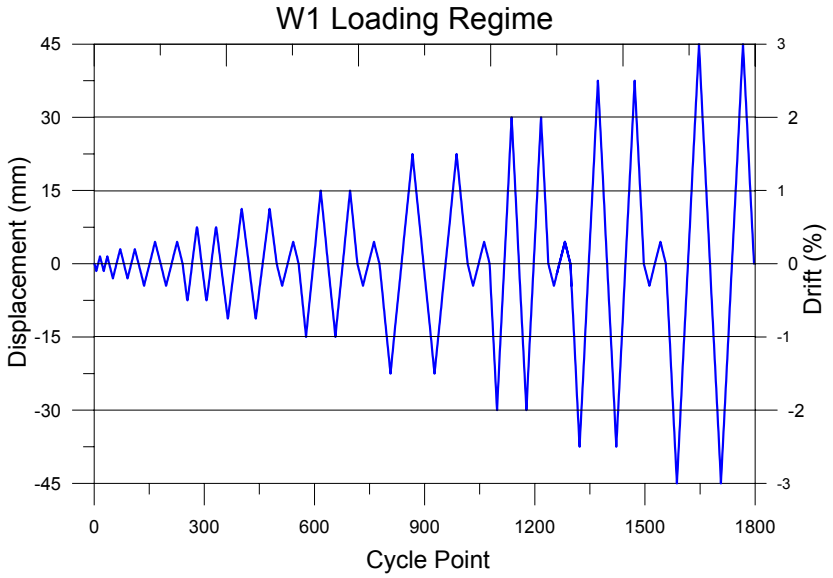

Figure 4-6: W1 Loading regime

4.6 Construction & Material Testing

W1 was constructed in two stages. Firstly the foundation block was prepared with starter bars 320mm (40 bar diameters) in length protruding to form the wall lap splice. The footprint area where the wall was to be formed was deliberately roughened to ensure that the construction joint did not provide a plane of weakness. The second stage of construction involved the erection of the wall and loading beam. The reinforcing cage for the wall & loading beam was constructed and then lifted on to the foundation block. The longitudinal wall reinforcement was spliced to the stater bars left protruding from the foundation block. Once the wall reinforcing cage was in place the wall and loading beam were cast vertically in a single concrete pour. **Figure 4-7** shows W1 during the construction phase.

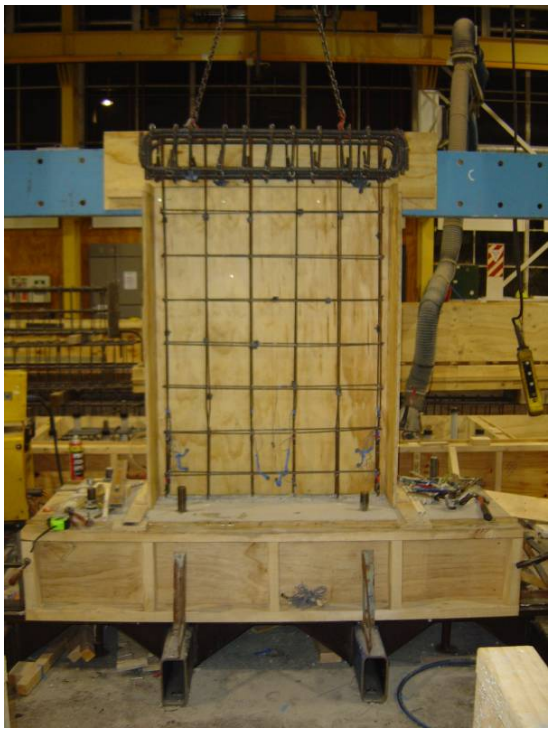

Figure 4-7: W1 under construction

Reinforcing Steel Properties

Tension tests were performed on samples of the longitudinal and transverse reinforcing steel to accurately determine the stress versus strain properties which are summarised in **Table 4-1**. In W1 R8 was used for the longitudinal reinforcement and R6 was used for the transverse reinforcement.

Table 4-1: W1, average reinforcement stress versus strain properties

Reinforcement	Bar size	f_y (MPa)	f_u (MPa)	ε_u
Transverse	R6	376	460	0.187
Longitudinal	R8	316	415	0.186

Concrete Cylinder Tests

Concrete cylinder tests were used to determine the concrete compressive strength of the concrete used in the wall at 28 days after casting and on test day. The results are summarised in **Table 4-2**.

Table 4-2: W1, average concrete cylinder strengths

Age	f'_c
28 day	34 MPa
Test day (100 day)	38 MPa

4.7 Force versus Displacement Predictions – W1

The force versus displacement response for W1 was predicted using standard hand calculation section analysis methods and by using section analysis program Response-2000 (Bentz, 2001). Response 2000 is a section analysis program which uses a modified compression field theory. The nominal section capacity was calculated assuming an ultimate concrete strain limit of ε_c=0.005, which represents the strain limit for unconfined concrete. A longitudinal reinforcing steel yield stress of 316MPa was used, which was the average steel yield stress from tested samples and a concrete compressive stress of 38MPa was used, which was the average measured test day cylinder strength.

The calculations determined the results in terms of moment versus curvature. These values were then used to determine the force versus displacement response. The yield curvature was estimated from a standard section analysis (ε_y=0.016). To calculate the peak displacement a plastic hinge length was required, an estimate of the plastic hinge length was found from Equation 4-1 (Priestley and Amaris, 2002), this was required to determine the plastic displacement contribution.

$$l_p = 0.2l_w + 0.03h_n \qquad \textbf{Equation 4-1}$$

Where l_w is the wall length and h_n is the wall height.

Figure 4-8 shows the force versus displacement backbone predictions from the two calculation methods discussed above. Comparing the resulting force versus displacement backbone curves it can be seen Response-2000 predicts a higher ultimate strength than the hand calculation method. This is likely due to Response 2000 accounting for the effects of strain hardening. A clearly defined yield point is not shown in the Response 2000 prediction as it is shown in the hand calculation method, this results in the hand method predicting a

higher initial stiffness. For both calculation methods the peak displacement at ε_c=0.005 corresponded to approximately 1.3% drift. This peak displacement calculation was highly dependent on the estimated plastic hinge zone length. For design purposes the peak allowable response would be governed by member ductility limits. The max allowable displacement ductility for a structural wall is 5 according to NZS3101:2006 (SNZ, 2006). For the hand calculation method a displacement ductility of 13.7 is calculated, meaning that the codified ductility limit would govern the allowable displacement. A ductility limit of 5 for W1 according to the hand method of calculation corresponds to a displacement of 7.5mm or a drift of 0.5%.

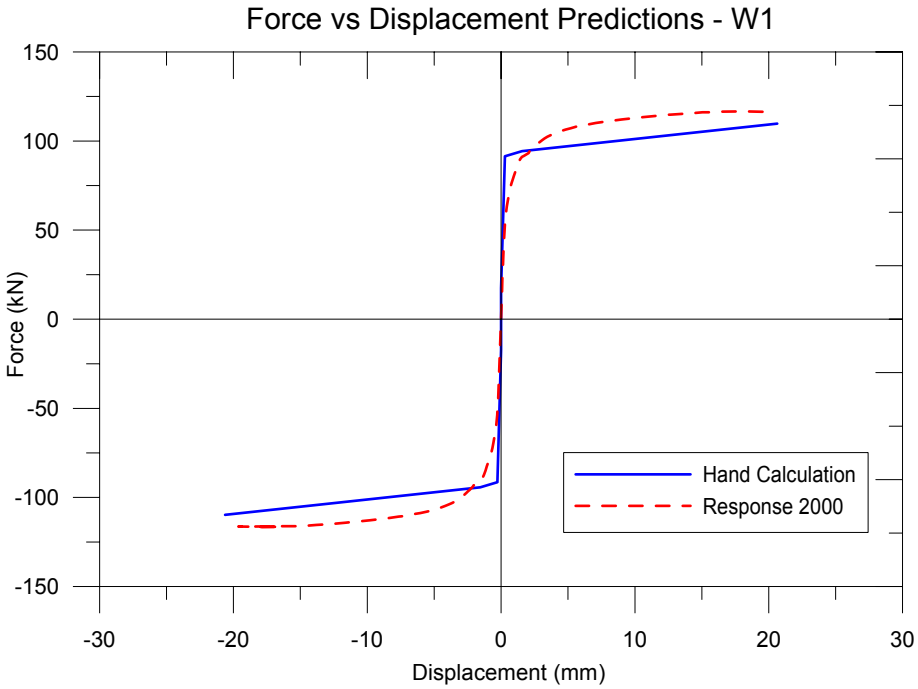

Figure 4-8: Force versus Displacement prediction for W1

4.8 Damage Observations – W1

Observations made during and post-testing on W1 are discussed in this section. Damage observations and instrumental data were used to draw conclusions about the wall behaviour.

4.8.1 Test Observations

Observations made during the testing of W1 are presented here. As an overview **Figure 4-9** shows W1 at its peak drift cycle of 3.0%. It can be seen that damage was limited to spalling at the wall corners and a single crack opening along the wall to foundation interface. The

opening of a single crack at the critical plane is quite typical behaviour for concrete sections reinforced with plain round bars.

Figure 4-9: W1 at peak drift of 3.0%

Notable damage observations made during the testing of W1 and the drift cycle at which they occurred are discussed in the following bullet points:

- 0.1% drift cycles, first hairline cracking appears at the wall to foundation interface near the ends of the wall.
- 0.2% drift cycles, crack along the wall to foundation interface extends across the full length of the wall.
- 0.3% drift cycles, cracking is still limited to a single crack at the wall to foundation interface.
- 0.5% drift cycles, wall is rocking on a single crack (gap) opening at the wall to foundation interface.
- 0.75% drift cycles, first signs of micro cracking evident at both ends of the wall, due either to concrete crushing or longitudinal reinforcement buckling.
- 1.0% drift cycles, extensive cracking developing at the wall corners, still only a single crack along the wall to foundation interface.

- 1.5% drift cycles, spalling of concrete at wall corners exposing buckled longitudinal reinforcement.
- 2.0% drift cycles, evidence of the longitudinal reinforcement lap splice providing sufficient capacity was observed by watching the longitudinal reinforcement buckle when in compression, then straighten out and yield in tension as the wall loading changed direction. Significant sliding of the wall along the horizontal crack at the wall to foundation interface was observed.
- 2.5% drift cycles, longitudinal reinforcement at one end of the wall ruptured in either tension or small cycle fatigue from repeated buckling and stretching. Substantial sliding of the wall along the horizontal crack at the wall to foundation interface was observed.
- 3.0% drift cycles, further rupture or failure of reinforcement at the other end of the wall. Only a single crack formed along the wall to foundation interface on which significant sliding of the wall panel was observed (in excess of 5mm).

Damage to W1 was limited to a single crack opening along the wall to foundation interface, spalling of cover concrete at the wall corners as well as buckling and rupture of longitudinal reinforcement at the wall ends. **Figure 4-10** show the spalling at one corner due to buckling of the longitudinal reinforcement. This occurred due to the large spacing of the transverse reinforcement. First cracking in the corner regions was observed on the 0.75% drift cycles and during the 1.5% drift cycles spalling occurred in the corner regions exposing the buckled longitudinal reinforcement.

Figure 4-10: Crushing in the toe region and longitudinal reinforcement buckling in W1

An example of the longitudinal reinforcement at the end of the wall rupturing in tension is shown in **Figure 4-11 (a)** and an example of the longitudinal reinforcement failing due to low cycle fatigue is shown in **Figure 4-11 (b)**. The first longitudinal bar failure occurred during the 2.5% drift cycles.

(a) (b)

Figure 4-11: (a) Longitudinal reinforcement failure in tension; (b) Longitudinal reinforcement failure due to low cycle fatigue.

4.8.2 Post Testing Damage Observations

Post testing damage observations were made after testing was complete and once the wall had been removed from the foundation block. **Figure 4-12** shows three starter bars that formed

the lap splice left protruding from the foundation block once the wall had been removed. This provides evidence that the lap splice could fail before the reinforcement ruptures. Only three starter bars were remaining, but others had been cut to allow the removal of the wall element or had ruptured during testing. It can be clearly seen that the lap provided sufficient capacity to allow the reinforcement in this wall to yield significantly. This can be seen by the variation in length of the starter bars left protruding from the foundation (they were the same length at the time of construction). The majority of this elongation from yielding did not occur during the test but occurred as the wall was removed from the foundation.

In no circumstance should the information gathered from this single test be used to conclude that a 40 bar diameter lap splice with plain round reinforcement provides sufficient strength to allow development of the full flexural capacity of a wall. The longitudinal reinforcement used in W1 had a high level of surface corrosion which would increase the bond capacity. It was also observed that the ends of the reinforcing bars were flared where it had been cut by a guillotine, this would further increase the capacity of the lap detail.

Figure 4-12: Starter bars left protruding from W1 foundation block once the wall had been removed

Figure 4-12 also shows how the starter bars have been deformed in shear at the wall to foundation interface. This was a result of dowel action as the wall attempted to slide on the crack interface that developed at the wall to foundation interface. It can also be seen that the single crack did not occur entirely along the construction joint at the wall to foundation interface.

4.9 Results & Analyses

This section discusses results and analyses of information gathered from the instrumentation attached to W1. This includes the force versus displacement response, axial load, neutral axis location, percentage of total wall displacement associated to rotation at the wall base and equivalent viscous damping.

4.9.1 Force versus Displacement Response

The force versus displacement response for W1 is shown in **Figure 4-13**. The hysteretic behaviour shows significant strength degradation occurred after the 1.5% drift cycles in both loading directions. A substantial level of pinching of the hysteresis was also evident, which is a common characteristic of reinforced concrete elements with plain round bars. Pinching of the hysteretic response is also a result of sliding of the wall along the crack that formed at the wall to foundation interface.

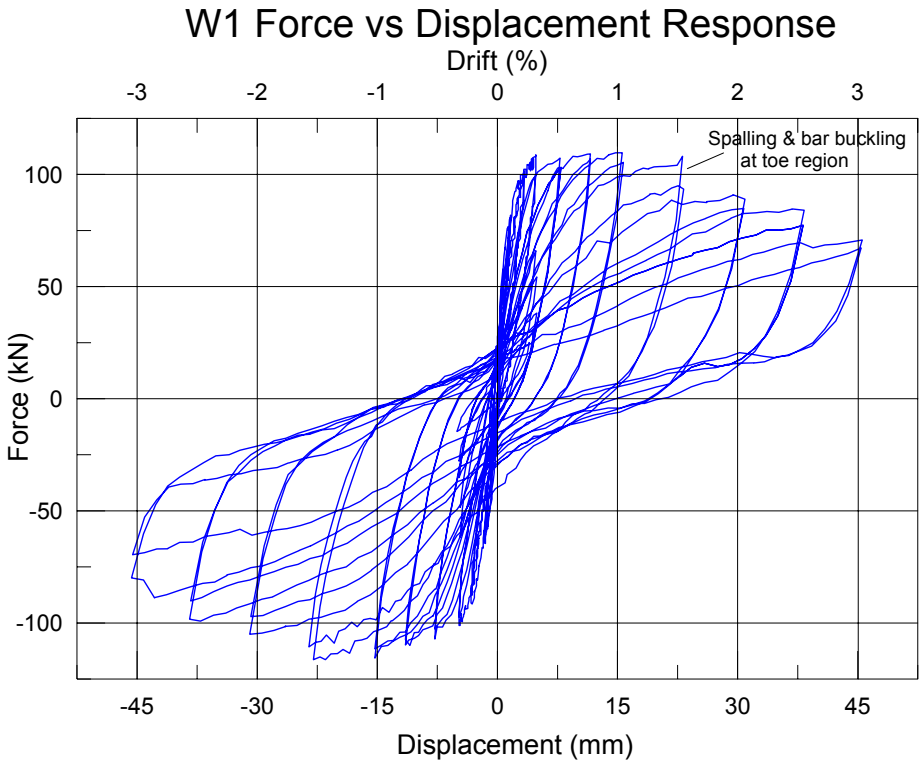

Figure 4-13: W1 force versus displacement response

4.9.2 Axial Load

Figure 4-14 shows the axial load versus lateral drift response for W1. The load was measured by the load cell on top of the post-tensioning jack, with the load equalling of the sum of the

forces in the four post-tensioning tendons. The post-tensioning, used to simulate an axial load remained relatively constant at 150kN for the duration of the test as was desired.

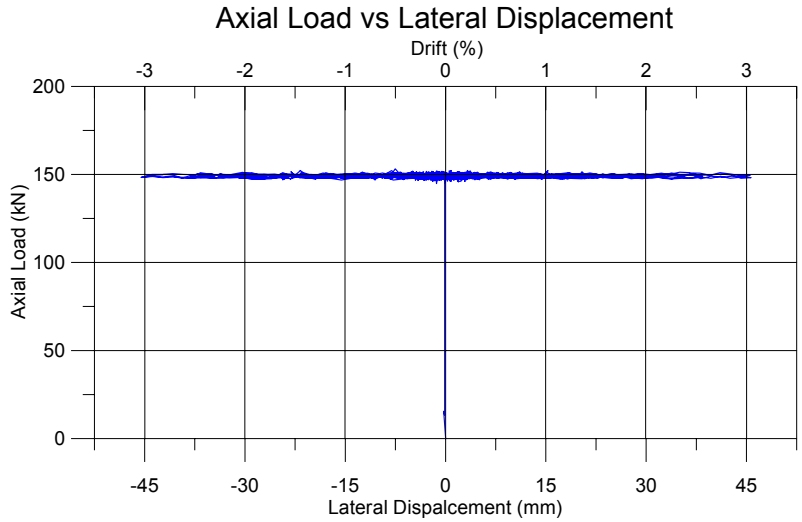

Figure 4-14: W1 post-tensioning load versus lateral displacement

4.9.3 Vertical Displacement at base of Wall & Base Rotation

The vertical elongation of linear potentiometers at the base of the wall as it was laterally loaded in the negative and positive directions were used to determine the neutral axis location and the percentage of the total displacement relating to the rotation at the base of the wall. The linear potentiometers crossed the critical plane and extended from the foundation block to a height of 200mm up the wall. The neutral axis and base rotation were determined at drift cycles up to 1.5% drift, the potentiometers were then removed at this point to avoid damaging to them. **Figure 4-15** and **Figure 4-16** show the extension of the linear potentiometers crossing the critical plane at the base of the wall versus their position along the length of the wall at the peak negative and positive drift cycles respectively. The line between the two data points was extrapolated to determine the neutral axis position. Between the 0.5-1.5% negative drift cycles the neutral axis location varied between 150-185mm, this equates to 0.15-0.185 of the of the wall length. The slope of the line equals the rotation at the base of the wall, between the 0.5-1.5% negative drift cycles the rotation at the base of the wall accounted for between 80-90% of the total wall displacement. The remaining proportion of the displacement would result form flexural deformation of the wall panel above the base section, shear deformation and sliding. **Figure 4-16** shows the potentiometer elongation at the bas of the wall for the positive drift cycles. Between 0.5%-1.5% positive drift cycles the neutral axis position ranged between 25-250mm, this equated to 0.025-0.25 of the wall length. The base

rotation in the positive direction accounted for between 70%-85% of the total displacement of the wall.

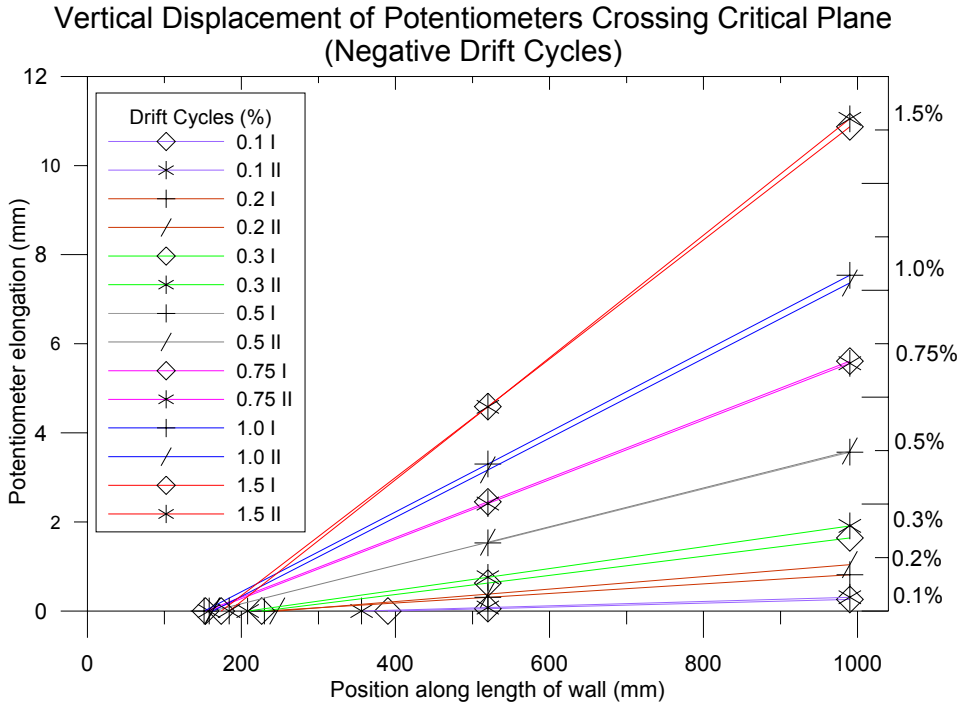

Figure 4-15: Elongation of potentiometers crossing the critical plane for the negative drift cycles.

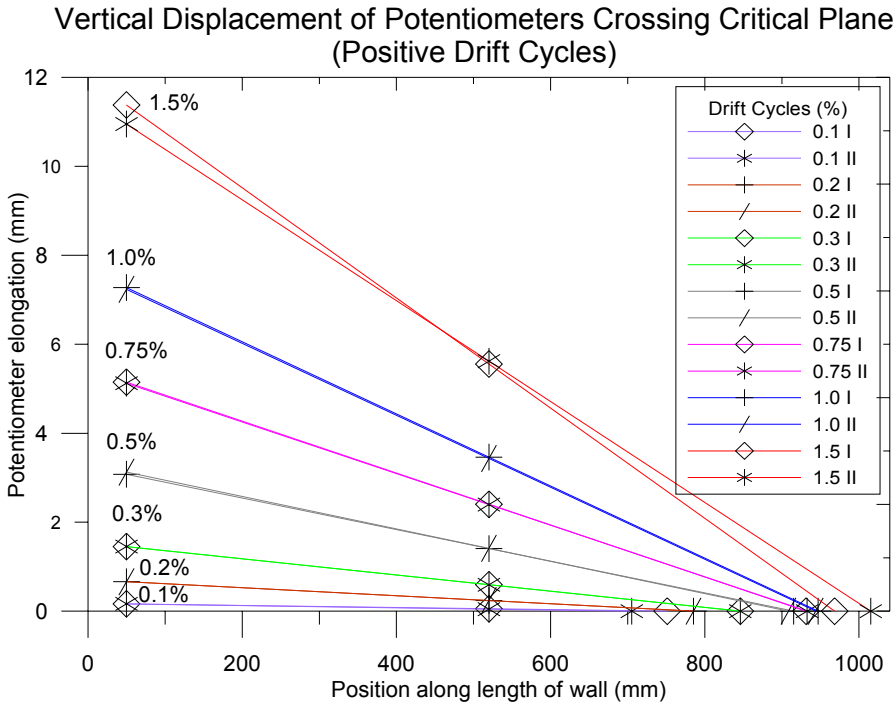

Figure 4-16: Elongation of potentiometers crossing the critical plane for the positive drift cycles]

Figure 4-17 shows the average c/d versus lateral drift for W1 (d=980mm) for the negative and positive loading direction of W1. The expected basic form of a c/d versus lateral drift was observed, with a general reduction in the c/d ratio as the lateral drift increases. The response was not quite symmetric which could be due to slight variations in the wall construction and the behaviour as the wall was laterally loaded in each direction. For the negative drift cycle an asymptote can be observed at approximately 0.15 c/d. After 1.0% drift a slight increase in the c/d ratio was observed, this is likely due to the crushing and bar buckling observed at the toe region of the wall. For the positive loading direction the c/d ratio reaches a minimum of 0.07, but the data is insufficient to define an asymptote.

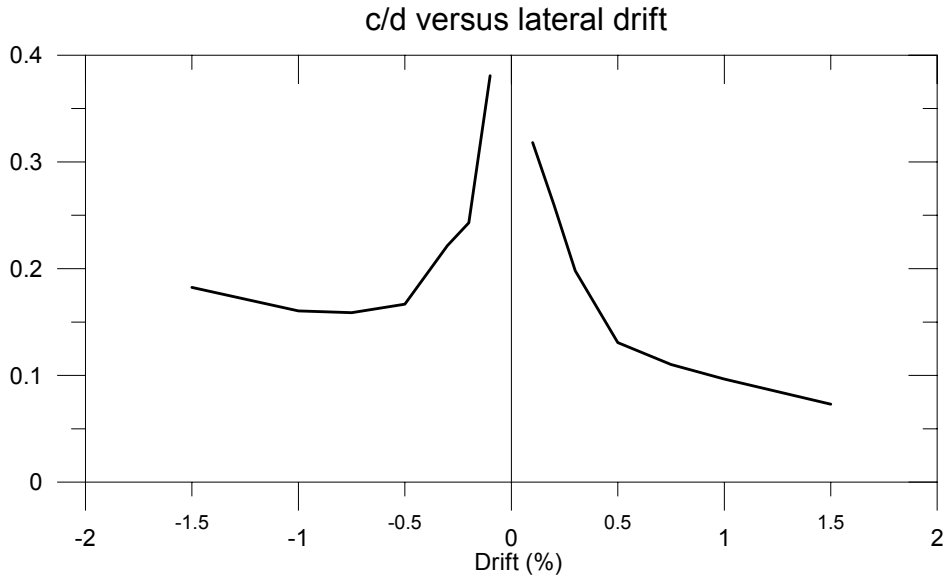

Figure 4-17: Average c/d versus lateral drift for W1

4.9.4 Equivalent Viscous Damping

The percentage equivalent viscous damping for W1 was calculated at the peak of the first and second cycle at each drift level, between 0.5-3.0%. **Figure 4-18** shows the percentage of equivalent viscous damping versus drift for W1 at each peak, the method used to calculate the percentage equivalent viscous damping can be found in Appendix C. It is typical to discuss the percentage equivalent viscous damping provided by an element in terms of the second cycle to each drift level, as the hysteretic response would have stabilised (un-conservative to consider first cycle to each drift level). The equivalent viscous damping for the first cycle to each drift level is shown so that the reduction in equivalent viscous damping can be seen as the hysteresis stabilises. For the second cycle, a peak equivalent viscous damping level of

24% was achieved on the 1.5% drift cycle. After the 1.5% drift cycle there is a significant reduction in the equivalent viscous damping which was related to the strength degradation observed in the force versus displacement response shown in **Figure 4-13**. For comparison the percentage equivalent viscous damping as predicted by an equation for a monolithic wall (Priestley, 2003) is shown. This equation (see section 10.3.5) is a function of ductility, for this calculation a yield drift of 0.3% was assumed.

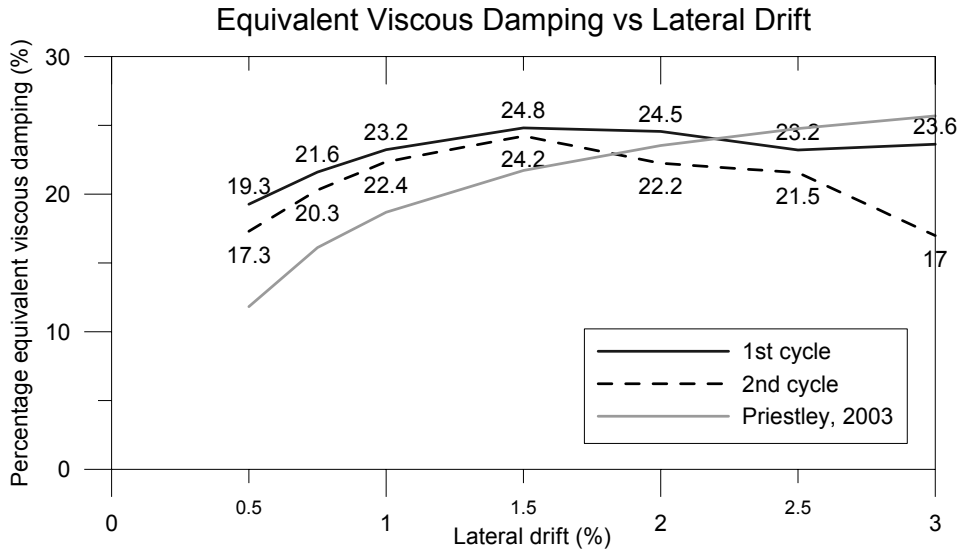

Figure 4-18: Equivalent viscous damping versus drift for W1

4.10 Predicted versus Experimental Response

Comparison between the predicted force versus displacement backbone curves (calculated in section 4.6 using hand method of analysis and Response-2000 (Bentz, 2001)) and the experimental force versus displacement response is shown in **Figure 4-19**. The original response prediction was slightly modified by changing the assumption of the plastic hinge length. The plastic hinge length was changed based on observed experimental response. It was seen that a plastic hinge did not develop, only a single crack opened at the wall to foundation interface. An equivalent plastic hinge length was back calculated form experimental data which showed a plastic hinge length of between 0.10-0.15m. Therefore an average plastic hinge length of 0.10m was used in these calculations instead of 0.23m as calculated by Equation 4-1 in section 4.6.

From **Figure 4-19** it can be seen that the hand calculation provides a good estimate of the peak section strength. The peak strength occurs at approximately 1.0% drift after the plastic

hinge length was changed to match that determined from experimental results. It can be seen that the initial stiffness is substantially overestimated especially in the negative drift cycle direction. This is due largely to the predicted cracking strength which is likely overestimated due to the approximate equations used to predict the tensile strength of the concrete.

A comparison of the experimental force versus displacement response to the backbone determined using Response-2000 (Bentz, 2001) is also shown in **Figure 4-19**. It can be seen that in the positive direction an accurate representation of the wall stiffness was achieved but that the peak strength was slightly overestimated. In the negative loading direction the stiffness was slightly overestimated but the peak force matched well. A limitation of Response-2000 for the assessment of existing walls is that it cannot account for the use of plain round bars.

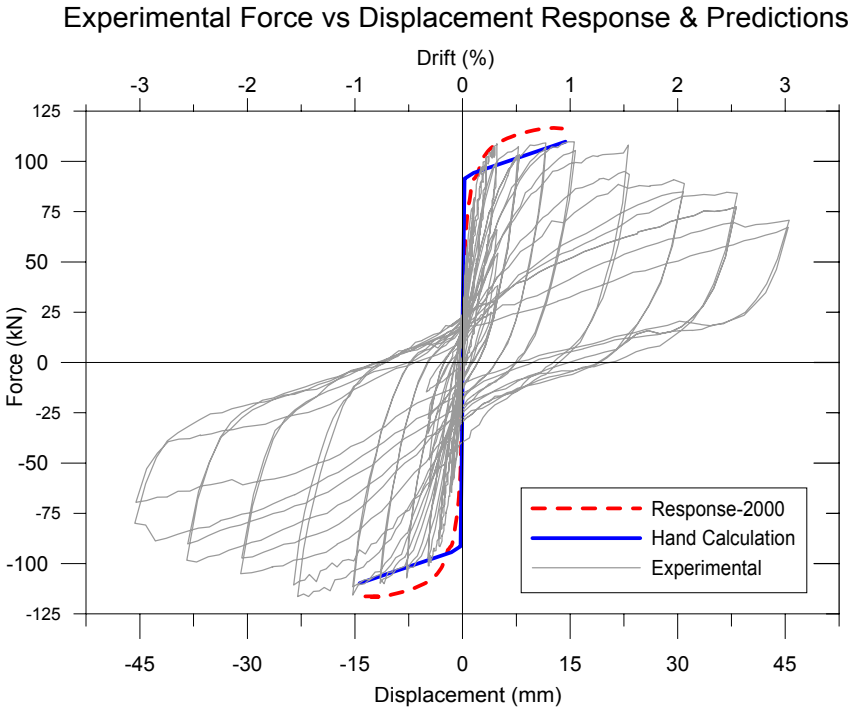

Figure 4-19: Predicted and experimental force versus displacement response, W1

References:

ACI T1.1-01, [2001], "Acceptance Criteria for Moment Frames Based on Structural Testing", ACI Standard, Reported by ACI Innovation Task Group 1 and Collaborators.

Bentz, E., [2001]. "Response-2000 User Manual". Department of Civil Engineering, University of Toronto, Canada.

Brunsdon, R.D., [1984]. “Seismic Performance Characteristics of Buildings Constructed Between 1936 & 1975”. Research Report 84-14, Department of Civil Engineering, University of Canterbury, Christchurch, New Zealand.

Chapman, H.E., [1991]. “Seismic Retrofitting of Highway Bridges”. Bulletin of New Zealand Society for Earthquake Engineering 24(2), 186-201pp.

NZSEE, [2005], “The Assessment and Improvement of the Structural Performance of Building in Earthquake”. Study group draft, October 2005.

Pinho, R, [2000], “Shaking Table Testing of RC Walls”, ISET Journal of Earthquake Technology, paper No. 45, Vol 37, No 4, December 2000, pp. 119-142

Priestley, M.J.N., [2003], “Myths and Fallacies in Earthquake Engineering, Revisited”, IUSS Press, Pavia, Italy.

Preistley, M.J.N., and Amaris, A.D. [2002] “Dynamic Amplification of Seismic Moments and Shear Forces in Cantilever Walls” Report No. Rose 2002/01, European School for Advanced Studies in Reduction of Seismic Risk, Pavia, 86pp.

SNZ. [2006]. Concrete Structures Standard NZS3101:2006, Volume 1 code of practice. Standards New Zealand, Wellington.

5 W2 – Shear Dominated Wall

5.1 Introduction

W2 was designed to be governed by a shear dominated inelastic mechanism. The purpose of this was to provide a severe scenario as a benchmark specimen for the selective weakening retrofit technique being developed. The development, testing and results for W2 are discussed in this Chapter.

5.2 Development of W2

W2 was designed to represent a scenario where the behaviour was dominated by a shear failure. In reinforced concrete seismic design shear dominated failure modes are avoided due to non-ductile response. A shear dominated failure might not be expected as typical behaviour of pre-1970's structural walls in New Zealand, but it has been observed in countries such as Turkey after seismic events. However in section 2.3.2 common deficiencies of existing New Zealand structural walls were discussed (as determined form previous research) and it was suggested that before the introduction of capacity design principles the contribution to the flexural capacity from the boundary element longitudinal reinforcement may have been neglected (considered as providing a conservative estimate of the flexural capacity). If this was the case a shear dominated inelastic mechanism may form. The shear dominated wall (W2) was created to act as a benchmark specimen for a selective weakening retrofit intervention to be performed later in the experimental program. The development of W2 in terms of geometry, reinforcement detailing and material properties is discussed in the following sections.

5.2.1 Experimental Specimen Geometry

The geometry of W2 was generally kept consistent with that used for W1 except for modifications to the wall thickness, foundation beam length and loading beam depth. Decisions regarding the geometry used for W1 are discussed in Section 5.2. An attempt to keep the geometry consistent with W1 was to ensure relative comparisons could be made between experimental specimens and for convenience relating to test rig compatibility. The most significant change between W1 and W2 was the wall panel thickness, this was reduced to 100mm (instead of 125mm for W1). This was to reduce the shear strength of the wall, as a

shear failure was being designed for. Cross sectional geometry significantly affects the shear strength, therefore to minimise the required flexural strength to cause shear failure the wall thickness was reduced accordingly. The strength of W2 needed to be minimised as it was approaching the capacity of the test rig. The main geometric details of W2 are shown in **Figure 5-1**.

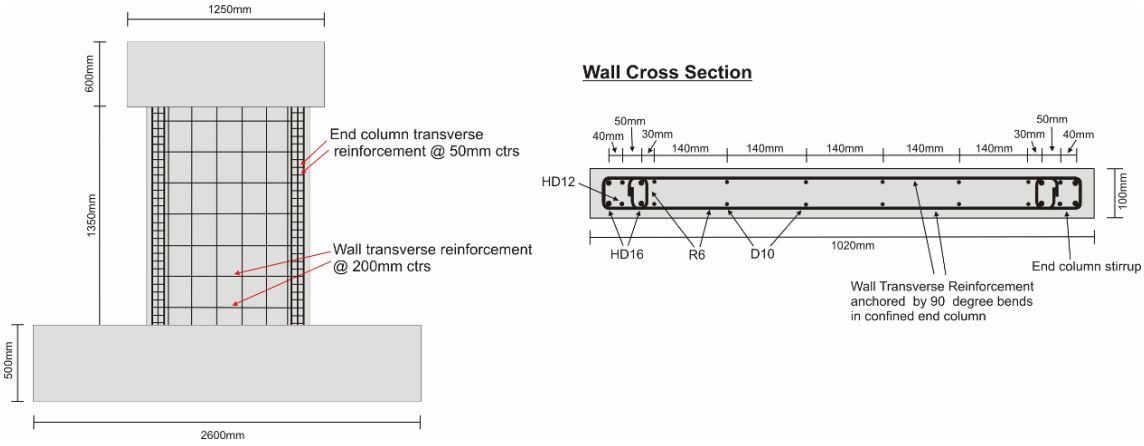

Figure 5-1: W2 reinforcement detailing and geometry

The size of the foundation and loading beams for W2 were increased in comparison to W1 to account for the increase in flexural strength. The length of the foundation block was increased to provide more anchorage points to the strong floor. This was required due to the high forces expected to develop within W2. The depth of the loading beam was increased due to geometric constraints relating to the steel channels used restrict out of plane movement and the 1000kN actuator. The 1000kN hydraulic actuator could not fit in between the steel channels restricting out of plane movement, as was the case in W1. Therefore the loading beam depth was increased to allow the actuator to be mounted at a height of 1.5m, with the steel channels positioned above (as shown in **Figure 5-2**).

5.2.2 Reinforcement Detailing

W2 was designed using an inverse capacity design approach, with the aim of achieving a shear dominated failure mechanism. To achieve a shear dominated failure mechanism a high flexural strength was required. Boundary element reinforcement was used within the rectangular wall cross section to provide a high flexural strength. The boundary elements were formed within the first 150mm from each end and consisted of 4 HD 16 and 2 HD 12 reinforcing bars. Confinement and anti- buckling resistance was provided to the end columns by a small hoop stirrup at 50mm centres. In the region between the boundary elements

minimal reinforcement was used, this consisted of two layers of D10 reinforcing bars at 140mm centres for the longitudinal reinforcement and two layers of R6 at 200mm spacing for the transverse reinforcement. The wall transverse reinforcement was anchored by 90 degree bends within the confined boundary elements. No lap splice was used in the longitudinal reinforcement as the purpose of this test was to achieve a shear dominated failure mode to act as a benchmark specimen, not to investigate lap splice behaviour. The reinforcement details of W2 are shown in **Figure 5-1**.

5.2.3 Material Properties

A combination of grade 300 and grade 500 deformed reinforcing bars were used within W2. Grade 500 steel was used in the boundary elements regions to achieve the required high flexural strength within the small cross sectional dimensions. Grade 300 deformed bar was used for the longitudinal reinforcement in the central section of the wall and grade 300 plain round bars were used for all transverse reinforcement.

Concrete with a specified 28 day compressive strength of 20MPa was used for W2. A relatively low strength concrete was used to minimise the concrete contribution to the shear capacity to help achieve the desired shear dominated failure mechanism. Due to the high density of reinforcement the aggregate size was reduced to 7mm.

5.3 Experimental Set-up

The test set-up used for W2 allowed for quasi-static in-plane uni-directional testing to be performed and is shown in **Figure 5-2**. The wall was loaded as a cantilever and had a constant axial load applied throughout the test. This was similar to that used for W1 which was discussed in section 4.3, except that the capacity of the horizontal hydraulic actuator was increased to 1000kN.

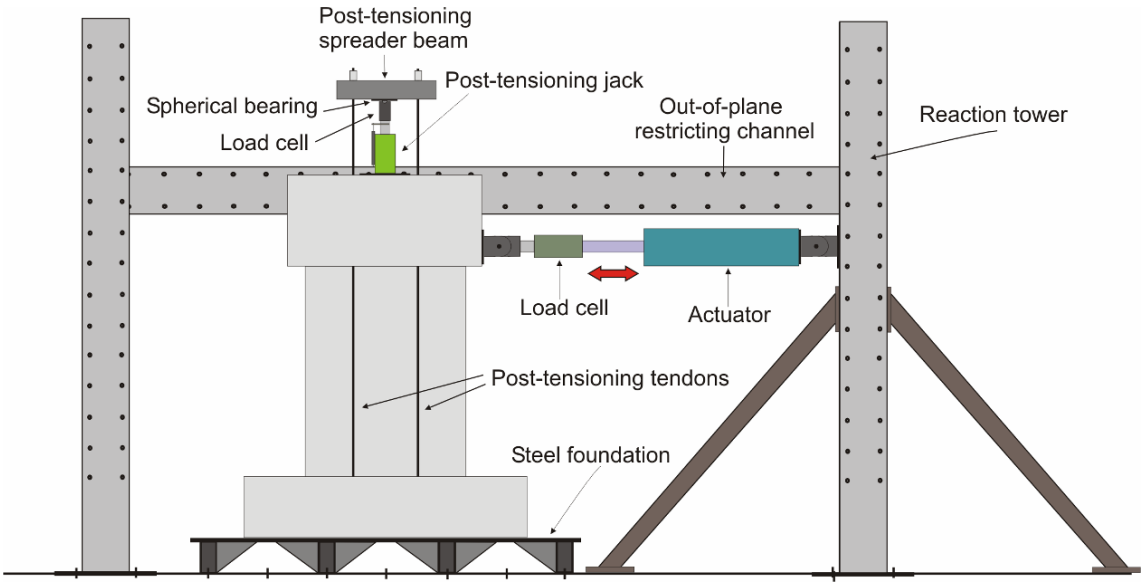

Figure 5-2: W2 experimental set-up

A displacement controlled lateral load was applied at a height of 1.5m from the base of the wall. The load was measured by a load cell attached to that actuator and the displacement was measured by a rotary potentiometer. As only uni-direction testing was being performed any out of plane movement was restricted by steel channels. The steel channels spanned between two reaction towers and passed down each side of the loading beam above the horizontal actuator as shown in **Figure 5-2**.

A constant axial load of 150kN was applied to W2 throughout the test. The axial load was applied via four 7-wire strand post-tensioning tendons (f_u=1860MPa); two on each side of the wall. The tendons passed through ducts cast into the foundation and loading beams and externally down the sides of the wall panel. To allow access to the tendons on the underside of the wall foundation, the wall was placed on a raised steel foundation. At the top of the wall the tendons were attached to a spreader beam which allowed the four tendons to be loaded simultaneously by a centrally located computer controlled post-tensioning jack. A spherical bearing was used to connect the spreader beam to the post-tensioning jack which ensured each of the tendons was loaded equally. The use of a controllable post-tensioning jack allowed the post-tensioning (axial) force to remain constant as the wall was laterally loaded, by accounting for any elongation of the tendons. Details of the post-tensioning system are shown in **Figure 5-2**.

5.4 Instrumentation Layout

A combination of linear potentiometers, rotary potentiometers, load cells and strain gauges were used to monitor the behaviour of W2. A complex array of linear and rotary potentiometers were used to monitor shear and flexural deformations and sliding of the wall and foundation block. The layout of the potentiometers is shown in **Figure 5-3**. As the wall was designed to be shear dominated an extensive array of potentiometers were used to monitor expected shear deformations. This consisted of a large diagonal configuration of 30mm linear potentiometers (±15mm) covering the entire wall panel and a more refined array consisting of three sets of diagonal potentiometers (see **Figure 5-3**). Incorporated into the shear array were a series of potentiometers which were used to monitor flexural deformations and the potential neutral axis position. Linear potentiometers were also placed to monitor sliding of the wall on the foundation interface.

Three rotary potentiometers were distributed up the height of the wall to determine the displacement profile (see **Figure 5-3**). A rotary potentiometer was also used to measure movement of the foundation block relative to the strong floor.

Two load cells were used to measure the magnitude of the lateral and axial loads applied to the wall. The location of the load cells is shown in the test set-up shown in **Figure 5-2**.

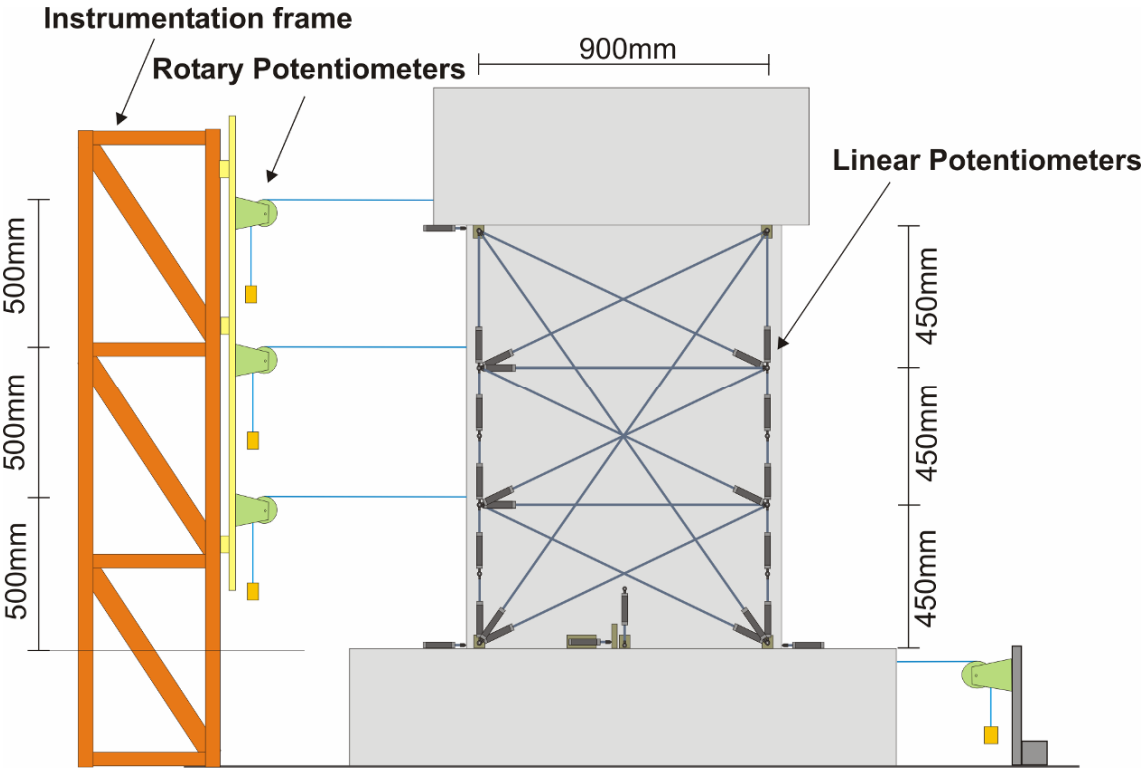

Figure 5-3: W2 potentiometer layout

Strain gauges were used in W2 to monitor strain development and strain profiles in the longitudinal and transverse reinforcement. The location of strain gauges on the longitudinal and transverse reinforcement of W2 can be seen in **Figure 5-4**. Strain gauges were placed on selected longitudinal reinforcing bars at the ends of the wall within the boundary elements and also near the centre of the wall. The strain gauges were placed at the wall to foundation interface to allow the strain profile across the wall to be monitored and to check if the longitudinal reinforcement reached yield limits. Strain gauges were also located on the transverse reinforcement up the full height of the wall on both faces. The strain gauges were located at the centre of each stirrup and were to be used to monitor the strain profile up the height of the wall.

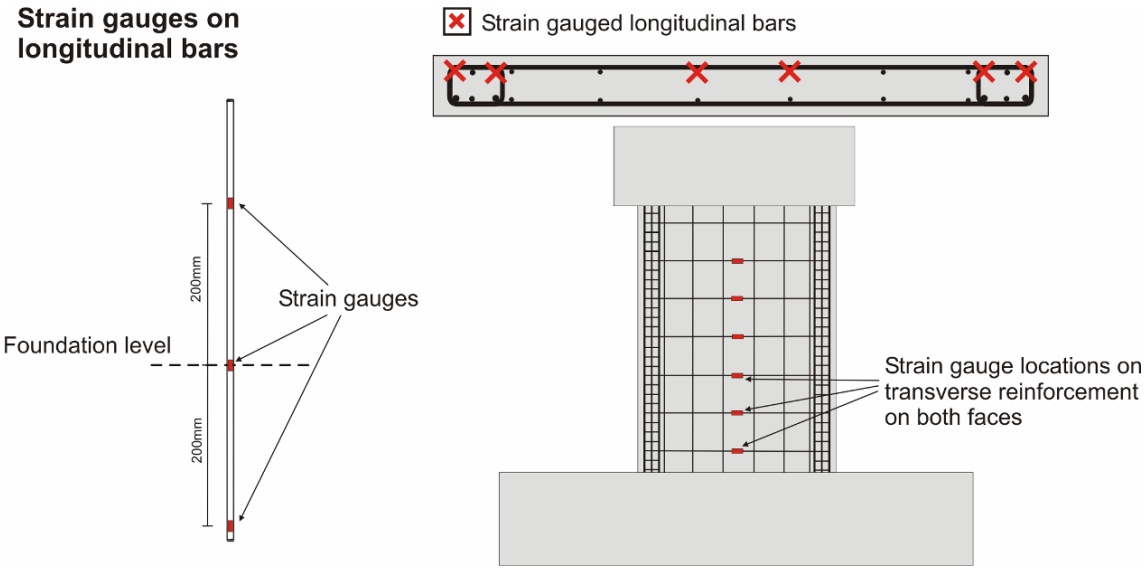

Figure 5-4: W2 strain gauge locations

5.5 Load Regime

The displacement based lateral loading regime used for W2 is shown in **Figure 5-5**. The load history was used to control the displacement applied to the wall by the horizontal actuator. It consisted of cyclically increasing drifts with two complete cycles at each drift level, up to a maximum of 2.5% drift. The peak drift was reduced to 2.5% from 3.0% which was used in W1 (section 5.5) to be in line with the NZSEE draft recommendations (NZSEE, 2005) for the peak acceptable drift for structural walls. The NZSEE draft guidelines suggest at drift limit of 2.5% if it was determined by time history analysis. The use of a displacement based load history and the use of two cycles at each drift level are discussed in section 4.5.

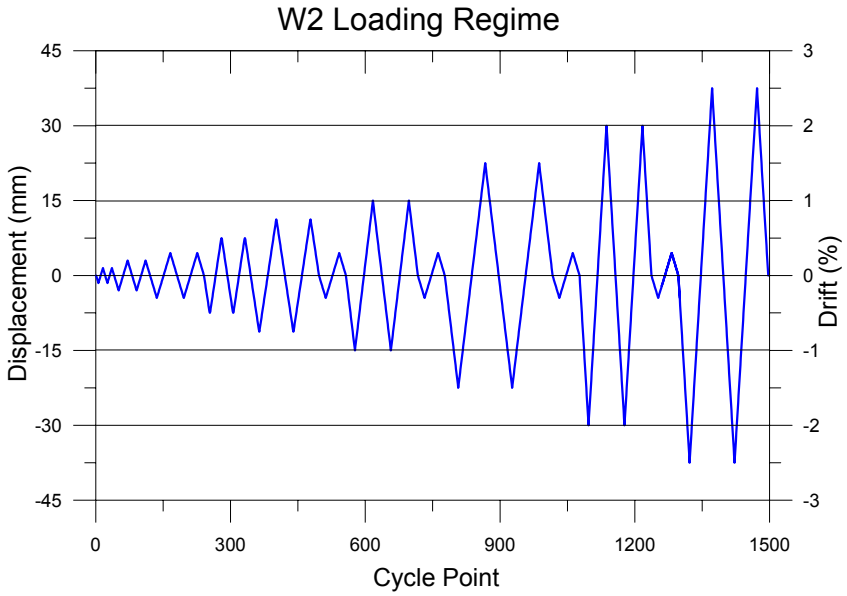

Figure 5-5: W2 loading regime

5.6 Construction & Material Testing

W2 was constructed in two phases, firstly the foundation block and then the wall and loading beam. No lap splice was used in the longitudinal reinforcement, so the foundation block was cast with the wall longitudinal reinforcement protruding. The cast foundation block with the wall and loading beam reinforcement in place is shown in **Figure 5-6**. The construction joint at the wall to foundation interface was deliberately roughened to ensure that it did not provide a plane of weakness. The wall and loading beam were cast vertically in the same pour.

Figure 5-6: W2 under construction

Reinforcing Steel Properties

Tension tests were performed on samples of the longitudinal and transverse reinforcement to accurately determine the stress versus strain characteristics. **Table 5-1** summarises the average yield stress, ultimate stress and minimum ultimate strain experienced during the material tests.

Table 5-1: Stress versus Strain properties of the reinforcement used in W2

Reinforcement	Bar size	f_y (MPa)	f_u (MPa)	$\varepsilon_{u(min)}$ (strain) x10^3
longitudinal	HD16	548	672	153
longitudinal	HD12	528	645	176
longitudinal	D10	326	449	172
transverse	R6	337	490	185

Concrete Cylinder Tests

Concrete cylinder tests were used to determine the concrete compressive strength achieved in W2. The specified concrete compressive strength was 20MPa, the average measured cylinder strength at 28 days was 24MPa. The wall was also tested 28 days after construction.

5.7 Force versus Displacement Predictions

A number of techniques were used to assess the likely behaviour of W2. Force versus displacement backbone curves were calculated assuming the wall was able to develop full flexural strength using conventional hand methods of analysis and section analysis program Response-2000 (Bentz, 2001). A shear strength envelope was calculated using the improved UCSD shear ductility model (Kowalsky and Priestley, 2000) which accounts for shear strength degradation as a function of ductility demand. The design shear strength as calculated by NZS 3101:1995 (NZS, 1995) was also used as a comparison. In an attempt to more accurately predict the behaviour a model that accounts for stiffness loss due to diagonal cracking was also implemented (Miranda et al., 2005), this model will be referred as the Miranda model in this Chapter. A strength envelope was predicted initially by the force versus displacement backbone curves of either the hand calculations, Response-2000 section analysis or the Miranda model until they intersected the shear ductility curve (improved UCSD), which then defines the remainder of the strength envelope. The predicted force versus displacement backbone curves for different methods of assessment and the shear

strength envelope are shown in **Figure 5-7**. In the predictions the average measured material properties were used. This corresponded to f'_c=24MPa, f_y=540MPa for the end column reinforced and f_y=337MPa for the transverse reinforcement.

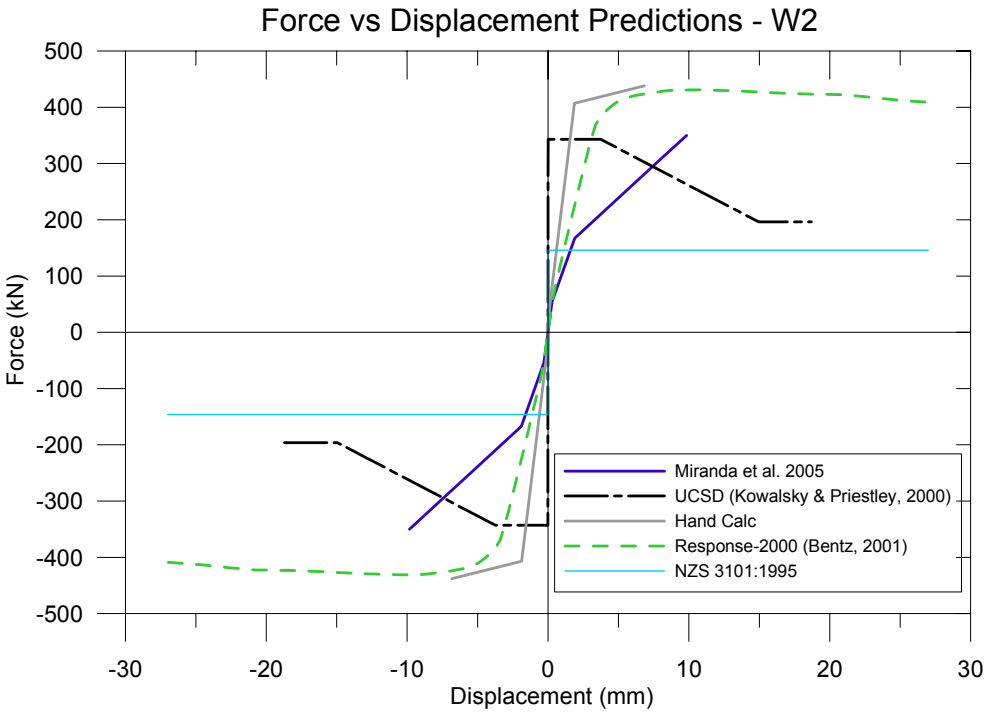

Figure 5-7: Predicted strength envelopes for W2

A predicted shear strength envelope was calculated using the improved UCSD model (Kowalsky and Priestley, 2000) and is shown in **Figure 5-7**. The model takes into account contributions to the shear strength from the concrete, reinforcing steel and axial load but also considers affects of the longitudinal reinforcement ratio and height to length aspect ratio of the element in question. The shear ductility model provides a shear strength envelope in which the shear strength from the concrete contribution degrades as the ductility demand increases. The model was used in combination with flexural backbone curves, when the flexural backbone intersected the shear ductility curve the shear ductility curve then became the strength envelope. For comparison the strength as predicted by NZS3101:1995 (NZS, 1995) was calculated and shown in **Figure 5-7**. This served to show that code design equations for shear strength are conservative for assessment purposes.

Force versus displacement responses assuming the full flexural strength could develop were calculated using conventional hand methods of analysis and by Response-2000 (Bentz, 2001). For the calculations a concrete compressive strain limit of ε_c=0.005 at nominal strength was

assumed and an average f_y of 540MPa was used for the end column reinforcement. **Figure 5-7** shows the two flexural force versus displacement curves and it can be seen that they intersect the shear ductility curve, therefore a shear failure was predicted.

In an attempt to more accurately predict the behaviour the model proposed by Miranda et al. 2005, which was developed for the assessment of columns with limited shear resistance was also used (referred to herein as the Miranda model). This Miranda model accounts for flexural deformations and incorporated stiffness loss due to diagonal shear cracking. In conventional (flexural) methods of assessment, deformations associated with shear cracking are typically neglected, which leads to conservative estimates of the displacement at which shear failure occurs but non-conservative estimates of the peak strength achieved in sections governed by a shear behaviour. This Miranda model was used in combination with the improved UCSD shear ductility curve (Kowalsky and Priestly, 2000) to define a strength envelope. The predicted force versus displacement curves using are shown in **Figure 5-7**. It was observed that there was a substantial reduction in stiffness to account for shear cracking when compared to the flexural backbone curves. This lead to a much higher predicted displacement for shear failure to occur but also results in a significant reduction in predicted peak strength.

5.8 Damage Observations

Observations made during the testing of W2 are discussed here. The following bullet points highlight observations made as the test progressed and the drift cycle at which they occurred:

- 0.1% drift cycles, first micro cracking was observed at wall to foundation interface. Horizontal cracking was also observed in the wall panel.
- 0.2% drift cycles, first shear cracking (diagonal) was observed in the wall panel, only very minor flexural cracking at the wall to foundation interface.
- 0.3% drift cycles, more shear cracks developed in the wall panel.
- 0.5% drift cycles, extensive shear cracking developed over the entire wall panel.
- 0.75% drift cycles, major diagonal tension crack developed on the first negative drift cycle to 0.75%, which extended from corner to corner of the wall panel. The crack was approximately 2mm in width.

- 1.0% drift cycles, on negative drift cycle the single diagonal tension crack was up to 8mm in width, on positive cycles two parallel diagonal tension cracks developed which stretch from corner to corner on wall panel.
- 1.5% drift cycles, significant spalling of concrete along major diagonal tension cracks observed.
- 2.0% drift cycles, significant spalling along major diagonal tension cracks, concrete at the toe region and top of wall panel has spalled to expose end column reinforcement. Significant shear deformation of the end column reinforcement was observed. At the centre of wall panel where diagonal tension cracks crossed a void through the entire thickness of the wall panel developed.
- 2.5% drift cycles, major pieces of concrete spalled from wall panel due to intersecting diagonal cracks. Test ended after one complete cycle to 2.5% drift as the wall was approaching collapse.

Figure 5-8 shows the first shear cracking that developed in the wall panel on the first cycle to 0.2% drift.

Figure 5-8: First shear cracking at 0.2% drift

Figure 5-9 show the major diagonal tension crack that developed in the negative loading direction. The crack is shown at a drift of 1.0% where it was approximately 8mm in width. Extensive shear cracking across the entire wall panel was observed.

Figure 5-9: Major diagonal tension crack at 1.0% drift

W2 at the end of testing is shown in **Figure 5-10**. The test was finished after one complete drift cycle to 2.5% drift as the wall was nearing collapse. It can be seen that major spalling of concrete occurred along the diagonal cracks and the toe regions of the wall, exposing the reinforcement. Where the diagonal cracks intersected at the centre of the wall panel a void that passed through the entire thickness of the wall formed. Note the pile of spalled concrete rubble sitting on the foundation block.

Figure 5-10: W2 exhibiting a shear dominated failure mode, after experiencing a peak drift of 2.5%

5.9 Results & Analyses

This section discusses the results determined from information gathered from instrumentation attached to W2. This includes the force versus displacement response, axial load versus lateral displacement, equivalent viscous damping and the strain profile up the height of the wall.

5.9.1 Force versus Displacement Response

Figure 5-11 shows the force versus displacement response for W2. It can be seen that a non-ductile response was exhibited, which was expected from the observed shear failure. The peak strength of 290kN was achieved on the 0.75% drift cycle, after which severe strength degradation occurred. A high level of degradation was also observed on repeating cycles to the same drift level. A high level of pinching of the hysteresis loop was observed due to slip from the opening and closing of the large shear cracks. The dissipation shown in the response was likely due to yielding of the transverse reinforcement that crossed the diagonal shear cracks.

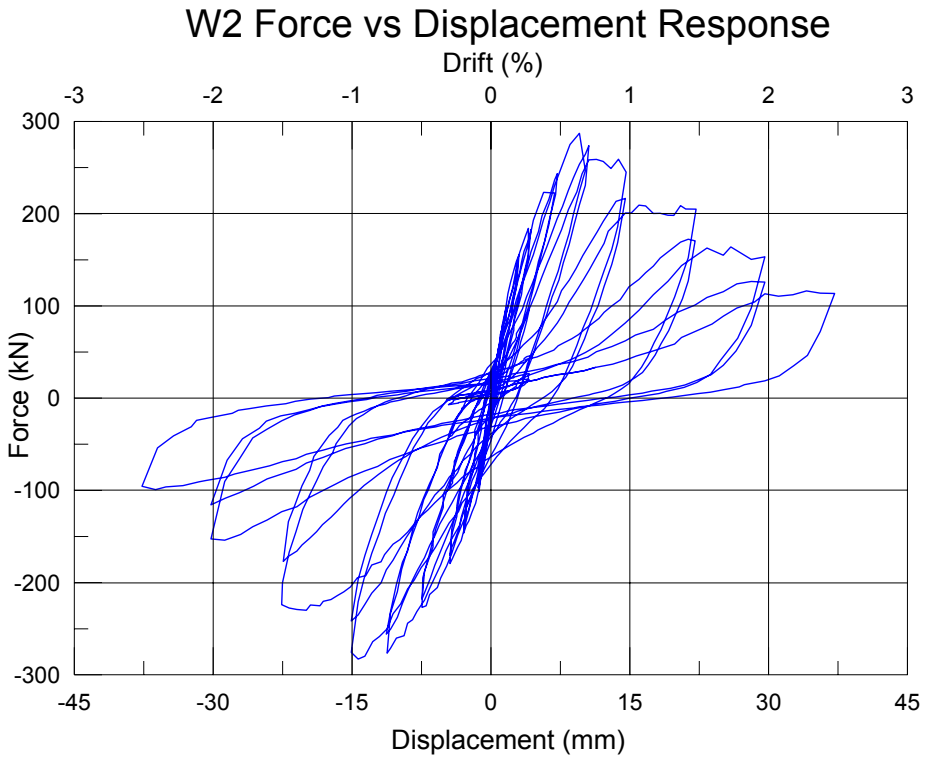

Figure 5-11: W2 force versus displacement response

Sliding of the foundation block relative to the strong floor was measured during the testing of W2. **Figure 5-12** shows relative sliding of the foundation block against the strong floor as the test progressed. It can be seen that substantial sliding occurred, particularly in the positive direction with a magnitude of nearly 4mm. It was also seen that the magnitude of the sliding decreased as the wall strength degraded. The measured foundation sliding was subtracted from the force versus displacement response to correct for this sliding.

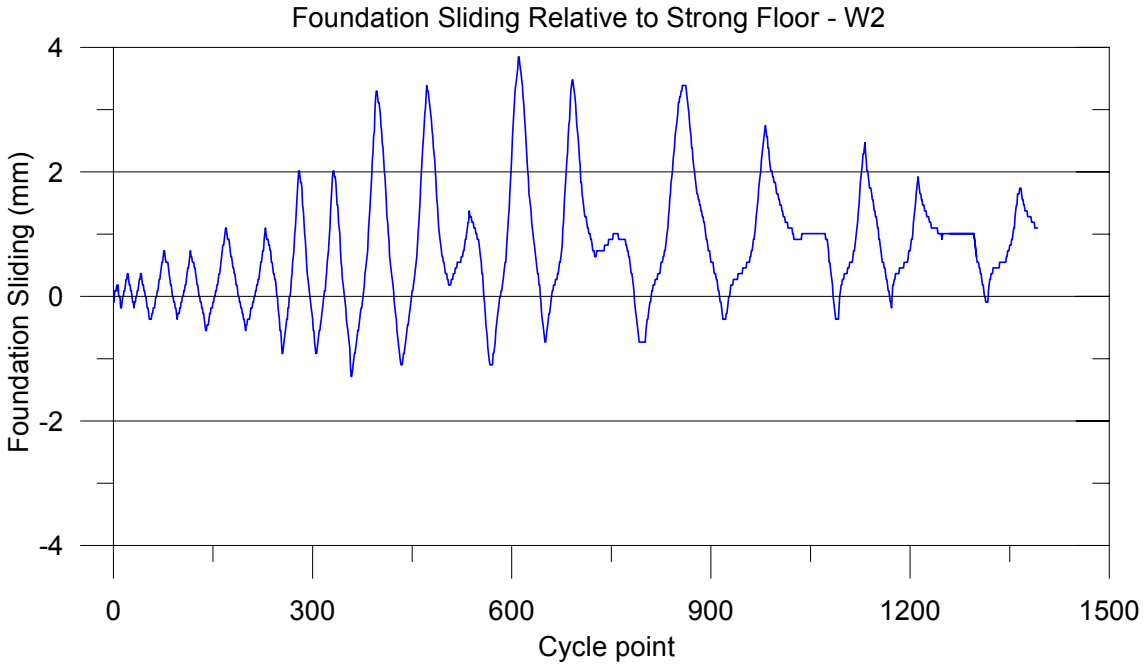

Figure 5-12: W2 foundation block sliding relative to strong floor

5.9.2 Axial Load

Figure 5-13 show the axial load versus lateral displacement for W2. The axial load was measured by a load cell on top of the post-tensioning jack and equalled the sum of the forces in the four post-tensioning tendons. A relatively constant 150kN axial load was achieved for the duration of the test with a maximum variation of ±5kN (12.5%) was observed.

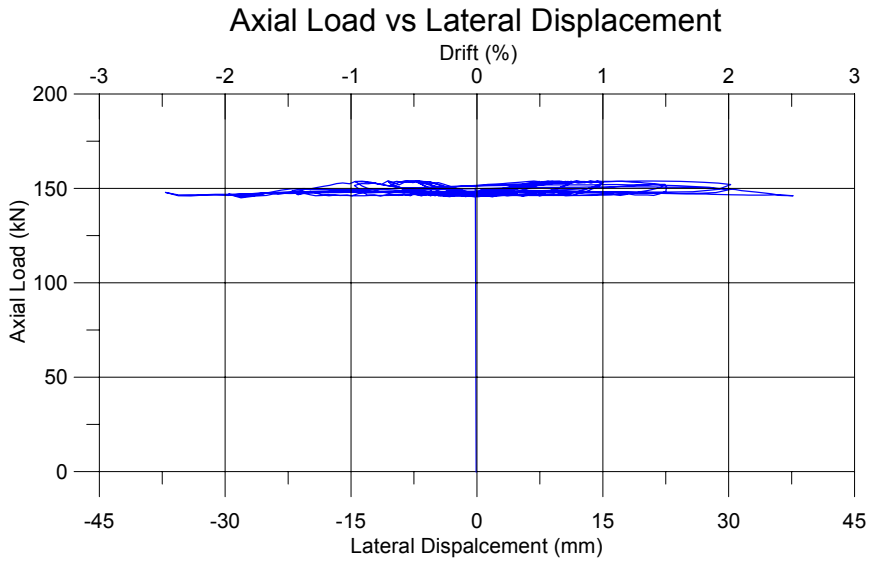

Figure 5-13: W2 axial load versus lateral displacement

5.9.3 Equivalent Viscous Damping

The percentage of equivalent viscous damping for W2 was calculated at peak drifts between 0.5-2.0%, for both the first and second cycle. For the second cycle the equivalent viscous damping was not calculated at the peak drift of 2.5%, as the test was stopped after the first cycle. **Figure 5-14** shows the percentage equivalent viscous damping versus drift calculated for W2, the method used for the calculations can be found in Appendix C. When determining the equivalent viscous damping provided by an element, the second cycle is usually considered as the hysteresis should have stabilised. It can be seen that the equivalent viscous damping provided in the second cycle is considerably less than that of the first cycle. A peak of 18.7% equivalent viscous damping was achieved on the second drift cycle to 2.0%. An estimate of the level of equivalent viscous damping, using an equation (section 10.3.5) for a well detailed structural wall (Priestley, 2003) is show for comparison in **Figure 5-14**. For tis calculation a yield drift of 0.5% was used and it can be seen that the equation slightly overestimated the provided percentage of equivalent viscous damping for the second cycle after 1.5% drift.

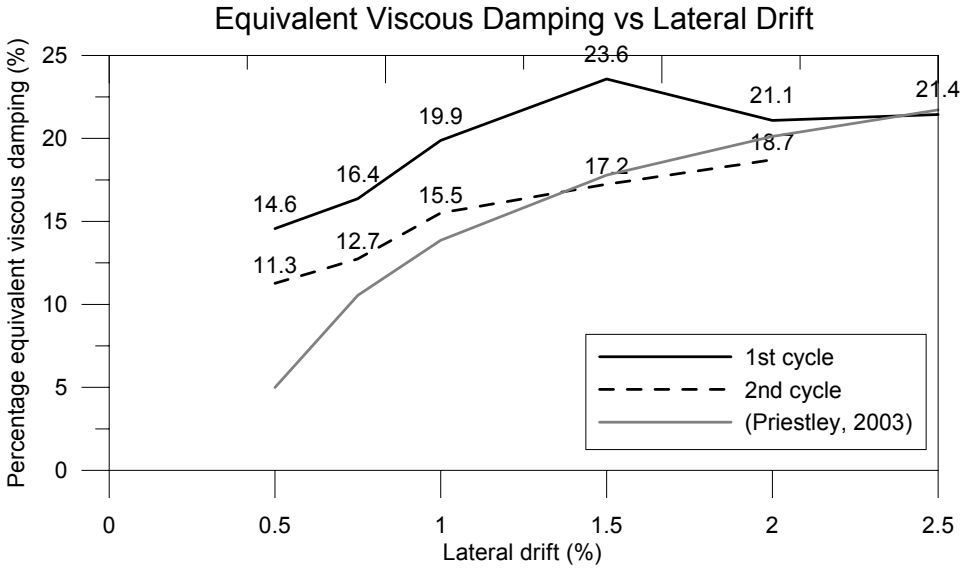

Figure 5-14: Equivalent viscous damping versus drift for W2

5.9.4 Strain Profile in Transverse Reinforcement

The strain profile up the height of W2 was measured by strain gauges located on the transverse reinforcement. **Figure 5-15** shows an example of the measured strain profile at the peak of the negative drift cycles between 0.2-0.5%. The strain profile was stopped after the 0.5% drift cycles as the strain gauges were damaged by the shear cracking. No strain profile

was observed on the 0.1% drift cycles. It can be seen that higher strains occurred near mid-height of the wall panel and diminished near the extremities. The yield strain of the transverse reinforcement was exceeded near the centre of the wall on the 0.5% drift cycles.

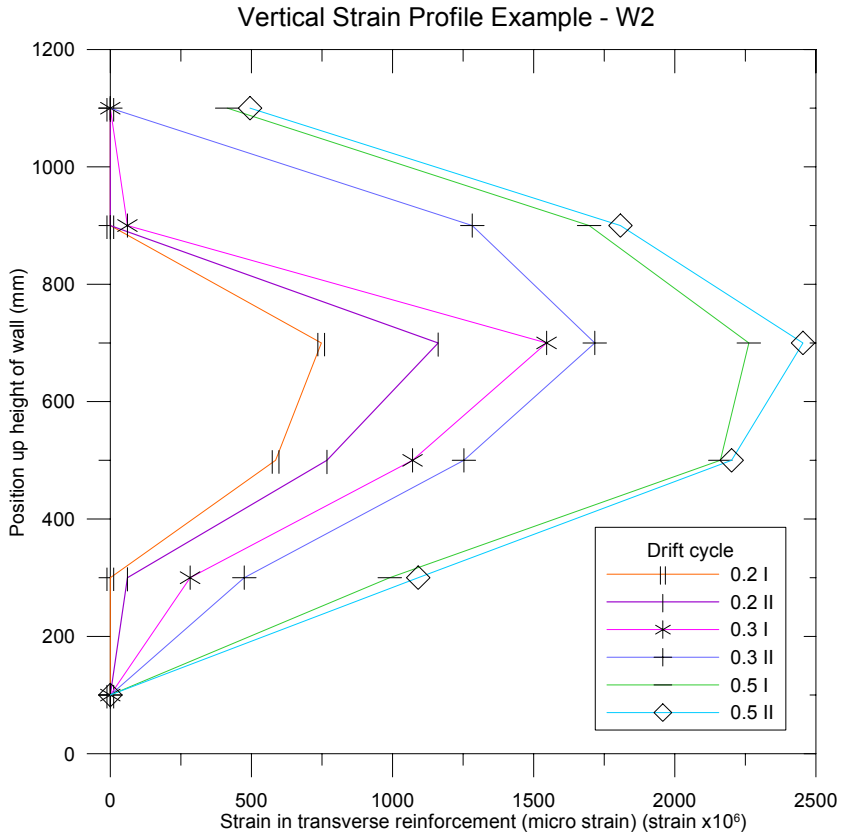

Figure 5-15: Example of the measured strain profile up the height of W2

5.10 Comparison of Experimental and Predicted Response

The predictions made in section 5.7 were compared with the experimental response by plotting the force versus displacement envelopes over the top of the experimental force versus displacement response, the results are shown in **Figure 5-16**.

The force versus displacement predicted assuming the full flexural strength could develop was performed using conventional hand methods of analysis and section analysis program Response-2000. From **Figure 5-16** it can be seen that a shear failure was predicted as both flexural force versus displacement curves cross the shear strength envelope (improved UCSD). However the stiffness was overestimated, due to stiffness loss attributed to shear cracking not being accounted for. The overestimated stiffness when used in combination with

the shear ductility model resulted in a conservative estimate of the displacement at which shear failure occurred but a un-conservative estimate of the peak strength achieved.

The prediction using the Miranda model (Miranda et al., 2005) which accounted for stiffness degradation due to the development of diagonal shear cracks was compared with the experimental response in **Figure 5-16**. It can be seen that when used in combination with the improved UCSD shear strength envelope an accurate prediction of the experimental response was achieved. The Miranda force versus displacement curve intersects the improved UCSD shear ductility model, defining a strength envelope that accurately predicts the displacement at which shear failure occurred and the required force to cause shear failure. The stiffness predicted by the Miranda model was still slightly higher than the experimental response, particularly on the negative displacement cycles. However it can be seen from **Figure 5-16** that it was important to consider the effects of stiffness loss due to shear cracking when assessing the behaviour of walls which are subject to high shear stresses as the flexural predictions provide unrealistic estimates of displacement and strength.

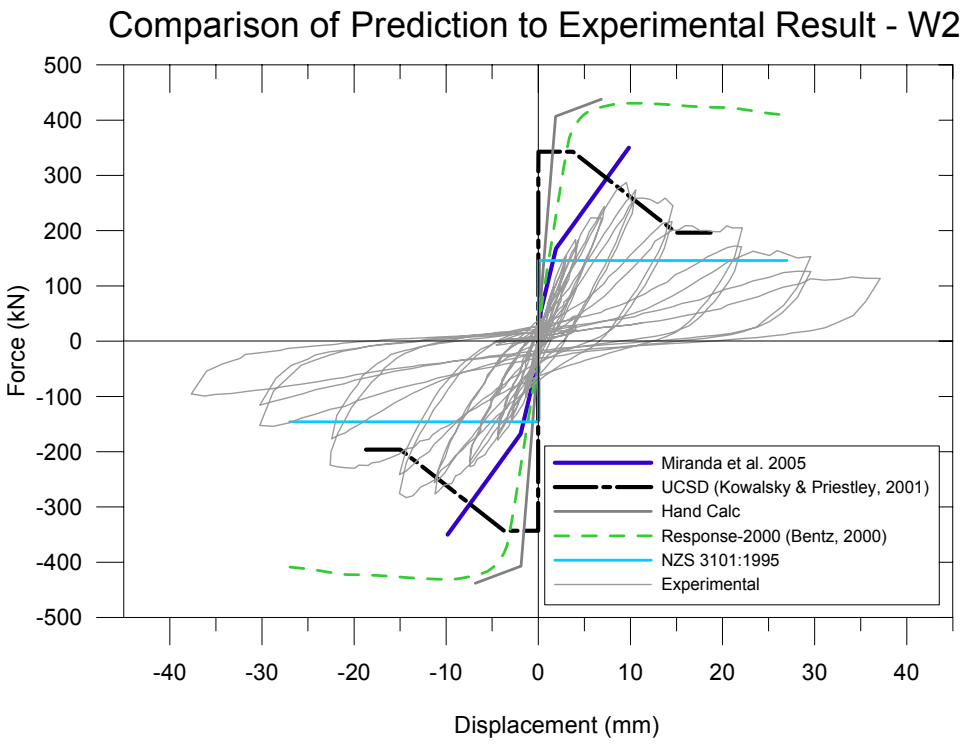

Figure 5-16: W2 Predicted response

References:

Bentz, E., [2001]. "Response-2000 User Manual". Department of Civil Engineering. University of Toronto.

Kowalsky, M.J, and Priestley, M.J.N. [2000]. "Improved Analytical Model for Shear Strength of Circular Reinforced Concrete Columns in Seismic Regions". ACI Structural Journal, Vol. 97, No. 3, pp. 388-396.

Miranda, P.A., Calvi, G.M., Pinho, R. and Priestley, M.J.N. [2005]. "Displacement-Based Assessment of RC Columns with Limited Shear Resistance". Report No. Rose 2005/04, European School for Advanced Studies in Reduction of Seismic Risk, Pavia.

NZSEE, 2005, "The Assessment and Improvement of the Structural Performance of Building in Earthquake". Study group draft, October 2005.

Priestley, M.J.N., [2003], "Myths and Fallacies in Earthquake Engineering, Revisited", IUSS Press, Pavia, Italy.

SNZ. [1995]. "Concrete Structures Standard NZS3101:1995", Volume 1 code of practice. Standards New Zealand, Wellington.

6 W1R – Selective Weakening Retrofit of a W1 Equivalent

6.1 Introduction

This Chapter discusses the development, testing and results of W1R, which was a retrofitted equivalent of W1 (discussed in Chapter 4). A selective weakening retrofit strategy was utilised with the aim of improving the seismic performance. Details of the selective weakening retrofit strategy that was implemented and the experimental outcomes are discussed.

6.2 Benchmark Specimen Summary – W1

W1 was constructed to represent an existing pre-1970's New Zealand structural wall and was tested to provide a benchmark specimen for the selective weakening retrofit strategy to be implemented on W1R. The construction details and results of testing on W1 are discussed in Chapter 4. The main features/deficiencies of the performance of W1 were:

- Single crack opening at the wall to foundation interface, typical of reinforced concrete element consisting of plain round reinforcement;
- Spalling of concrete at wall corners due to longitudinal reinforcement buckling;
- Substantial sliding along wall to foundation crack region;
- Pinched hysteresis with large residual displacements;
- Ruptured longitudinal reinforcement.

6.2.1 Retrofit Objectives

Retrofit objectives for W1R were developed from the outcomes of the testing on the benchmark specimen (W1). The retrofit solution for W1R involved implementing recent developments in building technology, for high performance jointed ductile (hybrid) seismic resisting systems (Priestley et al., 1999; fib 2003; Pampanin 2005), which focus on using a rocking response to ensure a self-centring behaviour and minimal damage. The retrofit solution aimed to provide the following advantages over the benchmark specimen:

- Minimise Damage after seismic response
- Eliminate bar buckling and bar rupture
- Provide a self centring behaviour
- Eliminate possibility of lap splice governing the behaviour
- Reduce the peak displacements during time-history response

6.3 Retrofit Configuration and Components

The details of the components required to implement the selective weakening retrofit solution used on W1R are discussed in this section. The retrofit solution initially involved weakening the as-built wall by a horizontal saw cut at the foundation level. This severed all the longitudinal wall reinforcement, and through a balanced contribution of un-bonded post-tensioning and energy dissipation devises the as-built monolithic wall was converted to a rocking wall. Corner armour and shear keys were also required to complete the retrofit solution. The details of each of the components which made up the retrofit solution are discussed in detail in the following sections. The overall configuration of the retrofit solution implemented for W1R is shown in **Figure 6-1**.

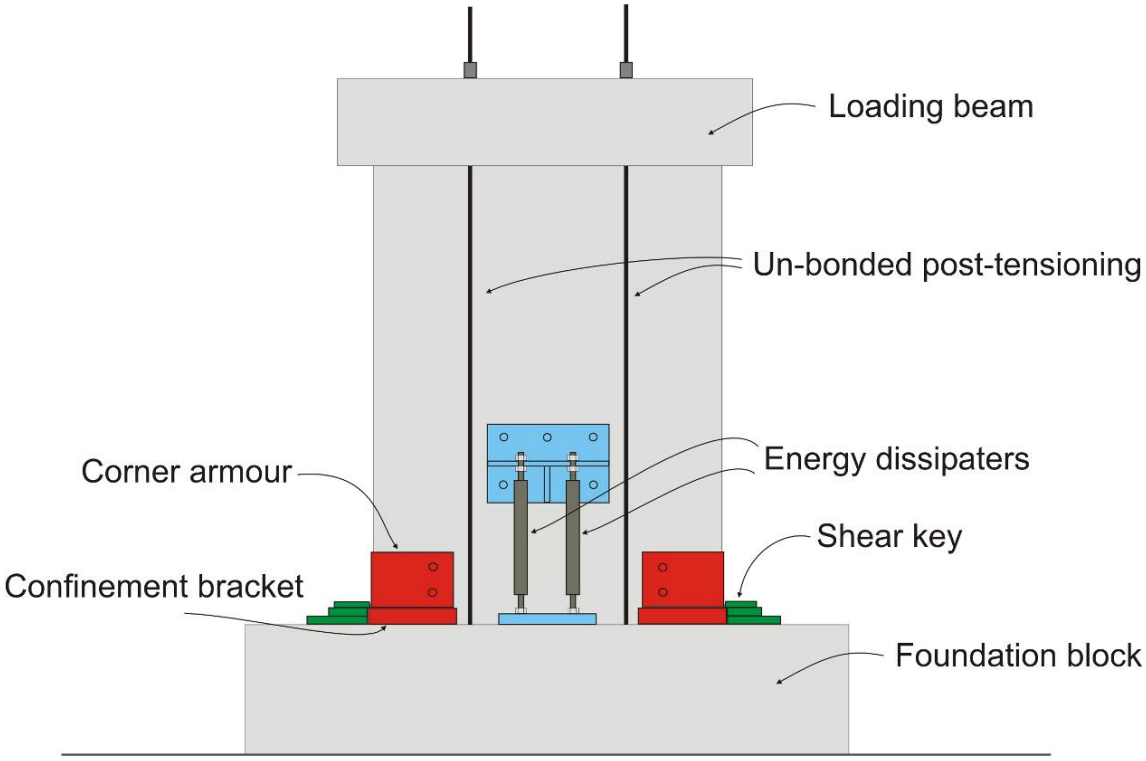

Figure 6-1: Selective weakening retrofit configuration for W1R

6.3.1 Horizontal Saw Cut

Selective weakening of W1R was performed by using a horizontal saw cut at foundation level. All of the longitudinal reinforcement was severed and the wall was completely separated from the foundation. The horizontal cut introduced a rocking behaviour, whilst eliminating the possibility of a lap splice failure and the possibility of bar buckling and/or rupture. The cut was made by a conventional concrete cutting saw, but due to geometric constraints relating to the saw the cut had to be made at a minimum of 50mm above the wall

to foundation interface. **Figure 6-2** shows the cutting in progress. Having the cut at a height of 50mm above the wall to foundation interface was an inconvenience as the section of wall below the cut region had to be confined to avoid potential crushing as the wall rocked. With the availability of a "wire saw" it would be possible for the cut to be made "flush" with the wall to foundation interface. A cementitious grout was applied over the cut region to ensure an even bearing surface was provided for the wall to rock on.

Figure 6-2: Implementation of horizontal foundation cut

6.3.2 Un-bonded Post-tensioning

Un-bonded post-tension was used to provide stability, increase the moment capacity (as all of the longitudinal reinforcement had been severed), control the rocking response and provide a self centring behaviour. The post-tensioning was provided by 7-wire post-tensioning tendons with an area of 99mm^2 and a specified ultimate stress of 1860MPa. The post-tensioning passed through ducts which were cast into the foundation block and loading beam, but were passed externally down the sides of the wall. The tendon locations in relation to the wall centreline are shown in **Figure 6-3**. It was important that un-bonded post-tensioning was used as this allowed the strain developed due to gap opening to be distributed along the un-bonded length of the tendon. If bonded post-tensioning had been used when the wall rocked a stress concentration due to the gap opening could result in the tendon yielding or rupturing.

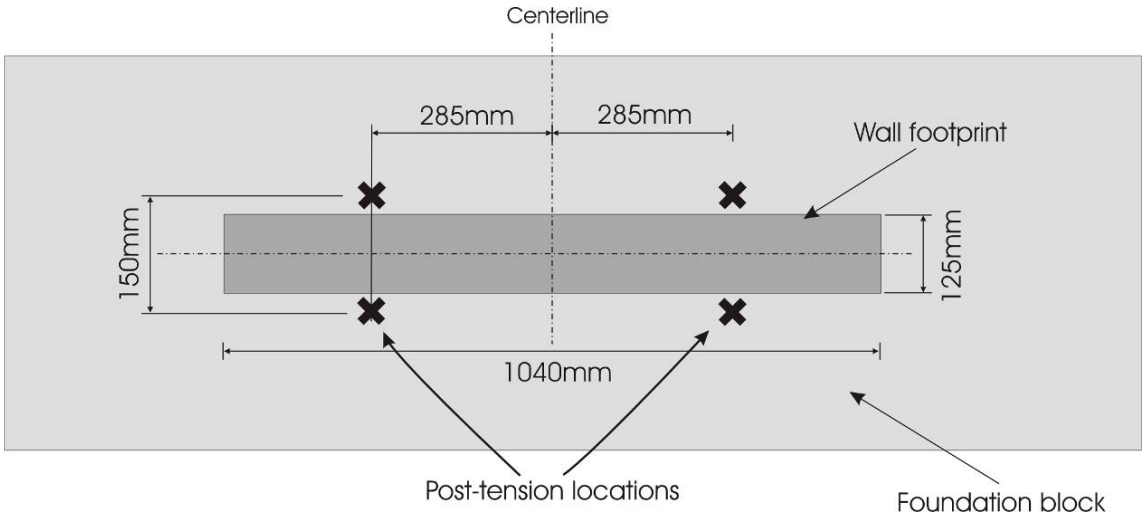

Figure 6-3: W1R post-tensioning tendon locations

To ensure a self centring behaviour was achieved an appropriate balance between the level of post-tensioning and the strength of the mild steel energy dissipaters was provided. This required that the total initial post-tensioning force was greater than the force required to yield the mild steel energy dissipaters in compression. The initial post-tensioning level also had to be low enough to ensure sufficient capacity was available in the post-tensioning so that they did not yield or rupture as the wall rocked. If the tendons yielded the initial post-tensioning level would reduce and the self centring capability might have been lost. When performance based design is used the elongation of the tendons can be estimated by determining the neutral axis depth at peak response and the rotation the wall will experience. The method for determining elongation due to gap opening is shown in **Figure 6-4**.

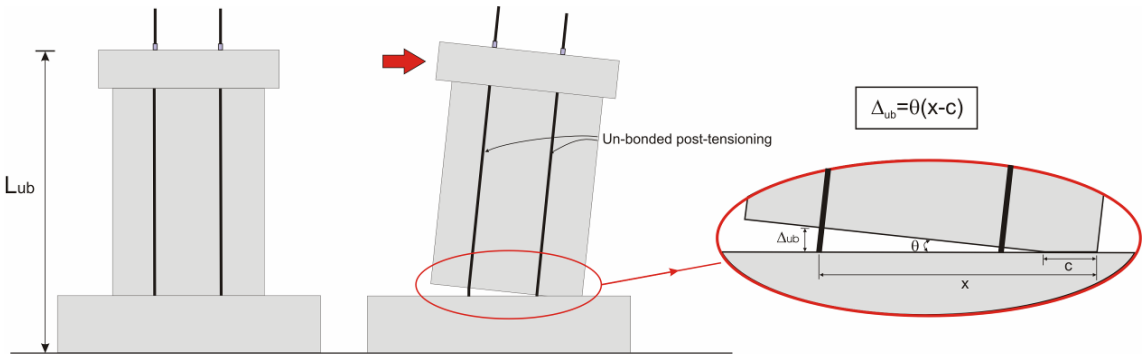

Figure 6-4: Elongation of post-tensioning tendons due to wall rocking

For W1R an initial post-tensioning of 40kN per tendon or 21% of ultimate was provided, with an un-bonded length of 2.85m. The level of initial post-tensioning ensured that a self centring

behaviour would be achieved and the tendons would not yield as the wall was laterally loaded.

6.3.3 Energy Dissipaters

Four energy dissipaters were attached to W1R to provide hysteretic energy dissipation and to increase the moment capacity. Without energy dissipaters the un-bonded post-tensioned wall would have a non-linear elastic hysteretic response, whilst with dissipaters it would have a desirable flag-shaped hysteresis (Pampanin, 2005). The energy dissipaters were provided in the form of mild steel black bar which was fused down to 10mm in diameter over a 150mm fuse length. The energy dissipaters were mounted on the wall so that they crossed the critical plane and yielded in tension as the wall rocked in either direction. The details and dimensions of the energy dissipaters used in W1R are shown in **Figure 6-5**.

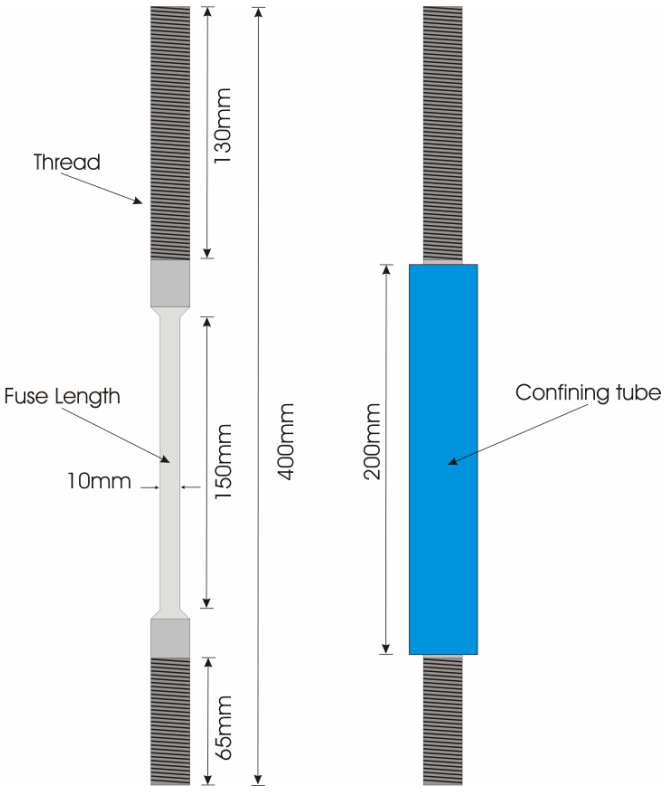

Figure 6-5: Details and dimensions of the energy dissipaters used on W1R

The fuse length of the dissipater was confined by a steel tube which prevented the fuse from buckling when it was loaded in compression. Confinement was provided by filling the steel tube with an epoxy. Buckling of the fuse length was undesirable as it reduces the efficiency of

the dissipater. The ends of the dissipater were threaded to allow them to be mounted to steel brackets attached to the wall and foundation. The use of threaded dissipaters meant that they could be easily replaced and the wall could then be re-tested. The fuse diameter was determined by the required axial yield force to ensure that the required moment capacity was achieved and that the initial un-bonded post-tensioning force was sufficient to yield the dissipaters in compression (to provide a self centring behaviour). Strain hardening was important to consider as if it was not accounted for the wall may not self centre.

A total of four dissipaters were mounted to the wall, 60mm either side of the wall centre line (as shown in **Figure 6-6**). The dissipaters were located near the centre of the wall to minimise the lever arm and therefore the required fuse length. The fuse length of the dissipater was determined from estimating the peak elongation expected in the dissipater, using the same method as was used to estimate the elongation due to gap opening in the post-tensioning tendons. Previous studies at the University of Canterbury using similar dissipaters (e.g. Marriott et al., 2006) have determined that an appropriate estimate of the max elongation that a dissipater of this form can sustain under cyclic loading is 10% of the fuse length. This was a significant reduction in the approximate 20% elongation which could be achieved if the dissipater was tested directly in tension. It was important that the fuse length was minimised, as when the fuse length increases the axial stiffness decreases. This allows more elastic deformation of the dissipater, which delays the onset of yield in the dissipater. Meaning the wall will displace further before any hysteretic energy dissipation was provided.

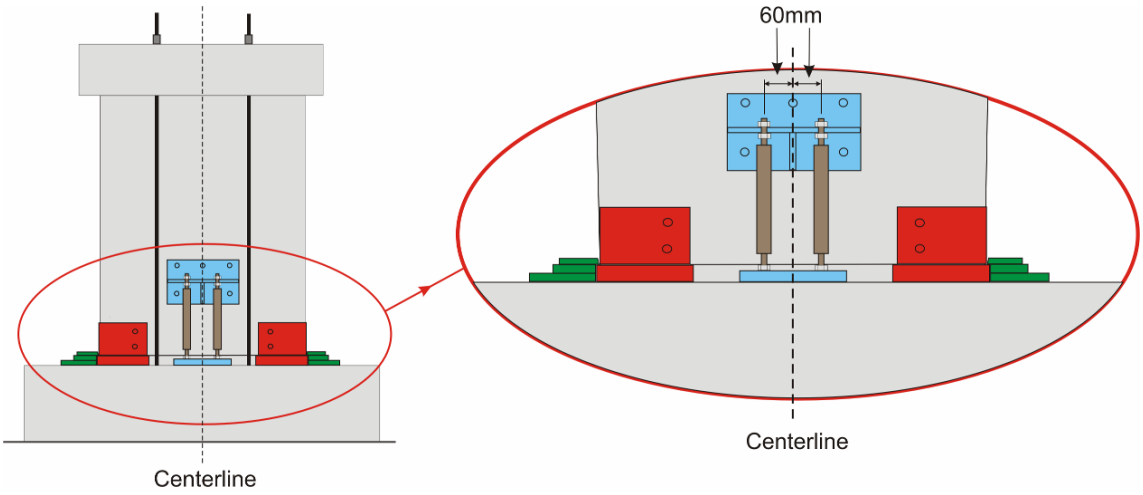

Figure 6-6: W1R dissipater locations

6.3.4 Protection of Corner Regions

Corner armour was used to provide confinement, to prevent the toe region of the wall crushing and spalling as the wall rocked. A U-shaped steel bracket consisting of 6mm thick by 150mm wide steel plate was welded into a U-shaped configuration and mounted to the wall corners. Two holes were drilled in each bracket and through the wall to allow the U-shape to be effectively closed by two 16mm bolts. The bolts improved the level of confinement provided by the bracket. To ensure a snug fit was achieved the bracket was deliberately mounted so that there was a void between the end of the wall the bracket. The void was filled with grout to ensure appropriate confinement was provided.

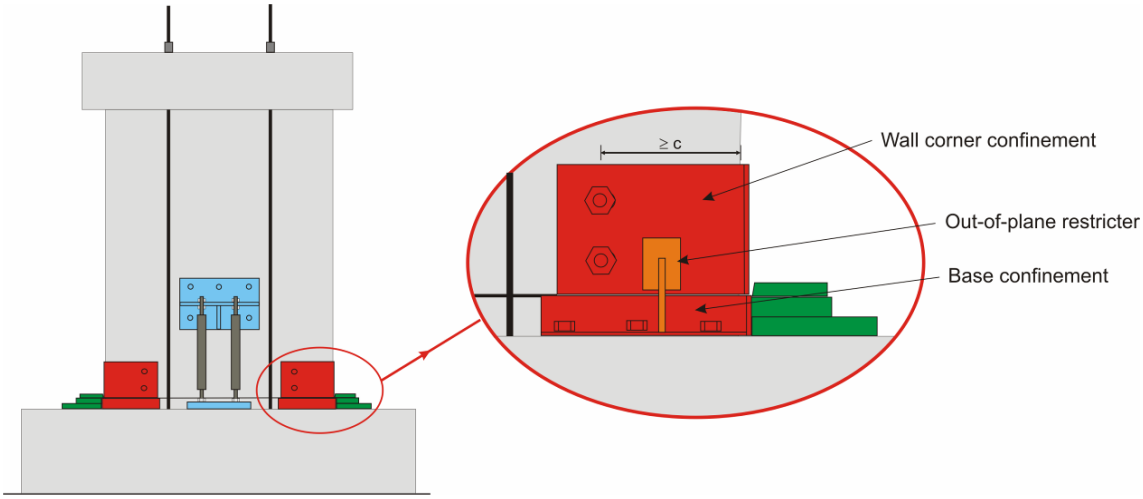

Figure 6-7: W1R corner armour

The required length of the corner armour was determined by calculating the neutral axis depth expected at the peak response. The length of the confinement brackets was then made slightly greater that the expected neutral axis depth to ensure that the entire compression zone was confined. In addition to providing confinement, the steel armour provided a surface for the shear keys to bear on. The shear keys would crush the toe region if no corner armour was provided.

In addition to the confinement armour provided on the wall corners above the horizontal cut, confinement was required for the 50mm section of wall that remained attached to the foundation. This base section resulted from the horizontal cut having to be made at a minimum of 50mm above the wall to foundation interface (due to geometric constraints

relating to the concrete cutting saw). This segment of wall needed to be confined as it was expected that it would crush when the wall sitting above it rocked. Confinement armour was provided by a 50x3mm steel angle bracket which was anchored to the foundation block. The confinement bracket was made slightly larger than the wall cross section to allow the remaining gap to be filled with grout to ensure appropriate confinement was provided. The length of the confinement bracket was made slightly larger than the expected neutral axis depth at peak response, as for the wall confinement bracket.

6.3.5 Shear Keys

Shear keys were required to ensure that the wall did not slide on the horizontal cut. The shear keys consisted of a 20mm steel plate with one edge milled to a 10% slope. This angle was used to ensure that the wall did not pivot about the top of the shear key, but instead simply slid up against the shear key. The shear key was provided as it was difficult to determine if adequate friction to prevent sliding could be provided along the cut region. The shear key was mounted upon 50mm of steel plates to ensure it was at the height of the horizontal cut. The steel plates upon which the shear keys were mounted were anchored to the foundation block. In addition to shear keys steel guides were placed to prevent the wall from moving out of plane.

6.4 Experimental Set-up

Quasi-static uni-directional in-plane testing was performed on W1R, with the wall acting as a cantilever. The experimental set-up is shown in **Figure 6-8**. This shows the hydraulic actuator, post-tensioning and reaction frame configuration. The experimental set-up was similar to that used for W1 which was discussed in Chapter 4.3. The only difference was that a constant axial load was not applied throughout the duration of the testing of W1R. The post tensioning tendons were initially loaded to 40kN each at the start of testing and then locked off. This was used to represent the gravity load (150kN total) with 2.5kN of initial post-tensioning per tendon. This meant that as the wall was laterally loaded the post-tensioning force increased.

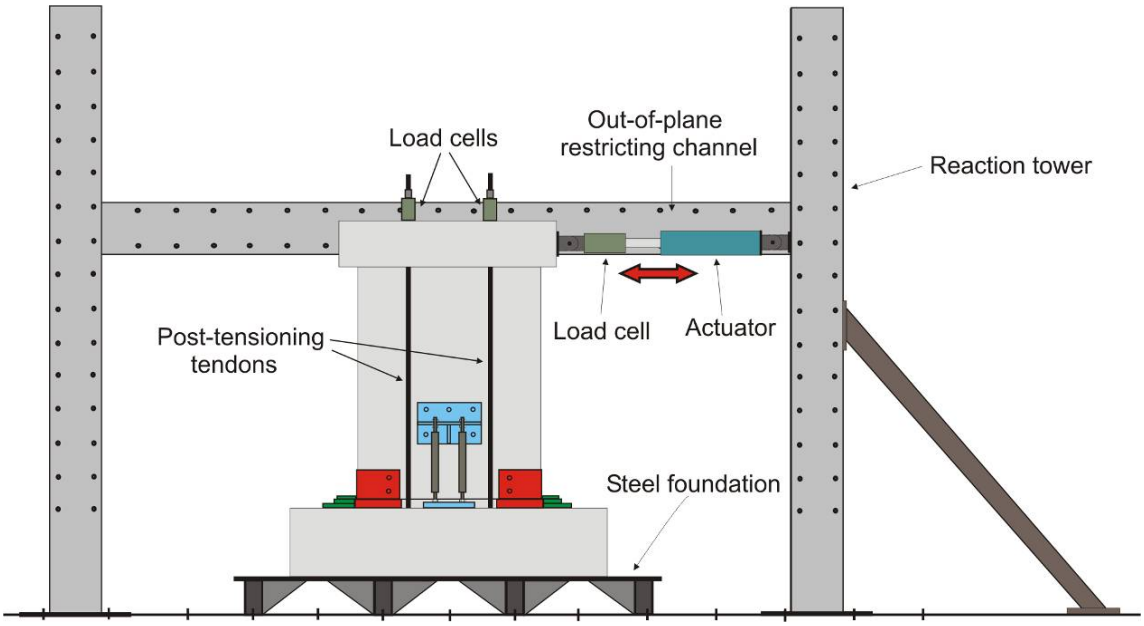

Figure 6-8: W1R test set-up

6.5 Instrumentation Layout

A combination of linear potentiometers, rotary potentiometers, load cells and strain gauges were used to monitor the behaviour of W1R. The layout of the potentiometers is shown in **Figure 6-9**. The potentiometers were used to monitor shear and flexural deformations, the neutral axis position, dissipater elongation and sliding of the wall and foundation.

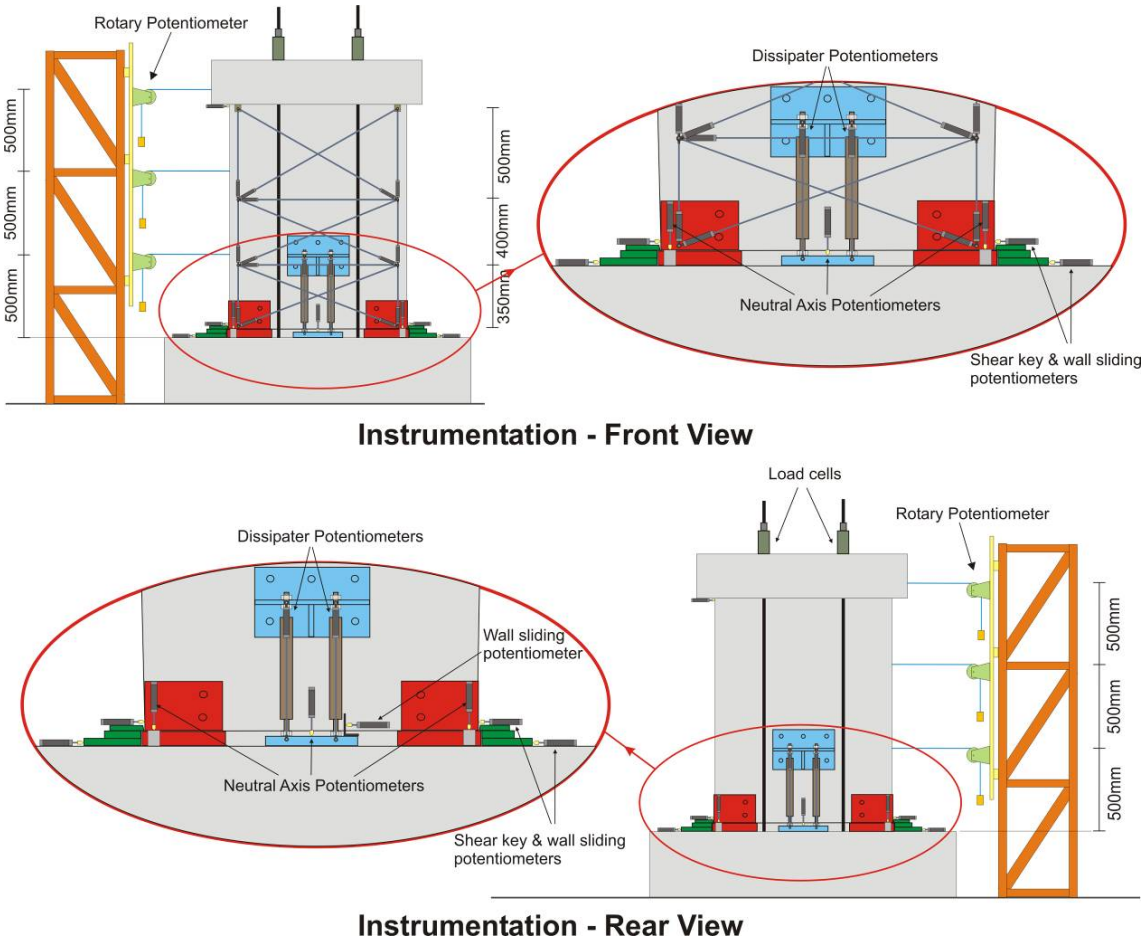

Figure 6-9: W1R instrumentation set-up

Shear deformations of the wall panel were monitored by a series of potentiometers in three diagonal configurations. Incorporated into the diagonal configurations were potentiometers to monitor flexural deformations of the wall panel. Three rotary potentiometers were distributed up the height of the wall to monitor the displaced shape and a rotary potentiometer was also used to monitor sliding of the foundation block relative to the strong floor. A series of linear potentiometers were mounter across the horizontal cut to be used to determine the neutral axis position. Potentiometers were also mounted across the foundation and wall dissipater mounts to measure the elongation experienced by the dissipaters. Strain gauges were also included on the fuse length of the dissipater to be used to determine when yielding started.

The load in the post-tensioning cables as testing progressed was monitored by load cells and strain gauges. Individual load cells were attached to each post-tensioning cable at the top of the wall as shown in **Figure 6-9**. Strain gauges were also attached to the post-tensioning cables at the horizontal cut level.

6.6 Load Regime

A displacement based lateral loading history was used for W1R and is shown in **Figure 6-10**. The load history consisted of cyclically increasing displacement up to a peak drift level of 2.5%. The details of how the load regime was determined are discussed in section 5.5.

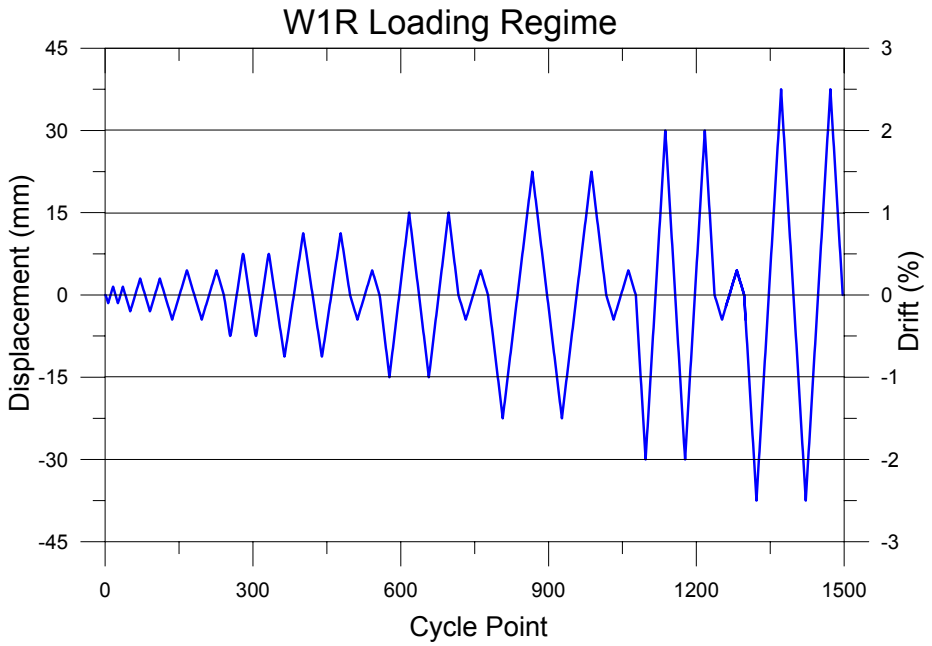

Figure 6-10: W1R Load History

6.7 Force versus Displacement Predictions – W1R

The force versus displacement backbone curve for W1R was predicted for the wall with and without energy dissipaters. The behaviour of the hybrid wall was determined using the monolithic beam analogy (Palermo, 2004; fib, 2003; NZS3101:2006 Appendix B), for a target drift of 2.5%. The response was predicted accounting for confined concrete strain of ε_c=0.01, to account for the steel corner armour. An un-bonded post-tensioning length of 2.85m was used with an initial post-tension force of 40kN per tendon. For the energy dissipaters a yield stress of 330MPa was used and the effects of strain hardening were accounted for. The predicted force versus displacement backbone curves for W1R with and without dissipaters are shown in **Figure 6-11**.

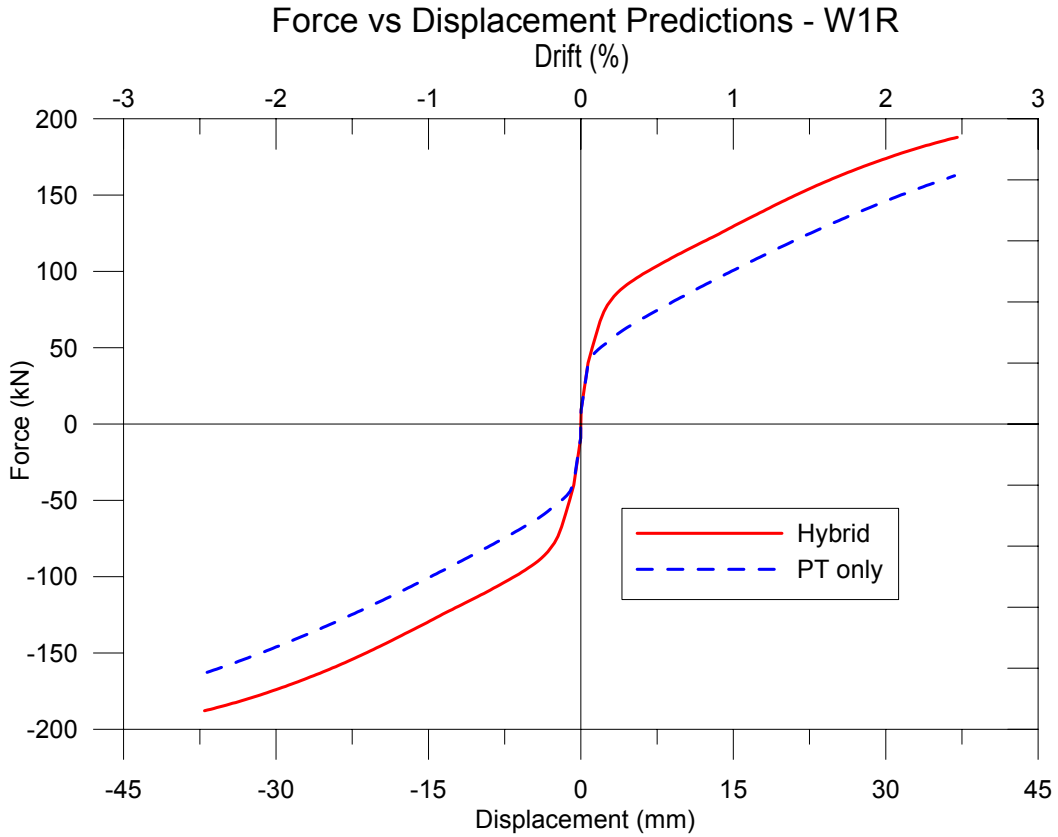

Figure 6-11: Force versus Displacement predictions, W1R

6.8 Sample Testing of Dissipater

A direct tension and a cyclic tension/compression test were performed on sample dissipaters that were to be used as part of the retrofit solution for W1R. The direct tension test was performed to determine the stress strain characteristics of the steel used to make the dissipaters. The cyclic tension/compression test was performed to determine the force versus displacement response of the dissipater and to monitor the effectiveness of the confinement method used to prevent buckling and to ensure that the dissipater did not rupture under the expected displacements.

The stress versus strain characteristic of the dissipater as determined from a tensile test are summarised in **Table 6-1** and shown in **Figure 6-12**. This test was performed of a sample dissipater without the confinement tube as it was to be loaded only in tension.

Table 6-1: Dissipater tensile test, steel stress-strain characteristics

yield stress	f_y (MPa)	330
ultimate stress	f_u (MPa)	463
ultimate strain	ε_u (strain) x10^3	200

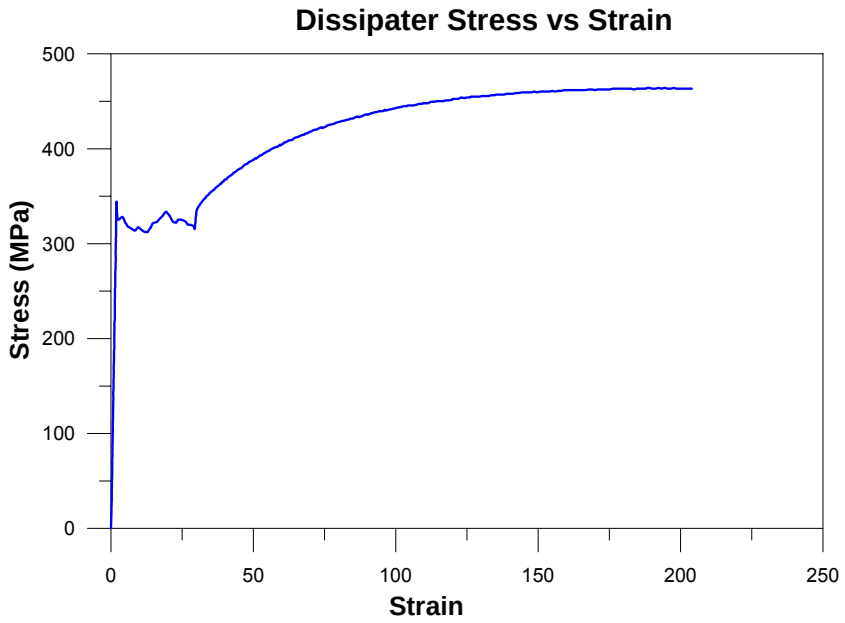

Figure 6-12: Dissipater tensile test, stress versus strain

A cyclic tension/compression test was performed on a sample dissipater to determine the force versus displacement response of the dissipater, the test was performed on a complete dissipater (including confining tube). An estimate of the likely displacements that the dissipater was going to be subjected to when attached to W1R was obtained from the wall lateral loading history and a calculated neutral axis depth (using the same method used to calculate the elongation in the post-tensioning tendons, section 6.3.2). Small cycles are used at the start in order to determine the pre-yield behaviour and the peak displacement in 12.6mm which corresponded to 8.4% of the fuse length. The displacement loading history used for the dissipater test is shown in **Figure 6-13**.

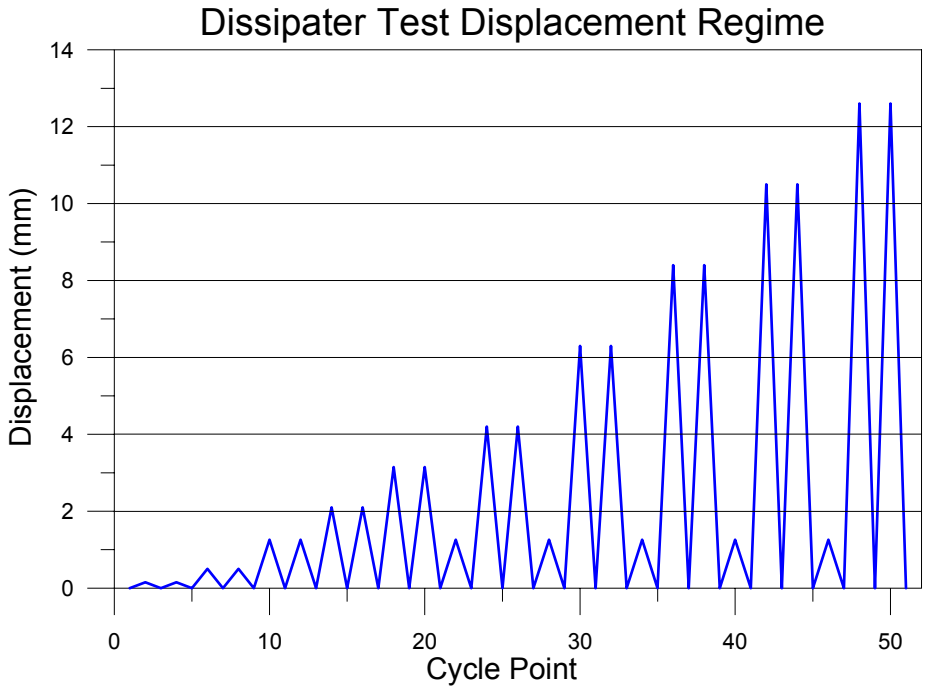

Figure 6-13: Dissipater test displacement loading regime

The measured force versus displacement response from the dissipater test is shown in **Figure 6-14**. The force versus displacement response shows that a stable hysteretic behaviour was achieved with no evidence of buckling of the dissipater when it was loaded in compression. It was seen that the dissipater yielded at a force of 26kN and that the ultimate tension force achieved at the peak displacement was 1.44 times the yield strength or 36kN. The peak compressive force achieved was 40kN, which corresponded to 1.54 times the tensile yield strength. The compressive yield force was not as evident from the force displacement response due to the Bauschinger effect. It can be seen that the yield displacement was approximately 0.25mm and the ultimate displacement achieved was 12.5mm.

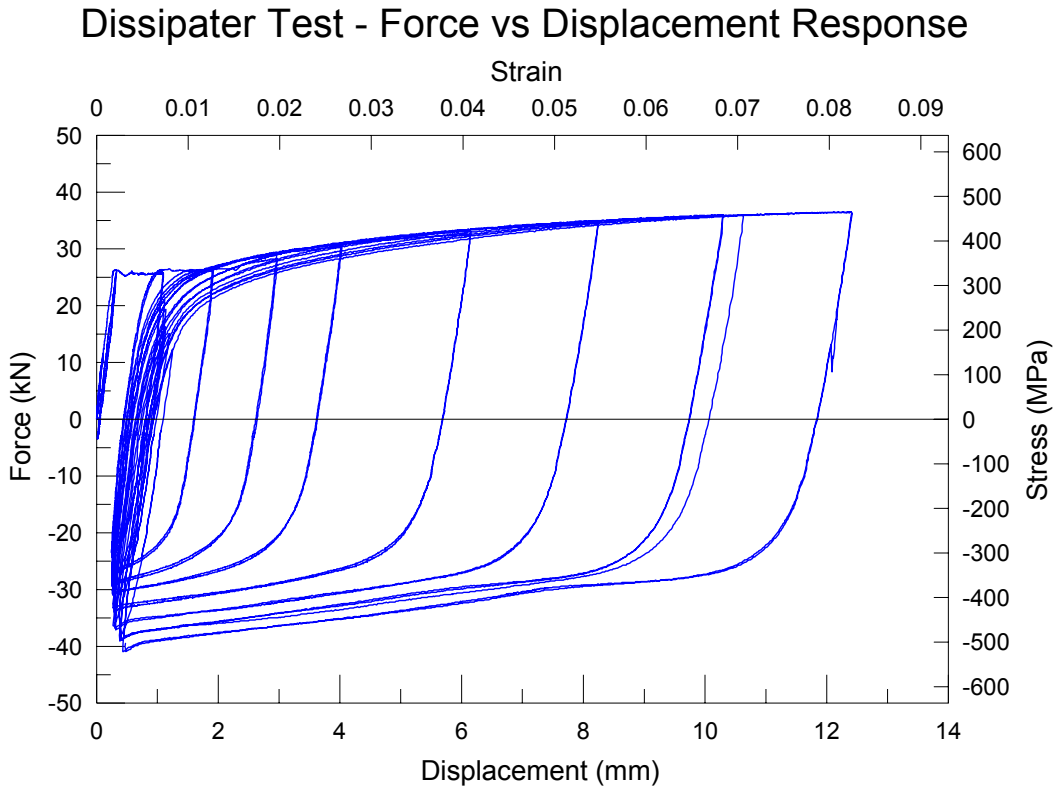

Figure 6-14: Dissipater test, force versus displacement response

6.9 Observations

As a result of the rocking behaviour, minimal damage and replaceable external energy dissipaters W1R was able to be tested multiple times. W1R was tested four times, two tests including energy dissipaters (hybrid) and two without (post-tensioned only). Observations made during and after the four tests are discussed in the following sections.

6.9.1 Test #1 Observations – 1st Hybrid Test

The first test conducted on W1R was with energy dissipaters (hybrid). Due to the rocking nature of the wall the observations were largely limited to a single gap opening along the horizontal cut region near foundation level. **Figure 6-15** shows the wall at its peak drift of 2.5%. It can be seen that all of the inelastic action was concentrated at a gap opening along the horizontal cut region, no cracks formed in the wall panel and no crushing was observed at the toe region of the wall.

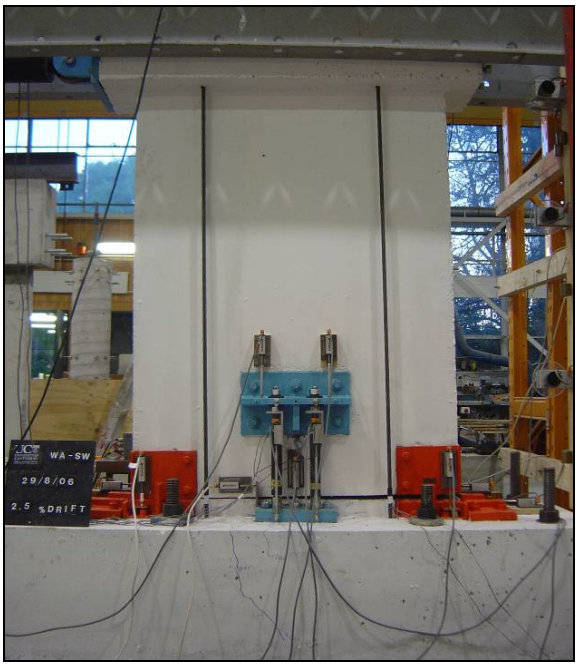

Figure 6-15: W1R at peak drift of 2.5%

Some notable observations made during the first test performed on W1R and the drift at which they occurred were:

- 0.3% drift cycles, an approximately 1mm wide crack opened along the horizontal cut region.
- 0.75% drift cycles, elongation of the dissipaters was observed by a crack forming in the epoxy between the dissipater and the confining tube.
- 2.0% drift cycles, cracks in the foundation formed near the dissipater mounts. No movement of the dissipater mounts was observed.
- 2.5% drift cycles, once drift cycles complete the wall returned to at rest position, no obvious damage.

Figure 6-16 shows the gap opening at one end of the wall when at the peak drift of 2.5%. A number of observations were made from observing the gap opening, which include:

- Grout pad on the horizontal cut region was intact, with no signs of crushing or breaking up when test was near completion.
- Noticeable wear on the paint at the bottom of the wall confining bracket where the wall has been bearing against the shear key.

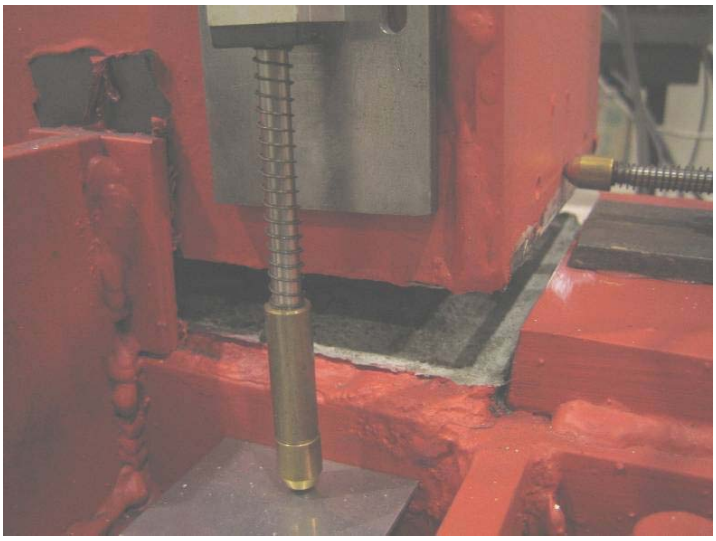

Figure 6-16: Gap opening at drift of 2.5%

Figure 6-17 shows one of the energy dissipaters mounted on the wall, when the wall was subject to 2.5% drift. It was seen that the dissipater has significantly elongated by the cracked epoxy which had moved relative to the confining tube.

Figure 6-17: Dissipater elongation at 2.5% drift

6.9.2 Test #2 – Test #4 Observations

The behaviour of W1R was governed by a single gap opening along the horizontal cut region as the wall rocked. A total of four tests were performed on this wall which included two with

energy dissipaters (hybrid) and two without (post-tensioned only). Significant observations made during the first test (with energy dissipaters) were discussed in the previous section. No significant observations different from those observed in the first test were made in the later tests of W1R. The second test was without dissipaters (post-tensioned only), the third was with dissipaters (hybrid) and the fourth was without dissipaters (post-tensioned only). **Figure 6-18** (a), (b) & (c) shows the W1R at 2.5% drift for the second, third and fourth tests respectively.

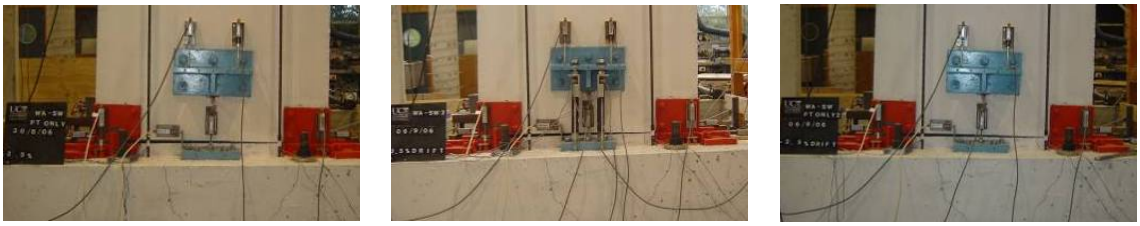

(a) (b) (c)

Figure 6-18: W1R peak response during the second, third & fourth tests

6.9.3 Post Test Observations

Once testing was complete on W1R a close inspection of overall performance of the wall around the horizontal cut region and of the dissipaters was made. **Figure 6-19** show the foundation side of the horizontal cut interface after testing and once the wall had been removed. It was seen that the grout pad on which the wall beared upon was still intact but with noticeable points of abrasion on the surface. Abrasion of the grout surface was visible at the end regions of the wall across the full width, to a length consistent with what would be the expected neutral axis depth at peak response. It was also seen that in the centre region of the wall a moderate level of abrasion was visible, which favoured one side of the wall. The reason the abrasion occurring on one side was likely due to the saw cut not being completely level (horizontal) across the width of the wall.

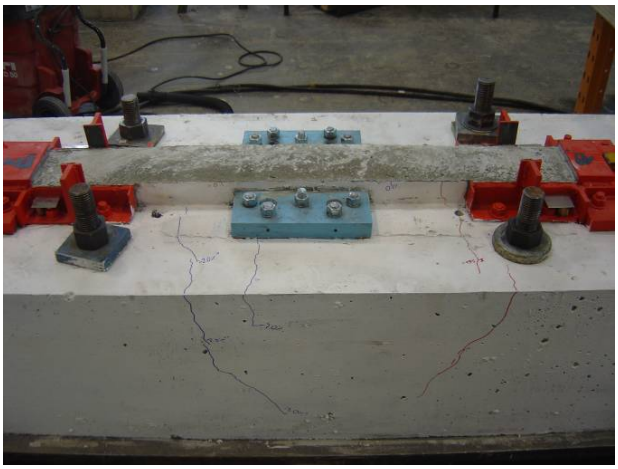

Figure 6-19: Horizontal cut foundation interface, post testing

Figure 6-20 shows the underside of the wall once it had been lifted off the foundation. Surface abrasion was visible on the end regions and also in the middle region, but favouring one side as was observed on the foundation interface. The corner regions of the wall showed no signs of crushing or cracking. This showed that the provided corner armour performed well by preventing damage to the toe region of the wall.

Figure 6-20: Underside of wall, post testing

Two of the four experiments conducted on W1R included energy dissipaters. After testing the dissipaters were removed and the confining tubes were cut away so that the behaviour of the

fuse length of the dissipater could be analysed. **Figure 6-21** (a) and (b) show one of the four dissipaters from each hybrid test, with the confining tube cut away for the first and second hybrid test respectively (test #1 & test #3 on W1R). The dissipater from the first test on W1R shows significant buckling at the centre of the fuse length. This was not a desirable feature of the performance as buckling lowers the efficiency of the dissipater. A possible cause of the buckling of the dissipater was thought to be the protective material which was applied over the strain gauges (which were located at the centre of the dissipater). This was a thick and malleable rubber tape, which was a lot softer than the surrounding epoxy and could have provided a starting point for buckling. In the second test involving dissipaters (test #3) the thick rubber tape used to protect the stain gauges was replaced with a thin plastic tape. When the confining tubes were cut from the dissipaters from the second test, it was seen that buckling was less predominant (**Figure 6-21** (b)).

(a) (b)

Figure 6-21: Dissipaters after testing for the first and second hybrid test

6.10 Results & Analyses – Test #1 (1st hybrid test)

The results and analyses of the first of four tests performed on W1R are presented in this section. This test was performed including a set of energy dissipaters, the results of tests excluding dissipaters will be discussed in a later section. The results and analyses that are

discussed include the force versus displacement response, post-tensioning forces, dissipater elongation, percentage of total displacement relating to rotation of the wall base and the equivalent viscous damping.

6.10.1 Force versus Displacement Response, test #1

The force versus displacement response for W1R is shown in **Figure 6-22**. A flag shaped hysteresis was formed which was expected and considered desirable for and un-bonded post-tensioned wall including energy dissipaters. A self centring behaviour was observed for the majority of the response, excluding the 2.0% and 2.5% negative drift cycles. A peak residual displacement of approximately 7mm (0.5% drift) was observed on after unloading. Given the flag-shape hysteresis loop, during a dynamic response it would be expected that the residual displacements would be reduced to negligible values. A negative attribute of the force versus displacement response was stiffness degradation as the test progressed. Reasons for this stiffness degradation include losses in the initial level of post-tensioning as the test progressed, dissipater buckling, sliding of the foundation block relative to the strong floor, sliding of the wall on horizontal cut and crushing damage at the toe regions of the wall.

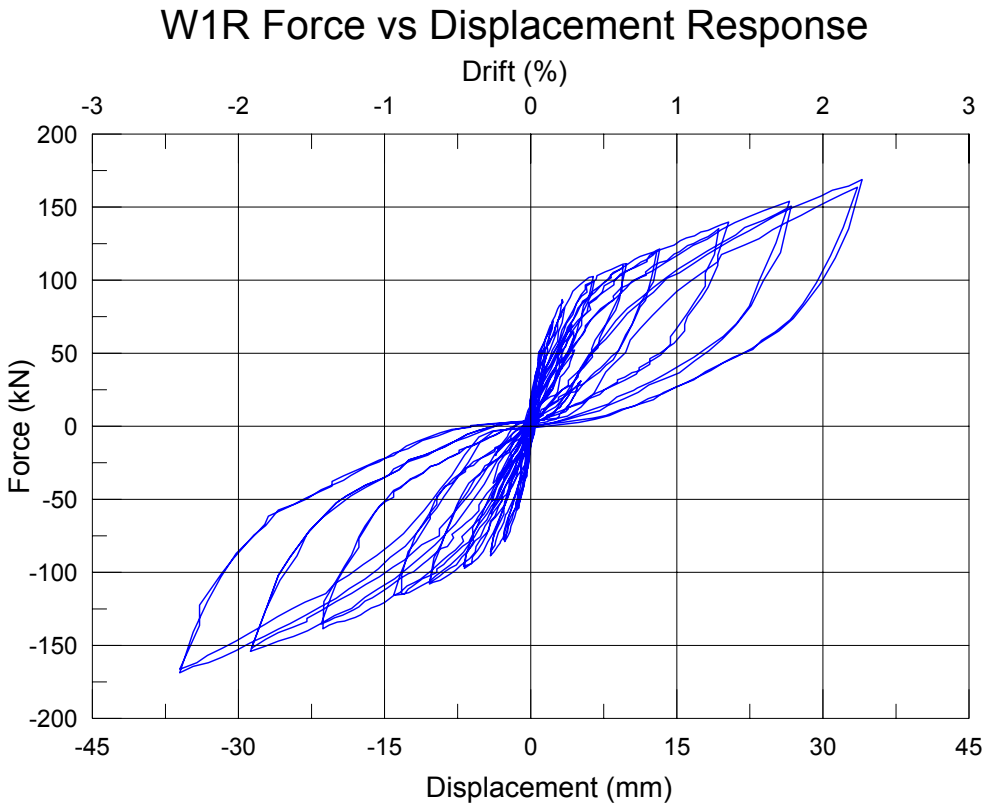

Figure 6-22: Force versus Displacement response, W1R, test #1

Sliding of the foundation block relative to the strong floor was observed. **Figure 6-23** shows the relative displacement between the foundation block and strong floor and it can be seen that the foundation block was sliding nearly 3.5mm in the negative direction whilst sliding less than 2mm in the positive direction.

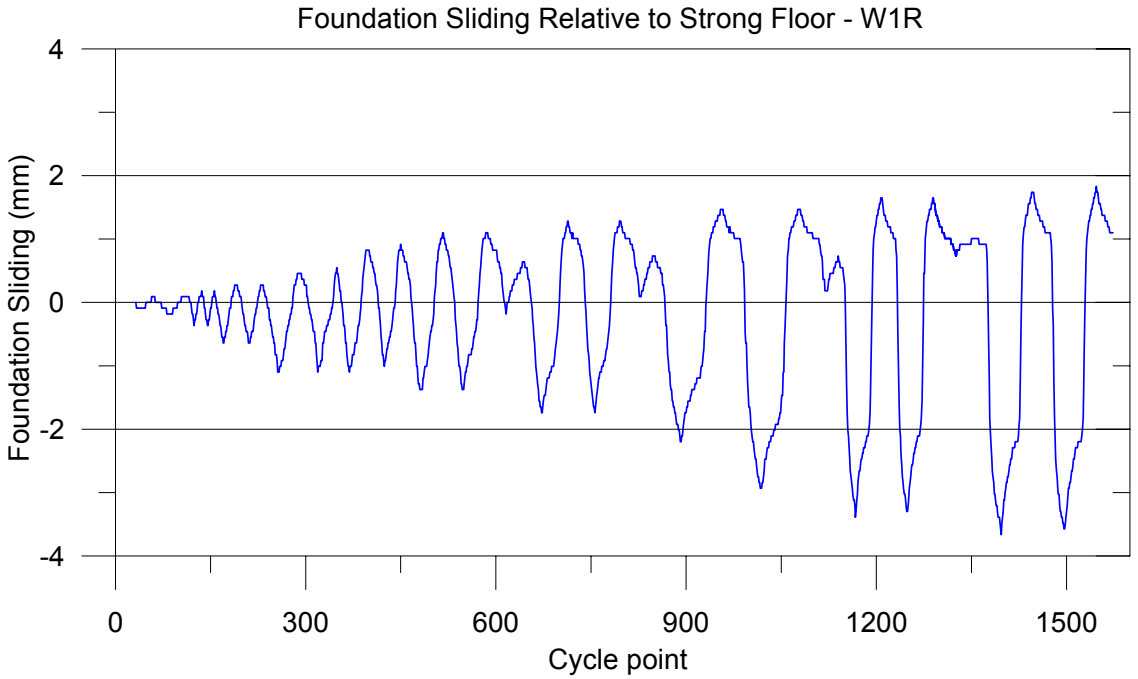

Figure 6-23: Foundation block sliding relative to strong floor, test#1

6.10.2 Un-bonded Post-tensioning Forces

An example of the cyclic change in post-tension force in one of the four post-tensioning cables, due to the lateral loading of the wall is shown in **Figure 6-24**. The post-tensioning force was measured directly by a load cell attached to each tendon and was also calculated from strain gauge readings. A good correlation between the post-tensioning forces measured directly by load cells and the measured strains was achieved.

An important feature shown in **Figure 6-24** was the substantial reduction of the initial post-tensioning force as the wall was cyclically loaded. An initial post-tensioning force of 40kN per tendon was used and by test completion this had reduced by nearly 50%, to just over 20kN per tendon. The reason for this loss was due to wedges used to lock off the cables slipping or bedding in, as the post-tensioning force increased (as the wall was laterally loaded). It can be seen that at peak response the post-tension force in each cable increased to

approximately 100kN per tendon. This was significantly higher than the initial post-tensioning force and highlights the need to initially overstress the tendons to avoid these losses. It was important to minimise the losses in the initial post-tensioning as it affected the walls ability to self centre.

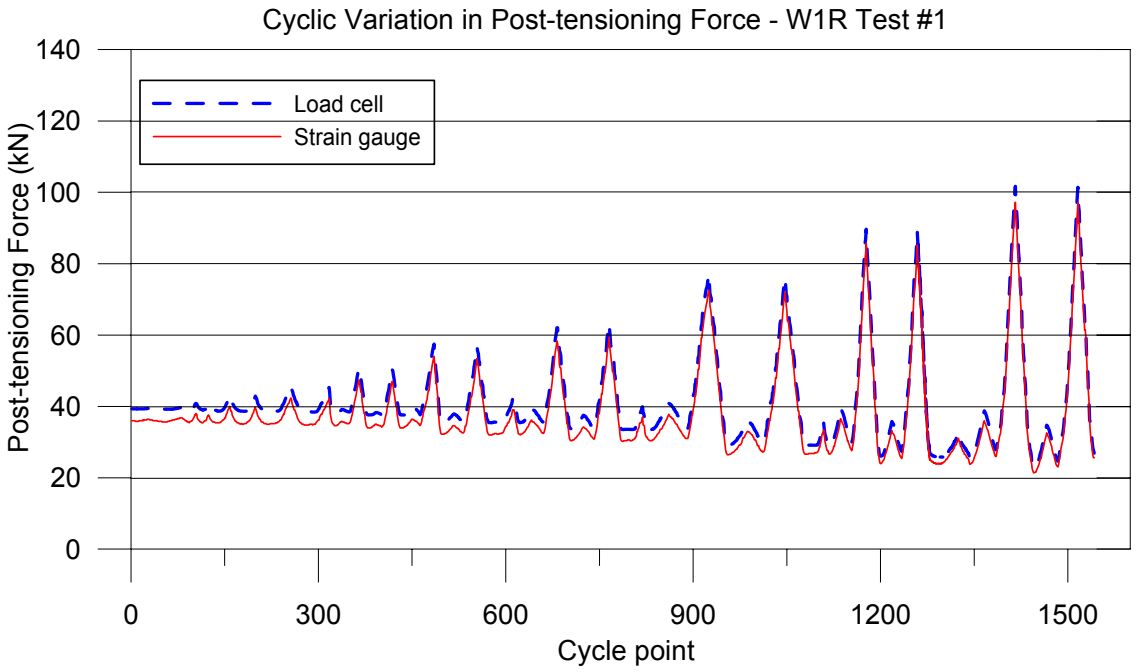

Figure 6-24: Example of the Change in post-tension force due to cyclic displacement, test #1

Figure 6-25 shows the post-tensioning force versus displacement for the four post-tensioning tendons in W1R. If there was no loss in the post-tensioning force during the test the plot would look like two equal and opposite condensed lines. Instead it can be seen that the plotted lines ratchet down after every cycle as a proportion of the initial post-tensioning was lost. From **Figure 6-25** it can also be seen that due to differing lever arms about the neutral axis (as the post-tensioning tendons were not centrally located), as the wall rocks and a gap opens the increase in the post-tensioning force in the tendons was substantially greater in one direction than the other. The post-tensioning tendon was located relatively close to the neutral axis position in one direction as there was only a moderate increase in the post-tensioning force as the wall was laterally loaded.

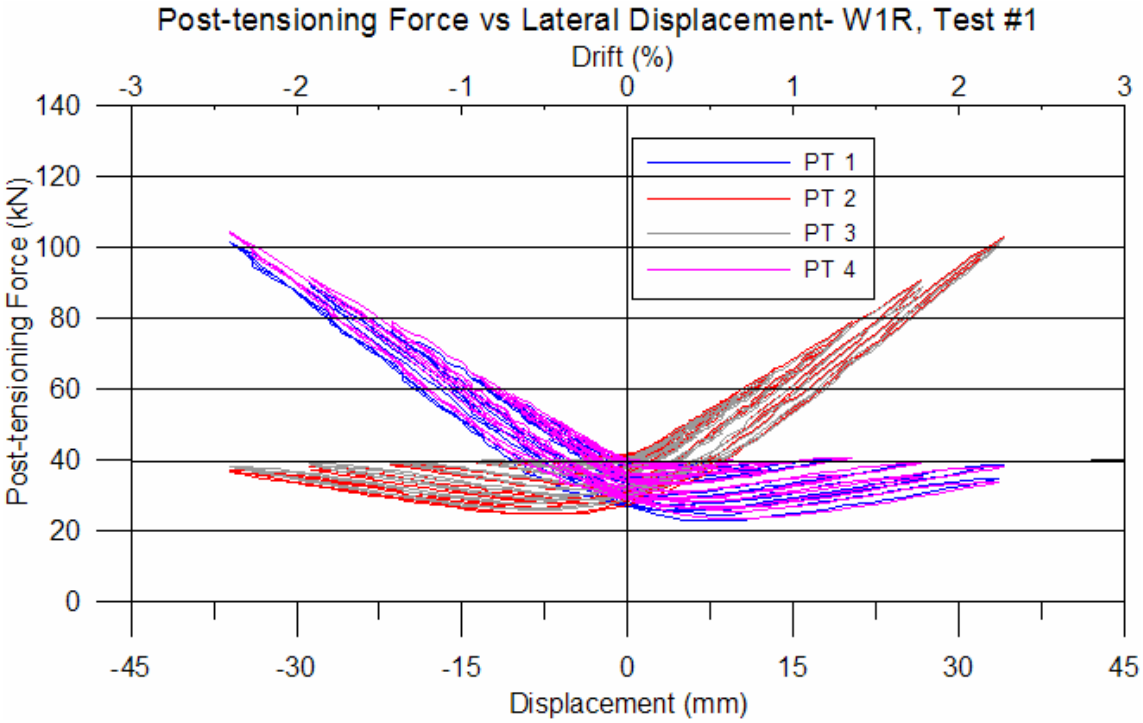

Figure 6-25: Post-tension force versus wall lateral displacement, test #1

6.10.3 Dissipater Displacement Demand

The displacement demand acting on the dissipaters was measured by a potentiometer extending between the two dissipater mounts. An example of the displacement profile that the dissipaters were subjected to is shown in **Figure 6-26**. Due the dissipaters not being located at the centre of the wall it can be seen that the displacement demand peaks vary between positive and negative cycles. This also shows that the dissipaters were always loaded in tension as the wall rocked in either direction.

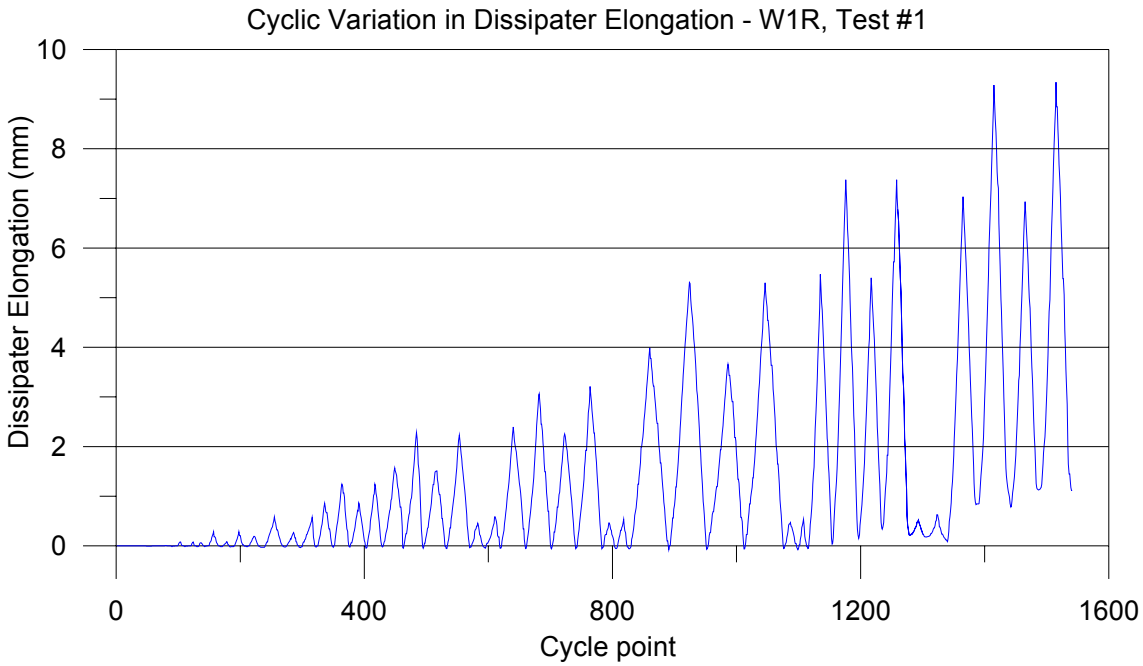

Figure 6-26: Displacement demand on dissipater, test #1

From **Figure 6-26** it can be seen that the peak displacement demand on the dissipaters was approximately 9.5mm, this was slightly less than the estimated 12.6mm used for the dissipater test but was well within the ultimate expected capacity of the dissipater. Another import feature was that in the final cycles the dissipater elongation profile was not returning to zero. It can be seen that there was (under static loading) approximately 1.0mm residual (static) displacement. This meant that the wall was not fully re-centring and that there would be a residual displacement within the wall at test completion. The reason for the residual displacement was due to a loss of nearly half of the initial post-tensioning force during the test, which was discussed in the previous section.

6.10.4 Vertical Displacement at Base of Wall & Base Rotation

Elongation of the linear potentiometers at the base of the wall were used to determine the neutral axis position and the percentage of the total displacement relating to the rotation at the base of the wall. **Figure 6-27** and **Figure 6-28** show the extension of the potentiometers at the base of the wall versus their position along the length of the wall, for the negative and positive drift cycles respectively. A line plotted between the two data points (from the potentiometer extension) was extrapolated to determine the neutral axis position and the slope was equal to the rotation at the base of the wall. For the negative loading direction the neutral axis varied

between 160-190mm (0.15-0.18 of the wall length) between the 0.5-2.5% drift cycles and the rotation at the base account for between 80-95% of the total wall displacement. For the positive loading direction the neutral axis depth varied between 160-260mm (0.15-0.25 of the wall length) between the 0.5-2.5% drift cycles and the base rotation accounted for 90-99% of the total wall displacement. The remaining proportion of the total displacement would have been due to flexural deformation of the wall panel above the base and sliding of the wall panel and/or foundation.

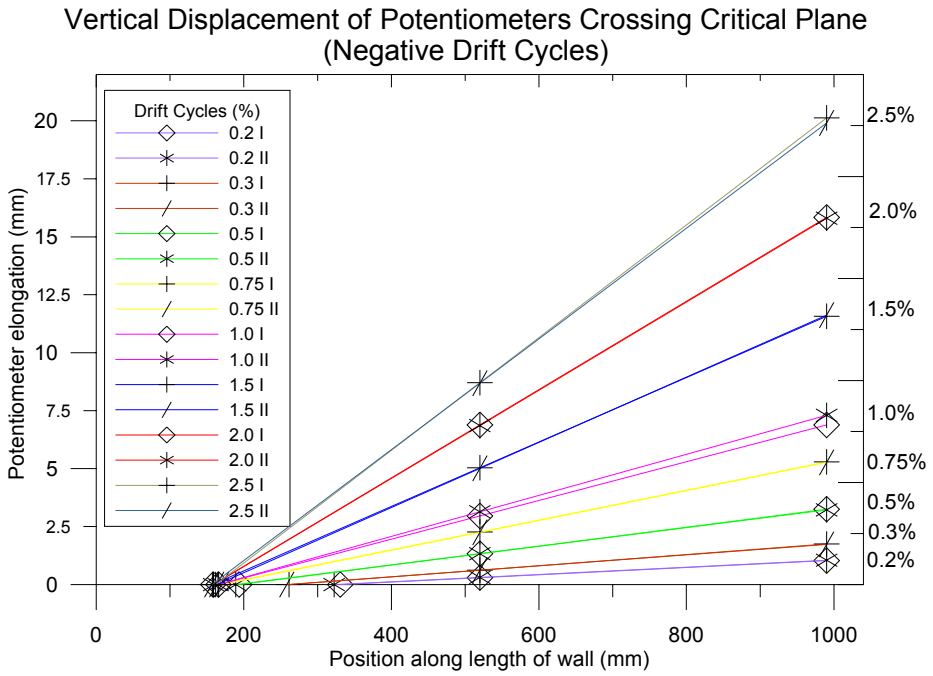

Figure 6-27: Elongation of potentiometers crossing the critical plane for negative drift cycles, test #1

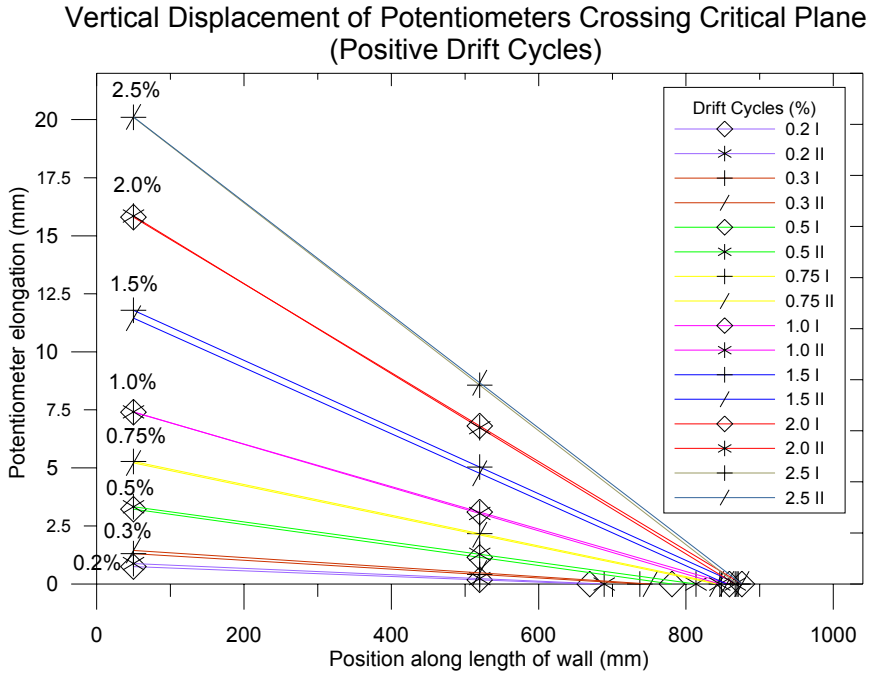

Figure 6-28: Elongation of potentiometers crossing the critical plane for the positive drift cycles, test #1

Figure 6-29 shows the average c/d versus lateral drift for the first hybrid test on W1R (assuming d=1020mm (length of wall)), for the negative and positive loading directions. The basic form of a c/d versus lateral drift diagram can be observed, with a general reduction in the c/d ratio as lateral drift increased. For both loading directions an asymptote of approximately at 0.15 c/d was observed.

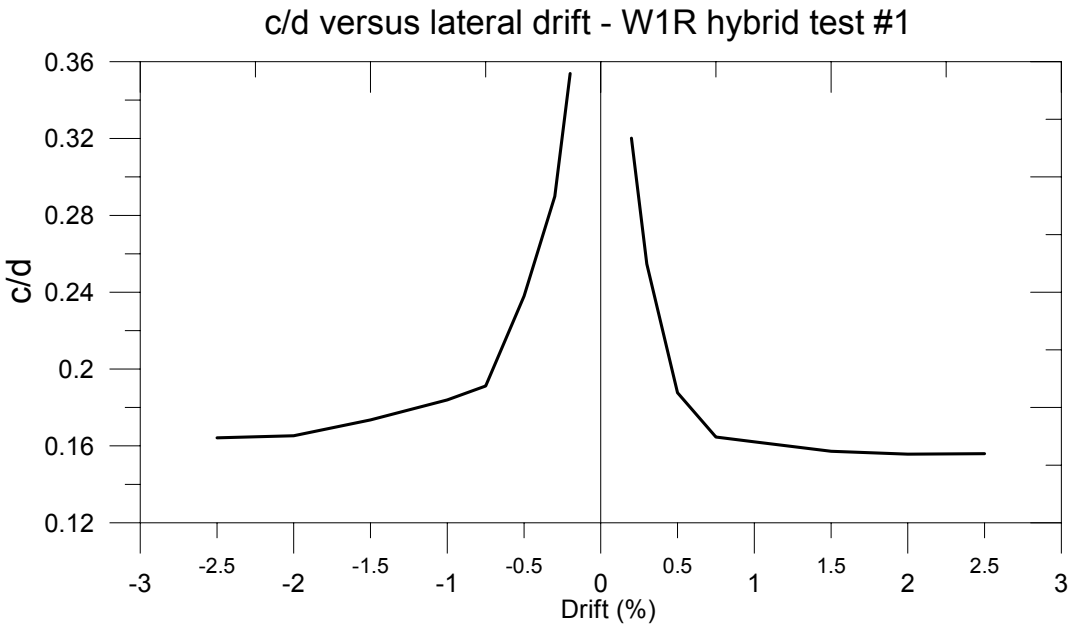

Figure 6-29: c/d versus lateral drift for W1R- 1st hybrid test

6.10.5 Equivalent Viscous Damping

The percentage of equivalent viscous damping present in the force versus displacement response of W1R (for the first and second cycles) was calculated and is shown verse lateral drift in **Figure 6-30** (5% elastic equivalent viscous damping is also included). A maximum of 14.9% percentage equivalent viscous damping was achieved on the second cycle at a drift level of 1.5% (second cycle considered to ensure that the hysteretic response had stabilised (Priestley, 2003)). This is reasonable for a rocking wall but less than what would be expected for an equivalent monolithic wall. After 1.5% drift the percentage of equivalent viscous damping degraded, this was due to the observed stiffness degradation in the force versus displacement response. The stiffness degradation also resulted in the second cycle exhibiting a slightly lower level of equivalent viscous damping. For comparison an estimate of the equivalent viscous damping was made using a combination of two equations for a post-tensioned wall and a monolithic wall (Priestley, 2003) (see appendix C). An approximate yield drift of 0.3% was assumed and it can be seen that the estimated equivalent viscous damping was slightly less than what was provided.

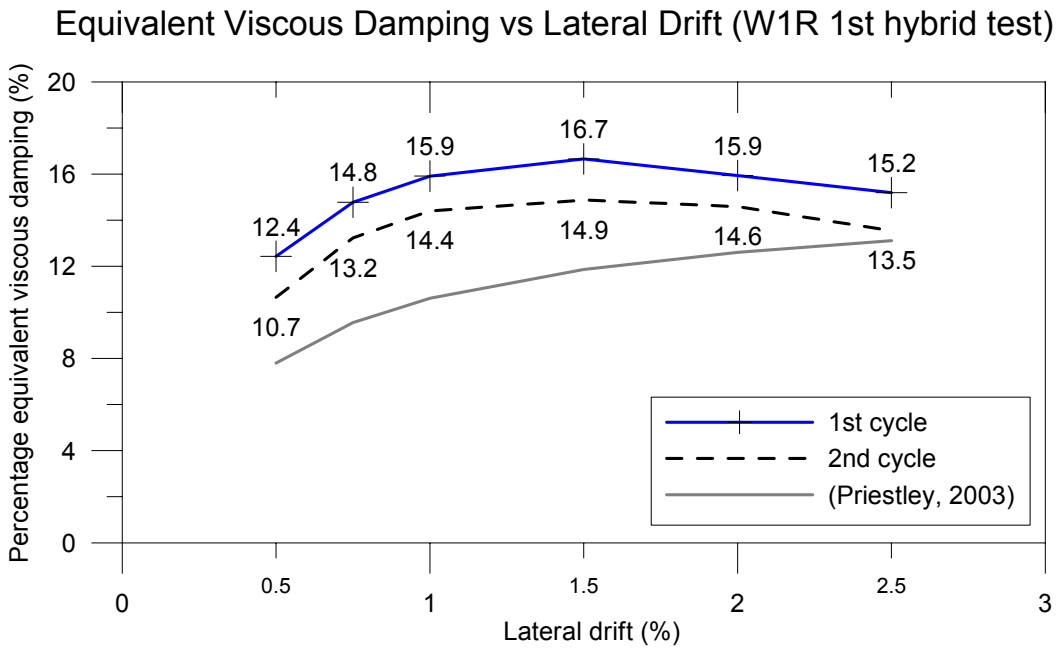

Figure 6-30: Equivalent Viscous damping versus drift, hybrid test #1

6.11 Results and Analyses - Test #2 (1st Post-tensioned only test)

This section discusses the results of the second test performed on W1R. The test was performed as a pure un-bonded post-tensioned only test (i.e. without any energy dissipaters), with an initial post-tensioning force of 40kN per tendon. The results include the force versus displacement and the variation in post-tensioning forces.

6.11.1 Force versus Displacement Response

The force versus displacement response for test #2 on W1R is shown in **Figure 6-31**. The resulting hysteresis loop was non-linear elastic, as would be expected because no energy dissipaters were included (the non linear nature was due to a geometric non-linearity not a material non-linearity). The non-linear elastic behaviour was not ideal (pure) due to sliding of the foundation block relative to the strong floor; this can be seen by comparing the max positive and negative displacements achieved.

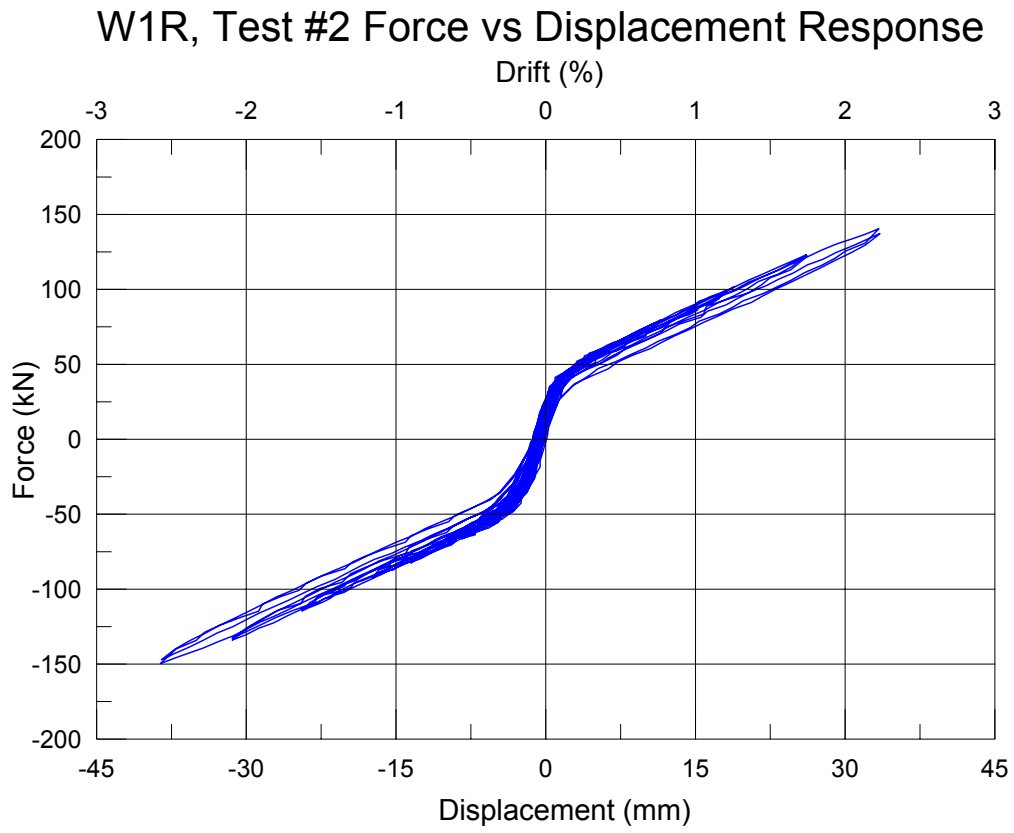

Figure 6-31: Force versus displacement response, test #2 (post-tensioned only)

Figure 6-32 shows the measured foundation block sliding relative to the strong floor. It can be seen that an offset occurred in the sliding occurs after the 300th cycle point, this was due to an attempt to restrict sliding of the foundation. As a result of the attempt to restrict foundation movement a permanent offset of approximately 2mm occurred, which led to a slightly asymmetrical hysteresis loop.

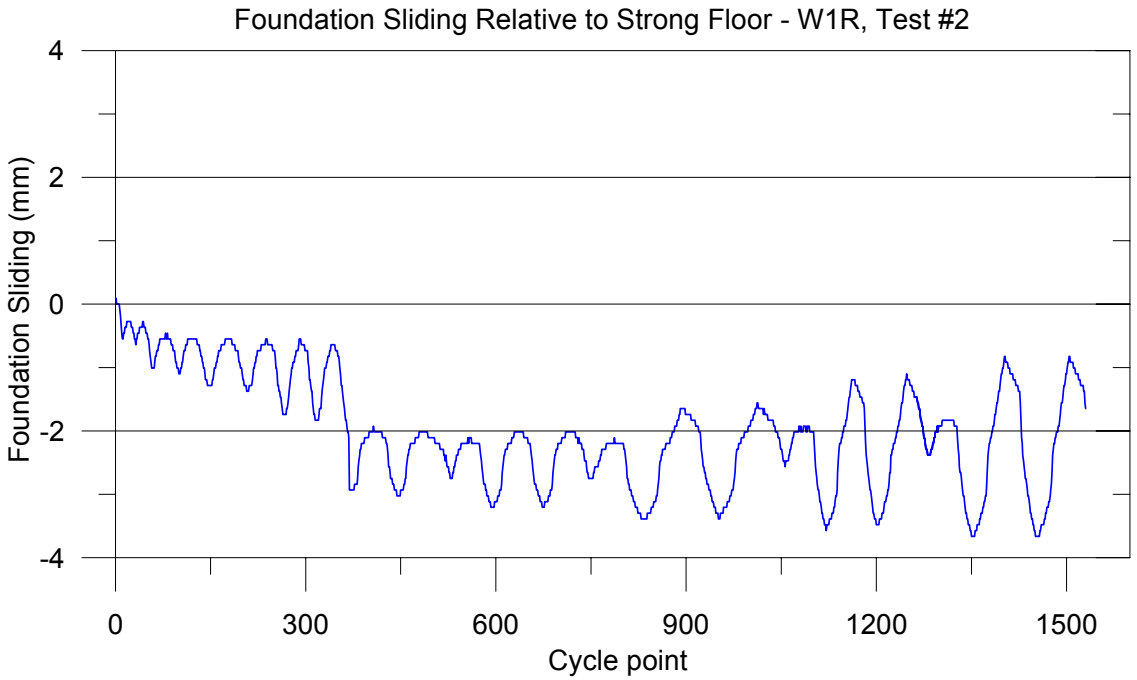

Figure 6-32: Foundation block sliding relative to strong floor, test #2

6.11.2 Post-tensioning Forces

The cyclic change in post-tensioning force in one of the four tendons due to the lateral displacement of W1R is shown in **Figure 6-32**. The peak tendon force achieved on the maximum drift cycle was 120kN which corresponds to 78% of yield. As with test #1 there was a substantial loss in the initial post-tensioning force by the end of the test. The loss was approximately 18% of the initial post-tensioning force. The loss was caused by the wedges (used to lock off the tendon) bedding in as post-tensioning force increased due to lateral loading. The max post-tensioning force achieved during test #2 was larger than the max post-tensioning force achieved during test #1. As the peak force achieved in the tendons increased from 100kN per tendon (max force experienced in test #1) to 120kN per tendon a further loss in the initial load was experienced.

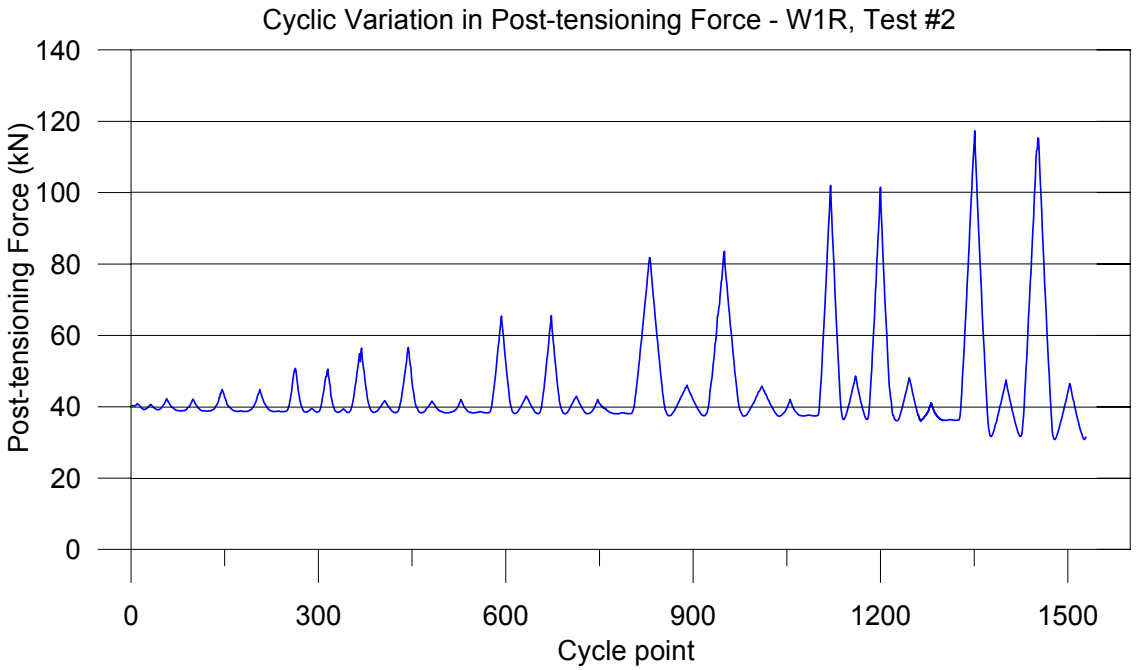

Figure 6-33: Change in post-tensioning force due to cyclic loading, test #2

Figure 6-34 show the tendon force plotted against the lateral displacement of the wall for each of the four tendons. The loss of initial post-tensioning can be seen as the graph ratchets down as the test progressed.

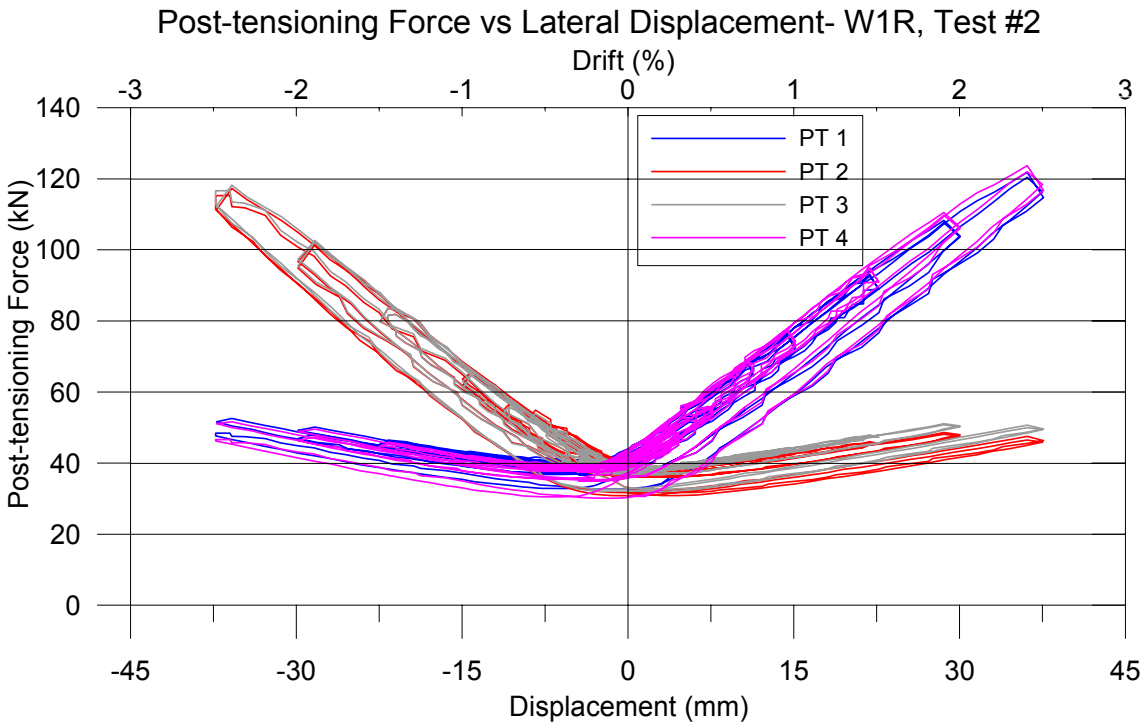

Figure 6-34: Post-tensioning force versus lateral displacement, test #2

6.12 Results and Analyses – Test #3 (2nd hybrid test)

The third test performed on W1R included energy dissipaters and was essentially the same as test #1. The test was performed in an attempt to improve the behaviour by eliminating post-tensioning losses, minimising foundation sliding and improving energy dissipater performance by reducing/eliminating buckling of the fuse length.

6.12.1 Force versus Displacement Response

The force versus displacement response for test #3 is shown in **Figure 6-35**. An improved flag-shaped hysteresis was achieved with negligible residual displacements and minimal stiffness loss as the test proceeds. Minimal losses in the initial post-tensioning force resulted in a peak force increase when the wall experienced its maximum drift. This increased from 170kN for test #1 to 190kN for test #3. The initial stiffness of was substantially less than that achieved during the test #1 on W1R, which was due to the repeated testing of W1R.

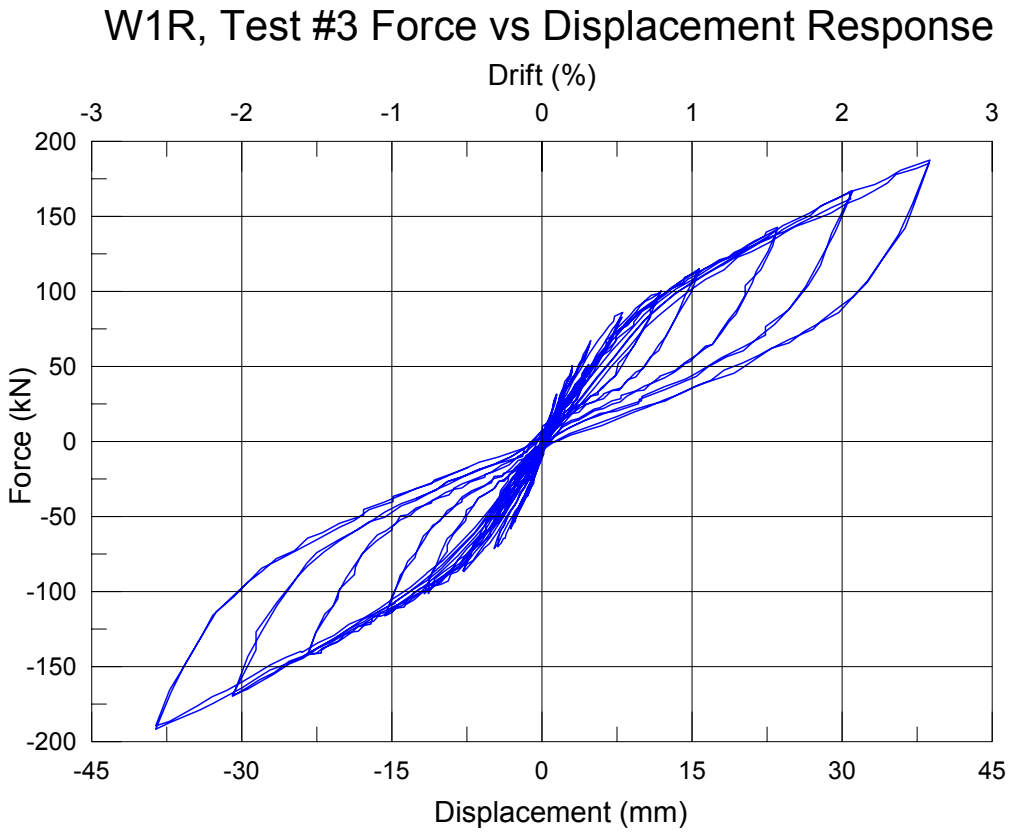

Figure 6-35: Force versus displacement response, test #3 (2nd hybrid)

Foundation block sliding relative to the strong floor is shown in **Figure 6-36**. An attempt to restrict the movement experienced in the first two tests performed on W1R minimised the foundation sliding to a maximum of approximately 2mm.

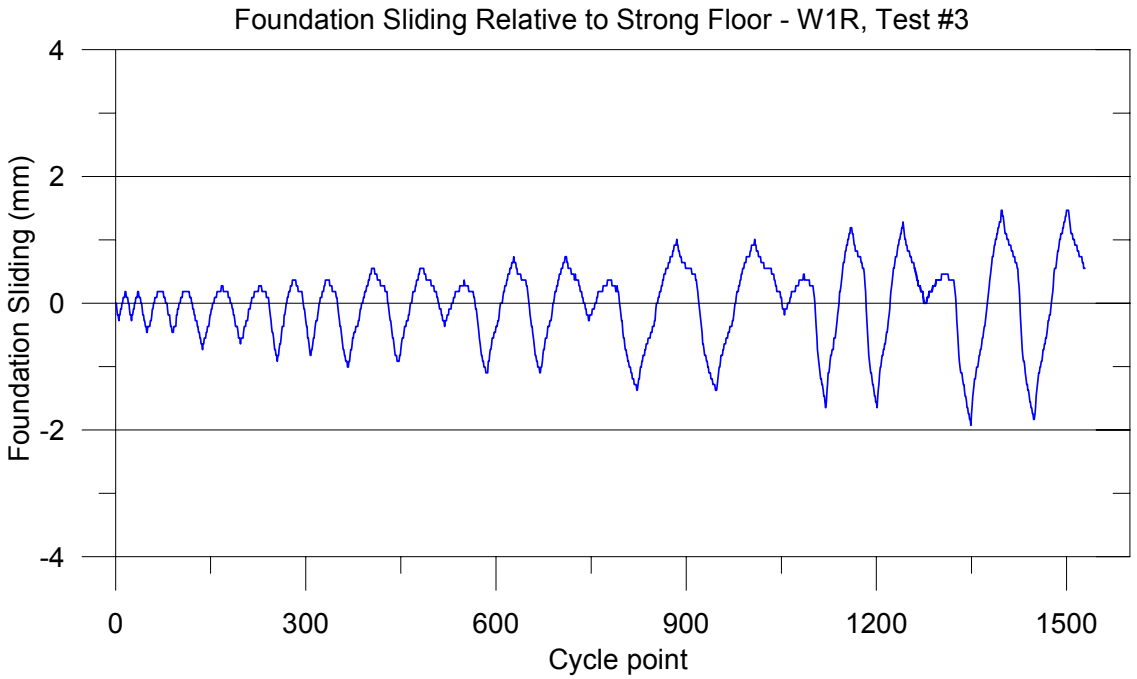

Figure 6-36: Foundation sliding relative to strong floor, test #3

6.12.2 Post-tensioning Forces

Figure 6-37 shows the cyclic change in post-tension force of one of the tendons, as the wall was subjected to lateral loading. A peak post-tensioning force of approximately 120kN was achieved which corresponded to about 78% of yield. Only a minimal loss in the initial post-tensioning force was experienced by the end of the test, which corresponded to about 5% of the initial post-tension force.

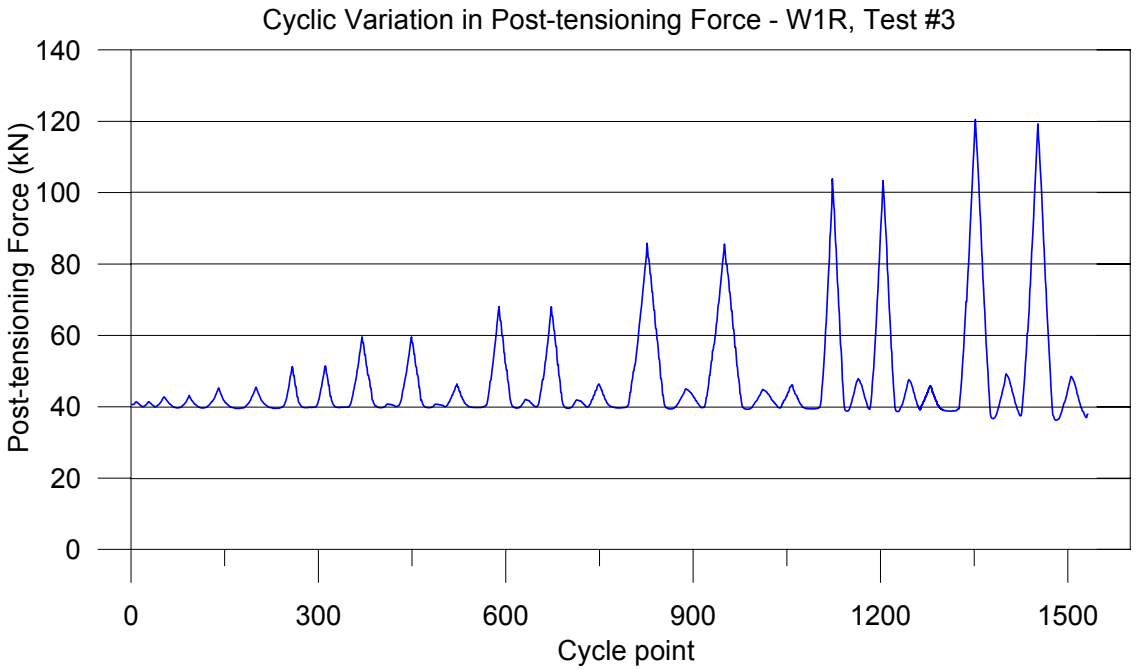

Figure 6-37: Cyclic change in post-tension force, test #3

Figure 6-38 show the post-tensioning force versus wall lateral displacement for the four post-tensioning tendons. Condensed lines were formed as the wall was cyclically loaded, without the ratchet effect which was experienced in the previous tests, as a proportion of the initial post-tensioning force was lost with each cycle.

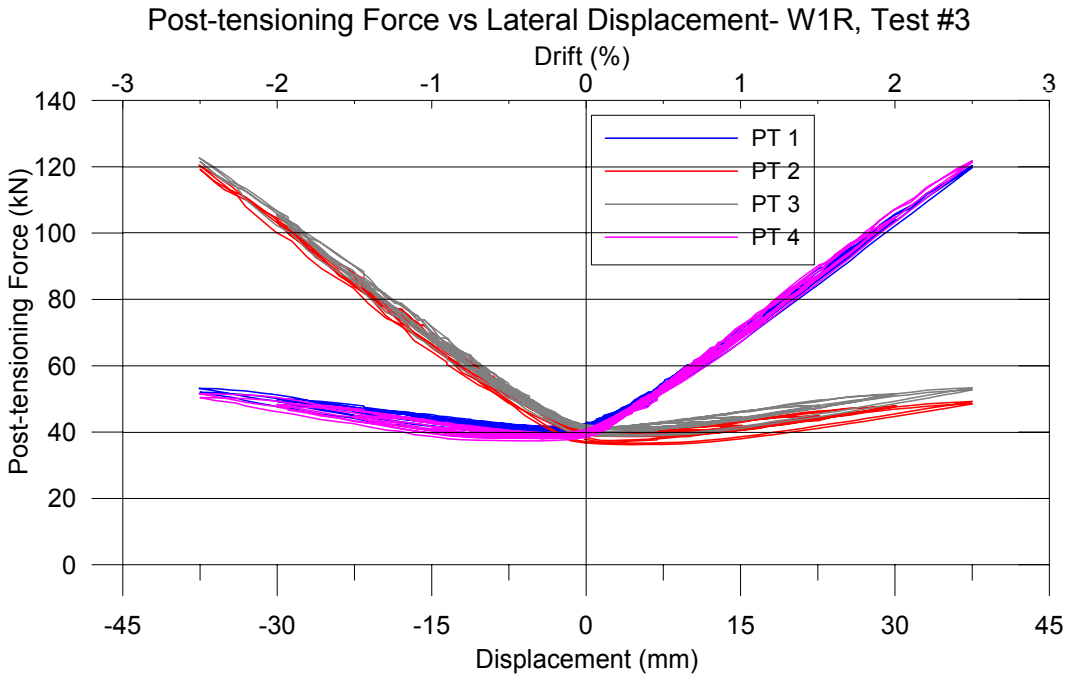

Figure 6-38: Post-tensioning load versus lateral displacement, test #3

6.12.3 Dissipater Displacement Demand

The displacement demand experienced by the dissipaters was measured by a potentiometer extending between the dissipater mounts. **Figure 6-39** shows the measured displacement demand of one of the dissipaters, which reached a peak displacement of 8.5mm. It can be seen that full re-centring was achieved as the dissipater displacement returned to zero at the end of the test; this was not achieved in the first dissipater test due to a substantial loss in the initial post-tensioning.

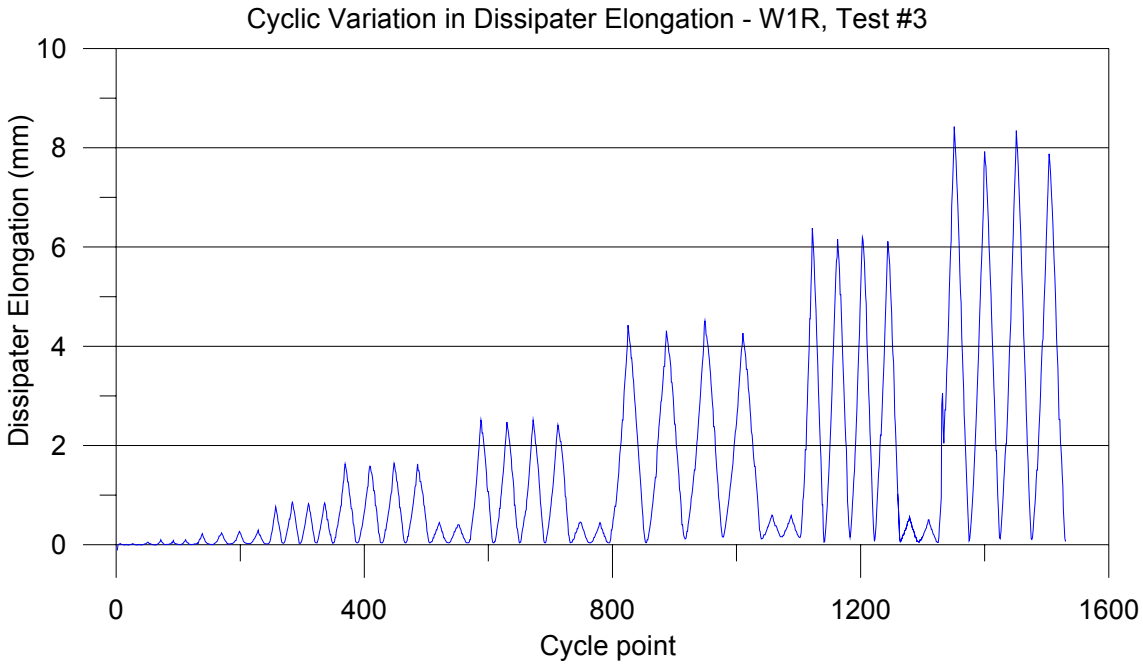

Figure 6-39: Dissipater displacement demand, test #3

6.12.4 c/d versus Lateral Drift

Figure 6-40 shows the average c/d versus lateral drift for the second hybrid test on W1R (assuming d=1020mm (length of wall)), for the negative and positive loading directions. The basic form of a c/d versus lateral drift diagram can be observed, with a general reduction in the c/d ratio as lateral drift increased. For both loading directions an asymptote of approximately at 0.15 c/d was observed

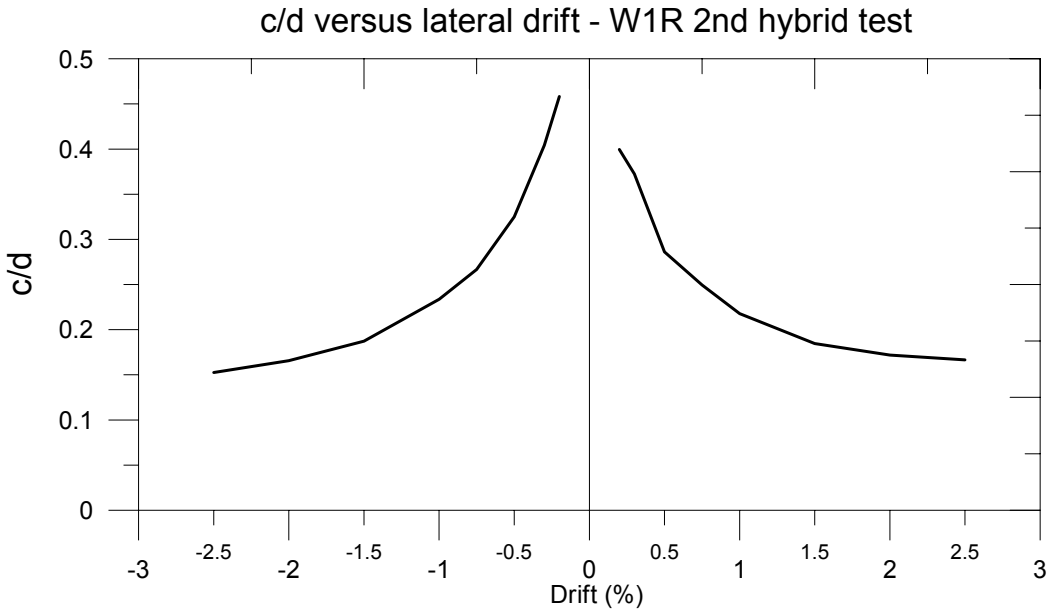

Figure 6-40: Average c/d versus lateral drift for the 2nd hybrid test on W1R

6.12.5 Equivalent Viscous Damping

Equivalent viscous damping versus drift for test #3 (2nd hybrid test) is shown in **Figure 6-41**, for the first and second cycles to each drift level. A peak of approximately 14.2% equivalent viscous damping was achieved at 2.5% drift, on the second cycle. For test #1 (1st hybrid test) 13.5% equivalent viscous damping was achieved on the second cycle to 2.5% drift. No reduction in the percentage of equivalent viscous damping was observed after the 1.5% drift cycle as it was for test #1. However the peak percentage of equivalent viscous damping achieved on the second cycle in test #1 was 14.9% (at 1.5% drift) which can be compared to 13.9% for test #3 at 1.5% drift. The damping was less in test #3 as the stiffness of the wall has reduced as a result of W1R being tested multiple times. Also due to minimal stiffness degradation and minimal post-tensioning losses in test #3 the difference between the percentage equivalent viscous damping observed on the first and second cycles is negligible. As in section 6.10.5 the level of equivalent viscous damping provided was estimated. The yield drift was assumed to be approximately 0.4%.

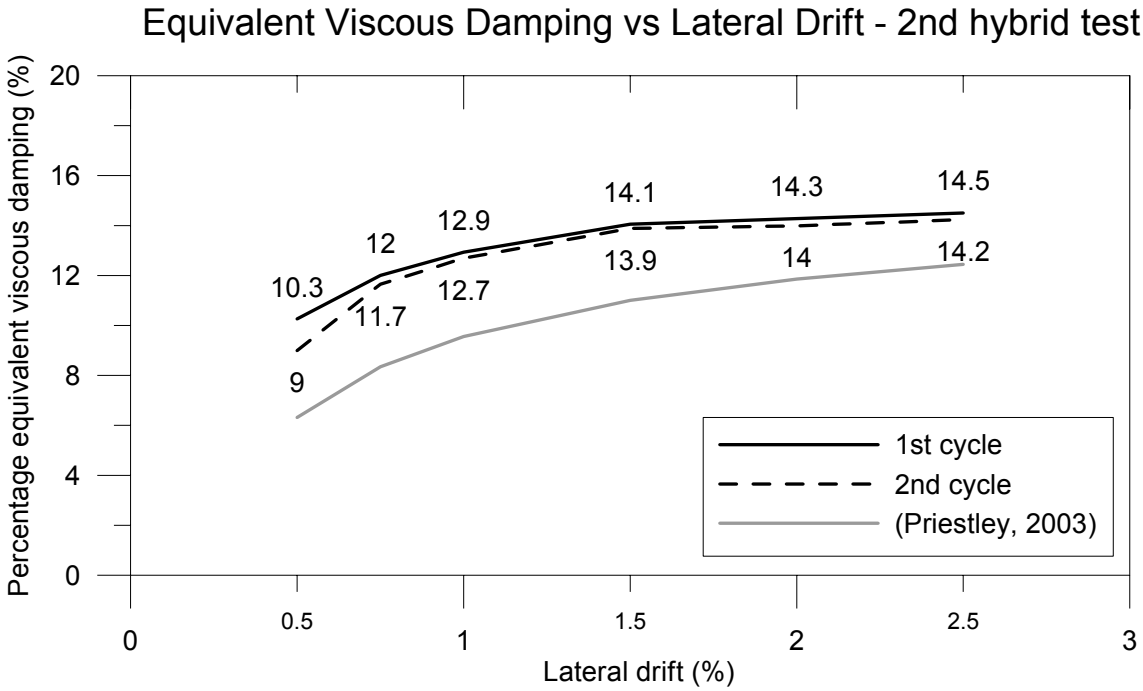

Figure 6-41: Equivalent viscous damping versus drift, test #3 (2nd hybrid test)

6.13 Results and Analyses – Test #4 (2nd Post-tensioned only Test)

A second post-tension only test was conducted on W1R to show that the wall can be subject to lateral loading a number of different times without suffering substantial damage. W1R was also re-tested to try and improve the performance by eliminating sliding between the foundation block and strong floor and to minimise losses in post-tensioning that were experienced in the first two tests.

6.13.1 Force versus Displacement Response

The force versus displacement response for test #4 is shown in **Figure 6-42**. A non-linear elastic hysteresis loop was achieved, which was more pure than that experienced in test #2. The improved performance was due to foundation block sliding being reduced along with losses in the initial post-tensioning force being minimised. The initial stiffness was substantially less that that of the test #2 due to the wall being tested multiple times.

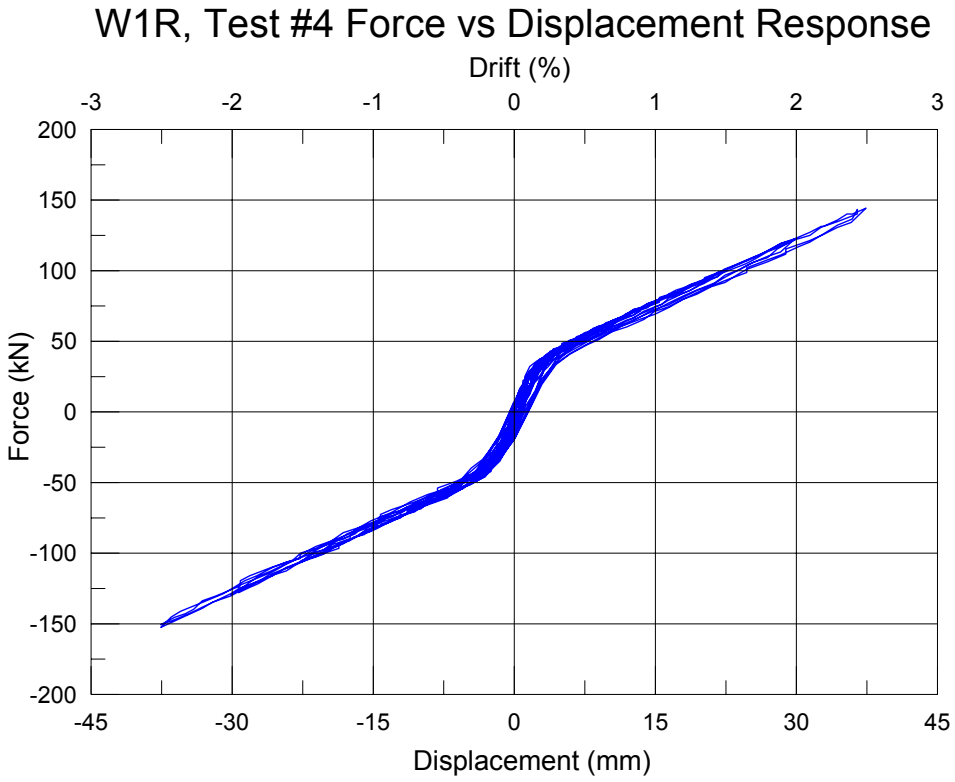

Figure 6-42: Force versus Displacement response, test #4

Figure 6-43 shows the relative sliding of the foundation block on the strong floor. A max of 2mm sliding was observed.

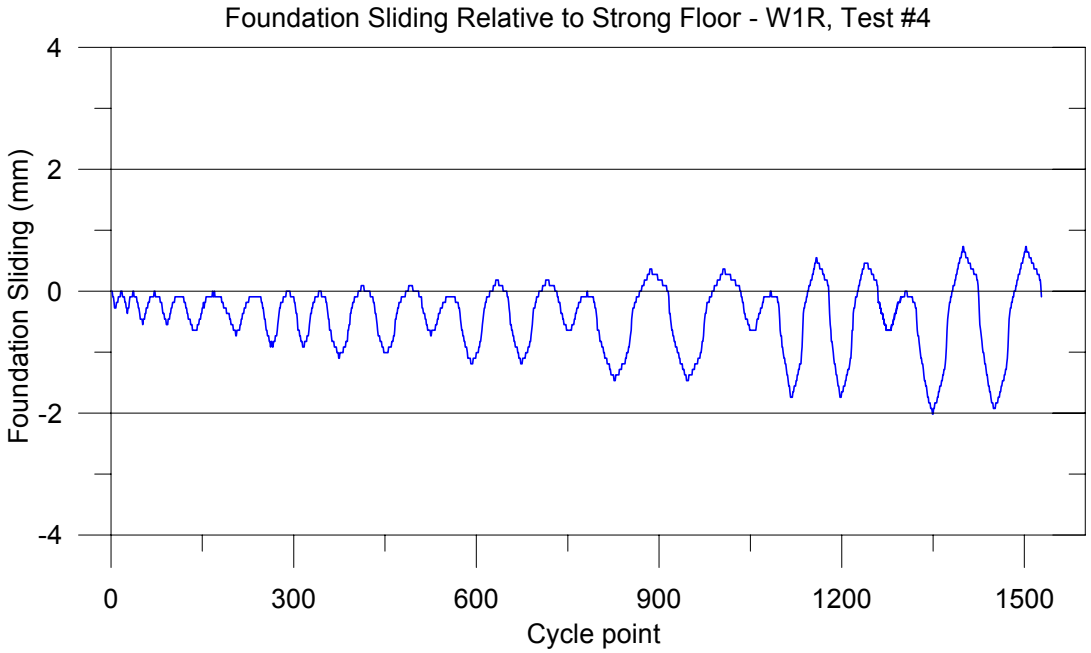

Figure 6-43: Foundation sliding relative to strong floor, test #4

6.13.2 Post-tensioning Forces

Figure 6-44 shows the change in post-tensioning force as the test progressed. Negligible losses in the initial post-tensioning force were observed.

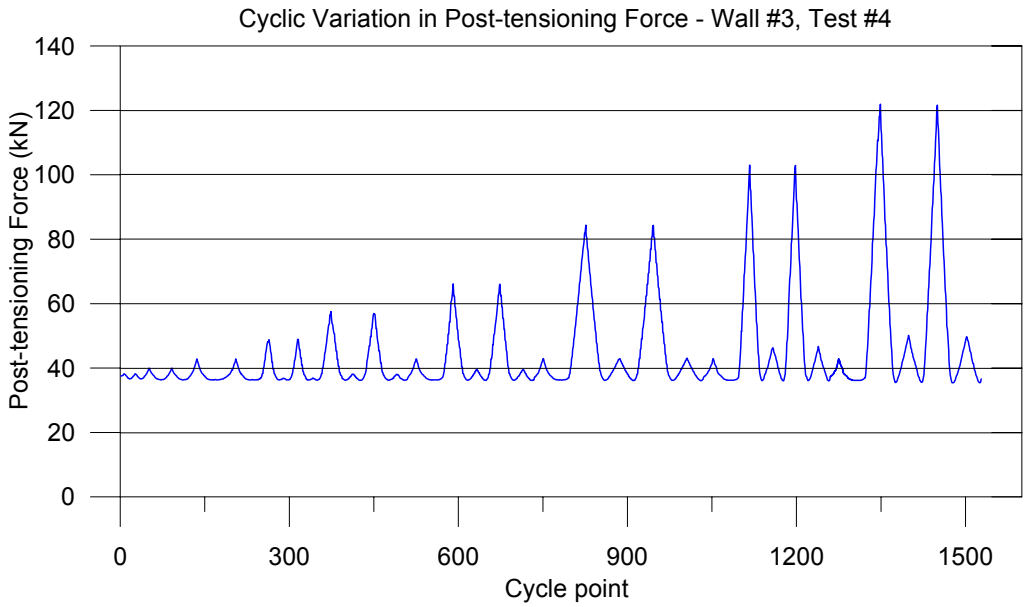

Figure 6-44: Post-tensioning force change due to lateral loading, test #4

Figure 6-45 shows the post-tensioning force in each tendon as the wall was cyclically loaded. The condensed lines show that minimal losses occurred as the wall was cyclically loaded.

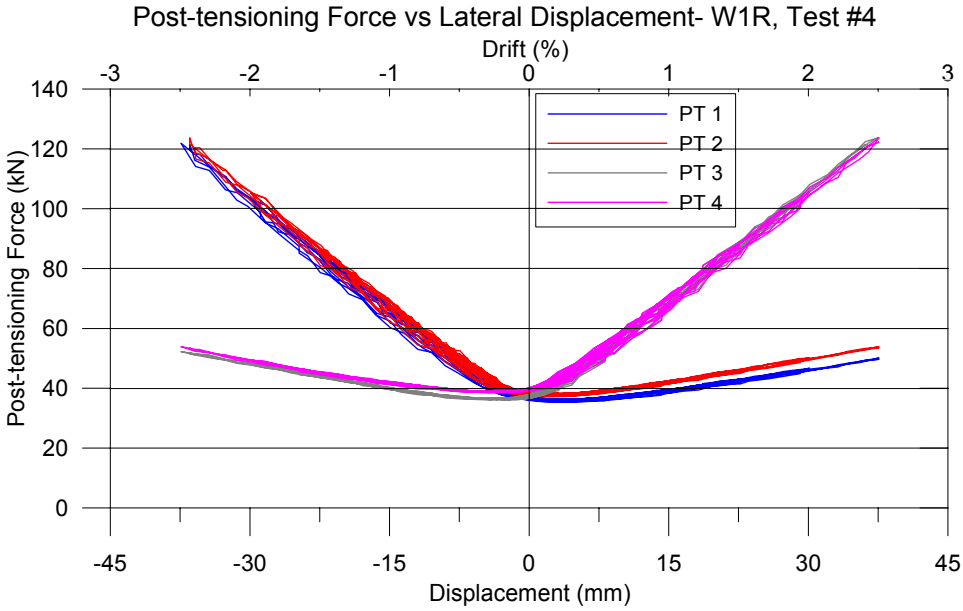

Figure 6-45: Change in post-tensioning load with wall lateral displacement, test #4

6.14 Analytical Experimental Comparison

In this section the predicted force versus displacement backbone curves calculated in section 6.7 (predictions) are compared to the experimental force versus displacement responses of the four tests performed on W1R.

Figure 6-46 compares the predicted force versus displacement response to the experimental response for test #1 and test #3 (hybrid) on W1R, which both included energy dissipaters. **Figure 6-46** (a) compares the predicted force versus displacement response to test #1. It can be seen that a very good estimate of the initial stiffness was achieved but that the peak strength was overestimated. The reason for the higher predicted strength was due to the loss of approximately 50% of the initial post-tensioning force by the end of testing. **Figure 6-46** (b) compares the experimental result of test #3 to the predicted response. A good estimate of the peak strength is achieved but the stiffness is substantially higher in the prediction. This shows that the stiffness of W1R reduced substantially from test #1 to test #3. The reduction in stiffness would be the result of two previous tests being performed on W1R, which must have caused minor damage.

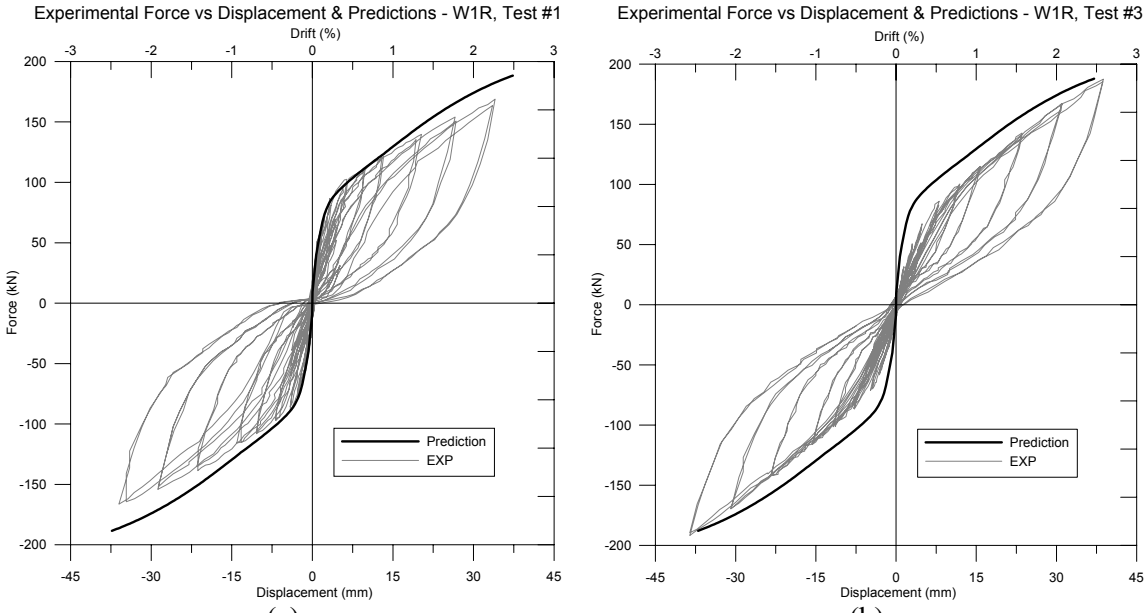

(a) (b)

Figure 6-46: Predicted versus Experimental response; (a) Test #1, (b) Test #3

Figure 6-47 compares the predicted force versus displacement backbone curve with test #2 and test #4 (post-tensioned only) on W1R, which were both post-tension only tests. **Figure 6-47** (a) compares the predicted response to test #2. It can be seen that the peak strength was

moderately overestimated; this was due to a loss of approximately 20% of the initial post-tensioning by the end of the test. Stiffness loss due to this being the second test performed on W1R would have also contributed to the experimental strength being less than the predicted strength. **Figure 6-47** (b) compares test #4 with the predicted response. The peak strength and non-linear point for test #4 were substantially overestimated by the predictions. This overestimate was believed to be the result of substantial stiffness loss to W1R being tested multiple times.

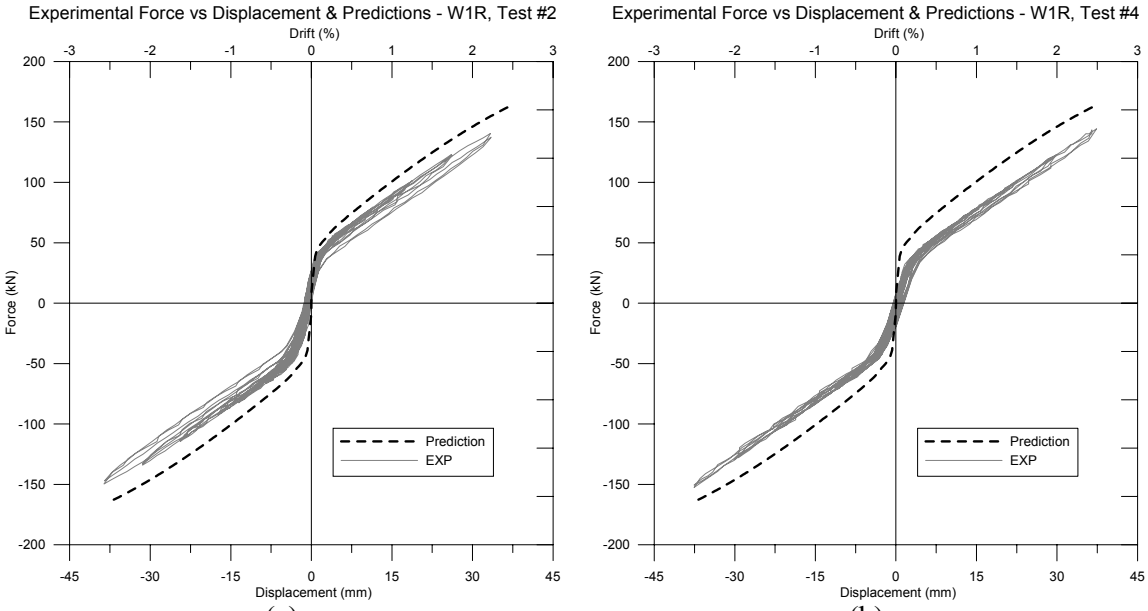

(a) (b)

Figure 6-47: Predicted versus Experimental response; (a) Test #2, (b) Test #4

References:

fib [2003], "Seismic Design of Precast Concrete Building Structures"

Marriott, D., Palermo, A. and Pampanin, S., [2006], "Quasi-static and Pseudo-dynamic Testing of Damage Resistant Bridge Piers with Hybrid Connections", First European Conference on Earthquake Engineering and Seismology, Geneva, Switzerland, Paper No. 794.

Palermo, A. [2004], "The use of Controlled Rocking in the Seismic Design of Bridges", Ph.D Dissertation, Technical University of Milan, Italy.

Pampanin S., [2005], "Emerging Solutions for High Seismic Performance of Precast/Prestressed Concrete Buildings", Journal of Advanced Concrete Technology (ACT), *invited paper* for Special Issue on "High performance systems", Vol. 3 (2), pp. 202-223

Priestley, M.J.N., [2003], "Myths and Fallacies in Earthquake Engineering, Revisited", IUSS Press, Pavia, Italy.

Priestley, M.J.N., Sritharan, S., Conley, J.R. and Pampanin, S., 1999 "Preliminary Results and Conclusions From the PRESSS Five-Storey Precast Concrete Test Building", PCI Journal, Nov-Dec 1999.

SNZ. [2006] "Concrete Structures Standard" NZS 3101:2006, Volume 1 Code of Practice and Volume 2 Commentary. Standards New Zealand, Wellington.

7 W2R - Selective Weakening Retrofit of a W2 Equivalent

7.1 Introduction

This Chapter discusses the development, testing and results of W2R, which was a selectively weakened equivalent of W2 (discussed in Chapter 5). Presented here are the details of the retrofit solution, experimental set-up, test observations and measured results.

7.2 Benchmark Specimen Summary – W2

W2 acted as the benchmark for the selective weakening retrofit of W2R. W2 was deliberately design to failure in shear, with the purpose of providing a severe scenario of a wall requiring retrofit. The behaviour of W2 was governed by large diagonal tension cracks (shear failure) which extended from corner to corner across the wall panel, in both directions. Severe degradation of the hysteretic response was observed and with the level of damage sustained, W2 would be considered as no longer capable of providing gravity or lateral load carrying capacity. Details of the construction, testing and results of W2 can be found in Chapter 5.

7.2.1 Retrofit Objectives

The main objective for the retrofit solution used for W2R was to alter the inelastic mechanism from shear to flexure, to ensure that after an inelastic response the wall can still provide adequate gravity carrying capacity. It was expected that W2R would contribute to the lateral load resisting system but that further lateral resistance would have to be provided other elements. The retrofit was aiming to improve the displacement capacity of W2R to allow it to sustain lateral displacements without loss of gravity carrying capacity. The magnitude of the lateral displacements would be governed by other elements in the lateral load resisting system and W2R be expected to be able to achieve the expected displacements.

7.3 Retrofit Configuration and Components

The retrofit solution for W2R was implemented on a wall equivalently detailed and constructed as W2. The retrofit involved a vertical saw cut to segment W2R into two wall segments acting in parallel. The decision to use this retrofit approach was based upon trailing a vertical cut for the development of selective weakening techniques. Details of other considered and possibly more suitable retrofit solutions for W2R are discussed in Chapter 8.

The retrofit solution involving a vertical cut served to highlight problems that need to be overcome to implement such a solution, as well as the effects it has on the wall behaviour. The benefits of using such an approach were that the slenderness of the wall was increased, the displacement capacity improved and the existing longitudinal reinforcement could be relied upon to provide energy dissipation by the means of flexural hinging. W2R was altered into a wall system consisting of two adjacent wall segments, but due to W2R having a large proportion of boundary element reinforcement the two wall segments exhibited asymmetric behaviour.

The selective weakening retrofit resulted in two equal but mirrored wall segments. A further degree of weakening was applied to one of the wall segments (involving partially severing boundary element reinforcement) so that more information could be gathered from a single test. One of the wall segments had the boundary element reinforcement partially severed by a horizontal saw cut. This was to lower the moment capacity of the wall segment, as the large proportion of boundary element reinforcement was going to result in a concrete compression failure. A concrete compression failure was considered to be more acceptable than a shear failure, though still to be avoided. From here on W2Ra will be used to describe the wall segment with the boundary element reinforcement partially severed and W2Rb will be used to describe the other wall segment with the boundary element reinforcement still in place.

Due to the vertical saw cuts all of the existing transverse reinforcement was severed, which meant that the shear capacity had to be reinstated to ensure a flexure dominated behaviour. The complete retrofit solution for W2R involved a combination of saw cutting, fibre reinforced polymers FRP, steel confinement armour and un-bonded post-tensioning. The details of each of these components are discussed in the following sections and the resulting retrofit solution is shown in **Figure 7-1**.

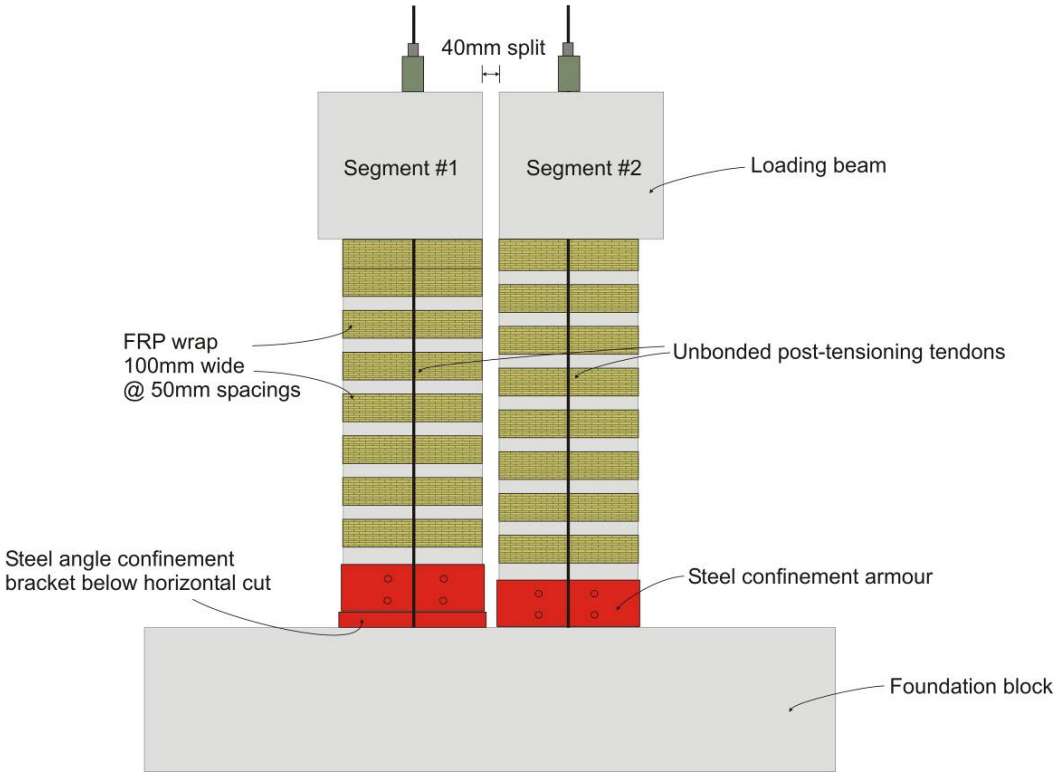

Figure 7-1: W2R selective weakening retrofit configuration

7.3.1 Saw Cuts

To achieve the selective weakening retrofit solution by segmenting the wall, two parallel vertical saw cuts 40mm apart were used. The saw cuts were made by a conventional concrete cutting saw and the cutting in progress can be seen in **Figure 7-2** (a). The two parallel cuts passed completely through the thickness of the wall panel and loading beam, resulting in two adjacent cantilever walls, as shown on the right in **Figure 7-2** (b). Two parallel vertical cuts were made at a spacing of 40mm to allow room for the FRP (used to reinstate shear capacity, discussed in more detail in the following section) to be applied.

In addition to the vertical cuts, one of the wall segments had its boundary element reinforcement partially severed by a horizontal saw cut. The horizontal cut made near foundation level, severed 2 HD16 and 2 HD12 reinforcing bars (leaving 2 HD16). The horizontal cut was 100mm in length, but as with the horizontal cut of W1R (Section 6.3.1) it had to be made at a height of 50mm above the wall-foundation interface (due to geometric constraints relating to the concrete cutting saw). Once the horizontal cut was complete the cut was filled with grout to provide a bearing surface for when the region was in compression. In an attempt to induce a rocking plane at the height of the horizontal cut the remaining portion

of wall was etched to a depth of 10mm. This introduced the possibility of inducing a stress concentration at the horizontal cut level which will be discussed in more detail in a later section.

(a) (b)

Figure 7-2: (a) W2R vertical saw cutting in progress; (b) W2R segmented

7.3.2 Fibre Reinforced Polymers (FRP)

Fibre Reinforced Polymers (FRP) were used to reinstate the shear capacity of the walls segments due to the vertical saw cuts severing the transverse reinforcement. The FRP applied was Sikawrap 100G which consisted of a unidirectional glass fibre matrix, the product details and design specifications can be found in appendix C. A single layer was applied in a banded nature, which formed external stirrups. The banded nature was used to reduce the quantities of FRP required, allowed inelastic action to be distributed up the wall.

Figure 7-3 shows the FRP application in progress. Firstly the wall segments were coated in a resin, and then resin impregnated FRP strips were applied to the wall. The strips of FRP were 100mm in width, and were spaced 50mm apart. The FRP served to provide shear resistance, prevent buckling of the reinforcing bars and provide confinement. Before the FRP was applied the corners of the concrete wall were rounded to a radius of 30mm.

Figure 7-3: FRP application in progress

7.3.3 Steel Confinement Armour

Due to the high concentration of reinforcement in the boundary elements, high compressive strains were expected in the toe region of the two wall segments. To prevent crushing and spalling of the concrete and bar buckling in these regions, steel confinement armour was provided at the base of the wall. The confinement armour consisted of 6mm thick by 150mm high steel plate, which formed a band around the base of the wall. Four 16mm bolts passing through the wall and confinement armour were used to improve confinement. The steel confinement armour was provided as a complete band around the base section of the wall due to the small geometry of the wall segments, had the wall segments been longer individual corner armour would have been provided (as for W1R, section 6.3.4). The confinement armour was deliberately made slightly longer that the wall to leave a void which could be filled with grout to ensure a tight fit. Steel armour was used at the base of the wall instead of FRP as it was simpler to achieve a higher level of confinement. By using steel plates holes could be drilled through steel plate and wall to allow bolts to be passed through, this is difficult to implement when using FRP.

Due to the high concentration of boundary element reinforcement and therefore high concrete compressive stresses the concrete above the steel confinement armour could crush in between

the FRP bands. This was particularly likely for W2Rb, for which the boundary element reinforcement had not been severed. This was unavoidable due to the large quantity of reinforcement, but the steel plate armour and FRP would prevent bar buckling which will minimise the negative side effects. A concrete compression failure was considered a more desirable failure than a shear failure, though it should be avoided where possible. This also serves as a good comparison to compare the effect of which severing the boundary element reinforcement had.

Another consideration was the possibility of the steel confinement armour causing a stress concentration in the longitudinal reinforcement if a single crack formed below the confining armour. This was thought as a high possibility for W2Ra as the horizontal cut provided a region for a stress concentration to develop. In fact a stress concentration was being induced by the concrete cover being etched along the horizontal plane for the rest of the wall length at the height of the horizontal cut. It was thought that the likelihood of the reinforcement rupturing would be reduced since the low concrete strength (20MPa) would allow significant strain penetration and the short wall length provides a short lever arm which reduces the expected strains in the reinforcement.

The region below the horizontal cut on W2Ra had to be confined to prevent crushing and spalling as the wall was cyclically loaded. The confinement was provided by a steel angle bracket which was anchored to the foundation block, as for W1R (section 6.3.4).

7.3.4 Un-bonded Post-tensioning

External un-bonded post-tensioning was provided by 7-wire tendons passing through ducts cast into the foundation and loading beams and externally down the sides of the wall panel. Two tendons were located near the centre of each wall segment and were loaded initially to 40kN per tendon, which was equivalent to the gravity loading used for W2 the benchmark specimen for this retrofit. The initial post-tensioning force was considered as acting a the gravity load, therefore it was assumed that in place the post-tensioning only provided an axial force when lateral displacement was applied.

7.3.5 Material Properties

Reinforcing Steel

Tension tests were performed on samples of the longitudinal and transverse reinforcement to accurately determine the stress-strain characteristics. **Table 7-1** summarises the average yield stress, ultimate stress and minimum ultimate strain experienced during the material tests.

Table 7-1: W2R reinforcement stress strain characteristics

Reinforcement	Bar size	f_y (MPa)	f_u (MPa)	$\varepsilon_{u(min)}$ (strain) x10^3
longitudinal	HD16	548	672	153
longitudinal	HD12	528	645	176
longitudinal	D10	326	449	172
transverse	R6	337	490	185

Concrete Cylinder Tests

Concrete cylinder tests were used to determine the concrete compressive strength achieved in W2. The specified concrete compressive strength was 20MPa, the average measured cylinder strength at 28 days was 16MPa. A test day concrete cylinder strength of 20MPa was achieved

7.4 Experimental Set-up

Quasi-static uni-directional in-plane testing was performed on W2R, with the two wall segments acting as separated cantilevers. The experimental set-up for W2R is shown in **Figure 7-4**, which shows the configuration of the hydraulic actuators and reaction frames.

Lateral loading was applied by two hydraulic actuators of 250kN capacity. One actuator was attached to each wall segment and they applied a displacement based loading regime which ensured the wall segments were subjected to the same displacement history. It was assumed that in a building the two wall segments would remain parallel when laterally loaded as they would be connected by a floor diaphragm. Out of plane movement of the wall segments was restricted by steel channels spanning between two reaction towers and passed down either side of the loading beam. Un-bonded post-tensioning was applied by two tendons in each wall segment. Each tendon was initially loaded to 40kN and then locked off.

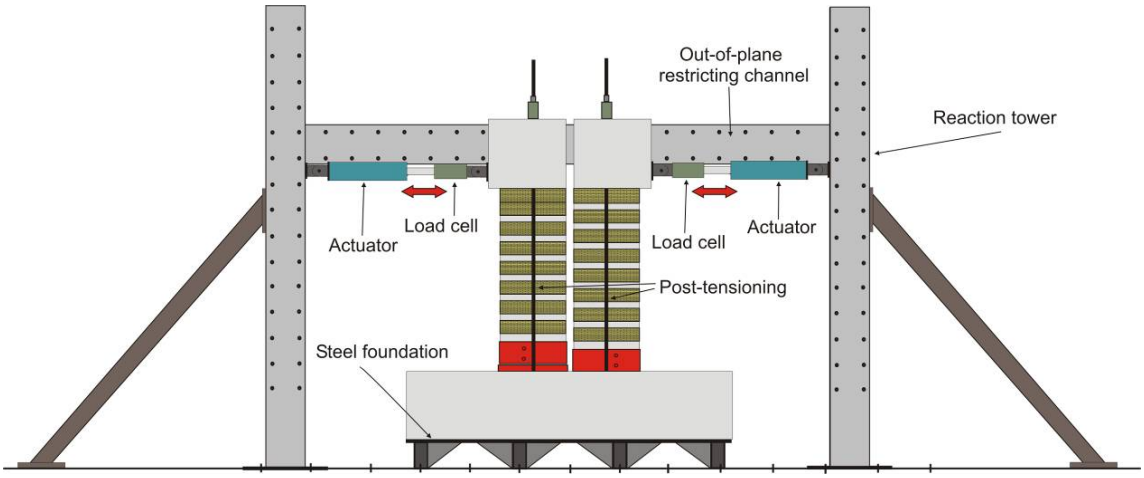

Figure 7-4: W2R Test set-up

7.5 Instrumentation Layout

A combination of linear potentiometers, rotary potentiometers, load cells and strain gauges were used to instrument the two wall segments of W2R, the instrumentation layout is shown in **Figure 7-5**.

On both wall segments shear deformations were monitored by three diagonal configurations of linear potentiometer, distributed up the height of the wall segments. Incorporated into the shear configuration were potentiometers used to monitor flexural deformations. At the base of the wall segments four linear potentiometer were used to monitor neutral axis position. Three rotary potentiometers were distributed evenly up the height of each wall segment to monitor the deformed shape and one rotary potentiometer was attached to the foundation block to measure sliding relative to the strong floor.

Load cells were attached to each actuator to measure the lateral load applied they were also attached to each post-tensioning cable to monitor the variation in post-tensioning as the test progressed. Strain gauges were also attached to the post-tensioning tendons to monitor strain development.

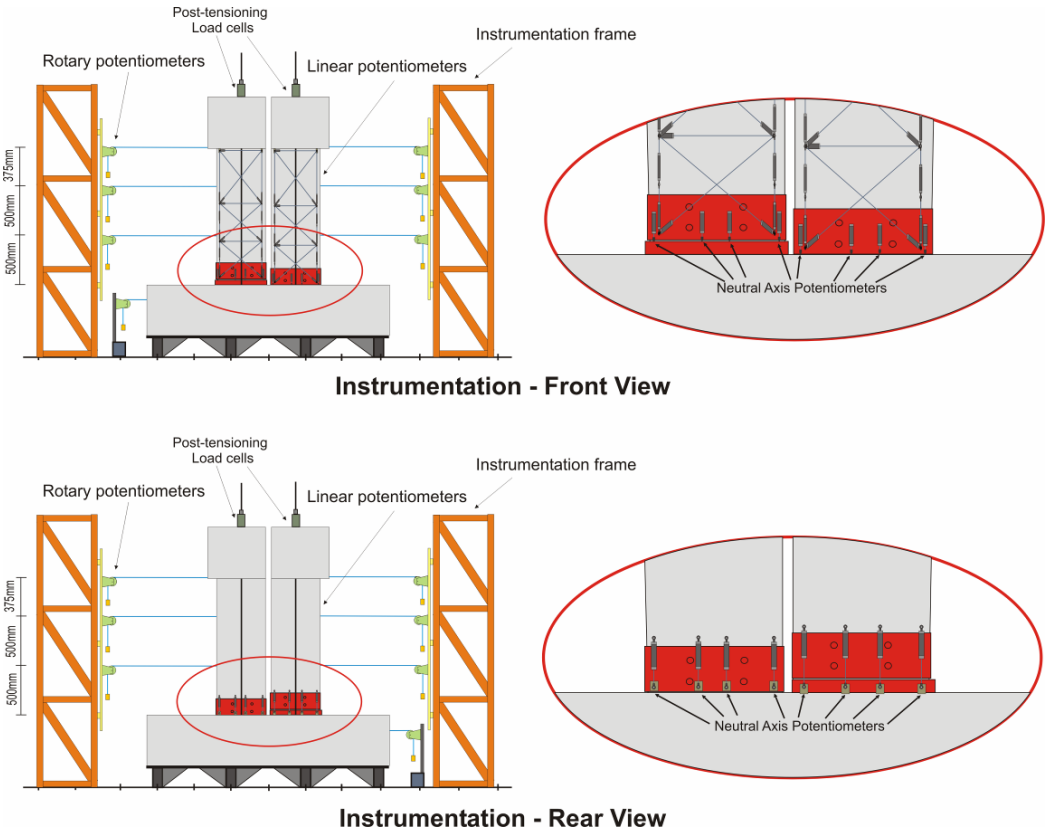

Figure 7-5: Instrumentation layout for W2R

7.6 Load Regime

A displacement based lateral loading history was used for W1R and is shown in **Figure 7-6**. The load history consisted of cyclically increasing displacement up to a peak drift level of 2.5%. The details of how the load history was determined are discussed in section 6.5.

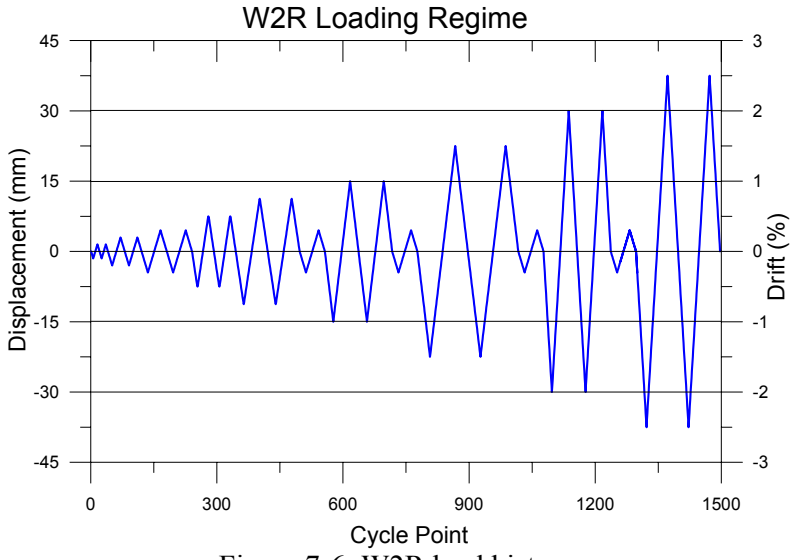

Figure 7-6: W2R load history

7.7 Damage Observations

Observations made during testing of the two wall segments of W2R are discussed in the following sections. The observations are discussed firstly for W2Ra and then for W2Rb.

7.7.1 W2Ra Observations

Observations made during testing of W2R in regards to W2Ra are discussed in this section. W2Ra was the wall segment which had the boundary element reinforcement partially severed by a horizontal saw cut near foundation level.

Significant observations made during testing of W2Ra are discussed in the following bullet points:

- 0.2% drift cycles, first cracking noticed on the internal edge (vertical cut region) of the wall between the steel confinement armour and first FRP band.
- 0.3% drift cycles, minor flexure and shear cracking in regions between FRP bands to about half height of the wall segment.
- 0.5% drift cycles, first cracking noticed below steel confinement armour. Cracks observed up to approximately 2/3 height of the wall on the internal edge, between FRP bands, whilst first cracking was observed on external wall edge of segment.
- 0.75% drift cycles, further development of flexure and shear cracking between FRP bands.
- 1.0% drift cycles, combination of shear and flexural cracks observed to nearly full height of the external wall edge and to approximately 2/3 height on the internal edge. Significant gap opening below steel confinement armour for both directions of loading.
- 1.5% drift cycles, micro cracking observed above steel confinement armour and below first FRP band on the internal edge of W2Ra. Major flexural crack forming between steel confinement armour and first FRP band as the wall was loaded in the negative direction (outside edge in compression).
- 2.0% drift cycles, further micro cracking observed on the internal edge of the wall between the top of the steel confinement armour and below the first FRP band. Shear

cracking which developed between FRP bands was restrained by the FRP resulting in diagonal cracks changing direction to form horizontally along top of FRP bands.

- 2.5% drift cycles, minor spalling of concrete on internal wall edge between steel armour and first FRP band. Major flexural crack developed above steel armour and below first FRP band when loaded of the wall segment in the negative direction. Significant cracking observed below wall steel confinement armour, along partial horizontal cut region. Cracking below armour formed along horizontal cut region for both directions of loading.
- End of test, wall elongation was evident with a crack of approximately 1mm in width remaining at the base section of the wall below wall confinement armour.

Figure 7-7 shows W2R at peak drift of 2.5% drift. W2Ra was on the left hand side and it can be seen that no significant damage was evident. The only damage that could be seen was the cracks which were highlighted during testing and minor amount of spalling on the internal edge of the wall between the steel confining armour and the first FRP band. The spalling that occurred in this region was relatively minor and only appeared to be a thin layer of the surface of the concrete. It was therefore thought that the resin coating applied to the wall surface during the application of the FRP made the surface of the concrete brittle. The spalling in this region post testing is shown in **Figure 7-8**.

Figure 7-7: W2R response at peak drift cycle of 2.5%

Figure 7-8: Crushing of concrete on W2Ra between confinement armour and FRP

During the demolition of W2Ra, it was observed that the horizontal cut used to partially sever the boundary element reinforcement only cut through the first two HD16's of the boundary element. The horizontal cut was meant to also cut through two HD12's (leaving two HD16's). This highlights the care needed to be taken in implementing such a solution as this resulted in an underestimate of the wall strength.

7.7.2 W2Rb Observations

Observations made during testing of W2R in regards to W2Rb are discussed in this section. W2Rb was the wall segment which the boundary element reinforcement was not cut, it can be seen that at a peak drift of 2.5% in **Figure 7-7**.

Significant observations made during the testing of W2Rb and the drift at which they occurred are discussed in the following bullet points:

- 0.3% drift cycles, first flexure and shear cracking observed to nearly half height of the wall, on both edges. No visible cracking was observed below steel confining armour.
- 0.5% drift cycles, further development of cracks to approximately half height of the wall segment. Evidence of crack development below steel confining armour.

- 0.75% drift cycles, cracking evident to nearly full height of the wall, particularly the external edge.
- 1.0% drift cycles, further development of cracking particularly on external wall edge. It was noticed that cracking and rocking of steel confining armour was only observed on positive drift cycles (evidence that large quantity of boundary element reinforcement was not yielding).
- 1.5% drift cycles, micro cracking formed in the region above the steel confinement armour and below the first FRP as the concrete crushed due to the large quantity of boundary element reinforcement being loaded in tension.
- 2.0% drift cycles, concrete starts to spall on the internal wall edge between the steel armour and first FRP band. Micro cracking starts to form above the first FRP band.
- 2.5% drift cycles, Major spalling occurs in region above steel confinement armour but below first FRP band, whilst moderate spalling occurs above first FRP band. The first FRP band delaminates from the concrete surface along the wall sides particularly near the internal edge of the wall segment. FRP still provides confinement at the wall ends and prevents reinforcing bars from buckling. As the wall rocks in the negative region there was still not significant gap opening below steel confinement armour.

Figure 7-7 shows W2R at its peak drift cycle of 2.5%, W2Rb is shown on the right hand side. It can be seen that cracking was predominant on the external wall edge and that significant spalling occurred on the internal wall edge above the steel confining armour. **Figure 7-9** show a close up view of the spalling that occurred on W2Rb, this shows that the steel confining armour and FRP bands provided confinement and prevented bar buckling.

Figure 7-9: Spalling of concrete on W2Rb

7.8 Results and Analyses – W2Ra

Results and analyses for W2R are presented individually for segments #1 and W2Rb and then as a whole for W2R. In this section the results for W2Ra (partially severed boundary element reinforcement) are discussed. They include the force versus displacement response and post-tensioning forces.

7.8.1 Force versus Displacement Response

The force versus displacement response for W2Ra is shown in **Figure 7-10**. The response was highly asymmetric due to the asymmetric reinforcement detailing. A ductile response was achieved with no strength degradation occurring, but substantial pinching was evident. Significant residual displacements are present as the un-bonded post-tension force was not large enough to provide a re-centring behaviour, particularly in the positive loading direction.

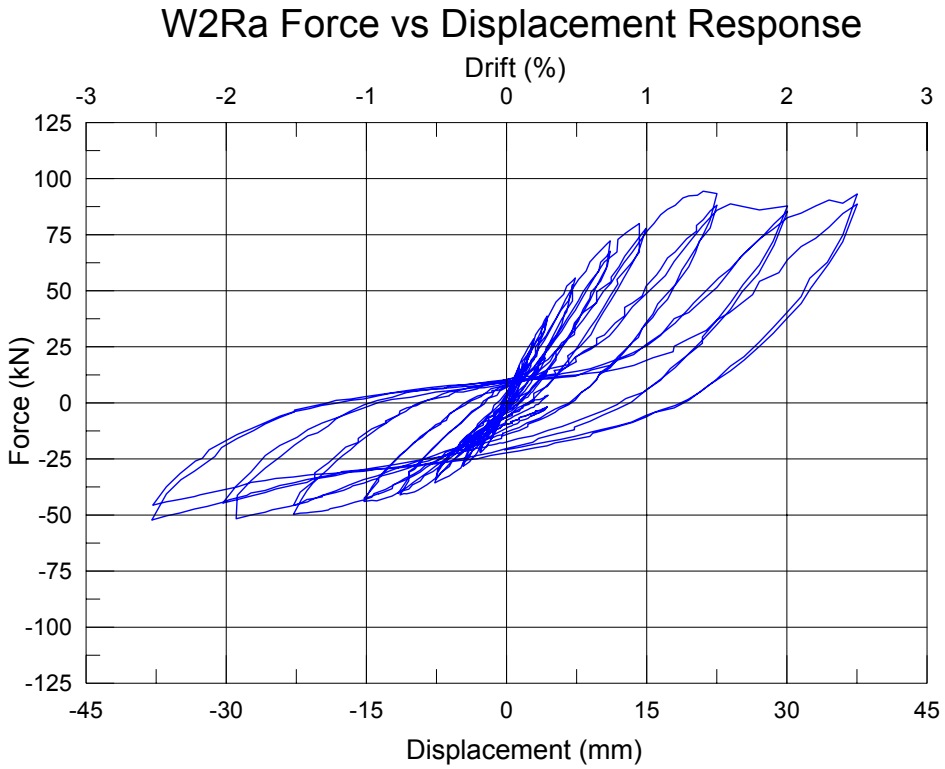

Figure 7-10: Force displacement response for W2Ra

Figure 7-11 shows the magnitude of foundation sliding relative to the strong floor as the test progressed. The measured foundation sliding was relevant to both wall segments and it can be seen that the displacements were typically less that 1mm in each direction.

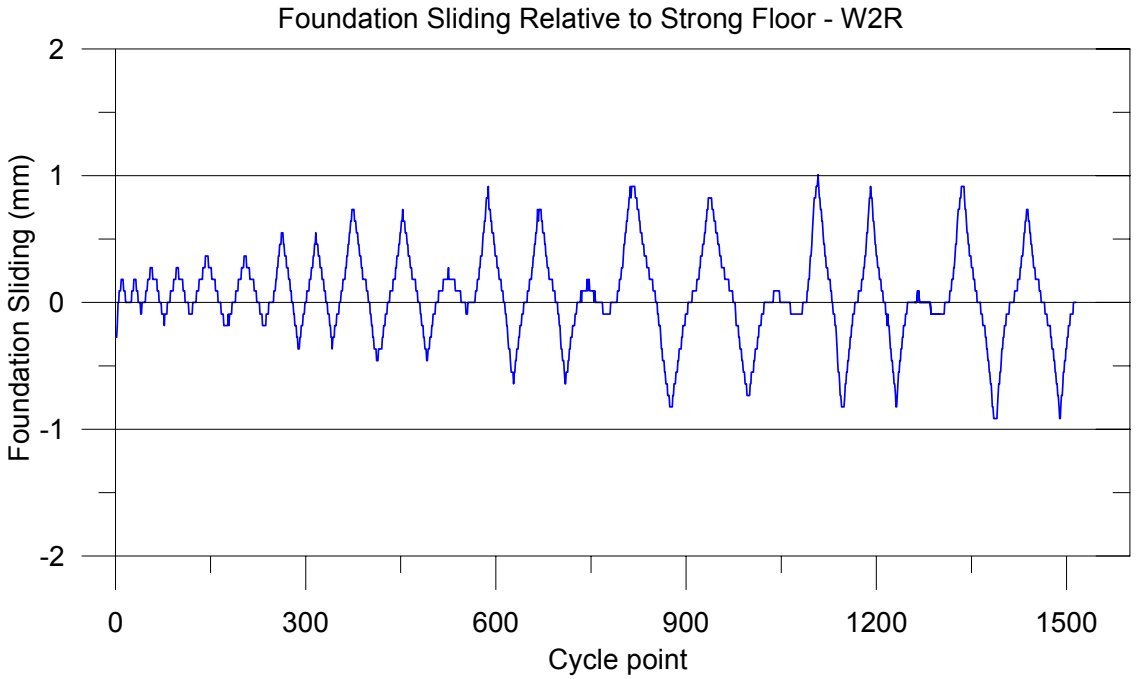

Figure 7-11: Foundation block sliding relative to strong floor

7.8.2 Post-tensioning

An example of the variation in the post-tensioning force as the testing progressed is shown in **Figure 7-12**. An initial post-tension force of 40kN per tendon was used and a peak of 70kN was reached during testing. At the end of the test the initial un-bonded post-tensioning force in both tendons had increased by approximately 10kN (25%). The increase was a result of the wall segment elongating as it was subjected to the cyclic lateral loading regime. This shows that the initial post-tensioning force was not large enough to provide a re-centring behaviour.

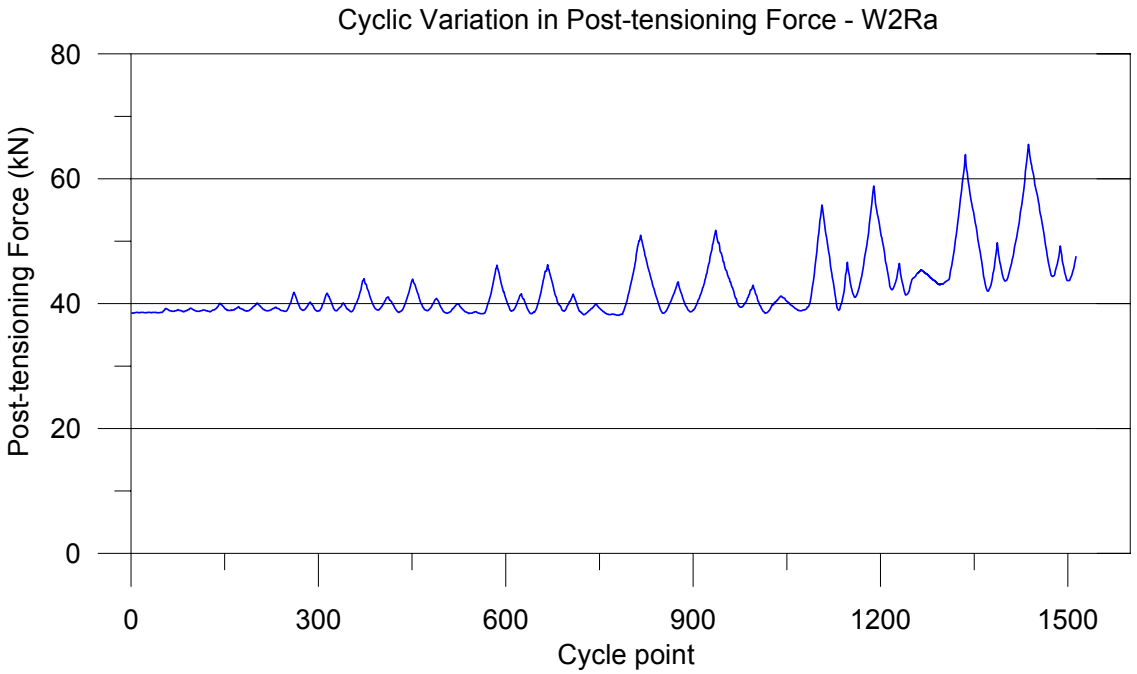

Figure 7-12: Change in post-tension force in W2Ra as test progresses

Figure 7-13 shows the post-tensioning force versus lateral displacement. Increases in the post-tensioning force due to lateral loading were much more substantial when the wall segment was loaded in the negative direction, due to a smaller neutral axis depth. The reason for this was that when the wall is subject to lateral loading in the positive direction the remaining boundary element reinforcement was put in tension, which resulted in a deep neutral axis. The deep neutral axis resulted in a small lever arm between the neutral axis and post-tensioning tendon, therefore only a slight increase in the initial post-tensioning force. The increase in initial post-tensioning can also be seen as the post-tensioning ratchets up as the segment was laterally loaded. This was due to elongation of the wall segment as it was cyclically loaded.

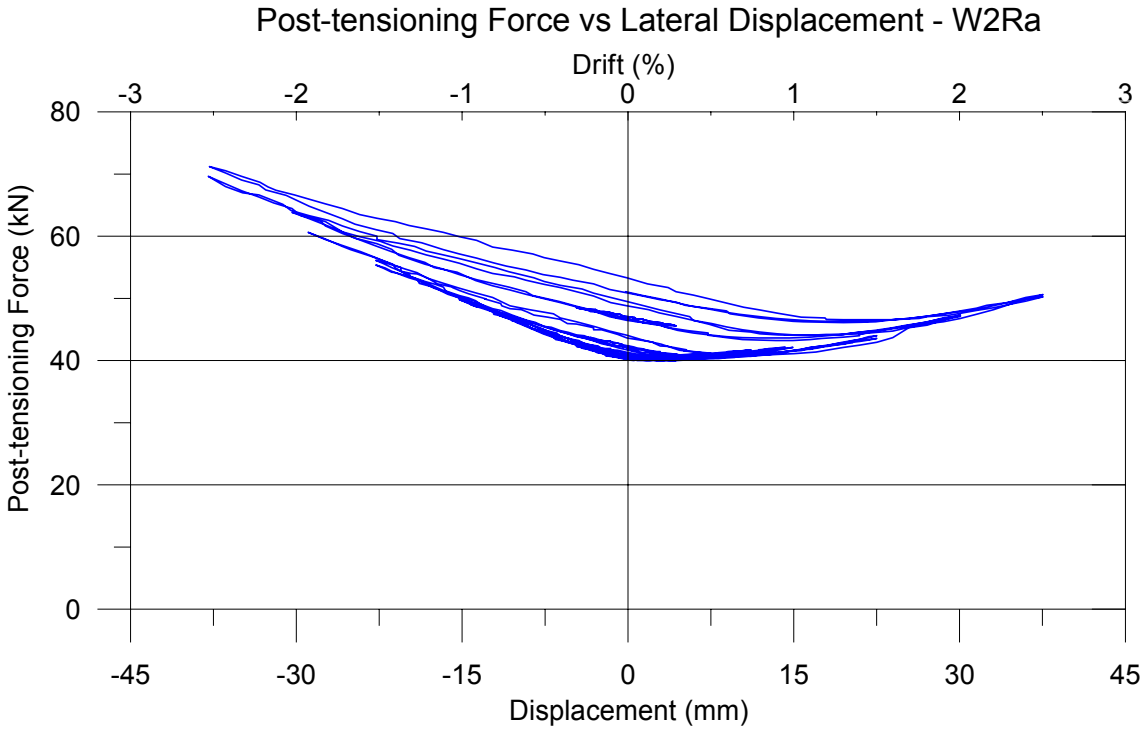

Figure 7-13: Post-tensioning force versus lateral drift, W2Ra

7.9 Results and Analyses – W2Rb

The results and analyses for W2Rb are presented within this section and include the force versus displacement response and variation in post-tensioning forces.

7.9.1 Force versus Displacement Response

Figure 7-14 show the force versus displacement response for W2Rb. It can be seen that the force versus displacement response was highly asymmetric and opposite to the force versus displacement response of W2Ra which is shown in **Figure 7-10**. A relatively ductile hysteretic response was achieved up to 2.0% drift. A significant loss in strength on the second cycle to -2.5% can be observed in the force versus displacement response, which was the result of substantial spalling.

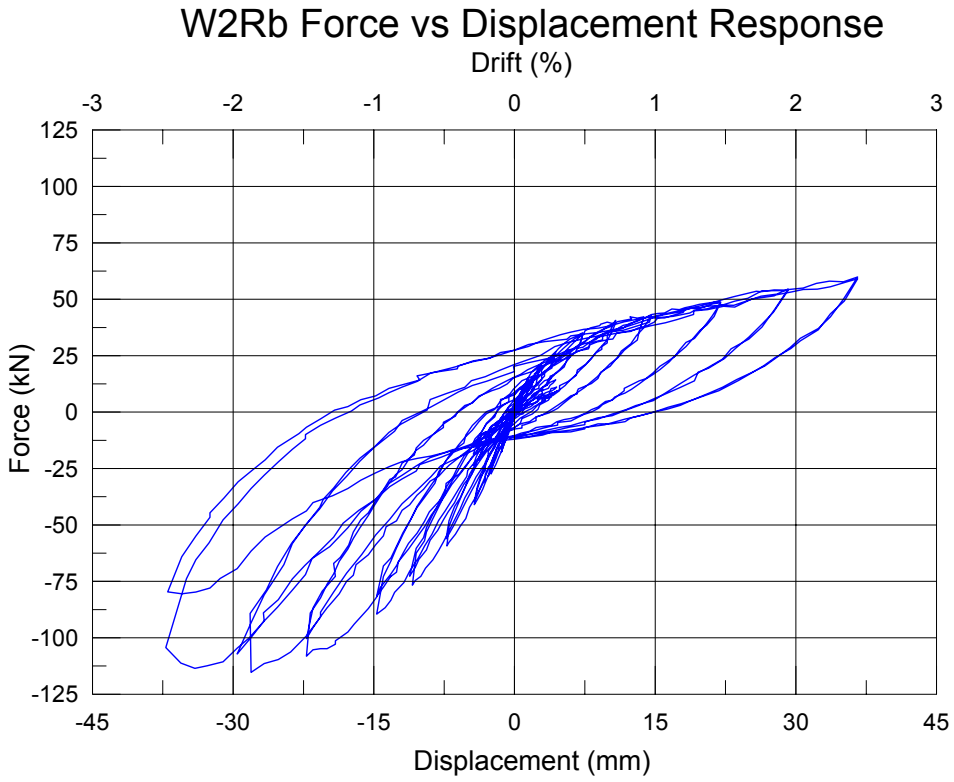

Figure 7-14: Force versus displacement response W2Rb

7.9.2 Post-tensioning

Figure 7-15 shows an example of the cyclic change in post-tensioning force in one of the tendons in W2Rb as the testing progressed. An initial post-tensioning force of 40kN per tendon was used and a peak of 65kN was reached during testing. There was no increase in the initial post-tensioning force at the end of the test as was observed for W2Ra. This shows that the wall did not elongate due to lateral loading.

It can be seen in **Figure 7-15** that there was a reduction in the post-tensioning load during the loading cycles of 1.0% drift and above. The reduction in post-tensioning load was not permanent as the initial post-tensioning load of approximately 40kN per tendon returned once the wall has returned to zero lateral displacement. The reason for this reduction in post-tension force was due to the tendon being located in the compression region and significant crushing/spalling occurring above the steel confining armour of W2Rb. The tendon was located in the compression region when the segment was loaded in the negative direction due to the large quantity of boundary element reinforcement being in tension and creating a large neutral axis depth.

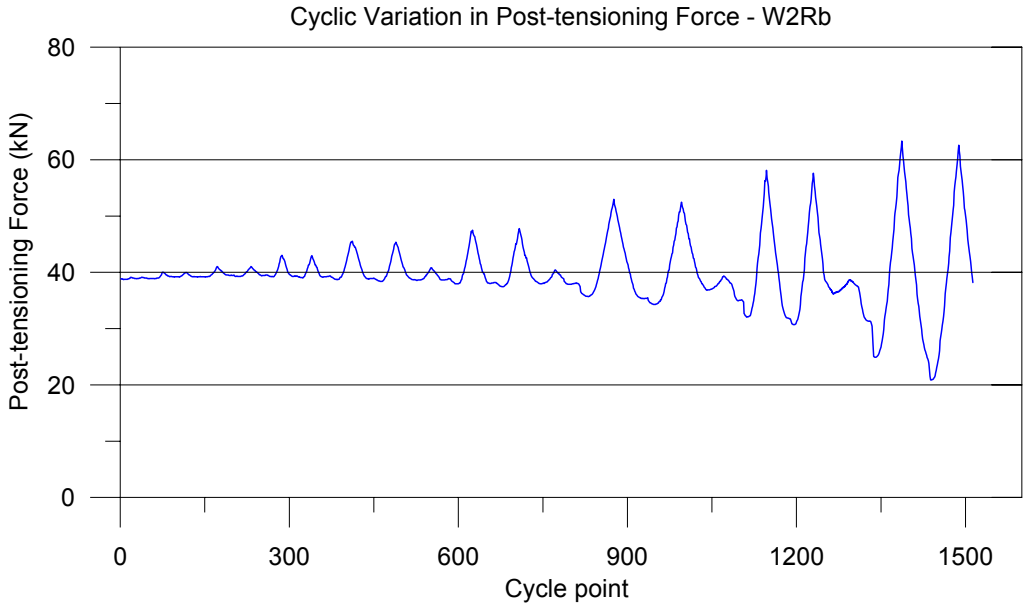

Figure 7-15: Change in post-tensioning force as wall progresses for W2Rb

Figure 7-16 shows the variation in post-tensioning force in one of the tendons as the wall segment was laterally loaded. A substantial increase was observed when the segment was loaded in the positive direction. When loaded in the negative direction the post-tensioning force remained relatively constant for the initial cycles but then reduced in the later cycles. The reduction in post-tensioning force as W2Rb was loaded in the negative direction was thought to be due to crushing and spalling in the compression region as the wall was loaded in the negative direction.

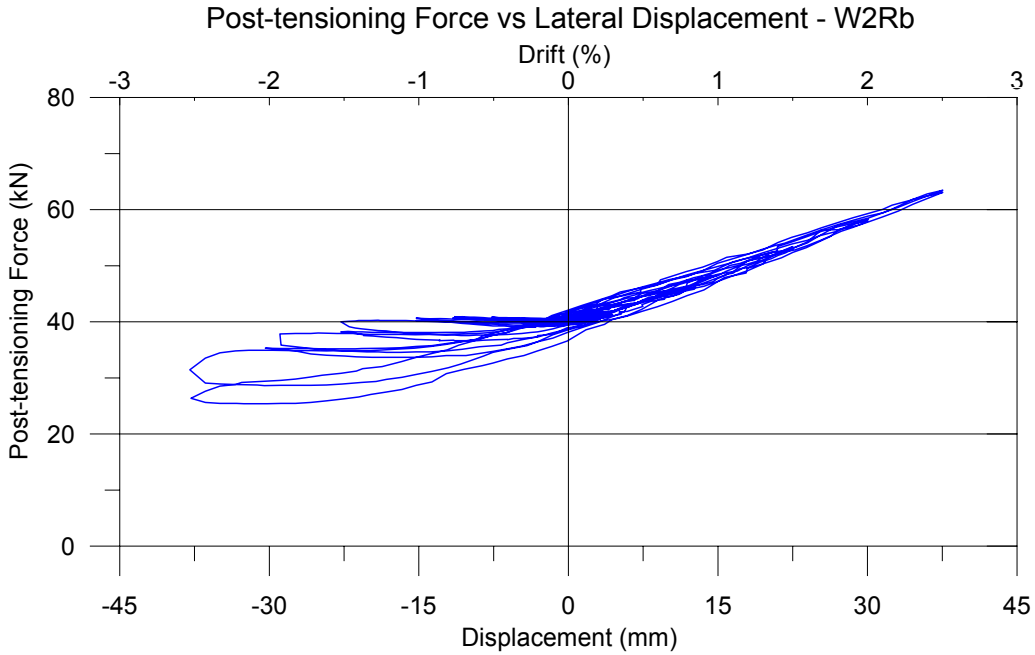

Figure 7-16: Post-tensioning force versus lateral displacement, W2Rb

7.10 Results and Analyses - W2R (W2Ra & W2Rb Combined)

The force versus displacement response for W2R was formed by adding the force versus displacement responses of W2Ra and W2Rb, shown in **Figure 7-10** and **Figure 7-14** respectively. The total (combined) force versus displacement response for W2R is shown in **Figure 7-17**. A relatively ductile force versus displacement response was achieved (when compared to the as-built wall, discussed in Chapter 5). A significant contribution to the lateral load resisting system would also be provided by W2R, as it exhibited a peak strength corresponding to 55% of the peak strength observed in W2. The peak strength of W2R was also higher than the degraded strength of W2. Strength degradation was only evident on the last drift cycle to negative 2.5%. A substantial degree of pinching was observed and large residual displacements are also evident.

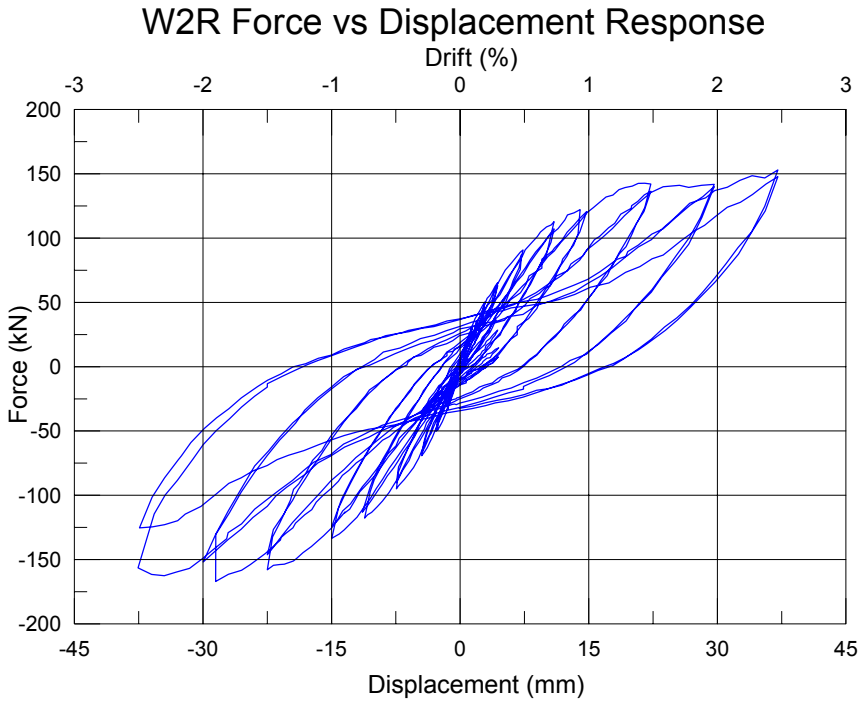

Figure 7-17: Force versus displacement response for W2R

7.10.1 Equivalent Viscous Damping

The percentage of equivalent viscous damping was calculated from the force versus displacement response for drift cycles between 0.5-2.5% and is shown in **Figure 7-18**. For the second drift cycles a peak equivalent viscous damping of 18.9% was achieved on the 2.5% drift cycle. It can be seen that there was a moderate reduction in the level of equivalent viscous damping provided, when comparing the first and second drift cycles. An equation (Priestley, 2003) was used to estimate of the equivalent viscous damping was also made, it can be seen that the estimate was substantially higher than the provided level of equivalent viscous damping.

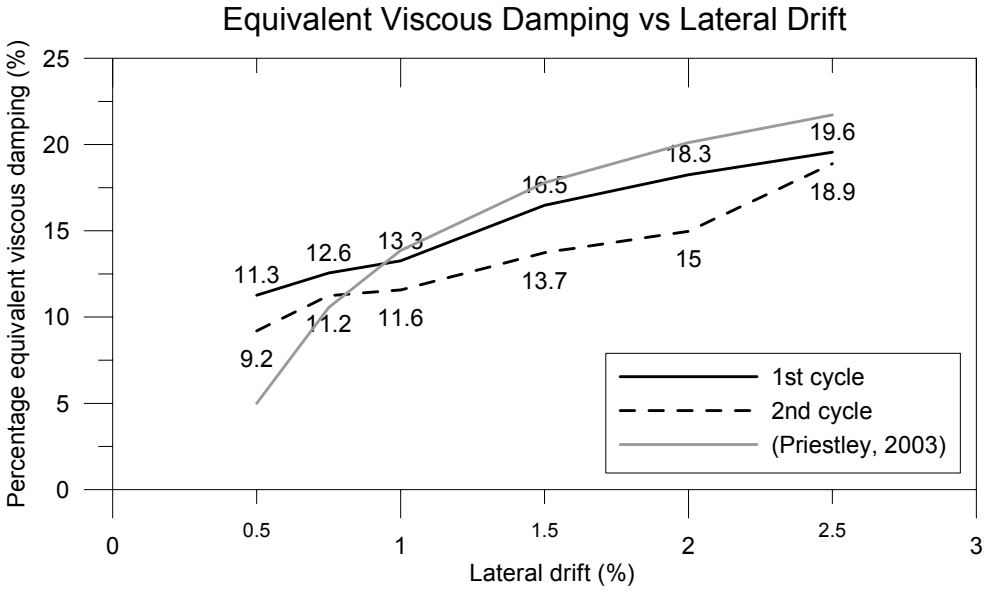

Figure 7-18: W2R equivalent viscous damping

7.11 Force versus Displacement Predictions

Force verse displacement predictions for W2R were calculated using standard hand analysis procedures. As W2R consisted of two wall segments, the force versus displacement response was calculated for each segment and then combined. Due to an asymmetric reinforcement layout in the wall segments, the positive force versus displacement response was dominated by the behaviour of W2Ra and the negative force versus displacement response was dominated the behaviour by W2Rb. The combined force versus displacement response for the two wall segments of W2R and the corresponding force predicted force versus displacement backbone curves are shown in **Figure 7-19**.

For the section analysis calculations a confined ultimate concrete compressive strain of ε_c=0.012 was used with f_y=540MPa for the HD16 and HD12 reinforcement and f_y=330MPa for D10 reinforcement. An empirical formula was used to predict the increase in the un-bonded post-tensioning force at the nominal flexural strength (appendix C). The calculations of the force verse displacement response for the wall segments are shown in Appendix C.

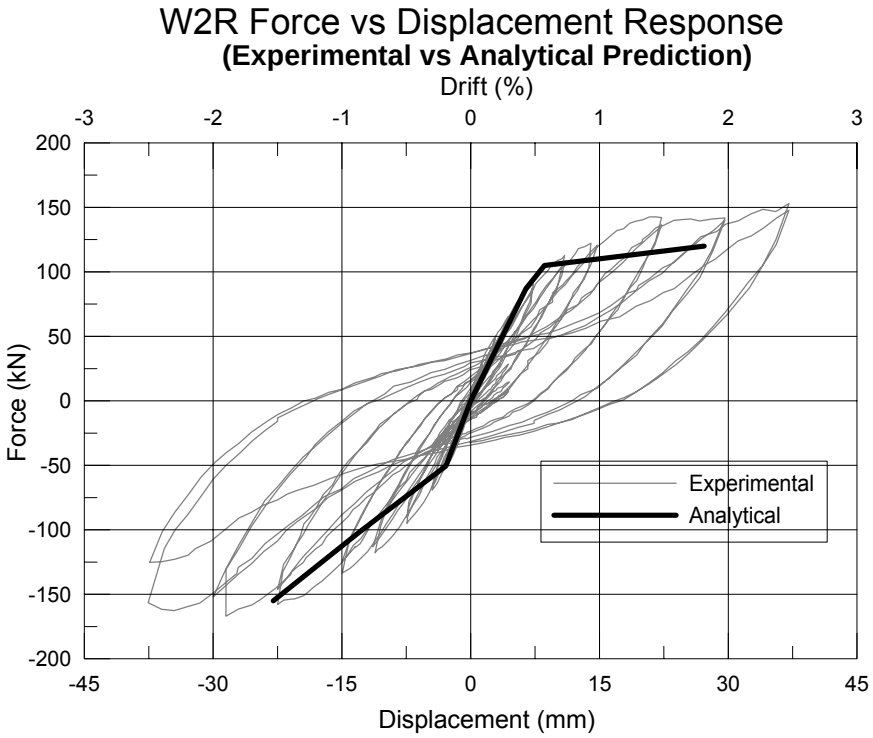

Figure 7-19: Experimental and analytical force versus displacement comparison

A reasonable representation of the experimental force verse displacement response for W2R was achieved using the hand calculations. An accurate representation of the stiffness in both loading directions was achieved. However the predicted strength in the positive displacement direction was substantially less that the experimentally observed force.

References:

Priestley, M.J.N., [2003], "Myths and Fallacies in Earthquake Engineering", Revisited, IUSS Press, Pavia, Italy.

8 Experimental Findings and Comparisons

8.1 Introduction

This Chapter provides a brief summary of the objectives and performance of the four structural wall experimental specimens. The first two specimens acted as benchmarks and the second two were retrofitted equivalents. Relevant comparisons of benchmark and retrofitted specimens are then discussed. Possible alternative retrofit solutions are discussed along with possible improvements to the retrofit solutions that were implemented. A brief overview of the behaviour of the benchmark and retrofitted walls can be found in **Figure 8-1** and **Figure 8-2**.

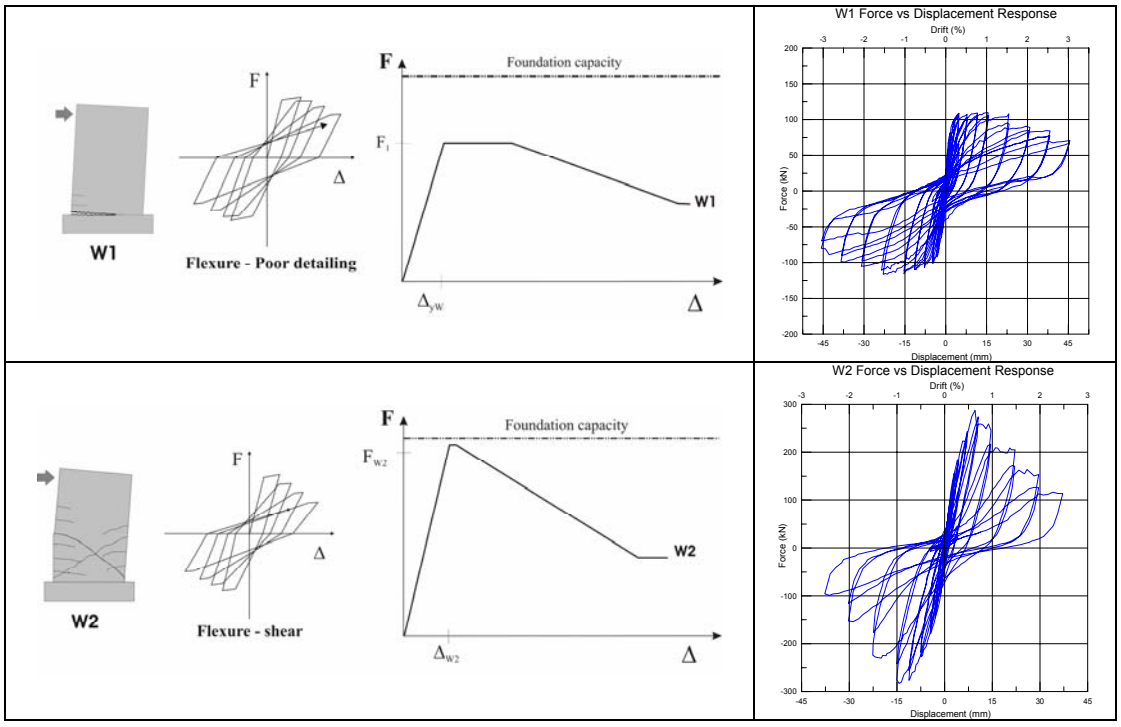

Figure 8-1: Summary of the behaviour of the benchmark walls (W1 and W2)

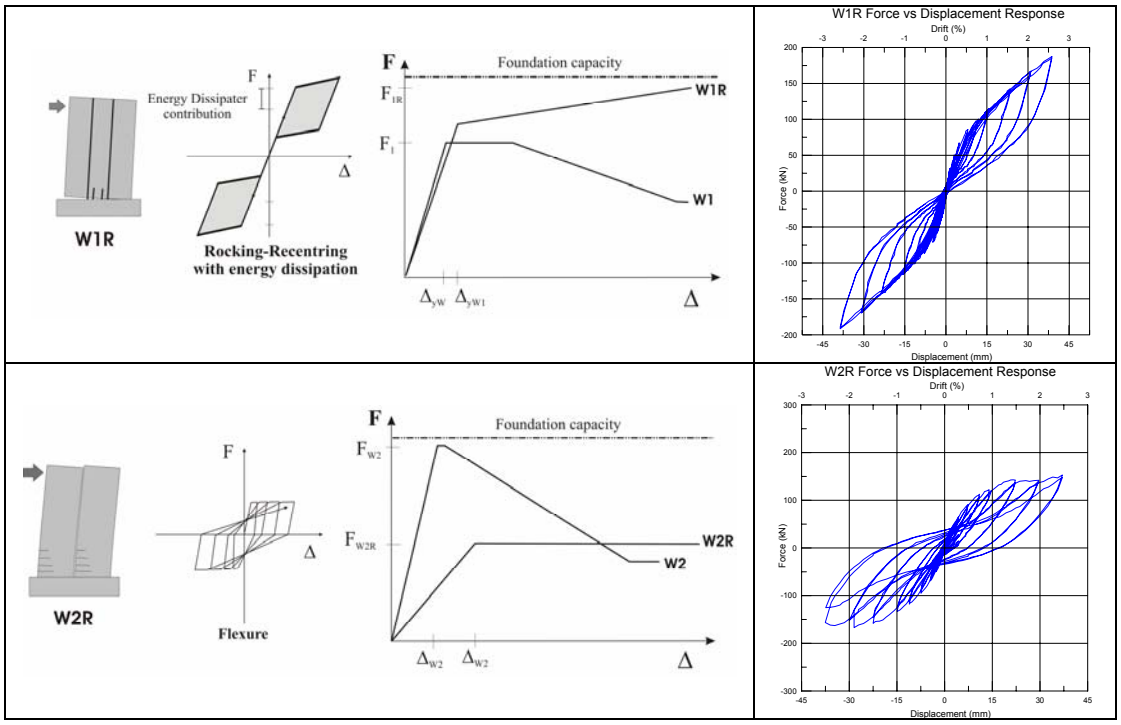

Figure 8-2: Summary of the behaviour of the retrofitted walls (W1R and W2R)

8.2 W1 – Pre-1970's Detailing

W1 was designed to represent pre-1970's construction practice in New Zealand. The objective of this test was to provide a benchmark specimen for the development of the selective weakening retrofit technique. W1 was reinforced with plain round reinforcement and was detailed with a straight lap splice of the longitudinal reinforcement, at the base of the wall. It was thought that the lap splice detail could govern the overall behaviour of the wall. A comprehensive discussion of the design, construction and testing of W1 can be found in Chapter 4.

W1 was tested to a drift level of 3.0% and is shown at this peak drift level in **Figure 8-3**. The observed behaviour was governed by a crack opening at the wall to foundation interface. This was the only flexural crack that developed in the wall panel. Substantial spalling and buckling of the longitudinal reinforcement was observed at the toe regions of the wall, this began at a drift level of 1.5%. By test completion the longitudinal reinforcement at the ends of the wall was observed to have ruptured. The lap splice detail in the longitudinal reinforcement did not have any detrimental affect on the overall behaviour.

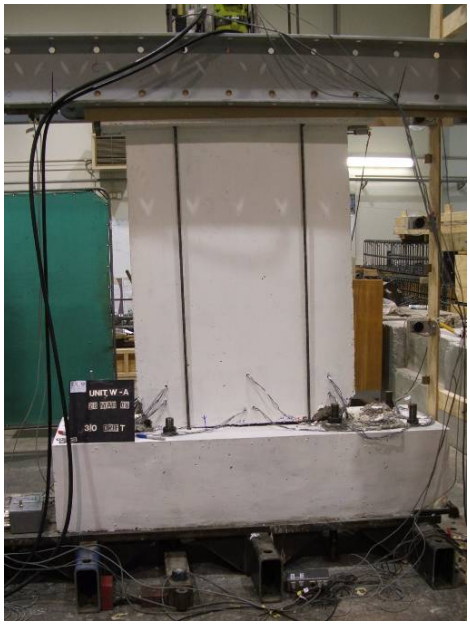

Figure 8-3: W1 at a peak drift of 3.0%

The behaviour of W1 in terms of the force versus displacement response is shown in **Figure 8-4**. A ductile force versus displacement response was achieved up to 1.5% drift, after which strength degradation was observed on the positive drift cycles. A substantial level of pinching of the force versus displacement response was also observed. A peak level of equivalent viscous damping of 24.2% was achieved on the second 1.5% drift cycle, the level of equivalent viscous damping degraded after this point. By the 3.0% drift cycle the percentage of equivalent viscous damping had reduced to 17.0%.

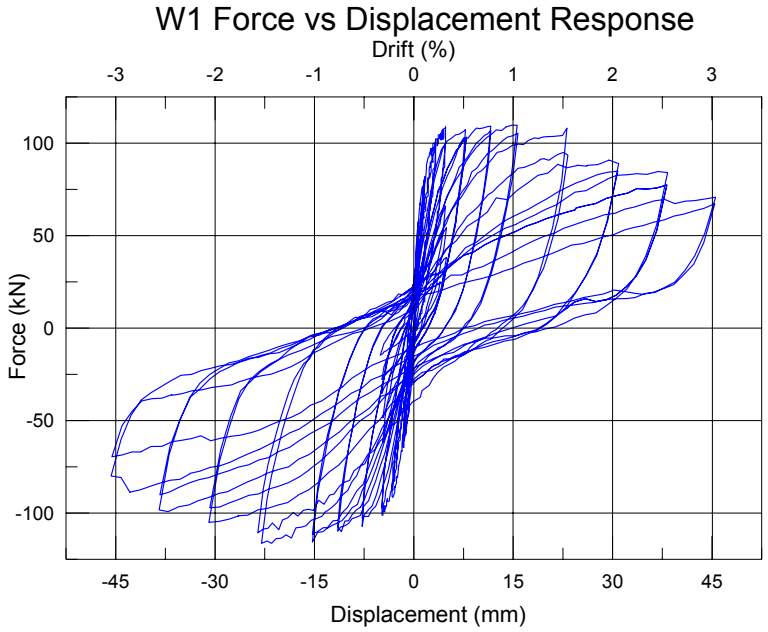

Figure 8-4: Force versus displacement response, W1

The performance of W1 is summarised in the following points:

- Substantial strength degradation was observed after drift cycles to 1.0%.
- Spalling and buckling of the longitudinal reinforcement was observed in the toe regions of the wall.
- Single crack opening at the wall to foundation interface resulted in rupturing of the longitudinal reinforcement at the end regions of the wall.
- Lap slice did not govern the behaviour.

8.3 W2 – Shear Dominated

W2 was designed and constructed to represent a severe scenario, where the inelastic behaviour of the wall was governed by shear. The objective of this was to provide a benchmark specimen for the development of the selective weakening retrofit technique. To achieve a shear dominated failure mode, a high flexural strength was required, this was achieved by using a large quantity of boundary element reinforcement within the rectangular cross section of the wall (at each end). A comprehensive discussion of the design, construction and testing of W2 can be found in Chapter 5.

W2 was tested to a drift level of 2.5%, after the first positive and negative drift cycle to 2.5% drift the test was stopped, as the wall was on the verge of collapse. The observed behaviour at

the end of testing is shown in **Figure 8-5**. The behaviour was dominated by diagonal tension cracks forming under both directions of loading. The large diagonal tension cracks extended from corner to corner across the wall panel. Extensive spalling was observed along the diagonal shear cracks. From the observed failure mode and level of damage sustained by W2 it was considered no longer capable of providing reliable gravity or lateral load carrying capacity.

Figure 8-5: Observed behaviour of W2 at test completion

The force verse displacement response for W2 is shown in **Figure 8-6**. A non-ductile shear dominated response was observed, with severe strength degradation, which began after the 0.75% drift cycles. On the negative drift cycle to 2.5% the peak strength had reduced to 35% of the peak strength achieved. A high level of slip (pinching) was also evident in the force versus displacement response which was due to the opening and closing of the large diagonal tension cracks. A peak level of equivalent viscous damping of 18.7% was achieved on the second 2.0% drift cycle.

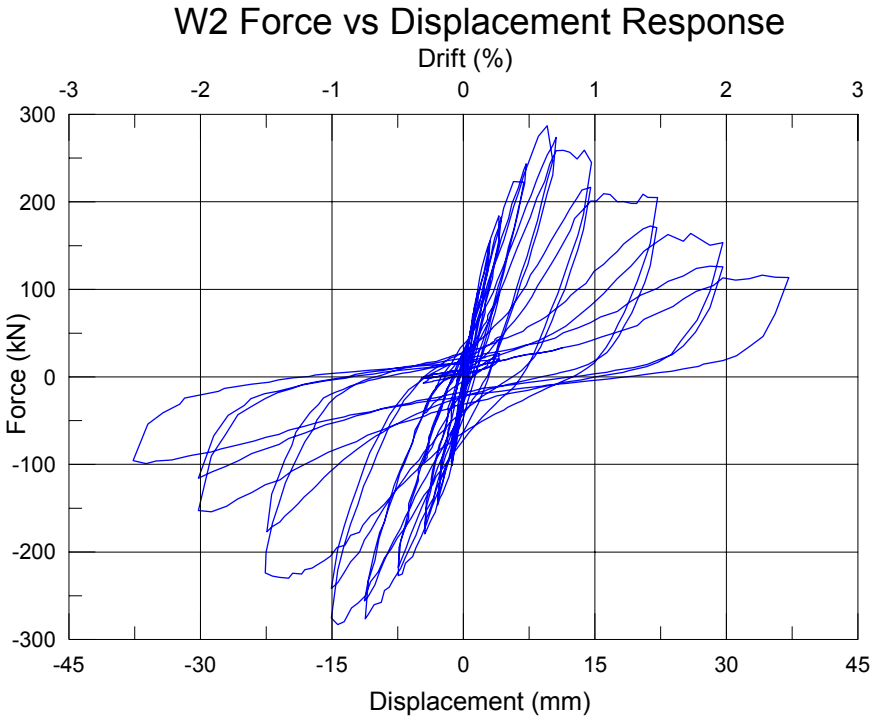

Figure 8-6: Force versus displacement response, W2

The performance of W2 is summarised in the following points:

- Inelastic behaviour dominated by a non-ductile diagonal tension failure (shear)
- Severe strength degradation observed after 0.75% drift cycles
- Substantial spalling was observed along diagonal crack regions
- Inability to provide reliable gravity carrying capacity after lateral loading

8.4 W1R – Selective Weakening Retrofit of W1 Equivalent

W1R was a selectively weakened retrofitted equivalent of W1. The selective weakening retrofit solution aimed to improve the inelastic behaviour by minimising damage, eliminating the possibility of a lap splice failure and to introduce a self-centring behaviour. The retrofit solution involved a horizontal saw cut at foundation level (severing all longitudinal reinforcement) to introduce a controlled rocking behaviour. Other components required to complete the retrofit solution were un-bonded post-tensioning, external energy dissipaters, confinement armour and shear keys (at the toe regions of the wall). The configuration of the selective weakening retrofit solution implemented for W1R is show in **Figure 8-7**. A comprehensive summary of the design, construction and testing of W1R can be found in Chapter 6.

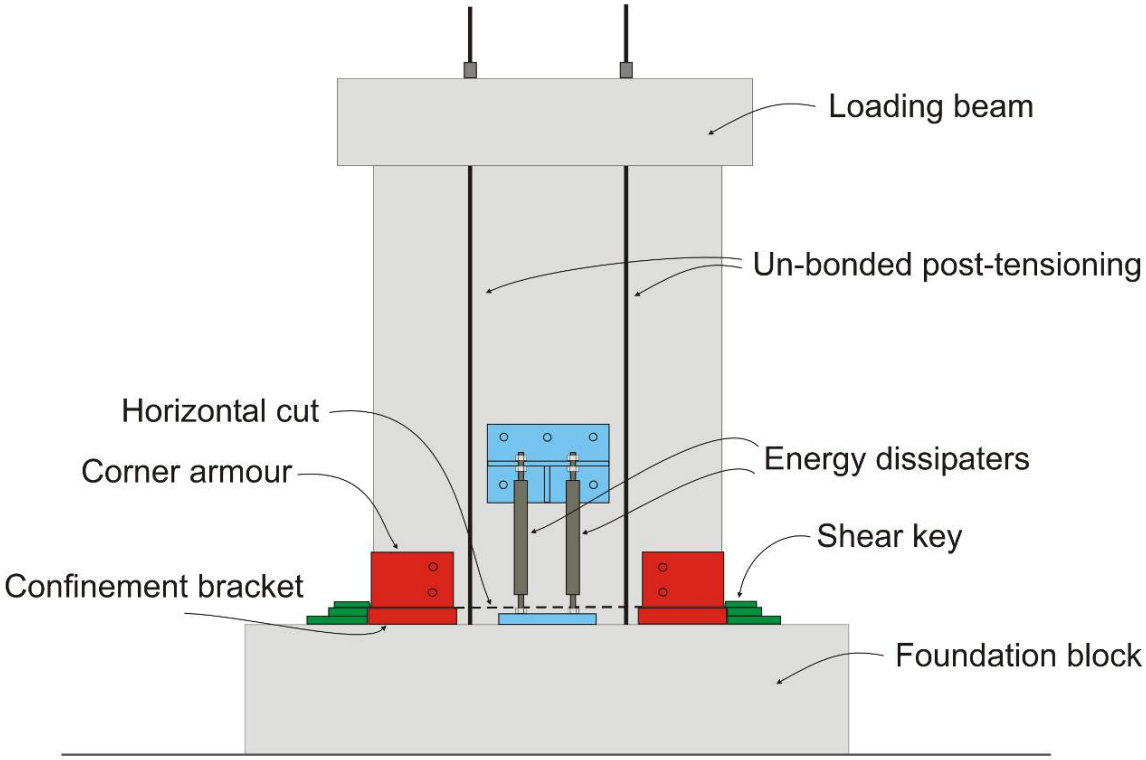

Figure 8-7: Retrofit configuration and components, W1R

A total of four tests were performed on W1R, two with energy dissipaters (hybrid) and two without (post-tensioned only). Multiple tests could be performed due to the negligible damage experienced. This was a result of the rocking nature and because the energy dissipaters were the only elements to experience inelastic behaviour. The energy dissipaters were easily replaceable for repeatable tests. The observed behaviour consisted of a gap opening along the horizontal cut region, with the wall re-centring as the lateral load was removed (due to the un-bonded post-tensioning). No cracking was observed in the wall panel and the confinement armour prevented spalling at the toe region of the wall.

The force versus displacement response of test #3 (2nd hybrid test) performed on W1R is shown in **Figure 8-8**. Test #3 was the second test with dissipaters to be performed on W1R and it can be seen that a flag-shaped (combined self-centring and energy dissipation) hysteresis loop resulted with minimal stiffness loss, a self centring behaviour and no sign of strength degradation. The force versus displacement response for test #3 was shown because the behaviour was improved form the first test including energy dissipaters. The behavioural improvements were achieved by minimising losses in the level of initial post-tensioning and

by reducing buckling of the dissipaters. A peak level of equivalent viscous damping of 14.2% was achieved during test #3. The tests performed without energy dissipaters exhibited a non-linear elastic hysteretic response (no hysteretic dissipation), the results can be seen in Chapter 6. A reduction in the initial stiffness was observed as multiple tests were performed on W1R. This was likely due to minor crushing/abrasion at the toe regions of the wall.

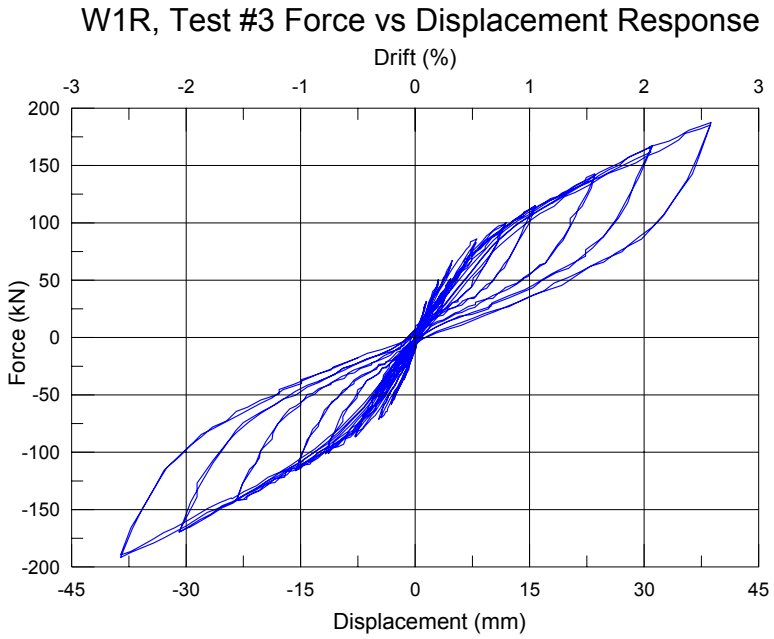

Figure 8-8: Force versus displacement response, W1R (test #3)

8.5 W2R – Selective Weakening Retrofit of W2 Equivalent

W2R was a selectively weakened equivalent of W2, which focused on improving the inelastic behaviour by introducing capacity design principles by changing the failure mode from shear to flexure. The aim was to ensure that after a seismic response the wall could still provide adequate gravity carrying capacity, the contribution to the lateral loading resisting system was a secondary objective. A comprehensive overview of the design, construction and testing of W2R can be found in Chapter 7.

The selective weakening retrofit strategy adopted involved vertically segmenting the wall with a 40mm split, creating two adjacent wall segments (see **Figure 8-9**). The two wall segments (W2Ra & W2Rb) were asymmetrically reinforced due to the large quantity of boundary element reinforcement present in the as-built wall. A horizontal cut partially severing the boundary element reinforcement was applied to W2Ra, this was used to avoid a

concrete compression failure. The horizontal cut through the boundary element reinforcement was not applied to W2Rb to allow the affects of the horizontal cut to be monitored, by comparing the behaviour of the two wall segments. In an actual retrofit situation the horizontal cut would have to be applied to avoid a concrete compression failure due to the high quantity of boundary element reinforcement. A combination of un-bonded post-tensioning, FRP and steel confinement armour was required to complete the retrofit solution, the configuration is shown in **Figure 8-9**.

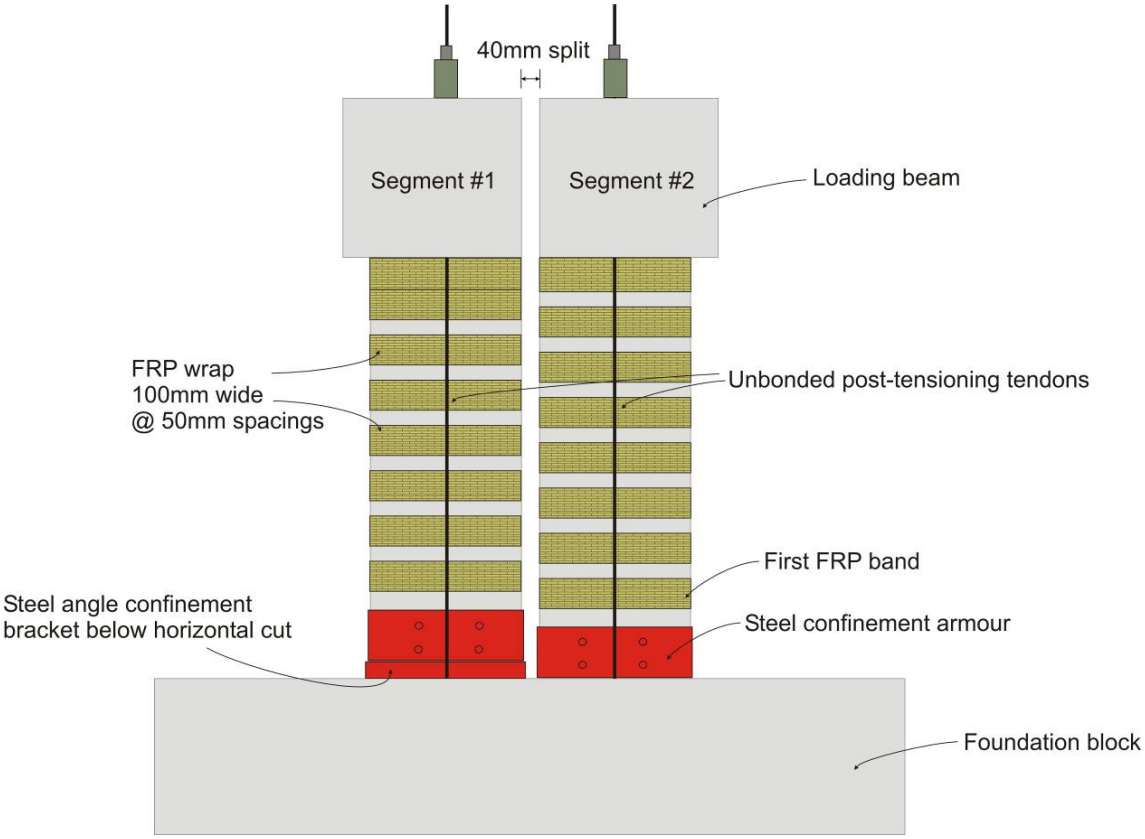

Figure 8-9: Retrofit configuration and components, W2R

The observed behaviour of W2Ra consisted of distributed cracking between the bands of FRP, which acted as external stirrups. At test completion minor spalling had occurred above the steel confinement armour, below the first band of FRP (from the base of the wall). During the demolition of W2Ra it was observed that the horizontal cut partially severing the boundary element reinforcement had not severed as many bars as was aimed for, this resulted in a higher flexural capacity and the observed crushing.

The observed behaviour of W2Rb was governed by a concrete compression failure. Substantial spalling occurred above the steel confinement armour and below the first band of FRP. Moderate spalling also occurred above the first FRP band. A concrete compression failure was expected due to the excessive quantity of boundary element reinforcement and the result can be compared to W2Ra where the boundary element reinforcement was partially severed.

The force versus displacement response for W2R, was formed by adding the force versus displacement response of the two wall segments, and is shown in **Figure 8-10**. A stable hysteresis loop was formed, with strength degradation only evident in the second cycle to -2.5% drift. Due to the asymmetric reinforcement detailing of the wall segments, W2Rb contributed the majority of the strength in the negative direction. The large amount of spalling due to the concrete compression failure was likely the reason for the strength degradation observed on the negative cycle. A peak of 18.9% equivalent viscous damping was achieved at 2.5% drift.

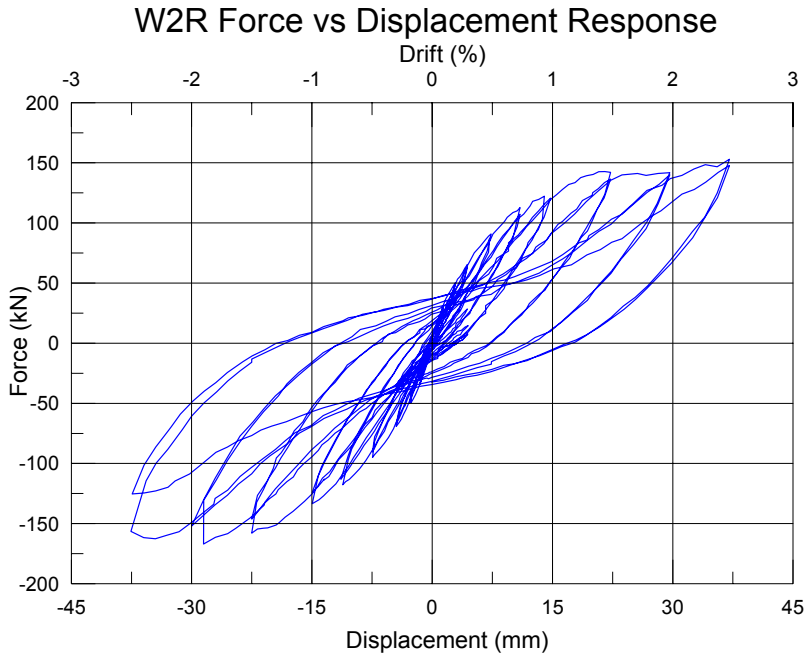

Figure 8-10: Force versus displacement, W2R

8.6 W1 versus W1R Comparison

The performance of the selective weakening retrofit solution implemented on W1R is discussed in this section. The observed and measured behaviour of W1 (benchmark) and W1R (retrofitted) is compared and the negative and positive aspects are highlighted.

8.6.1 Observed Behaviour – Benchmark and Retrofitted

The observed behaviour of W1 was dominated by a single crack opening at the interface between the wall and foundation, and substantial spalling at the toe region of the wall with bucking of the longitudinal reinforcement. For W1R the observed behaviour was dominated by a single gap opening at the horizontal cut region (50mm above wall-foundation interface). The confinement armour provided at the toe regions of W1R prevented any crushing or spalling. By severing all the longitudinal reinforcement the possibility of buckling or rupturing of the outermost bars was also eliminated. Substantial sliding along the single crack region in W1 was observed during testing, this was reduced in W1R by providing shear keys at each end of the wall. **Figure 8-11** compares the observed behaviour at peak response for W1 and W1R.

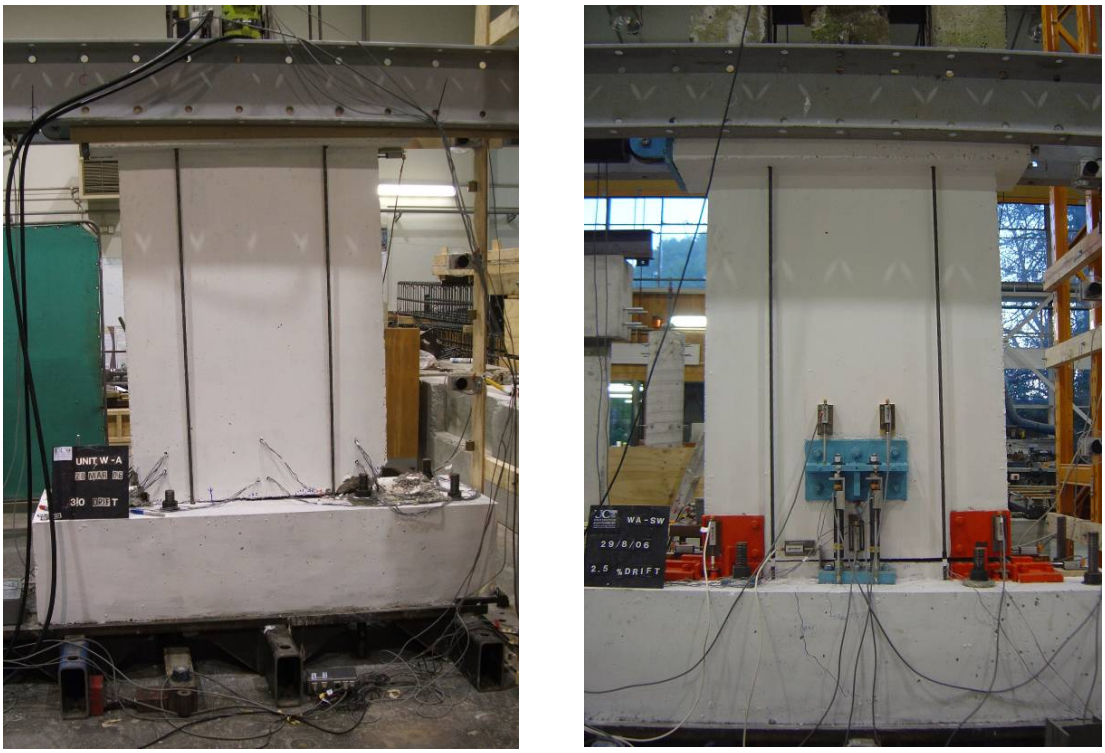

(a) (b)

Figure 8-11: (a) W1 at peak response, (b) W1R at peak response

8.6.2 Force versus Displacement Response – Benchmark and Retrofitted

The force versus displacement response for W1 (benchmark) and W1R (retrofitted) are shown in **Figure 8-12**. For W1 the hysteretic response was stable up to 1.0%, drift after which substantial strength degradation occurred. The force versus displacement response of W1R offers the advantages of no strength degradation and negligible residual displacements. At the completion of testing on W1 the strength had degraded to approximately 60% of the peak strength achieved and substantial residual displacements were observed (greater than 1.0% residual drift).

Disadvantages observed from the force versus displacement response of W1R when compared to W1 are the peak strength achieved and a lower level of equivalent viscous damping. The peak strength achieved in W1R was 190kN compared to 115kN for W1 which was a 65% increase. This could be considered a negative attribute as it would substantially increase the demand on the foundation and would increase the shear actions induced in the wall panel. The percentage of equivalent viscous damping exhibited by W1R was also substantially less that that of W1. At 2.5% drift W1 had a percentage of equivalent viscous damping of 21.5% and for W1R it was only 14.2%. For rocking re-centring elements a lower level of equivalent viscous damping is considered as a side effect of being able to achieve a re-centring behaviour.

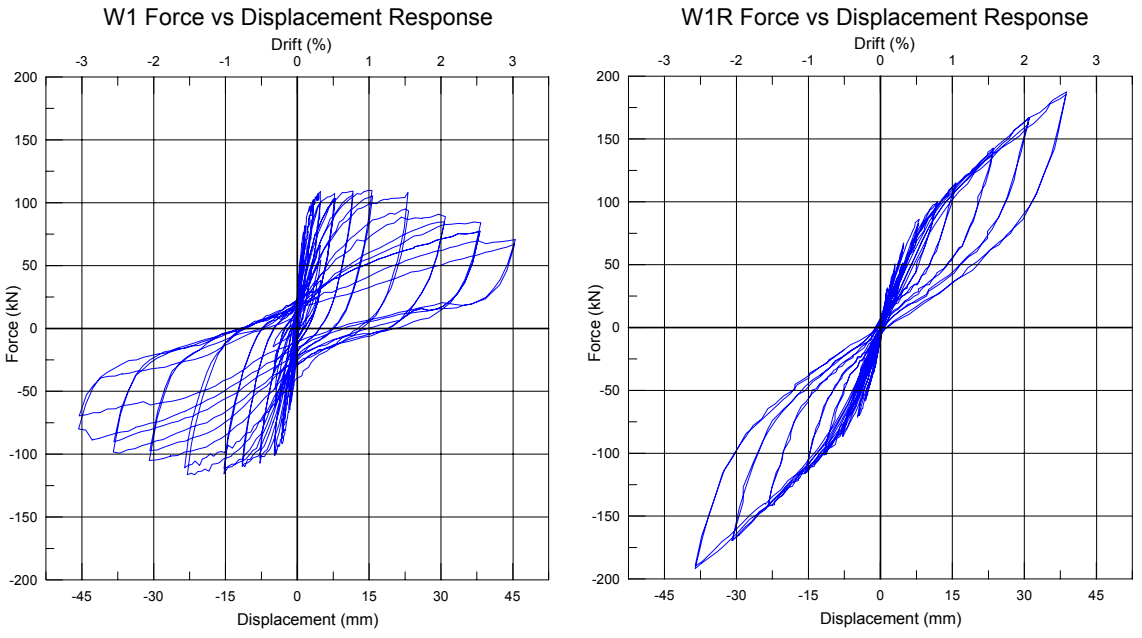

(a) (b)

Figure 8-12: (a) W1 force versus displacement response, (b) W1R force versus displacement response

8.6.3 Possible Improvements to the Retrofit Solution

Possible improvements to the retrofit solution adopted for W1R, include reducing the cost and difficulty of implementing the retrofit solution.

The retrofit solution could be made considerably easier/cheaper to implement if the horizontal cut was made at the interface between the wall and foundation. Due to geometric restraints relating to the concrete cutting saw used the cut was made at 50mm above the wall to foundation interface. This would simplify the retrofit solution as there would be no "stub" of wall below the cut region which would have to be confined. It would also make it easier to mount shear keys as they would not have to be raised to the cut height. It would be possible with the use of a "wire saw" to make the cut at the interface.

An investigation into using the existing reinforcement to provide energy dissipation would lead to a much more cost effective and less invasive retrofit solution. The solution adopted required large dissipater mounts to be attached to the wall panel and foundation block, as well as purpose built energy dissipaters. Problems to overcome to be able to use the existing reinforcement are such as the reinforcement rupturing (need to provide an un-bonded length) and possible a lap splice creating discontinuous longitudinal reinforcement at the critical section.

8.6.4 Other Possible Retrofit Scenarios for W1R

Alternative retrofit solutions for W1R appropriate for different retrofit situations, such as when the capacity of the foundation is critical, were investigated analytically. In these situations it would not be suitable to increase the capacity of the wall as the foundation capacity would be exceeded and a costly foundation upgrade would be required. Therefore a selective weakening retrofit may be suitable as it could be used to ensure that the capacity of the foundation was not exceeded. As a result of the selective weakening retrofit the peak displacements due to an acceleration response may be increased or other structural elements may be require to provide sufficient lateral load carrying capacity.

A proposed alternative retrofit solution for W1R, for a situation where the foundation capacity is substantially inadequate is discussed (**Figure 3-3** (a)). In this situation it would be appropriate to reduce the walls capacity to such a level, that the foundation would not be

damaged if the wall was laterally loaded. As a consequence, existing or new structural elements may have to be relied on to provide lateral load resistance. To minimise the flexural capacity of the wall a horizontal cut could be applied at foundation level (severing all longitudinal reinforcement) and the moment capacity could rely on the axial load alone (i.e. no longitudinal reinforcement, post-tensioning or energy dissipaters). An analytical investigation was performed, to determine the effect on the response if the proposed retrofit solution was applied. **Figure 8-13** compares the force versus displacement response of W1 (benchmark) with the analytical representation of the force versus displacement response for the proposed alternate retrofit solution. The peak force achieved in for the proposed retrofit solution is less than 50% of that achieved in the benchmark specimen, which would considerably reduce the demand on the foundation. The resulting force verse displacement response is non-linear elastic which means there will be minimal energy dissipation.

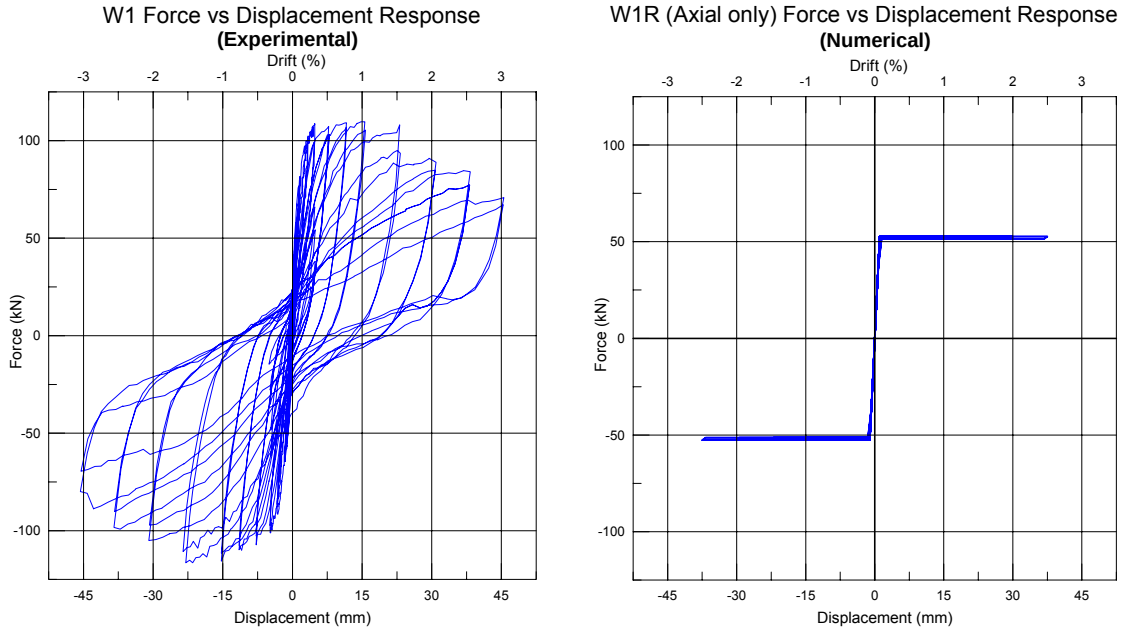

(a) (b)

Figure 8-13: (a) W1 Force versus Displacement response (experimental); (b) Alternative retrofit solution for W1R, force versus displacement response (numerical), axial load only solution

A second proposed alternative retrofit solution for W1R, is suitable for a situation where the capacity of the wall cannot be increased as it is on the limit of the foundation capacity (**Figure 3-3** (b)). The retrofit solution could be designed to maximise the possible contribution to the lateral load resisting system (without exceeding foundation capacity),

whilst introducing the advantages of a self-centring behaviour, increased ductility and minimal damage. The proposed alterative retrofit solution was investigated analytically and was determined to require a horizontal cut at foundation level, two centrally located 7-wire strand post-wire strand post-tensioning tendons with an unbonded length of 6.5m (scaled height of prototype wall) and 4-10mm energy dissipaters. The difference between this alternative solution and W1R is that the unbonded length of the post tensioning was increased. This resulted in a lower increase in the post-tensioning force as the wall was laterally loaded. This more accurately represents a real life situation where the majority of the axial load would result from the dead and live loads. **Figure 8-14** compares the force versus displacement response of W1 (benchmark) and the analytical representation of the proposed alternative retrofit solution and it can be seen that the ultimate force capacity of the benchmark (as-built) wall was not exceeded and that a self-centring behaviour was introduced. This retrofit solution would result in a slightly increased displacement demand, due to a lower level of damping.

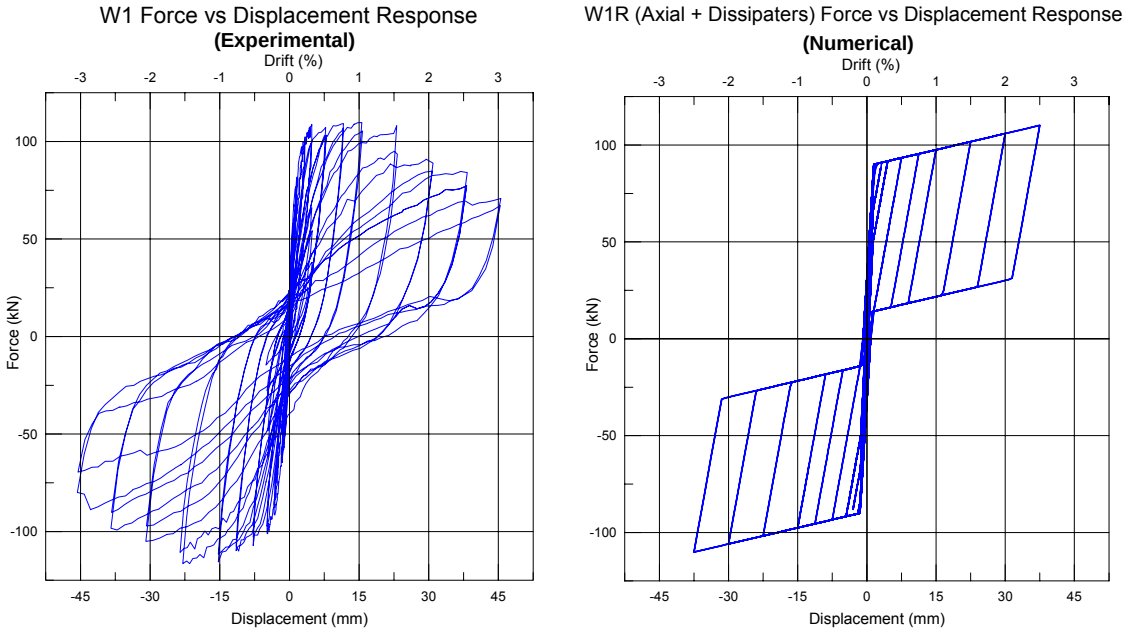

(a) (b)

Figure 8-14: (a) W1 Force versus Displacement response (experimental); (b) Alternative retrofit solution for W1R, force versus displacement response (numerical), two central PT-tendons & 4-10mm dissipaters

8.7 W2 versus W2R Comparison

The performance of the selective weakening retrofit solution implemented on W2R is discussed in this section. The observed and measured behaviour of W2 (benchmark) and W2R (retrofitted) is compared the negative and positive aspects are discussed.

8.7.1 Observed Behaviour- Benchmark and Retrofitted

The behaviour of W2 was dominated by large diagonal tension cracks forming from corner to corner across the wall panel in both loading directions. This resulted in substantial spalling along the crack regions and the test was stopped on the first cycle to 2.5% drift due to immanent collapse. The observed behaviour led to the conclusion that the W2 was no longer capable of providing adequate or reliable gravity carrying capacity. The retrofit solution for W2R created two wall segments (discussed in Chapter 7), both of which exhibited flexural behaviour. A series of minor flexure and shear cracks formed up the height of each wall segment, but were restrained by the bands of FRP. W2Rb exhibited a concrete compression failure due to the large quantity of boundary element reinforcement at one end. This resulted in substantial spalling above the steel confinement armour. W2Ra only exhibited relatively minor levels of spalling. It could be concluded from the observed behaviour that the W2R could still provide adequate and reliable gravity carrying capacity. Elongation of W2Ra was also observed. The behaviour of W2 and W2R is compared in **Figure 8-15**.

(a) (b)

Figure 8-15: (a) W2 at end of test, (b) W2R at 2.5% drift

8.7.2 Force versus Displacement Response – Benchmark and Retrofitted

The force versus displacement responses for W2 and W2R are shown in **Figure 8-16** (for W2R the force versus displacement response is a combination of the behaviour of the two wall segments). W2 exhibited severe strength degradation which began at 0.75% drift and the strength had degraded to 35% by the end of testing. The peak strength reached by W2R corresponded to 55% of the peak strength achieved in W2, which was greater than the degraded strength. The behaviour was much more stable/reliable with strength degradation only evident on the last cycle to -2.5% drift. For loading in the negative direction the force versus displacement response was dominated by W2Rb, which exhibited a concrete compression failure.

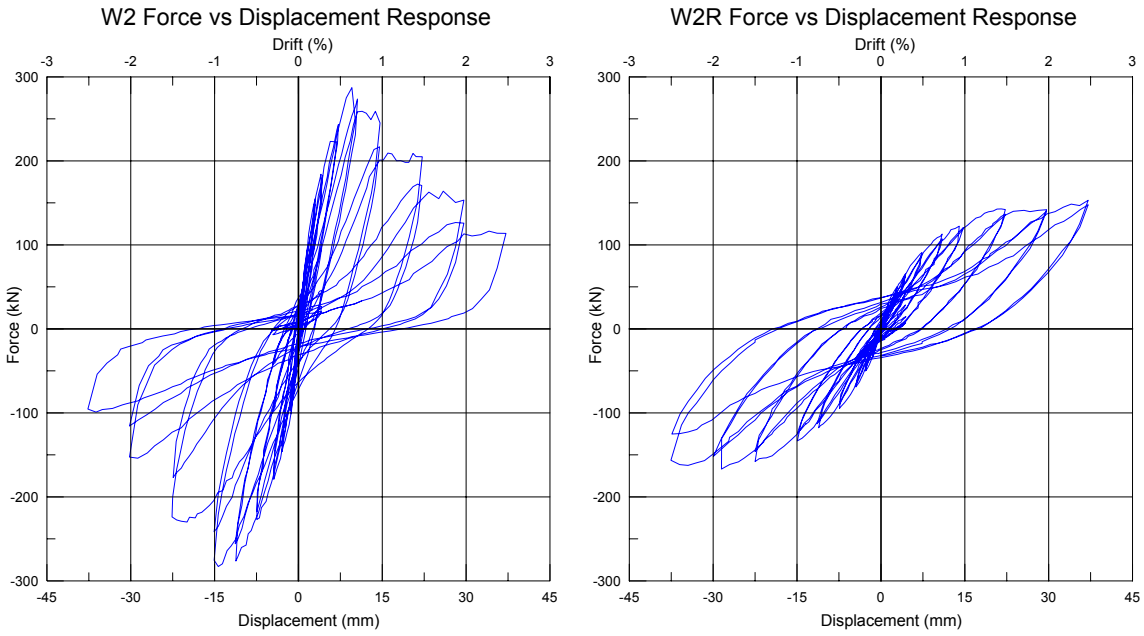

(a) (b)

Figure 8-16: (a) W2 force versus displacement, (b) W2R force versus displacement

8.7.3 Possible Improvements to the Retrofit Solution

The performance of the retrofit solution adopted for W2R could be improved by applying a horizontal cut partially severing the boundary element reinforcement as was used on W2Ra. This would avoid the concrete compression failure that was observed in W2Rb and eliminate the strength degradation that was observed on the last cycle to -2.5% drift. This was not

applied to allow the behaviour with and without the severed boundary element to be compared.

The implementation cost of the retrofit solution could be reduced if the horizontal cut applied in the boundary element region was made at the wall to foundation interface. As for the horizontal cut in W1R, the cut was made at 50mm above the interface between the wall and foundation. This created a more costly/difficult retrofit solution as the region below the cut region had to be confined to prevent crushing.

8.7.4 Other Possible Selective weakening Retrofit Solutions for W2R

Alternative selective weakening retrofit solutions possible for W2R are discussed in this section. The choice of selective weakening retrofit solution implemented on W2R was based on trailing a vertical cut. This served to highlight points that need to be considered when using such a technique. Two possibly alternative selective weakening retrofit solutions involving horizontal saw cuts will be proposed in this section.

The first alternative retrofit solution would be to use a retrofit approach similar to that used for W1R (i.e. use a horizontal cut at foundation level to severe reinforcement and introduce a rocking behaviour). The solution used for W1R could easily be applied to W2R as it was independent of the wall longitudinal reinforcing details, as all longitudinal reinforcement would be severed at foundation level by a horizontal saw cut. This would substantially lower the flexural capacity and therefore the shear demand on the wall. This retrofit solution could be applied with the aim of retaining the gravity carrying capacity of W2R, therefore further lateral load carrying capacity may have to be supplied by other structural components. The only difference between W1R and W2R was the wall thickness, which was 125mm and 100mm respectively. The capacity of W2R could be expected to be slightly less than that observed for W1R. This retrofit solution would have been a viable option for the retrofit of W2R as it would have eliminated a shear failure and introduced a rocking re-centring behaviour. The retrofit configuration used for W1R is shown in **Figure 8-7**.

A second alternative selective weakening retrofit solution considered for W2R was similar to the first alternative but the horizontal cut was to be applied only through the boundary element longitudinal reinforcement. This would substantially reduce the flexural capacity and

therefore shear demand on the wall, introducing capacity design principles if correctly balanced. The existing reinforcement between the boundary elements could then be used to provide energy dissipation and flexural capacity. The benefit of using the existing reinforcement to provide energy dissipation would be that it removes the costly and invasive approach of having to provide energy dissipaters and dissipater mounts externally on the wall. Important considerations that need to be made when considering such a solution would be that un-bonded post-tensioning may be required to provide a re-centring behaviour and to increase the flexural capacity. Also by applying horizontal cuts only at the ends of the wall a stress concentration would be introduced. This could lead to the remaining reinforcement rupturing as the wall was laterally loaded. It would likely be necessary to somehow create an un-bonded length along the existing reinforcement which would allow the strain to be distributed and prevent it from rupturing.

The two alternative selective weakening retrofit solutions proposed for W2R, where possibly more suitable retrofit approaches for W2R, than the retrofit solution that was implemented. The alternative solutions were not implemented, as for the purpose of developing selective weakening retrofit techniques the effect of vertically segmenting a wall was trailed. Another reason for not implementing the first alternative selective weakening retrofit solution was that the likely behaviour from the first alternative solution could be interpolated from the behaviour of W1R (see **Figure 8-7** & **Figure 8-8**). In situations such as very squat walls or where a strength eccentricity needs to be removed a selective weakening retrofit solution involving a vertical cut may be required.

8.8 Summary

The observed and measure behaviour of the four experimental walls was discussed in this section. Relevant comparisons between the benchmark and retrofitted specimens were made to asses the performance of selective weakening retrofit.

W1 was designed and constructed to represent a pre-1970's structural wall in New Zealand and W1R an equivalent wall that was retrofitted using a selective weakening solution. The retrofit solution involved a horizontal saw cut at foundation level which introduced a rocking behaviour and removed the possibility of a lap splice failure. The behaviour was improved by increasing the displacement capacity of the wall, minimising damage and introducing a self

centring behaviour. Negative attributes of the retrofitted solution included a higher base shear capacity and reduced level of equivalent viscous damping.

W2 was designed to failure in shear to provide a severe retrofit scenario which could be expected in situations where the principles of capacity design are not met. W2R was an equivalent that was retrofitted using selective weakening. The retrofit solution involved a vertical split which segmented the wall in two. A horizontal cut partially severing the boundary element reinforcement of one segment was also applied to avoid a concrete compression behaviour. The retrofitted wall had a significantly lower lateral load carrying capacity than the benchmark wall specimen. This was justified by a ductile response being achieved and reliable gravity carrying capacity after lateral loading. In this situation further lateral resistance would likely have to be provided by new and/or existing elements in the building. A retrofit solution as used for W1R would likely be more suitable for this situation.

The selective weakening retrofit solutions were successful in improving the displacement capacity of the experimental walls. For the application in actual buildings global affects of the behaviour would have to be considered. The retrofit solutions adopted were used to prove a concept, therefore the retrofit solutions require refinement to improve the cost effectiveness and to solve practicality issues.

9 Numerical Modeling of Prototype Wall & Sensitivity Analysis

9.1 Introduction

This Chapter discusses the calibration of hysteretic models to experimental tests performed in this investigation, the selection and scaling of earthquake records and the results of time history analyses on single degree of freedom (SDOF) and multi degree of freedom (MDOF) systems. The analyses were used monitor the sensitivity of peak drifts, residual drifts and peak base shear to strength degradation, p-delta and higher mode effects.

9.2 Hysteretic Calibration to Experimental Results

To determine the appropriate hysteretic parameters to use for the lumped plasticity SDOF and MDOF models, hysteretic calibration to experimental results was performed. This was carried out using RUAUMOKO (Carr, 2005), a non-linear dynamic analysis program. The calibration was performed by creating a lumped plasticity model consisting of an elastic beam element (1.5m in height) representing the experimental wall specimen, which was attached to a zero length inelastic rotational spring at the base. An example of the model used for the calibration of the hysteresis models is shown in **Figure 9-1**. The inelastic behaviour of the spring was defined by different hysteresis rules depending on which experimental wall the calibration was being performed for. The calibration was performed using a push-pull analysis using the same displacement based loading regime as was applied to the experimental walls. The resulting force versus displacement response from the push-pull analysis was compared to the experimental response. The parameters defining the shape of the hysteresis were adjusted until an appropriate representation was achieved. The hysteretic response was calibrated with and without including the effects of strength degradation where appropriate. The calibration was only performed for W1 and W1R as they could be appropriately represented by a lumped plasticity model. W2 could not be represented by the lumped plasticity model as it was dominated by shear.

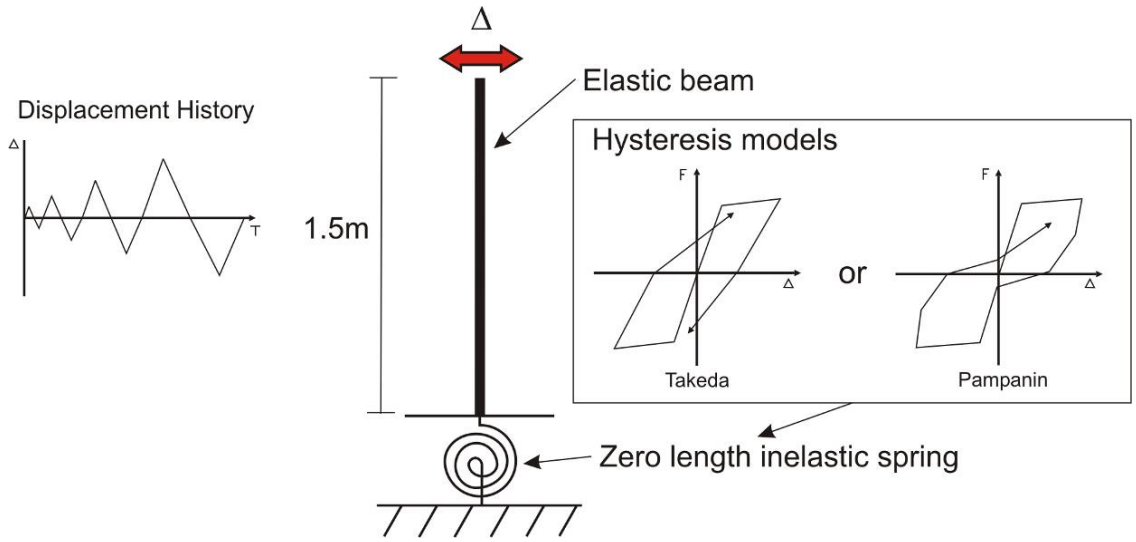

Figure 9-1: Lumped plasticity calibration model

9.2.1 Hysteresis Rules – W1

The inelastic behaviour exhibited by W1 was represented by a modified Takeda and a Pampanin hysteresis rule (Carr, 2005). These two rules are appropriate to use to represent the behaviour of monolithic reinforced concrete elements. For W1R two inelastic springs were used in parallel to represent the behaviour of the un-bonded post-tensioned rocking wall. The two hysteresis rules used were non-linear elastic and elasto-plastic.

The modified Takeda hysteresis rule (as per Carr, 2005) was calibrated to the force versus displacement response resulting form the testing of W1. The modified Takeda hysteresis used was appropriate to define the cyclic behaviour of reinforced concrete elements, but is better suited for reinforced concrete sections that are well detailed that exhibit little or no pinching. The modified Takeda rule offers a bi-linear reloading and linear unloading slope and an example of the hysteresis loop is shown in **Figure 9-2**. Ruaumoko (Carr, 2005) offers two options to describe the unloading behaviour of the modified Takeda hysteresis, the first is Emori unloading and the second is Drain-2D unloading. For the calibration and time history analyses in this investigation Drain-2D unloading was used because it was simpler to assess the effect the parameter used to define the unloading will have of the shape of the hysteresis.

To define the shape of a modified Takeda hysteresis in **Figure 9-2** four parameters are required and are listed in **Table 9-1**. An α factor governs the unloading stiffness, a β factor defines the reloading stiffness, a NF factor relates to the reloading stiffness power factor (a

factor of 1.0 is usually taken) and a KKK factor determines the type of unloading used. A KKK of 1 ensures that Drain-2D unloading is used.

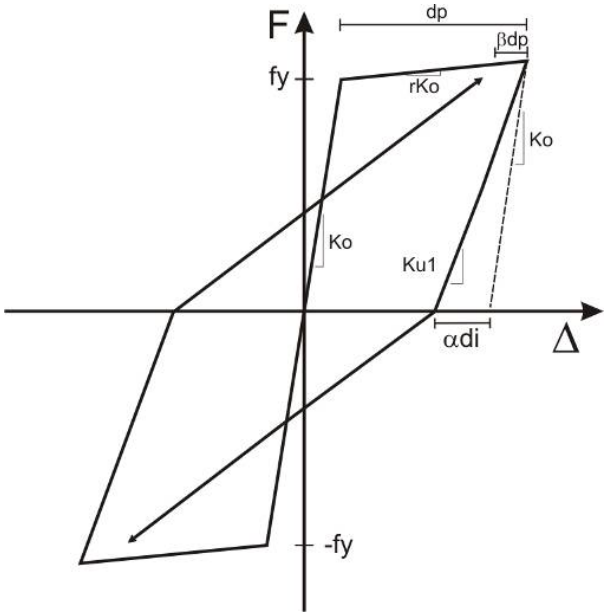

Figure 9-2: Modified Takeda reinforced concrete hysteresis rule, with Drain-2D unloading (as per Carr, 2005)

Table 9-1: Modified Takeda hysteresis parameters

Takeda Hysteresis Parameters	Description
α	Unloading Stiffness
β	Reloading Stiffness
NF	Reloading Stiffness Power Factor
KKK	Type of Unloading

The Pampanin hysteresis rule (Carr, 2005) was also calibrated to the experimental force versus displacement response of W1. The Pampanin hysteresis rule was developed to represent the behaviour of pre-1970's reinforced concrete beam column joints. The Pampanin hysteresis differs from the modified Takeda rule as it offers bilinear unloading and a slip on reloading (an example of the Pampanin hysteresis is shown in **Figure 9-3**). These differences make it suitable for defining the behaviour of concrete sections reinforced with plain round bars, as the characteristic pinching behaviour can be described. The loop requires the definition of seven different parameters to describe the unloading and reloading behaviour (Carr, 2005). The names and a description of these parameters a are listed in **Table 9-2**. The Pampanin hysteresis was under development at the University of Canterbury and was awaiting confirmation and implementation of the small cycle behaviour at the time of this research. The Pampanin hysteresis was therefore only suitable for calibration purposes until

these changes are complete. Two options are available for the definition of slip on reloading, the option used depends on the IOP parameter, in this contribution an IOP of 2 was used.

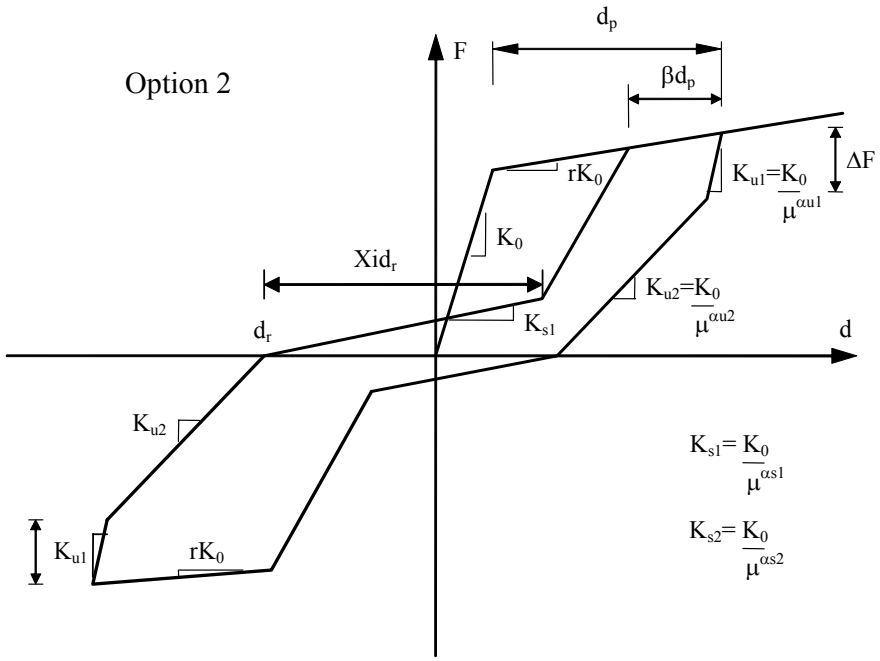

Figure 9-3: Pampanin, beam-column joint hysteresis rule, IOP=2 (as per Carr, 2005)

Table 9-2: Description of Pampanin hysteresis parameters (as per Carr, 2005)

Pampanin Hysteresis Parameters	Description
IOP	Options for the Definition of Slip on Reloading
AlfaS1	Slip Stiffness Power Factor
AlfaS2	Reloading Factor
AlfaU1	Initial Unloading Power Factor
AlfaU2	Final Unloading Power Factor
DeltaF	Unloading Force Factor
Beta	Reloading Factor

9.2.2 Strength Degradation

Calibration of the hysteretic models for W1 was performed with and without strength degradation. The sensitivity of the time history response to strength degradation could then be monitored. The incorporation of strength degradation in the hysteretic models provides a much more accurate representation of the experimental response. Two types of strength degradation were implemented the first was a function of the maximum ductility experienced by the wall and the second was a function of the number of inelastic cycles (Carr, 2005).

The level of strength degradation was defined by a degradation envelope, shown in **Figure 9-4**. The strength degradation envelope defines the ductility or cycle number at which strength degradation begins and when strength degradation stops. There are two options to define when strength degradation stops in Ruaumoko, the first is when a specified residual strength level is reached and the second is when the strength reaches 1% of the initial strength. In this contribution strength degradation ended when a specified residual strength was reached. For this three parameters were required to describe the strength degradation characteristics, the parameters are described in Table 9-3.

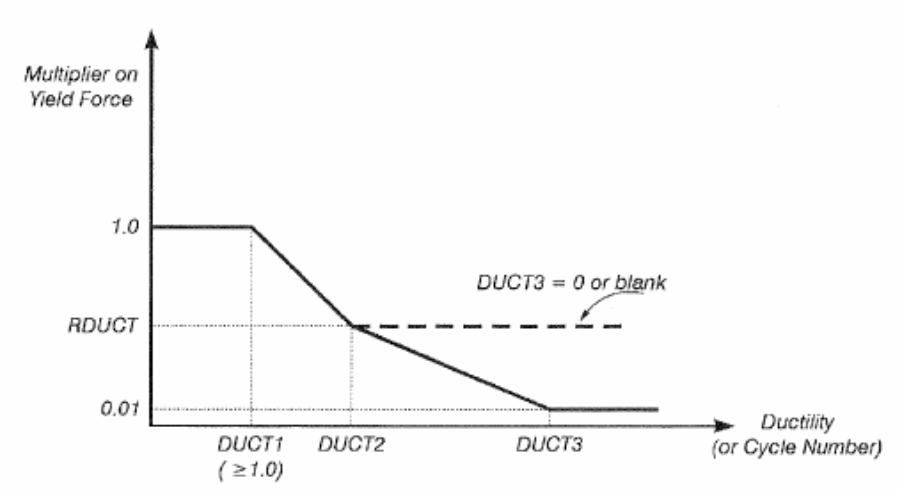

Figure 9-4: Definition of strength degradation envelope (as per Carr, 2005)

Table 9-3: Strength degradation parameters (as per Carr, 2005)

Strength Degradation Parameters	Description
DUCT1	Ductility (or Cycle) at which degradation begins
DUCT2	Ductility (or Cycle) at which degradation stops
RDUCT	Residual strength as fraction of the initial strength

9.2.3 Hysteresis Rules – W1R

To represent the inelastic behaviour of W1R two zero length, rotational inelastic springs were used in parallel. W1R was an un-bonded post-tensioned rocking wall and the two springs were used to represent the contributions to the force versus displacement response from the un-bonded post-tensioning and the energy dissipaters. The contribution from the un-bonded post-tensioning was represented by a bilinear elastic hysteresis and the contribution form the energy dissipaters was represented by an elasto-plastic hysteresis. The bilinear elastic rule used to define the contribution to the post-tensioning exhibits a non-linear behaviour due to a

geometric non-linearity not a material non-linearity. The two hysteresis rules are shown in **Figure 9-5**. The contributions from the bilinear elastic hysteresis and the elasto-plastic were appropriately balanced to achieve the flag shaped hysteresis observed in the experimental results.

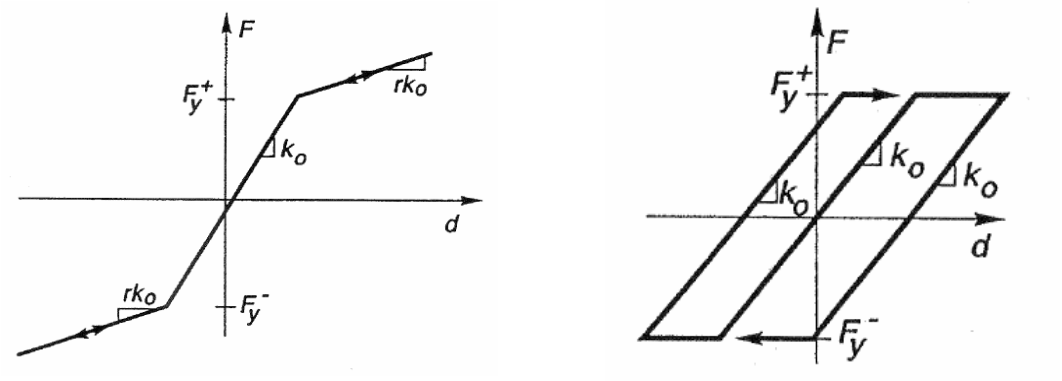

(a) (b)

Figure 9-5: (a) Bilinear elastic rule (as per Carr, 2005), (b) Elasto-plastic rule (as per Carr, 2005)

9.3 W1 – Hysteretic Calibration

For W1 a push versus pull analysis was performed to calibrate the hysteretic response used in the lumped plasticity models to the experimental force versus displacement response. Modified Takeda and Pampanin hysteresis rules were used with and without strength degradation. The calibrated hysteretic responses for different hysteresis rules are shown plotted over the top of the experimental hysteretic response in the following sections.

9.3.1 Modified Takeda

Figure 9-6 (a) shows the hysteretic force versus displacement response of the calibrated modified Takeda hysteresis loop compared to the experimental response of W1. A reasonable match was achieved, but the representation was limited by no strength degradation being included, and pinching not being accounted for. The calibrated parameters used to define the shape of the modified Takeda hysteresis are shown in **Table 9-4**. Equivalent viscous damping versus lateral drift for the experimental and calibrated hysteresis loops is shown in **Figure 9-6** (b). It can be seen that the calibrated modified Takeda with no strength degradation, exhibited a substantially higher level of equivalent viscous damping (nearly double) than the experimental response.

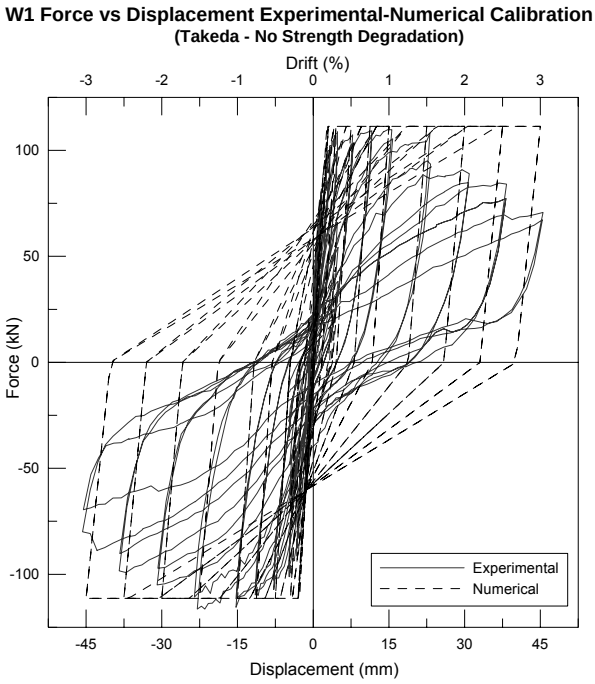

(a)

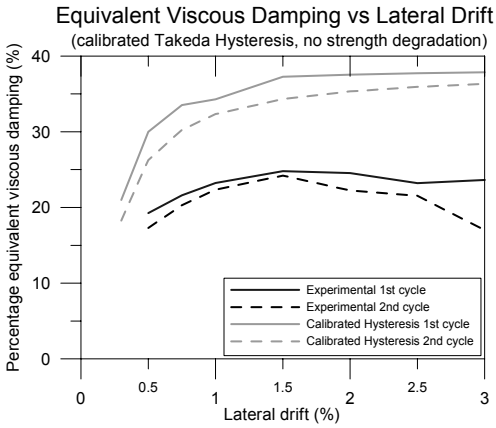

(b)

Figure 9-6: (a) W1, Takeda hysteresis calibration with no strength degradation; (b) equivalent viscous damping of experimental and calibrated hysteresis loops

Table 9-4: Calibrated Takeda hysteresis parameters for W1

Calibrated Takeda Parameters	Alpha	Beta	NF	KKK
	0.05	0.2	1	1

9.3.2 Modified Takeda – Max Ductility Strength Degradation

A modified Takeda hysteresis with strength degradation (dependent on the maximum ductility a section has experienced) was calibrated to the experimental response of W1 and is shown in **Figure 9-7** (a). The parameters used to define the hysteresis loop were the same as those determined for the calibration without strength degradation and are shown in **Table 9-4**. The inclusion of strength degradation significantly improved the calibration to the experimental results, the parameters used to describe the strength degradation are shown in **Table 9-5**. The calibration could be improved significantly if pinching could be accounted for with the hysteresis loop. Equivalent viscous damping versus lateral drift for the experimental and calibrated hysteresis loops is shown in **Figure 9-7** (b). It can be seen that the calibrated modified Takeda with max ductility based strength degradation, exhibited a substantially higher level of equivalent viscous damping than the experimental response. The inclusion of strength degradation only had a minor influence on the level of equivalent viscous damping experienced in the calibrated response.

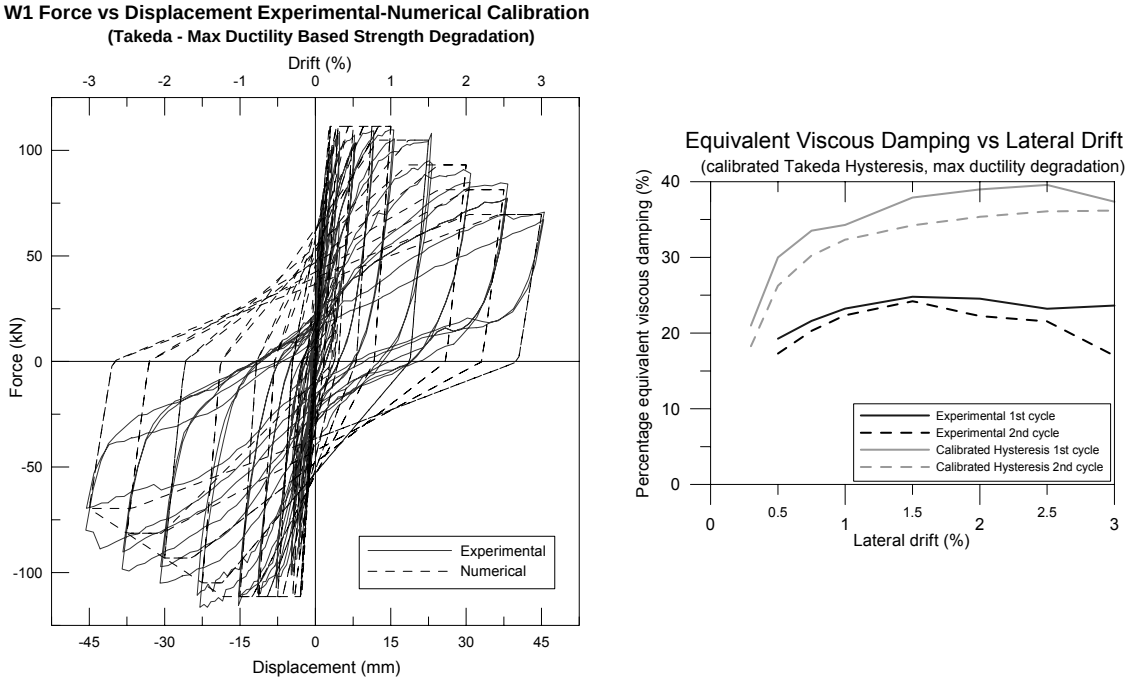

(a) (b)

Figure 9-7: (a) W1, Takeda hysteresis calibration with max ductility strength degradation; (b) equivalent viscous damping of experimental and calibrated hysteresis loops

Table 9-5: W1 modified Takeda calibration, max ductility base strength degradation parameters

Max Ductility strength degradation parameters	DUCT1	DUCT2	RDUCT
	8	24	0.5

9.3.3 Modified Takeda – Number of Inelastic Cycles Based Strength Degradation

A modified Takeda hysteresis with strength degradation as a function of the number of inelastic cycles was calibrated to the experimental response of W1 and is shown in **Figure 9-8** (a). The parameters used to define the shape of the modified Takeda hysteresis were the same as for the calibration without strength degradation, which are shown in **Table 9-4**. A substantially improved calibration was achieved with regards to the modified Takeda calibration without strength degradation. The parameters used to define the cyclic based strength degradation are shown in **Table 9-6**. As W1 was loaded to repeated cycles at the same drift strength degradation was observed. This showed that strength degradation is dependent on the number of cycles. To improve the calibration a hysteresis model including bilinear unloading and a slip on reloading to account for pinching would be required. Equivalent viscous damping versus lateral drift for the experimental and calibrated hysteresis loops is shown in **Figure 9-8** (b). It can be seen that the calibrated modified Takeda with

cyclic based strength degradation, exhibited a substantially higher level of equivalent viscous damping than the experimental response. The inclusion of strength degradation only had a minor influence on the level of equivalent viscous damping experienced in the calibrated response.

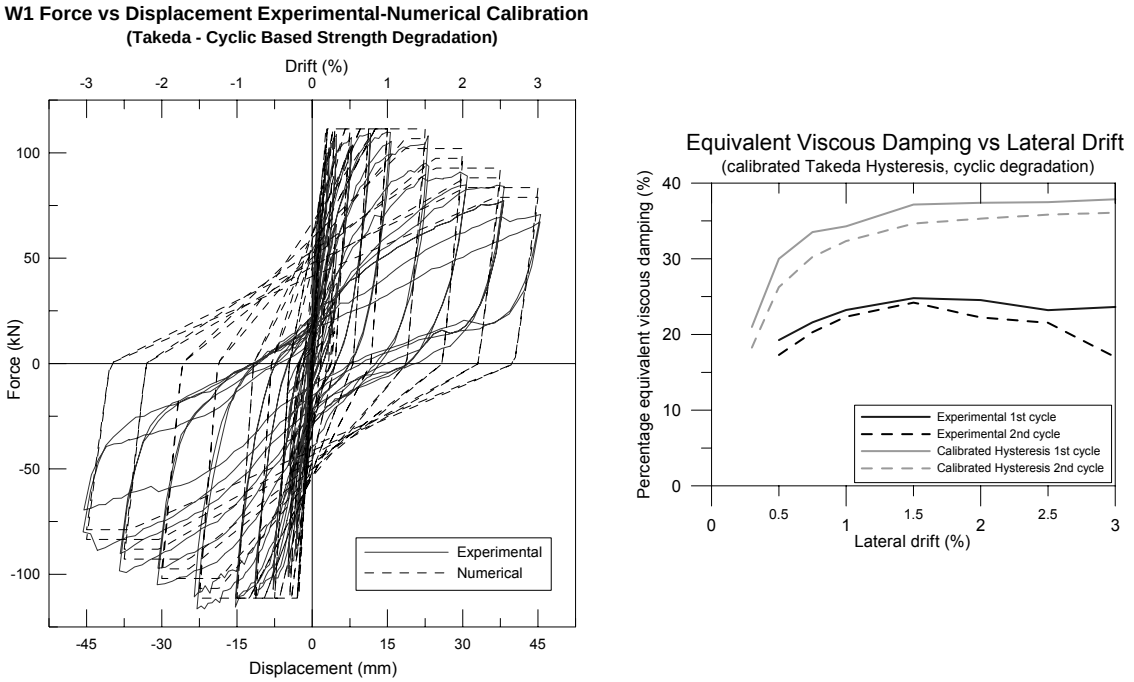

(a) (b)

Figure 9-8: (a) W1, Takeda hysteresis calibration with cyclic strength degradation; (b) equivalent viscous damping of experimental and calibrated hysteresis loops

Table 9-6: W1 modified Takeda Calibration with strength degradation based on the number of cycles

Cycle based strength degradation parameters	DUCT1	DUCT2	RDUCT
	4	12	0.5

9.3.4 Pampanin Calibration

The Pampanin hysteresis rule without strength degradation was calibrated to the experimental response of W1 and is shown in **Figure 9-9** (a). A reasonable fit was achieved, which was better than the calibrated modified Takeda hysteresis (without strength degradation) as it incorporated a bilinear unloading and a slip on reloading which allowed pinching to be accounted for. **Table 9-7** summarises the input parameters used to define the shape of the calibrated Pampanin hysteresis. Equivalent viscous damping versus lateral drift for the experimental and calibrated hysteresis loops is shown in **Figure 9-8** (b). The calibrated

response used a Pampanin hysteresis rule, but the equivalent viscous damping could only be calculated for the first drift cycle as the small cycle behaviour of the Pampanin hysteresis is still under development. The calibrated response exhibited a moderately higher level of equivalent viscous damping when compared to the experimental response, but it was substantial improvement when compared to the calibrated response using the modified Takeda hysteresis. This showed the importance of accounting for pinching in a hysteresis rule.

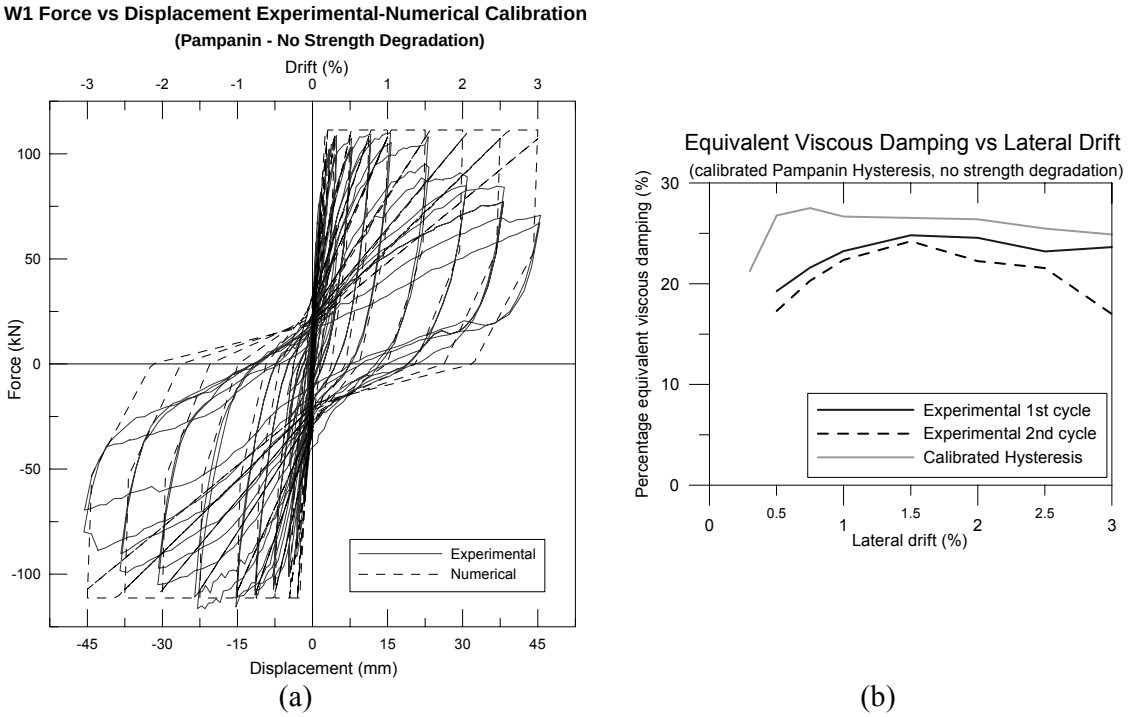

(a) (b)

Figure 9-9: (a) W1, Pampanin hysteresis calibration with no strength degradation; (b) equivalent viscous damping of experimental and calibrated hysteresis loops

Table 9-7: Calibrated Pampanin hysteresis parameters

Calibrated Pampanin Parameters	IOP	AlphaS1	AlphaS2	AlphaU1	AlphaU2	DeltaF	Beta
	2	1.5	1.0	-0.6	0.8	50	-0.05

9.3.5 Pampanin Calibration – Max Ductility Based Strength Degradation

A Pampanin hysteresis with strength degradation based on max ductility was calibrated to the experimental response of W1 and is shown in **Figure 9-10** (a). The parameters used to define the shape of the calibrated Pampanin hysteresis were that same as used for the calibration without strength degradation, the parameters are listed in **Table 9-7**. A very good representation of the hysteretic response was achieved in terms of the level of strength

degradation and the degree of pinching. The parameters used to define the maximum ductility based strength degradation are listed in **Table 9-8**. The use of strength degradation significantly improved the representation of the experimental results. **Figure 9-10** (b) shows the equivalent viscous damping versus lateral drift for the experimental response and the calibrated Pampanin hysteresis with the inclusion of max ductility based strength degradation. The inclusion of strength degradation only had a minor influence on the level of equivalent viscous damping.

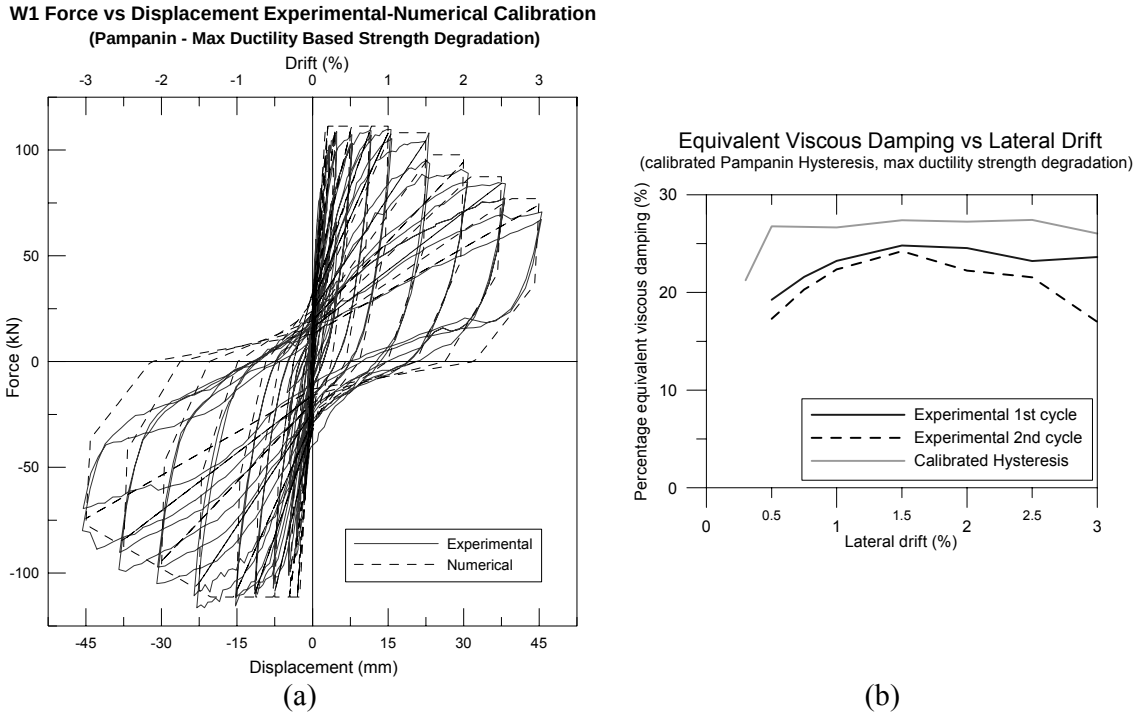

(a) (b)

Figure 9-10: (a) W1, Pampanin hysteresis calibration with max ductility strength degradation; (b) equivalent viscous damping of experimental and calibrated hysteresis loops

Table 9-8: Max ductility based strength degradation parameters for Pampainin hysteresis, W1

Max ductility based strength degradation parameters	DUCT1	DUCT2	RDUCT
	8	24	0.5

9.3.6 Pampanin Calibration – Number of Cycles Based Strength Degradation

A Pampanin hysteresis with strength degradation based on the number of inelastic cycles was calibrated to the experimental response of W1 and is shown in **Figure 9-11** (a). The parameters used to define the cycle based strength degradation are shown in **Table 9-9**. The parameters used to define the shape of the Pampanin hysteresis were the same as those used for the calibration without strength degradation and are listed in **Table 9-7**. A very good

representation of the experimental hysteresis was achieved, which was considerably better than that achieved using the modified Takeda hysteresis. This was due to the Pampanin hysteresis having the ability to define a bilinear unloading and pinching. **Figure 9-10** (b) shows the equivalent viscous damping versus lateral drift for the experimental response and the calibrated Pampanin hysteresis with the inclusion of cyclic based strength degradation. The inclusion of strength degradation only had a minor influence on the level of equivalent viscous damping.

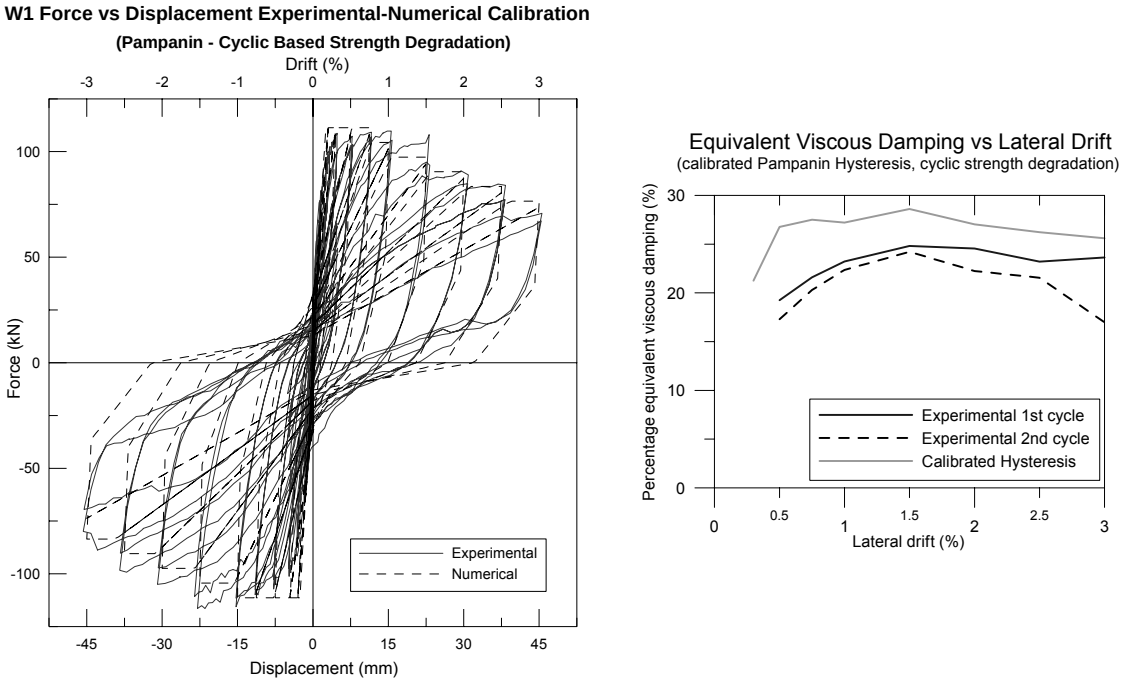

(a) (b)

Figure 9-11: (a) W1, Pampanin hysteresis calibration with cyclic strength degradation; (b) equivalent viscous damping of experimental and calibrated hysteresis loops

Table 9-9: Cyclic based strength degradation parameters for Pampanin hysteresis

Cyclic based strength degradation parameters	DUCT1	DUCT2	RDUCT
	4	12	0.5

9.4 W1R – Hysteretic Calibration

Hysteretic calibration to the experimental force versus displacement response for W1R was performed using two rotational springs in parallel. The first rotational spring was a bilinear elastic, which was used to represent the contribution from the un-bonded post-tensioning. The second spring was elasto-plastic, which represented the contribution from the external energy dissipaters mounted to the wall. **Figure 9-12** (a) shows the calibrated response compared to

the experimental response. The only hysteretic parameter required was the post-yield slope of the bilinear elastic hysteresis representing the contribution from the un-bonded post-tensioning, a value of 0.042 was used (4.2% of the elastic stiffness). The post-yield slope was not due to the post-tensioning yielding but was due to a geometric non-linearity. The flag shaped hysteresis was achieved by using an appropriate balance of the bilinear elastic and elasto-plastic hysteresis loops, this balance was determined from the design calculations (Appendix C).

A reasonable representation of the experimental response was achieved. Differences between the experimental and calibrated response occurred as there was substantial stiffness loss as testing on W1R progressed. This led to the calibrated response over estimating the reloading stiffness, especially in later cycles. As an elasto-plastic hysteresis rule was used to define the contribution from the energy dissipaters, however the bauschinger effect could not be accounted for. A loss in the level of initial post-tensioning resulted in a decrease in the peak strength achieved and in some small residual displacements being observed in the experimental response. This was not captured in the calibrated response. No strength degradation was required as strength degradation was not evident in the experimental response.

Figure 9-12 (b) shows the equivalent viscous damping versus lateral drift for the experimental and calibrated response. The equivalent viscous damping versus lateral drift for the calibrated response was moderately higher than that of the experimental response. The majority of the difference is likely due to the stiffness degradation experienced in the experimental response.

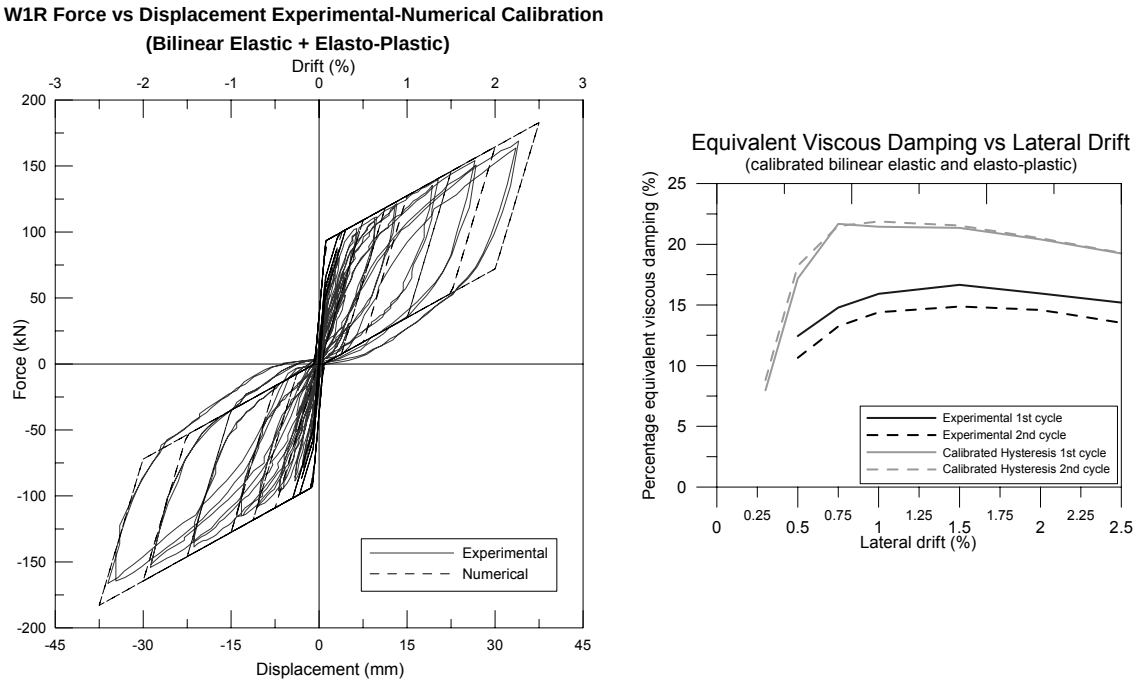

(a) (b)

Figure 9-12: (a) W1R, hysteresis calibration for the 1st hybrid test; (b) equivalent viscous damping of experimental and calibrated hysteresis loops

9.5 Selection and Scaling of Earthquake Records

An assortment of 16 earthquake records from the California region were selected for the time history analyses on the SDOF and MDOF models. The records were scaled to a 5% damped NZS1170.5 (NZS, 2005) elastic target spectrum with a 1/500 year annual probability of exceedence for soil type "D". Three different intensity levels were used, which corresponded to a PGA of 0.14g (Auckland), 0.21g (Christchurch) and 0.45g (Wellington). **Table 9-10** shows the name and relevant information regarding the 16 selected earthquake records used. The selected records did not include near fault effects and were recorded of soils of the type "C" & "D" according to the NEHRP guidelines (FEMA, 1997).

Table 9-10: Earthquake Record Information (Pampanin et.al, 2002)

Record Number	Earthquake Event	Year	Mw	Station	Soil Type (NEHRP)	Duration (s)	Original PGA (g)
1	Cape Mendocino	1992	7.1	Fortuna Fortuna Blvd	C	44.0	0.44
2	Cape Mendocino	1992	7.1	Rio Dell Overpass - FF	C	36.0	0.46
3	Landers	1992	7.3	Desert Hot Springs	C	50.0	0.39
4	Landers	1992	7.3	Yermo Fire Station	D	44.0	0.31
5	Loma Prieta	1989	6.9	Capitola	D	40.0	0.46
6	Loma Prieta	1989	6.9	Gilroy Array # 4	D	40.0	0.54
7	Loma Prieta	1989	6.9	Hollister Diff. Array	D	39.6	0.36
8	Loma Prieta	1989	6.9	Saratoga - W Valley Coll.	D	40.0	0.47
9	Northridge	1994	6.7	Beverly Hills 14145 Mulhol	C	30.0	0.34
10	Northridge	1994	6.7	Canoga Park - Topanga Can	D	25.0	0.37
11	Northridge	1994	6.7	LA - Hollywood Stor FF	D	40.0	0.42
12	Northridge	1994	6.7	N. Hollywood - Coldwater Can	C	21.9	0.43
13	Northridge	1994	6.7	Sunland - Mt Gleason Ave	C	30.0	0.46
14	Superstition Hills	1987	6.7	Brawley	D	22.0	0.29
15	Superstition Hills	1987	6.7	El Centro Imp. Co. Cent.	D	40.0	0.49
16	Superstition Hills	1987	6.7	Plaster City	D	22.2	0.36

The scaling procedure involved the use of two scale factors which were applied to the elastic acceleration spectra of each record. The first scale factor "k1" the record scale factor, was calculated for each individual record and was found by minimising function shown in Equation 9-1, over a target period range.

$$f(T) = \log\left(\frac{k_1 SA_{component}(T)}{SA_{T\,\arg et}(T)}\right) \qquad \textbf{Equation 9-1}$$

Where:

$SA_{component}$ = Record spectral acceleration component at time T

SA_{Target}= Target spectrum acceleration at time T

The target period range used was 0.5-2.5 seconds which was considered a suitable range for the models to be considered. It was suggested that "k1" should typically range between 0.33< k1< 3.0. The second scale factor "k2" the family scale factor was applied to all selected records and was used to ensure that over the entire specified period range at least one record exceeded the target spectrum. The "k2" factor must be at least 1.0. The scaled PGA and scale factors for each record are shown in **Table 9-11**.

Table 9-11: PGA of scaled earthquake records and the scale factors used

Target Spectrum PGA 0.14g (AUCK)			Target Spectrum PGA 0.21g (CHCH)			Target Spectrum PGA 0.45g (WGTN)		
Record	Scaled PGA (g)	Scale factor (k1*k2)	Record	Scaled PGA (g)	Scale factor (k1*k2)	Record	Scaled PGA (g)	Scale factor (k1*k2)
CM1	0.10	0.24	CM1	0.14	0.34	CM1	0.30	0.73
CM2	0.13	0.44	CM2	0.18	0.63	CM2	0.39	1.35
Lan1	0.10	0.29	Lan1	0.15	0.46	Lan1	0.31	0.97
Lan2	0.12	0.37	Lan2	0.17	0.53	Lan2	0.37	1.13
Lp1	0.20	0.48	Lp1	0.28	0.69	Lp1	0.60	1.47
Lp3	0.20	0.51	Lp3	0.29	0.73	Lp3	0.61	1.56
Lp5	0.15	0.46	Lp5	0.21	0.65	Lp5	0.46	1.40
Lp6	0.10	0.28	Lp6	0.14	0.40	Lp6	0.30	0.85
Nor2	0.13	0.45	Nor2	0.18	0.65	Nor2	0.39	1.36
Nor3	0.19	0.34	Nor3	0.27	0.49	Nor3	0.55	1.03
Nor5	0.19	0.43	Nor5	0.27	0.62	Nor5	0.56	1.30
Nor9	0.14	0.42	Nor9	0.20	0.61	Nor9	0.43	1.27
Nor10	0.16	0.39	Nor10	0.23	0.56	Nor10	0.47	1.18
Sup1	0.11	0.42	Sup1	0.16	0.60	Sup1	0.33	1.27
Sup2	0.07	0.26	Sup2	0.10	0.38	Sup2	0.21	0.80
Sup3	0.18	0.48	Sup3	0.26	0.68	Sup3	0.53	1.41

Figure 9-13 shows the target acceleration spectrum and the mean spectrum of the 16 scaled earthquake records for the 0.21g PGA intensity level (CHCH) (spectrum comparisons for 0.14g PGA (AUCK) & 0.45g PGA (WGTN) intensity levels can be found in Appendix C). It can be seen that the mean achieved a reasonable fit when compared to the target spectrum. The mean was consistently less than the target spectrum for larger period ranges, this is due to a typical trait of target spectrum to be conservative for long periods, to ensure a minimum strength level (Priestley, 1995).

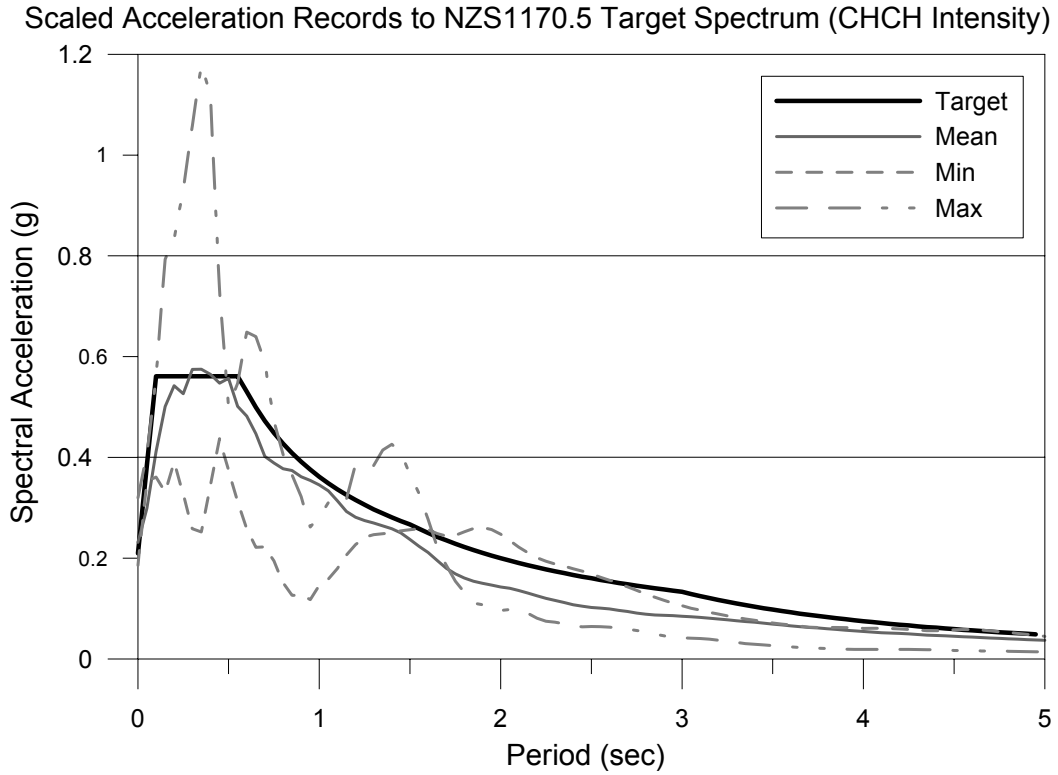

Figure 9-13: Comparison of target spectrum to mean of 16 scaled records, for PGA of 0.21g (CHCH)

9.6 SDOF Time History Analysis

A single degree of freedom model of the prototype wall was created in Ruaumoko (Carr, 2005) and used to investigate peak and residual displacements. The SDOF model was subject to 16 earthquake records, scaled to three intensity levels (PGA of 0.14g, 0.21g and 0.45g), as discussed in section 9.4. The SDOF model was used to monitor the sensitivity of peak and residual drifts of the model wall to strength degradation and p-delta. In a later section the peak base shear will be compared to that of a MDOF system to monitor the effects of higher modes.

Figure 9-14 shows a representation of the SDOF model used which consisted of a zero length inelastic spring at the base, an elastic beam element representing the wall and an effective seismic mass assigned at the top of the wall element. The equivalent SDOF system had an effective height of 7.94m (78% of the total height) with an effective mass of 76.9t (85% of the total seismic mass) and 5% critical damping was used. The process used to develop the equivalent SDOF system can be found in Chapter 10. The hysteretic properties of the inelastic spring were defined using the calibrated modified Takeda hysteresis and strength degradation parameters (for both types of strength degradation used) determined in section 9.2. The stiffness and yield moment capacity were scaled up from the experimental values to represent the prototype wall following the rules of similitude (Appendix C). The calibrated parameters for the Pampanin hysteresis were not used for the SDOF time history analyses as the hysteresis rule was still under development (small cycle behaviour).

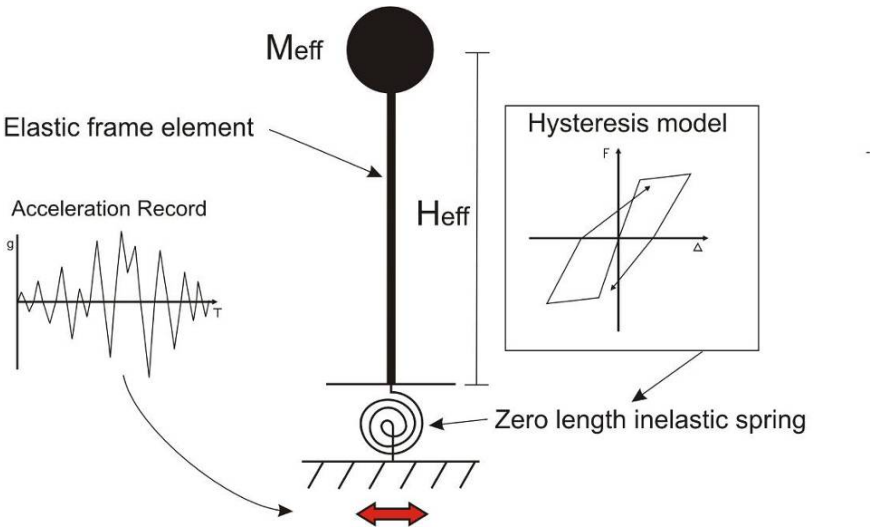

Figure 9-14: SDOF model used to represent prototype wall

9.6.1 SDOF Results – With & Without Strength Degradation

The sensitivity of peak and residual drifts to strength degradation was monitored using a series of non-linear time history analyses on a SDOF system representing the prototype wall. Calibrated modified Takeda hysteresis parameters were used with and without strength degradation. Two different types of strength degradation were used, the first was based on the maximum ductility the section was subjected to and the second was based off the number of inelastic cycles the section was subjected to. The parameters used to define the degrading strength envelope were calibrated to the experimental response in section 9.3. **Table 9-12** summarises the mean and standard deviation of maximum drifts experienced by the SDOF with and without the inclusion of strength degradation for the 16 scaled earthquake records at three different intensity levels. P-delta effects were not included in these analyses.

Table 9-12: Comparison of maximum drifts for SDOF systems, with & without strength degradation

	Maximum Drift (%)					
	Intensity					
	0.14g (PGA) (Auckland)		0.21g (PGA) (Christchurch)		0.45g (PGA) (Wellington)	
No SD	MEAN	0.53	MEAN	0.89	MEAN	2.60
	STDEV	0.14	STDEV	0.27	STDEV	0.93
Max ductility based SD	MEAN	0.53	MEAN	0.89	MEAN	2.80
	STDEV	0.14	STDEV	0.27	STDEV	1.26
Cyclic based SD	MEAN	0.53	MEAN	0.89	MEAN	2.68
	STDEV	0.14	STDEV	0.27	STDEV	1.17

For 0.14g (PGA) and 0.21g (PGA) intensity levels it was seen that there was no difference between the peak drifts for the SDOF systems when strength degradation was included. This was due to the drift levels experienced being smaller or on the limit of where strength degradation begins. From the calibrated hysteretic responses in section 9.3 it can be seen that strength degradation did not begin until after 1.0% drift.

When subject to a 0.45g (PGA) intensity level a small increase in the mean peak drift was experienced due to strength degradation. Strength degradation based on the maximum ductility resulted in the largest increase in the mean peak drift. This resulted in an 8% increase in peak drifts and a large increase in the standard deviation was observed. The accuracy of the strength degradation modelling is difficult to determine as it was based of experimental results of a wall subject to a cyclically increasing displacement regime. When subject to an acceleration record the displacement regime would not follow a cyclically increasing profile, this could substantially modify the strength degradation behaviour.

The sensitivity of residual drifts to strength degradation is compared in **Table 9-13**. For the 0.14g (PGA) and 0.21g (PGA) intensity levels it was seen the inclusion of strength degradation had no effect on the residual drifts. This was consistent with what was observed for the peak drifts. For the three SDOF systems subject to a 0.45g(PGA) intensity level it was seen that the mean residual drift corresponded to 18-23% of the mean maximum drift experienced. The effect of strength degradation on the mean residual drift was variable. Strength degradation based on maximum ductility resulted in a small decrease in the mean residual drift (8%) and strength degradation based on the number of cycles resulted in a small increase (7%) in the observed residual drift. It should be noted that there was a high standard deviation in the residual drifts observed.

Table 9-13: Comparison of residual drifts for SDOF systems with & without strength degradation

	Residual Drift (%)					
	Intensity					
	0.14g (PGA) (Auckland)		0.21g (PGA) (Christchurch)		0.45g (PGA) (Wellington)	
No SD	MEAN	0.07	MEAN	0.16	MEAN	0.58
	STDEV	0.06	STDEV	0.11	STDEV	0.45
Max ductility based SD	MEAN	0.07	MEAN	0.16	MEAN	0.53
	STDEV	0.06	STDEV	0.11	STDEV	0.60
Cyclic based SD	MEAN	0.07	MEAN	0.16	MEAN	0.62
	STDEV	0.06	STDEV	0.11	STDEV	0.59

9.6.2 SDOF Results – With and Without P-delta

The sensitivity of the peak and residual drifts to p-delta effects was monitored for the SDOF models representing the prototype wall. The SDOF models included a calibrated modified Takeda hysteresis and were performed with and without strength degradation. The peak drifts for the SDOF models with and without p-delta effects are summarised in Table 9-14.

Table 9-14: Comparison of maximum drifts of SDOF systems, with and without p-delta

	Maximum Drift (%)								
	Intensity								
	0.14g (PGA) (Auckland)			**0.21g (PGA) (Christchurch)**			**0.45g (PGA) (Wellington)**		
		No P-Δ	With P-Δ		No P-Δ	With P-Δ		No P-Δ	With P-Δ
No SD	MEAN	0.53	0.54	MEAN	0.89	0.91	MEAN	2.60	2.71
	STDEV	0.14	0.14	STDEV	0.27	0.27	STDEV	0.93	1.09
Max ductility based SD	MEAN	0.53	0.54	MEAN	0.89	0.91	MEAN	2.80	3.13
	STDEV	0.14	0.15	STDEV	0.27	0.27	STDEV	1.26	1.57
Cyclic based SD	MEAN	0.53	0.54	MEAN	0.89	0.91	MEAN	2.68	2.66
	STDEV	0.14	0.15	STDEV	0.27	0.27	STDEV	1.17	0.96

The inclusion of p-delta effects generally resulted in a small increase in the mean peak drifts experienced. For all situations except for the two 0.45g (PGA) intensity levels including

strength degradation the increase in maximum drift was less that 5%. The most significant increase in peak drift was observed for the 0.45g (PGA) intensity with max ductility based strength degradation. This resulted in a 12% increase in the mean peak drift. For the 0.45g (PGA) intensity level including strength degradation based on the number of cycles a slight reduction (2%) in the peak drift was observed.

The sensitivity of residual displacements to p-delta effects for the SDOF systems is summarised in **Table 9-15**. It was seen that the inclusion of p-delta effects substantially increases the magnitude of the observed residual displacements for all the SDOF systems considered. A general trend was observed that as the earthquake intensity level increased the effect of p-delta on residual displacements also increased. This was in line with expectations as when the intensity level increases the peak displacements also increase, which increases the effect of p-delta. For the 0.45g (PGA) intensity the SDOF system without strength degradation exhibited a 125% increase in residual drifts due to p-delta effects. The most significant increase was observed for the 0.45g (PGA) intensity and the SDOF system including maximum ductility based strength degradation. In this case the observed increase in residual drift due to p-delta effects was 280%. The substantial increase in residual drifts was likely due to the p-delta effects resulting in a negative post-yield stiffness. The post-yield stiffness of the calibrated modified Takeda hysteresis was zero.

Table 9-15: Comparison of residual displacements of SDOF system, with and without p-delta

	Residual Drift (%)								
	Intensity								
	0.14g (PGA) (Auckland)			0.21g (PGA) (Christchurch)			0.45g (PGA) (Wellington)		
		No P-Δ	With P-Δ		No P-Δ	With P-Δ		No P-Δ	With P-Δ
No SD	MEAN	0.07	0.09	MEAN	0.16	0.23	MEAN	0.58	1.31
	STDEV	0.06	0.07	STDEV	0.11	0.16	STDEV	0.45	1.10
Max ductility based SD	MEAN	0.07	0.09	MEAN	0.16	0.23	MEAN	0.53	2.02
	STDEV	0.06	0.07	STDEV	0.11	0.16	STDEV	0.60	1.95
Cyclic based SD	MEAN	0.07	0.09	MEAN	0.16	0.23	MEAN	0.62	1.21
	STDEV	0.06	0.07	STDEV	0.11	0.16	STDEV	0.59	0.88

9.6.3 SDOF Results – As-built Prototype versus Retrofitted Prototype

The as-built and retrofitted performance of the prototype wall (W1 versus W1R) was assessed using the SDOF models. The hysteretic response for the as-built and retrofitted prototype wall was calibrated to the experimental results in section 9.3 and 9.4. For the as-built prototype wall the hysteretic model including strength degradation based upon maximum ductility was used, as it resulted in the highest peak and residual drifts.

Table 9-16 provides a comparison of the maximum drift levels for the as-built and retrofitted walls when subject to the 16 earthquake records scaled to the three intensity levels.

Table 9-16: Comparison of maximum drifts for as-built and retrofitted prototype

	Maximum Drift (%)								
	Intensity								
	0.14g (PGA) (Auckland)			0.21g (PGA) (Christchurch)			0.45g (PGA) (Wellington)		
		No P-Δ	With P-Δ		No P-Δ	With P-Δ		No P-Δ	With P-Δ
As-built Prototype	MEAN	0.53	0.54	MEAN	0.89	0.91	MEAN	2.80	3.13
(Max Ductility SD)	STDEV	0.14	0.15	STDEV	0.27	0.27	STDEV	1.26	1.57
Retrofitted Prototype	MEAN	0.63	0.64	MEAN	0.98	0.99	MEAN	2.40	2.42
	STDEV	0.16	0.17	STDEV	0.25	0.25	STDEV	0.76	0.80

The displacement capacity of the as-built prototype was governed by a code specified ductility limit of five. This was used to calculate a displacement capacity in Appendix A which was determined to be 1.45% drift. From the results of the SDOF analyses it was seen that the maximum drifts were within the specified limit for the 0.14g (PGA) and 0.21g (PGA) intensities, but were not for the 0.45g (PGA) intensity.

Comparison of the peak drifts for the as-built and retrofitted situation showed that at lower intensity levels (0.14g (PGA) & 0.21g (PGA)) the retrofitted wall resulted in slightly increased peak drift levels. However for the 0.45g (PGA) intensity level the peak drift experienced by the retrofitted wall was significantly reduced. For the situation including p-delta the retrofit solution resulted in a 23% reduction in the mean peak drift. P-delta effects were also noted to be of less significance for the retrofitted wall.

The residual drift levels of the as-built and retrofitted prototype wall for the three intensity levels are compared in **Table 9-17**. When subjected to earthquake records of the 0.14g (PGA) and 0.21g (PGA) intensity it can be seen that the residual drifts were relatively minor, which was consistent with the low peak drifts experienced for these intensities. A comparison of the residual drifts for the as-built and retrofitted situation, when subject to 0.45g (PGA) intensity level excitations, shows the distinct advantage of a controlled rocking structure with re-centring capabilities. The retrofitted wall had negligible residual drifts after seismic excitation but the as-built wall experienced a mean residual drift of 2.0% drift with a standard deviation of 1.95% drift. With residual drift levels of this magnitude the structure could not be repaired and would have to be demolished.

Table 9-17: Comparison of residual drifts for as-built and retrofitted prototype

	Residual Drift (%)								
	Intensity								
	0.14g (PGA) (Auckland)			0.21g (PGA) (Christchurch)			0.45g (PGA) (Wellington)		
		No P-Δ	With P-Δ		No P-Δ	With P-Δ		No P-Δ	With P-Δ
As-built Prototype	MEAN	0.07	0.09	MEAN	0.16	0.23	MEAN	0.62	2.02
(Max Ductility SD)	STDEV	0.06	0.07	STDEV	0.11	0.16	STDEV	0.59	1.95
Retrofitted Prototype	MEAN	0.01	0.01	MEAN	0.01	0.01	MEAN	0.01	0.01
	STDEV	0.01	0.01	STDEV	0.01	0.01	STDEV	0.00	0.00

9.6.4 Example – As-built versus Retrofitted Prototype

An example of the drift versus time response for the as-built and retrofitted prototype wall is shown in **Figure 9-15**. The example is for the Nor9 earthquake record scaled to a 0.45g (PGA) intensity level. It was seen that the retrofitted wall resulted in a moderate decrease in the peak drift experienced. The most substantial feature was that the retrofitted wall resulted in zero residual drift whilst the as-built prototype resulted in 0.8% residual drift.

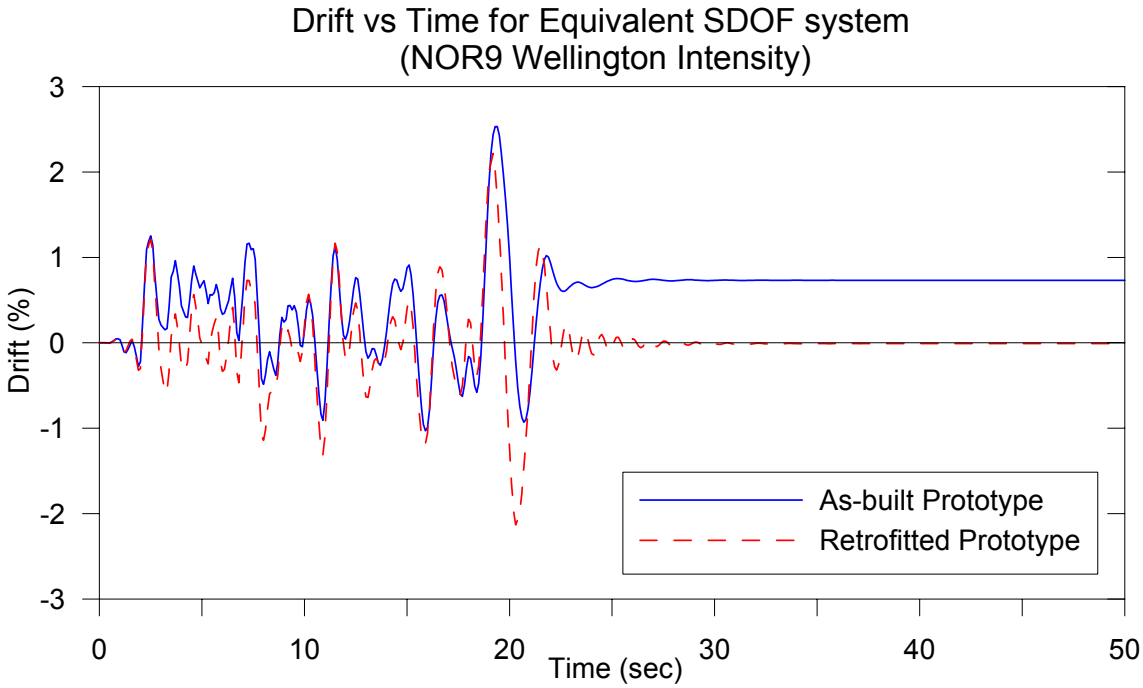

Figure 9-15: Peak displacement versus time for as-built and retrofitted prototype for Nor9 earthquake record (0.45g (PGA) intensity)

Examples of the hysteretic response of the as-built and retrofitted prototype wall when subject to Nor9 scaled to a 0.45g (PGA) intensity level are shown in **Figure 9-16**. The modified Takeda and flag shaped hysteresis loops of the two systems can be observed.

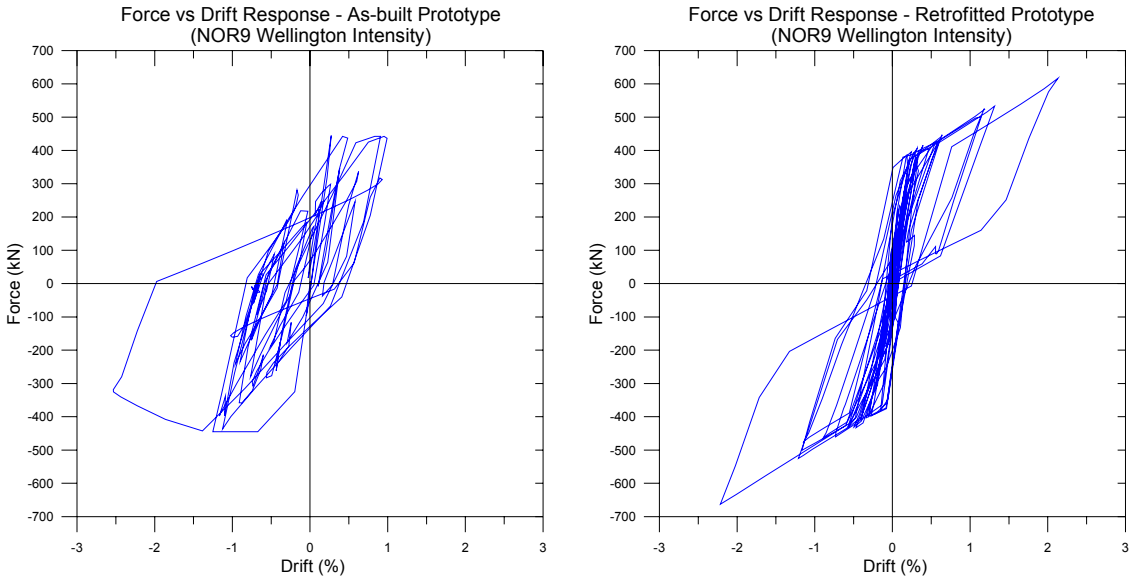

(a) (b)

Figure 9-16: Force versus displacement response for Nor9 earthquake record (0.45g (PGA) intensity); (a) As-built prototype wall, (b) Retrofitted prototype wall

9.7 MDOF Time History Analysis

A multi degree of freedom model of the prototype wall was created in Ruaumoko (Carr, 2005) and used to monitor peak drifts, residual drifts and peak base shear. The MDOF model was subject to 16 earthquake records scaled to three intensity levels corresponding to 0.14g (PGA), 0.21g (PGA) and 0.45g (PGA). The sensitivity of peak and residual drifts to strength degradation and p-delta effects was monitored. The effect of higher modes on the base shear was also monitored by comparing the SDOF and MDOF analyses.

Figure 9-17 shows the MDOF lumped plasticity model used which consisted of a zero length inelastic rotational spring at the base of the wall, elastic beam elements representing the wall with a seismic mass assigned at each floor level. An inter-storey height of 3.4m and a floor mass of 30t were used. The damping used consisted of 5% critical damping of the first and third modes. The hysteretic properties of the inelastic spring were defined using the calibrated hysteresis and strength degradation parameters determined in section 9.3. The stiffness and yield moment capacity were scaled up from the experimental values to represent the prototype wall, following the rules of similitude (Appendix C). The calibrated parameters for the Pampanin hysteresis were not used for the MDOF time history analyses as the hysteresis rule was still under development.

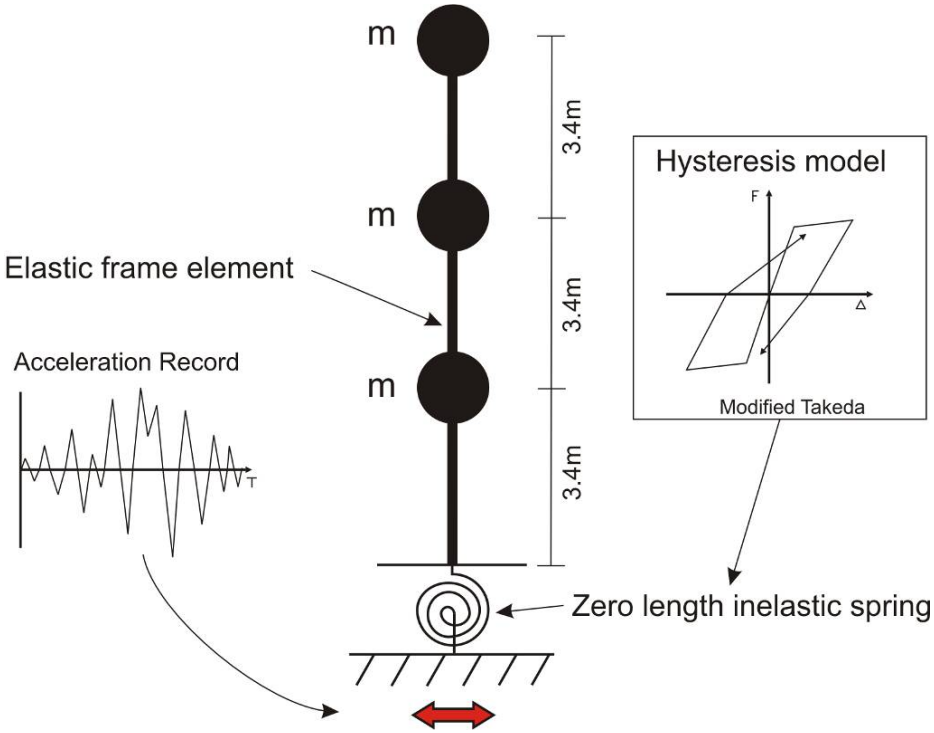

Figure 9-17: MDOF lumped plasticity model used to represent prototype wall

9.7.1 MDOF Results – Sensitivity to Strength Degradation and P-delta

The sensitivity of the mean peak drift to strength degradation and p-delta effects for MDOF systems was monitored by a series of time history analyses. Calibrated modified Takeda hysteresis parameters (section 9.3) were used with and without strength degradation. Two different types of strength degradation were used, the first was based off the maximum ductility the section was subjected to and the second was based off the number of cycles the section was subjected to. The parameters used to define the degrading strength envelope were calibrated to the experimental response in section 9.3. The analyses were performed with and without p-delta effects. **Table 9-18** summarises the mean and standard deviation of the maximum drift experienced by the MDOF systems.

Table 9-18: Comparison of maximum drifts of MDOF systems, with and without p-delta

	Maximum Drift (%)								
	Intensity								
	0.14g (PGA) (Auckland)			0.21g (PGA) (Christchurch)			0.45g (PGA) (Wellington)		
		No P-Δ	With P-Δ		No P-Δ	With P-Δ		No P-Δ	With P-Δ
No SD	MEAN	0.53	0.54	MEAN	0.89	0.91	MEAN	2.60	2.70
	STDEV	0.13	0.13	STDEV	0.26	0.26	STDEV	0.91	1.02
Max ductility based SD	MEAN	0.53	0.54	MEAN	0.89	0.91	MEAN	2.80	3.36
	STDEV	0.14	0.14	STDEV	0.26	0.26	STDEV	1.22	2.28
Cyclic based SD	MEAN	0.53	0.54	MEAN	0.89	0.91	MEAN	2.60	2.70
	STDEV	0.14	0.14	STDEV	0.26	0.26	STDEV	0.91	1.02

The sensitivity of MDOF systems to strength degradation and p-delta, was similar to the conclusions drawn from the results of the SDOF analyses. For low intensity levels (0.14g (PGA) and 0.21g (PGA)) strength degradation had no effect on maximum drift experienced. For the 0.45g (PGA) level intensity there was a small increase in the peak drift (8%) when strength degradation based on maximum ductility was used. P-delta effects generally resulted in a increase in mean maximum drifts of less that 5%. The only exception was for the 0.45g (PGA) intensity when max ductility strength degradation was used. In this case p-delta effects resulted in a 20% increase in the mean peak drift.

The sensitivity of residual displacements to strength degradation and p-delta effects is summarised in **Table 9-19**. It was seen that at low intensity levels (0.14g (PGA) and 0.21g (PGA)) strength degradation had no effect on the residual displacements for the MDOF systems. For the 0.45g (PGA) intensity level strength degradation resulted in no change, or a slight reduction in the residual drift when p-delta effects were not included. P-delta effects were observed to have a significant influence on the level of residual displacements. As the intensity of the earthquake record increased effect of p-delta on residual displacements increased. The largest increase was for the 0.45g (PGA) intensity, with maximum ductility based strength degradation. In this situation the mean residual drift increased by 300%.

Table 9-19: Comparison of residual drifts of MDOF systems, with and without p-delta

	Residual Drift (%)								
	Intensity								
	0.14g (PGA) (Auckland)			0.21g (PGA) (Christchurch)			0.45g (PGA) (Wellington)		
		No P-Δ	With P-Δ		No P-Δ	With P-Δ		No P-Δ	With P-Δ
No SD	MEAN	0.07	0.08	MEAN	0.16	0.21	MEAN	0.61	1.19
	STDEV	0.06	0.07	STDEV	0.11	0.14	STDEV	0.43	0.91
Max ductility based SD	MEAN	0.07	0.08	MEAN	0.16	0.21	MEAN	0.53	2.12
	STDEV	0.06	0.07	STDEV	0.11	0.14	STDEV	0.59	2.72
Cyclic based SD	MEAN	0.07	0.08	MEAN	0.16	0.09	MEAN	0.61	1.19
	STDEV	0.06	0.07	STDEV	0.11	0.24	STDEV	0.43	0.91

The sensitivity of the mean peak base shear to strength degradation and p-delta is summarised in **Table 9-20**. It was observed that strength degradation and p-delta effects had no influence on the maximum observed mean base shear, which would be expected.

Table 9-20: Comparison of base shear of MDOF systems, with and without p-delta

	Maximum Base Shear (kN)								
	Intensity								
	0.14g (PGA) (Auckland)			0.21g (PGA) (Christchurch)			0.45g (PGA) (Wellington)		
		No P-Δ	With P-Δ		No P-Δ	With P-Δ		No P-Δ	With P-Δ
No SD	MEAN	96	96	MEAN	106	106	MEAN	143	143
	STDEV	11	10	STDEV	15	15	STDEV	30	31
Max ductility based SD	MEAN	96	96	MEAN	106	106	MEAN	141	142
	STDEV	11	10	STDEV	15	15	STDEV	30	31
Cyclic based SD	MEAN	96	96	MEAN	106	106	MEAN	143	143
	STDEV	11	10	STDEV	15	15	STDEV	30	31

9.7.2 MDOF Results – As-built Prototype versus Retrofitted Prototype

The as-built and retrofitted performance of the prototype wall was assessed using MDOF models. The hysteretic response for the as-built and retrofitted prototype wall was calibrated to the experimental results in section 9.3 and 9.4. For the as-built prototype wall the hysteretic model including strength degradation based upon maximum ductility was used as it resulted in the highest peak and residual drifts. **Table 9-21** provides a comparison of the maximum drift levels for the as-built and retrofitted situation when subject to the series of earthquake records scaled to three different intensity levels.

Table 9-21: Comparison of maximum drifts for as-built and retrofitted prototype wall

	Maximum Drift (%)								
	Intensity								
	0.14g (PGA) (Auckland)			0.21g (PGA) (Christchurch)			0.45g (PGA) (Wellington)		
		No P-Δ	With P-Δ		No P-Δ	With P-Δ		No P-Δ	With P-Δ
As-built Prototype	MEAN	0.53	0.54	MEAN	0.89	0.91	MEAN	2.80	3.36
(Max ductility SD)	STDEV	0.14	0.14	STDEV	0.26	0.26	STDEV	1.22	2.28
Retrofitted Prototype	MEAN	0.63	0.64	MEAN	0.96	0.98	MEAN	2.39	2.40
	STDEV	0.17	0.18	STDEV	0.25	0.25	STDEV	0.75	0.79

Similar results were obtained for the MDOF system as were observed for the SDOF system when maximum drifts were compared for the as-built and retrofitted prototype wall. Comparison of the mean peak drifts for the as-built and retrofitted situation showed that at lower intensity levels (0.14g (PGA) & 0.21g (PGA)) the retrofitted wall resulted in slightly increased peak drift levels. However for the 0.45g (PGA) intensity level the peak drift experienced by the retrofitted wall was significantly reduced. For the situation including p-delta the retrofit solution resulted in a 42% reduction in the mean peak drift. P-delta effects had a smaller influence on the mean peak drift observed for the retrofitted situation.

The residual drift levels of the as-built and retrofitted prototype wall for the three intensity levels are compared in **Table 9-22**. When subjected to earthquake records of 0.14g (PGA) and 0.21g (PGA) intensity it can be seen that the residual drifts were relatively minor, which was consistent with the low peak drifts experienced for these intensities. A comparison of the

residual drifts for the as-built and retrofitted situation, when subject to 0.45g (PGA) intensity level excitations again shows the distinct advantages of a controlled rocking structure with re-centring capabilities. The retrofitted wall had negligible residual drifts after seismic excitation but the as-built wall experienced a mean residual drift of 2.1% drift with a standard deviation of 2.7% drift. With residual drift levels of this magnitude the structure could not be repaired.

Table 9-22: Comparison of residual drifts for as-built and retrofitted prototype wall

	Residual Drift (%)								
	Intensity								
	0.14g (PGA) (Auckland)			0.21g (PGA) (Christchurch)			0.45g (PGA) (Wellington)		
		No P-Δ	With P-Δ		No P-Δ	With P-Δ		No P-Δ	With P-Δ
As-built Prototype	MEAN	0.07	0.08	MEAN	0.16	0.21	MEAN	0.53	2.12
(Max ductility SD)	STDEV	0.06	0.07	STDEV	0.11	0.14	STDEV	0.59	2.72
Retrofitted Prototype	MEAN	0.01	0.01	MEAN	0.01	0.01	MEAN	0.01	0.01
	STDEV	0.00	0.01	STDEV	0.01	0.01	STDEV	0.00	0.00

The peak observed base shear for the as-built and retrofitted prototype wall at the three intensity levels is summarised in **Table 9-23**. As the intensity of the earthquake record was increased it was observed that the base shear increased substantially. The increase in base shear for the as-built situation was due to higher mode effects. For the retrofitted situation the increase in base shear was due to a combination of higher mode effects and the higher post-yield stiffness of the flag shaped hysteresis. The retrofitted wall resulted in a mean peak base shear increase of 15% for the 0.45g (PGA) intensity level.

Table 9-23: Comparison of maximum base shear for as-built and retrofitted prototype wall

	Maximum Base Shear (kN)								
	Intensity								
	0.14g (PGA) (Auckland)			0.21g (PGA) (Christchurch)			0.45g (PGA) (Wellington)		
		No P-Δ	With P-Δ		No P-Δ	With P-Δ		No P-Δ	With P-Δ
As-built Prototype	MEAN	96	96	MEAN	106	106	MEAN	141	142
(Max ductility SD)	STDEV	11	10	STDEV	15	15	STDEV	30	31
Retrofitted Prototype	MEAN	93	94	MEAN	112	114	MEAN	160	163
	STDEV	13	13	STDEV	13	15	STDEV	19	21

9.8 SDOF versus MDOF Time History Results

The results of the SDOF and MDOF analyses were compared to monitor how well the equivalent SDOF represent the MDOF prototype wall and to monitor the effect of higher modes on the peak base shear. The comparisons made between the SDOF and MDOF systems in this section are for analyses performed with p-delta effects.

Table 9-24 summarises the mean and standard deviation of the peak drift for the SDOF and MDOF system. In all cases the difference in mean peak drift between the SDOF and MDOF system was less that 8%.

Table 9-24: SDOF versus MDOF maximum drift comparisons

	Maximum Drift (%)								
	Intensity								
	0.14g (PGA) (Auckland)			0.21g (PGA) (Christchurch)			0.45g (PGA) (Wellington)		
		SDOF	MDOF		SDOF	MDOF		SDOF	MDOF
As-built Prototype	MEAN	0.54	0.54	MEAN	0.91	0.91	MEAN	2.71	2.70
No SD	STDEV	0.14	0.13	STDEV	0.27	0.26	STDEV	1.09	1.02
As-built Prototype	MEAN	0.54	0.54	MEAN	0.91	0.91	MEAN	3.13	3.36
Max ductility based SD	STDEV	0.15	0.14	STDEV	0.27	0.26	STDEV	1.57	2.28
As-built Prototype	MEAN	0.54	0.54	MEAN	0.91	0.91	MEAN	2.66	2.70
Cyclic based SD	STDEV	0.15	0.14	STDEV	0.27	0.26	STDEV	0.96	1.02
Retrofitted Prototype	MEAN	0.64	0.64	MEAN	0.99	0.98	MEAN	2.42	2.40
	STDEV	0.17	0.18	STDEV	0.25	0.25	STDEV	0.80	0.79

The mean and standard deviation of the residual drift for the SDOF and MDOF systems are summarised in **Table 9-25**. The difference in residual drift between the SDOF and MDOF systems was generally less than 10%. One exception was the as-built wall with cyclic based strength degradation, in this case the difference was 61%.

Table 9-25: SDOF versus MDOF residual drift comparisons

	Residual Drift (%)								
	Intensity								
	0.14g (PGA) (Auckland)			0.21g (PGA) (Christchurch)			0.45g (PGA) (Wellington)		
		SDOF	MDOF		SDOF	MDOF		SDOF	MDOF
As-built Prototype	MEAN	0.09	0.08	MEAN	0.23	0.21	MEAN	1.31	1.19
No SD	STDEV	0.07	0.07	STDEV	0.16	0.14	STDEV	1.10	0.91
As-built Prototype	MEAN	0.09	0.08	MEAN	0.23	0.21	MEAN	2.02	2.12
Max ductility based SD	STDEV	0.07	0.07	STDEV	0.16	0.14	STDEV	1.95	2.72
As-built Prototype	MEAN	0.09	0.08	MEAN	0.23	0.09	MEAN	1.21	1.19
Cyclic based SD	STDEV	0.07	0.07	STDEV	0.16	0.24	STDEV	0.88	0.91
Retrofitted Prototype	MEAN	0.01	0.01	MEAN	0.01	0.01	MEAN	0.01	0.01
	STDEV	0.01	0.01	STDEV	0.01	0.01	STDEV	0.00	0.00

The maximum base shears for the SDOF and MDOF systems are compared in **Table 9-26**. The base shears were compared to monitor the potential increase due to dynamic magnification as a result of higher mode effects. The maximum base shear of the SDOF system representing the as-built prototype wall could not be amplified by higher modes and was constant at 84kN as the post-yield slope was zero. The inclusion of strength degradation did not alter the observed peak mean base shear of the as-built prototype wall for both the SDOF and MDOF models. Significant increases in the mean peak base shear were however observed for the MDOF system due to higher modes. The effect of higher modes increased as the intensity of the earthquake records increase. For 0.14g (PGA), 0.21g (PGA) and 0.45g (PGA) intensity levels there was a 14%, 26% and 70% increase in the peak mean base shear respectively, due to higher mode effects, for the as-built prototype wall.

The mean peak base shear for the SDOF model of the retrofitted prototype wall was not constant because of the post-yield stiffness of the hysteretic response. The effect of higher modes was monitored by comparing the peak mean base shear of the SDOF and MDOF

systems. For the 0.14g (PGA), 0.21g (PGA) and 0.45g (PGA) intensity levels the increase in peak mean base shear due to dynamic magnification was 24%, 33% and 28% respectively. The mean peak base shears for the as-built and retrofitted situations were also compared. The difference in mean peak base shear was -2%, 8% and 14% for the 0.14g (PGA), 0.21g (PGA) and 0.45g (PGA) intensity levels respectively.

Table 9-26: SDOF versus MDOF maximum base shear comparisons

	Maximum Base Shear (kN)								
	Intensity								
	0.14g (PGA) (Auckland)			0.21g (PGA) (Christchurch)			0.45g (PGA) (Wellington)		
		SDOF	MDOF		SDOF	MDOF		SDOF	MDOF
As-built Prototype	MEAN	84	96	MEAN	84	106	MEAN	84	143
No SD	STDEV	0	10	STDEV	0	15	STDEV	0	31
As-built Prototype	MEAN	84	96	MEAN	84	106	MEAN	84	142
Max ductility based SD	STDEV	0	10	STDEV	0	15	STDEV	0	31
As-built Prototype	MEAN	84	96	MEAN	84	106	MEAN	84	143
Cyclic based SD	STDEV	0	10	STDEV	0	15	STDEV	0	31
Retrofitted Prototype	MEAN	76	94	MEAN	86	114	MEAN	127	163
	STDEV	6	13	STDEV	7	15	STDEV	23	21

9.9 Summary of Time History Results

A series of non-linear time history analyses were performed of equivalent SDOF and MDOF lumped plasticity models representing the as-built and retrofitted 3-storey prototype wall, which was developed in Chapter 3. The analyses were used to monitor the sensitivity of peak drifts, residual drifts and peak base shear to strength degradation, p-delta effects and higher mode effects. The analyses were also used to compare the as-built and retrofitted behaviour of the prototype wall.

Conclusions drawn from the results of the analyses included:

- Strength degradation only slightly increased the mean peak drift observed for the SDOF and MDOF models when subject to high intensity earthquake records (0.45g (PGA)). The effect can be more substantial when p-delta effects are included.
- Strength degradation can have a variable effect on the observed residual drifts. The effect is usually only minor but can be significant when used in combination with p-delta effects.
- P-delta effects usually only resulted in a minor increase in the peak mean drift for the SDOF and MDOF systems, but can be more substantial when used in combination with strength degradation.
- P-delta effects resulted in a major increase in the observed mean residual displacements for the SDOF and MDOF systems.

- The equivalent SDOF and MDOF models resulted in very similar mean peak drifts and mean residual drifts.
- Higher modes can significantly increase the peak base shear. A maximum increase of 70% was observed.
- The effects of higher modes on peak base shear increase with increasing earthquake record intensity.

The results of the SDOF and MDOF analyses were used to draw conclusions about the performance of the as-built versus retrofitted prototype wall. Significant points included:

- The mean peak drift experienced by the retrofitted wall was moderately reduced for the 0.45g (PGA) intensity level. For the lower intensity levels the mean peak drift of the retrofitted wall was slightly higher than the as-built wall.
- The retrofitted wall resulted in zero or negligible residual drifts, which was a significant advantage over the as-built wall.
- P-delta effects have little or no effect on the behaviour, unless strength degradation was include.
- The amplification of the base shear in the retrofitted wall due to higher mode effects was smaller at higher intensity levels (0.45g PGA), when compared to the as-built wall.

References:

Carr, A.J. [2005] "Ruaumoko – A program for Inelastic Time-History Analysis". Department of Civil Engineering , University of Canterbury, New Zealand.

FEMA [1997], "NHERP Guidelines for the Seismic Rehabilitation of Buildings". FEMA Report No. 273. Federal Emergency Management Agency, Applied Technology Council, Washington. D.C.

NZS [2005], NZS 1170.5:2004, "Structural Design Actions", Part 5: Earthquake actions – New Zealand, Standards New Zealand.

Pampanin, S., Christopoulos, C., and Priestley, M.J.N. [2002] “Residual Deformations in the Performance-Based Seismic Assessment of Frame Structures”. Research Report No. ROSE 2002/02, IUSS Press, Pavia, Italy, August 2002, 203pp.

Priestley, M.J.N. [1995] “Displacement-based Seismic Assessment of Existing Reinforced Concrete Buildings” Proceedings of Pacific Conference on Earthquake Engineering 2:225-44, 1995, Melbourne.

10 Assessment of Structural Walls

10.1 Introduction

This Chapter provides a review and extension of the recommendations made in NZSEE assessment and retrofit guidelines (NZSEE, 2005), for the displacement based assessment of reinforced concrete structural walls. A compilation of parameters and procedures appropriate for the assessment of structural walls is provided, with particular emphasis on the assessment of pre-1970's structural walls. A displacement based design procedure to determine the base shear capacity required for a retrofit solution is also briefly discussed.

10.2 Displacement Based Assessment

A displacement based assessment procedure for structural walls is discussed in this section. The NZSEE guidelines outline both force based and displacement based assessment procedures. The NZSEE displacement based assessment procedure (modified from Priestley, 1997) is discussed in this section, as it offers a more logical (accurate) assessment approach than the traditional force-based approach.

10.2.1 Steps to Displacement Based Assessment

The main steps in the displacement based seismic assessment procedure outlined in the NZSEE guidelines (NZSEE, 2005) are summarised in the following points (the procedure will be discussed in regards to the assessment of reinforced concrete structural walls):

1. Determine the probable flexural and shear strengths of the critical section. This is to be performed assuming that there is no degradation of strength due to cyclic loading.
2. Determine the inelastic mechanism and the base shear capacity.
3. Calculate the member plastic rotation capacity using moment curvature analysis.
4. Determine if a shear failure will occur before the peak flexural response is reached. If a shear failure is likely to occur, reduce the plastic rotation capacity to the value at the onset of shear failure.
5. Determine the displacement capacity and displacement ductility of the wall.
6. Create an equivalent SDOF substitute structure, with an effective stiffness at maximum displacement. The effective period of vibration can then be determined and an estimate the percentage of equivalent viscous damping can be made.

7. Use an elastic displacement spectrum to determine the spectral displacement demand.
8. Compare the displacement capacity to the spectral displacement demand.

The displacement based assessment procedure is summarised in **Figure 10-1**. The displacement capacity can be compared to the spectral displacement demand to determine if retrofit is required. The capacity and demand could also be compared in terms of base shear and overturning moment. The base shear demand can be determined from $V_{b(Demand)} = k_e \Delta_{demand}$.

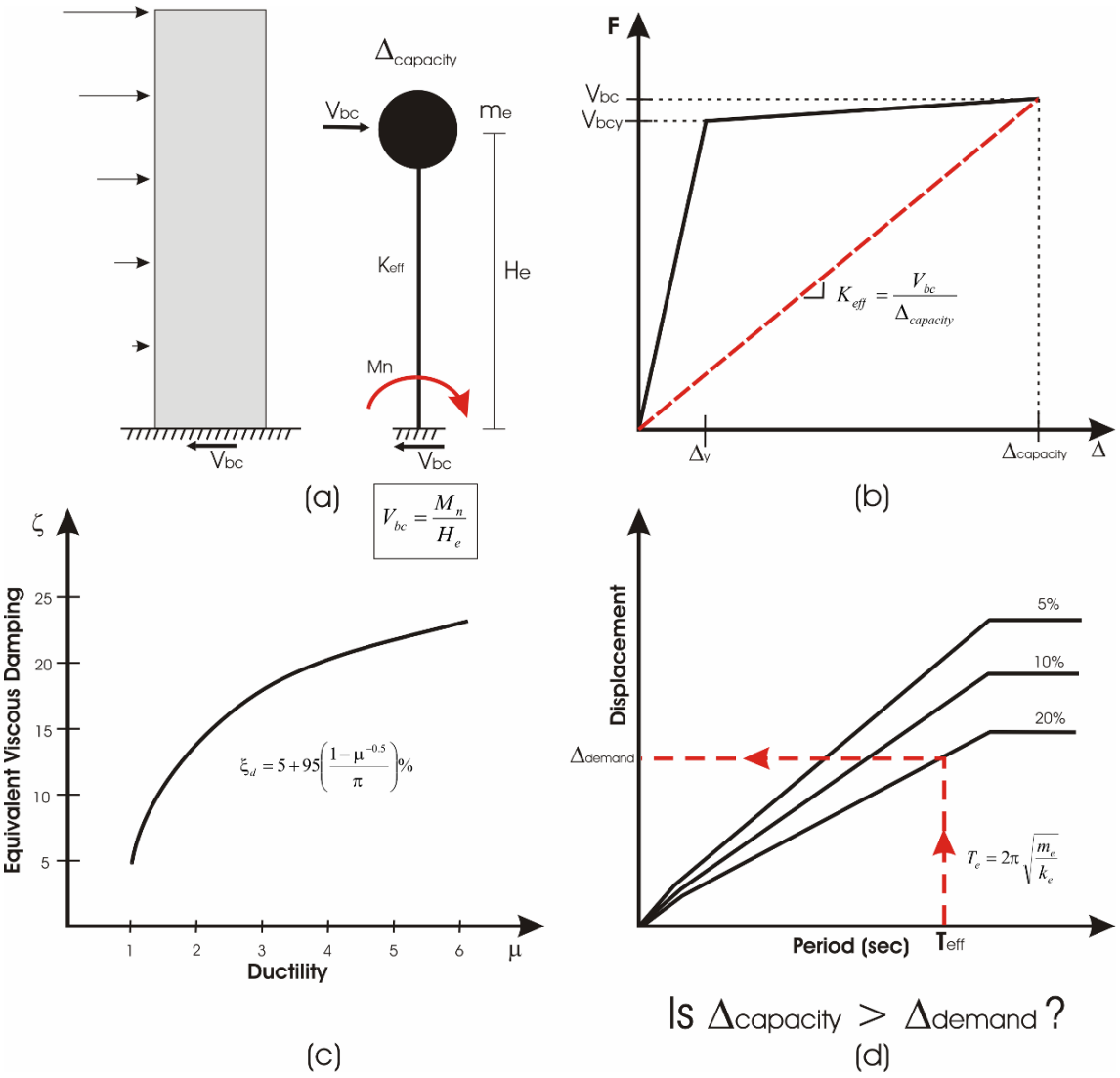

Figure 10-1: Displacement based assessment of a structural wall (modified after Priestley, 2003)

10.2.2 Creation of a SDOF Substitute Structure

The creation of an equivalent single degree of freedom (SDOF) substitute structure, which represents the multi degree of freedom (MDOF) structure at peak response is required to perform the displacement based assessment. The development of the SDOF substitute structure (with an emphasis on structural walls), will be discussed in this section. Clarification and extension of certain points and assumptions made during the procedure will be performed, as the development of the SDOF substitute structure is not fully discussed in the NZSEE guidelines. Particularly, more detail will be given on how to determine the effective height, effective mass and effective stiffness of the SDOF substitute structure (Shibata and Sozen, 1976; Priestley, 1998). The representation of a MDOF system as an equivalent SDOF substitute structure is shown in **Figure 10-2**.

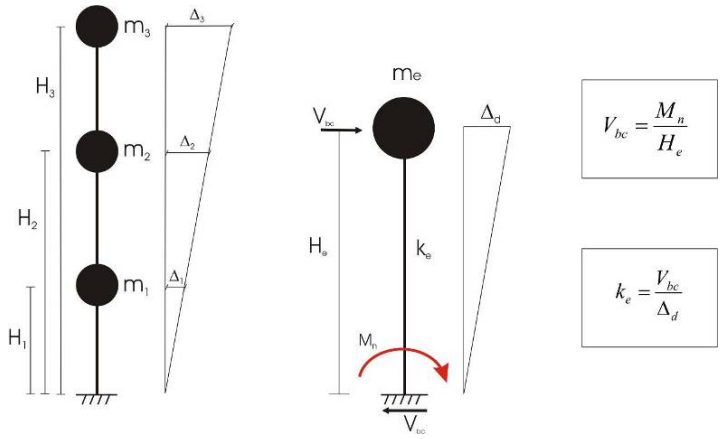

Figure 10-2: Representation of a MDOF system as an equivalent SDOF substitute structure according to Shiata and Sozen approach (1997).

For structural walls the NZSEE guidelines (NZSEE, 2005), assume an effective height of $0.67H_w$ (where H_w is the total height of the wall). If the actual effective height of the structure was greater than $0.67H_w$ this assumption would result in an un-conservative estimate of the base shear capacity. A more accurate estimate of the effective height can be made using Equation 10-1 (Priestley, 2003).

$$H_e = \frac{\sum_{i=1}^{n}(m_i \Delta_i H_i)}{\sum_{i=1}^{n}(m_i \Delta_i)} \qquad \textbf{Equation 10-1}$$

Where m_i, Δ_i and H_i are the mass, displacement and height at the n significant locations of mass (generally at each floor level of the building).

The displaced shape of the wall is required to determine the displacement at the n significant locations of mass. For low rise structural walls, a linear displacement profile can be used. This will result in Equation 10-1 giving an effective height as a proportion of the total wall height. Equation 10-2 can be used to determine the displacement at the n significant locations of mass when a linear displacement profile is assumed.

$$\Delta_i = 1.0\frac{H_i}{H_w}$$ **Equation 10-2**

Where H_w is the total height of the wall.

The effective mass of the SDOF substitute structure can be calculated using Equation 10-3 (Priestley, 2003). The effective mass relates to the mass participating in the first inelastic mode of response. The design displacement (Δ_d), required for the effective mass calculation is given by Equation 10-4 (Priestley, 2003).

$$m_e = \frac{\sum_{i=1}^{n}\left(m_i\Delta_i\right)}{\Delta_d}$$ **Equation 10-3**

The design displacement (Δ_d), as calculated using Equation 10-4 (Priestley, 2003) reduces the magnitude of the peak displacement of the MDOF wall to an appropriate value for the equivalent SDOF substitute structure. The calculation requires knowledge of the displaced shape of the wall, but as for the calculation of the effective height, an approximation of a linear profile with a value of 1.0 at the top of the wall can be used. This will result in Equation 10-4 giving the design displacement as a proportion of the peak displacement (or displacement capacity) of the MDOF system.

$$\Delta_d = \frac{\sum_{i=1}^{n}\left(m_i\Delta_i^2\right)}{\sum_{i=1}^{n}\left(m_i\Delta_i\right)}$$ **Equation 10-4**

The base shear capacity of the SDOF substitute structure can be calculated using Equation 10-5 (Priestley, 1995).

$$V_{bc} = \frac{M_n}{H_e} \qquad \textbf{Equation 10-5}$$

Where M_n is the nominal moment capacity at peak response.

The effective elastic stiffness of the substitute structure can be calculated using Equation 10-6 (Priestley, 1995), the effective stiffness is a secant stiffness at peak response as shown in **Figure 10-1 (b)**. The displacement capacity of the SDOF substitute structure ($\Delta_{capacity(SDOF)}$) can be determined using moment-curvature analysis, which will be discussed in section 10.3.2. The displacement capacity will be governed by either code specified ductility limits, drift limits or the walls ductility capacity.

$$k_e = \frac{V_{bc}}{\Delta_{capacity(SDOF)}} \qquad \textbf{Equation 10-6}$$

The effective period of the SDOF substitute structure can be calculated using Equation 10-7 (NZSEE, 2005). The effective period is used to enter the displacement spectrum to determine the displacement demand expected on the SDOF substitute structure. The spectral displacement demand can then be compared to the displacement capacity to see if retrofit will be required. An estimate of the equivalent viscous damping will also be required to determine the level of damping to apply to the displacement spectrum. The displacement based assessment procedure is outlined in **Figure 10-1**.

$$T_e = 2\pi\sqrt{\frac{M_e}{k_e}} \qquad \textbf{Equation 10-7}$$

10.2.3 Assessment of Multiple Structural Walls

The displacement based assessment procedure discussed above only considered the assessment of an individual wall, whereas in structural wall buildings it is likely that there will be more than one wall contributing to the seismic resisting system. In this section a

modification to the assessment procedure, so that it can be used for the assessment of structural walls systems will be discussed.

The first step for the assessment of a wall system is to determine the effective height of the wall system (not the individual walls). This can be determined using Equation 10-1, where m_i will be the mass associated to the entire wall system, at the n significant locations of mass. The base shear capacity of each of the individual wall elements in the system can then be determined using Equation 10-5. The base shear capacity of each of the individual walls can be added together to determine the base shear capacity of the entire wall system.

The next step will be to determine the displacement capacity of the multiple wall system. This will involve determining the displacement capacity of each of the individual walls, with the critical wall governing the displacement capacity of the entire wall system. The displacement capacity of each of the individual walls could be governed by code specified ductility limits, drift limits or the section ductility capacity.

With the system base shear capacity and the system displacement capacity determined the effective stiffness of the system can be determined using Equation 10-6 or as shown in **Figure 10-3**. With the effective stiffness of the system determined the displacement based assessment procedure will then follow the same steps as outlined for the assessment of an individual wall element or as shown in **Figure 10-1**.

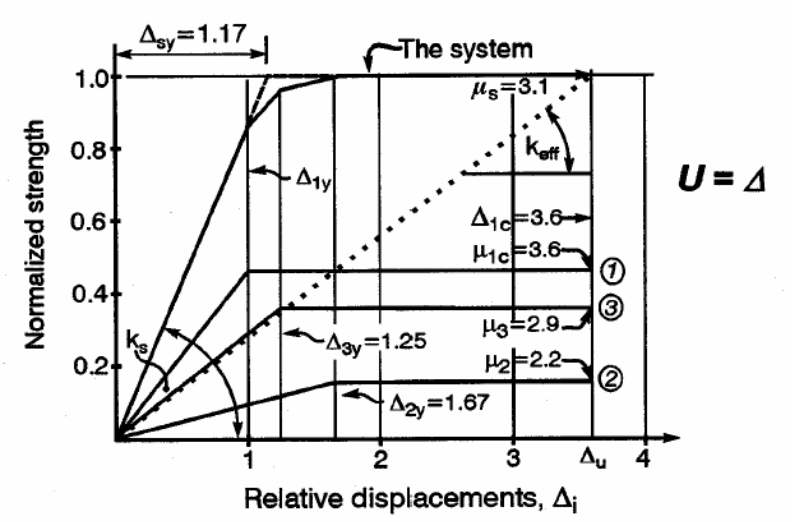

Figure 10-3: Strength versus displacement response for multiple walls (wall system) and the corresponding effective stiffness as per NZSEE (2005) (modified after Paulay, 1998).

10.2.4 Consideration of Performance Based Design

Performance based design principles (briefly discussed in section 2.4) can be easily incorporated into the displacement based assessment procedure previously discussed. The typical performance objective of newly designed structures is to achieve a life safety performance level when the structure is subjected to a rare seismic event (typically considered as having a 1/500 year return period). This is accounted for in the assessment procedure by using a displacement spectrum corresponding to a 1/500 year return period. Higher or enhanced performance objectives can be taken into account by using a displacement spectrum which corresponds to a higher seismic intensity level. An example would be the displacement spectrum corresponding to the maximum considered seismic event, which typically corresponds to a 1/2500 year event. The definition of material strain limits at different performance levels is also required.

10.3 Structural Wall Assessment Parameters and Procedures

This section discusses the steps required to assess the behaviour of a reinforced concrete structural wall, with particular emphasis on steps 1-5 of the displacement based assessment procedure (Section 10.2.1). This involves checking the assumption that a flexural hinge forms at the base of the wall, evaluating the ductility capacity and the hierarchy of strength of the critical section. The steps required to check the assumptions made during the displacement based assessment procedure, with specific emphasis on structural walls are:

1. Determine the flexural capacity at the base of the wall and the corresponding base shear capacity of the equivalent SDOF substitute structure;
2. Distribute the base shear capacity up the wall using an inverted triangular distribution and determine the moment and shear demand envelopes;
3. Adjust the moment and shear demand envelopes for tension shift, higher modes and over strength where appropriate;
4. Calculate the flexural and shear capacity at critical points up the height of the wall, due to curtailment of the longitudinal reinforcement or changes in the transverse reinforcement;
5. Check that the critical section occurs at the base of the wall;

6. If the critical section is at the base of the wall check the hierarchy of strength. If the strength hierarchy is not governed by a flexural mechanism adjust the base shear capacity accordingly.

Calculation of the nominal flexural capacity, ductility capacity, moment and shear demand envelopes and the hierarchy of strength of the critical section will be discussed in the following sections. Special considerations regarding pre-1970's structural walls will be made.

10.3.1 Nominal Flexural Capacity

Calculation of the nominal moment capacity is required to determine the base shear capacity of the wall (Equation 10-5) and to assess the hierarchy of strength at the critical section. The nominal flexural capacity can be calculated using standard section analysis procedures. A review of appropriate concrete and reinforcement, stress and strain limits to use for the section analysis and particularly for the assessment of pre-1970 structural walls is performed.

Concrete Compressive Stress

The typical specified compressive strength values of concrete for pre-1970's structural walls (in New Zealand) were for an "ordinary" grade concrete 2000-2500 psi (13.8-17.2 MPa) (NZSS 1900, 1964). It is suggested that as a conservative estimate of the compressive strength of the concrete increasing with age and due to conservative mix designs, the specified compressive strength be multiplied by a factor of 1.5 (NZSEE, 2005 and Priestley, 1995). As an estimate of the confined compressive strength (f'_{cc}) it is suggested that the compressive strength of the concrete (f'_c) is multiplied by 1.5 (Priestley, 1995).

Unconfined Concrete Strain Limit

An unconfined compressive concrete strain limit of 0.005 is assumed appropriate for the assessment of reinforced concrete structures (Priestley, 1995). This compressive strain limit is appropriate to use as the ultimate compressive strain limit for poorly detailed reinforced concrete structures, or as an estimation as to when the cover concrete on a well detailed reinforced concrete element will spall.

Suggested deficiencies in reinforcement detailing which lead to the concrete in beams and columns (also for walls) being considered as unconfined include (Priestley, 1995):

- Only reinforcing bars at the corner of a section being restrained by transverse reinforcement
- Ends of stirrups not anchored within core (confined) concrete
- Spacing of transverse reinforcement exceeding d/2 or 16 bar diameters

A comparison of these detailing deficiencies to the typical detailing characteristics of pre-1970's structural walls in New Zealand, leads to the assumption that in assessing the capacity it would be appropriated to assume unconfined concrete conditions. Typical reinforcement detailing deficiencies in pre-1970's structural walls effecting concrete confinement include:

- Transverse reinforcement anchored by 90 degree bends within the cover concrete (Priestley, 1995).
- Large spacing of transverse reinforcement, typically 12" (304mm), approximately 24-32 bar diameters.

Confined Concrete Strain Limit

An appropriate value to use for the ultimate compressive strain for confined concrete is given by Equation 10-8 (Paulay and Priestley, 1992). This provides a conservative estimate for the ultimate achievable compressive strain and values typically range between 0.006-0.015 (Paulay and Priestley, 1992).

$$\varepsilon_{cu} = 0.004 + \frac{1.4\rho_s f_{yh}\varepsilon_{su}}{f'_{cc}} \qquad \textbf{Equation 10-8}$$

Where, f_{yh} represents the transverse reinforcement yield stress, ε_{su} transverse reinforcement ultimate strain, f'_{cc} confined concrete compressive strength. ρ_s represents the volumetric ratio of transverse reinforcement and can be estimated using Equation 10-9 (Priestley, 1995).

$$\rho_s = \frac{1.5A_v}{b_c s} \qquad \textbf{Equation 10-9}$$

Where A_v represents the total area of transverse reinforcement in a layer, b_c equals the width of the concrete core area and s the spacing of the transverse reinforcement. When calculating

the section capacity, using a confined compressive strain value, it should be ensured that the compression region considered corresponds only to the region of concrete appropriately confined (i.e. to the centre line of the confining reinforcement, do not include the cover concrete) (Priestley, 1995).

Confined concrete is defined as that being confined by details satisfying recent design standards such as NZS 3101:1995. Typical detailing characteristics representative of a confined concrete element (beam or column) are (Priestley, 1995):

- All longitudinal reinforcement restrained against buckling by an appropriately size leg of transverse reinforcement, if bar is at the top or bottom edge of a section.
- All transverse reinforcement adequately anchored, such as by 130 degree hooks in core concrete
- Transverse reinforcement meets spacing requirements of being less than $6d_b$, d/4 or 150mm

An example of appropriate transverse reinforcement detailing to provide adequate confinement in the compression region of a structural wall is shown in **Figure 10-4**. Confinement reinforcement is required when the compressive strain is excessive, which is determined from a critical neutral axis depth (as per NZS 3101:2006). **Figure 10-4** shows how the confinement reinforcement is anchored by 135 degree hooks within the confined concrete and that all the longitudinal reinforcement bars are restrained against buckling in the compression region. It can also be seen that the shear reinforcement is anchored via 90 degree hooks within the zone of confined concrete (not outside the outer most longitudinal bars). The transverse confining reinforcement is only required to extend vertically over the zone of expected inelastic behaviour (plastic hinge zone).

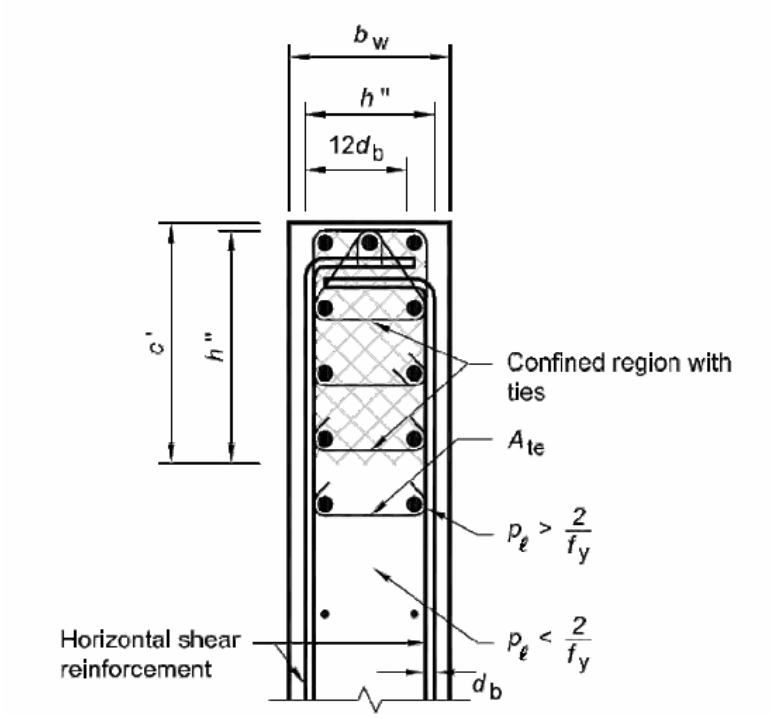

Figure 10-4: Typical detailing requirements for confinement at the end of a structural wall and for anchoring shear reinforcement as per NZS 3101:2006

Reinforcing Steel Stress

Between the period of 1930-1970 the specified yield strength of structural grade reinforcement was originally 227 MPa, later increased to 275 MPa (NZSEE, 2005). After 1964 a high grade reinforcement with a yield strength of 414 MPa was also available. Sampling of reinforcement concluded that the 5th percentile yield stress was typically 15%-20% higher than the specified yield stress (Chapman, 1991). An appropriate value for assessment purposes is $1.1f_y$ where f_y is the specified yield stress (Priestley, 1995).

Steel Strain Limits

Limits on the ultimate strain of reinforcement, with particular emphasis to older buildings have been suggested as $\varepsilon_{su} = 0.15$ for 275 MPa reinforcement or $\varepsilon_{su} = 0.1$ for 420 MPa reinforcement (Priestley, 1995).

Yield Limit States

When performing a section analysis the strain at first yield should be either $\varepsilon_s = \frac{f_y}{E_s}$ or $\varepsilon_c = 0.002$, depending which strain limit is reached first (Priestley and Kowalsky, 1998).

10.3.2 Ductility Capacity

The ductility capacity of a structural wall can be governed by the section ductility capacity or by code specified ductility or drift limits. The first requirement to be able to determine the ductility capacity is to estimate the yield curvature. The potential plastic hinge length and a plastic curvature will also have to be determined, so that the ductility capacity of the wall can be calculated. This can be compared to code specified limits to see if they will govern the allowable displacement or ductility. All displacements should be determined at the effective height of the wall. The increase in peak displacement due to p-delta when a wall is loaded in-plane need not be considered, as it will be minimal, as reported in Chapter 9.

The yield curvature can be estimated from a standard section analysis (using strain limits of section 10.3.2) or by an approximate equation. An approximate estimate for the yield curvature for a rectangular structural wall can be calculated using Equation 10-10 (Priestley, 2003).

$$\phi_y = \frac{2\varepsilon_y}{l_w} \qquad \textbf{Equation 10-10}$$

Where ε_y is the steel yield strain and l_w is the length of the wall. The yield displacement can then be calculated using moment curvature analysis.

The plastic curvature can be calculated from a standard section analysis at the nominal moment capacity (using strain limits specified in Section 10.3.1). An estimate of the potential plastic hinge length will be required to calculate the ultimate displacement capacity of the wall. The calculated ultimate displacement and corresponding ductility capacity is quite sensitive to the assumed plastic hinge length. An overestimation of the plastic hinge length results in a considerable overestimation of the ductility capacity. The NZSEE guidelines (NZSEE, 2005) assume an approximate plastic hinge length of $0.5l_w$ for structural walls. This is very approximate and is potentially not suitable for the assessment of pre-1970's structural walls, which are reinforced with plain round bars. Concrete sections reinforced with plain round bars do not typically develop plastic hinge regions, as the behaviour is usually governed by a single crack opening at the critical section (as was observed in the experimental investigation on W1, in Chapter 4). A back-calculation to determine the equivalent plastic hinge length from an experimental test on a wall detailed as a pre-1970's structural wall in

this investigation was performed and is shown in appendix C. The equivalent plastic hinge length was determined to be in the region of $0.10l_w$. Although the results of a single experiment cannot be expected to predict the behaviour of all pre-1970's structural walls, they can be used to show that an estimate of $0.5l_w$ may not be appropriate for pre-1970's structural walls. A more accurate estimate of the plastic hinge length can be obtained from Equation 10-11 (Paulay & Priestley, 1992), which is meant for sections reinforced with deformed bars.

$$l_p = 0.08l_w + 0.022d_b f_y \qquad \textbf{Equation 10-11}$$

Where l_w is the length of the wall, d_b is the reinforcing bar diameter and f_y is the steel yield stress.

Alternatively the plastic hinge length can be estimated by the larger of Equation 10-12 or Equation 10-13 (Priestley, 2003), which are specifically for structural walls.

$$l_p = 0.054H_w + 0.022 f_y d_b \qquad \textbf{Equation 10-12}$$

or

$$l_p = 0.2l_w + 0.03H_w \qquad \textbf{Equation 10-13}$$

The ultimate displacement capacity and section displacement ductility can be found from moment curvature analysis. The allowable displacement capacity is determined by comparing the section capacity with code specified ductility and drift limits to see which governs.

10.3.3 Base Shear Distribution

The base shear capacity calculated using Equation 10-5 can be distributed up the height of the wall using an inverted triangular distribution (Priestley, 1995). This can be used to calculate shear and bending moment demand envelopes up the height of the wall. These are then used to check the assumption that the critical section occurs at the base of the wall. Example bending moment and shear demand envelopes for a 5-storey wall, resulting form the inverted triangular distribution of base shear are shown in **Figure 10-5**.

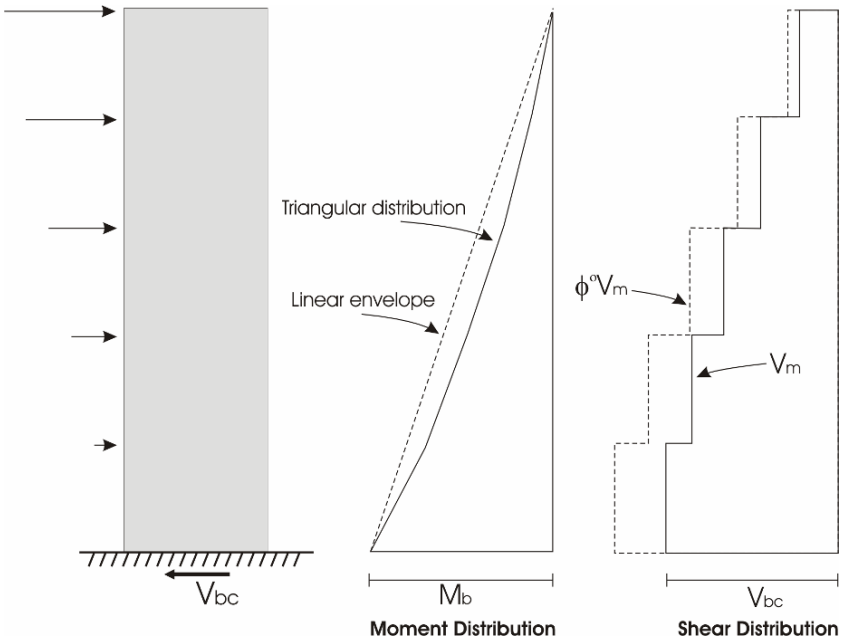

Figure 10-5: Base shear capacity and resulting bending moment and shear envelopes (modified after Priestley, 1995)

The inverted triangular distribution of base shear results in a multi-linear bending moment envelope up the height of the wall. It has been suggested that the bending moment envelope be modified to account for the effects of higher modes by assuming a linear distribution of bending moment with height, as shown in **Figure 10-5** (Paulay & Priestley, 1992). To ensure that the principles of capacity design are followed the shear demand envelope is to be amplified. In design situations it is typical to amplify the shear demand to account for material over strength and higher mode effects). For assessment purposes it is unduly conservative to assume that the peak over strength and peak dynamic amplification occur at the same time (Priestley, 1995). It is therefore suggested that the shear demand envelope is only amplified to account for material over strength, a factor of 1.25 is appropriate (Priestley, 1995).

The over strength shear demand is used to determine if a tension shift of the moment demand envelope will be required (Priestley, 1995). A tension shift accounts for a shift in the moment profile due to the development of diagonal cracking. It has been suggested that if the wall shear stress is less than $0.2\sqrt{f_c^{'}}MPa$ then a tension shift will not be required, as diagonal cracking is unlikely to develop (Priestley, 1995). The shear stress distribution can be calculated form the over strength shear force distribution as shown in **Figure 10-6**. If the shear stress is greater than $0.2\sqrt{f_c^{'}}MPa$ a tension shift of $0.5l_w$ should be applied (Priestley,

1995). This is reduced from a tension shift of $1.0l_w$ which is used for design purposes (Priestley, 1995). This removes excessive conservatism, as it is for an assessment procedure (rather than design). The tension shift only needs to be applied to the moment demand envelope over the region of the wall where the shear stress exceeds the specified limit, as shown in **Figure 10-6**.

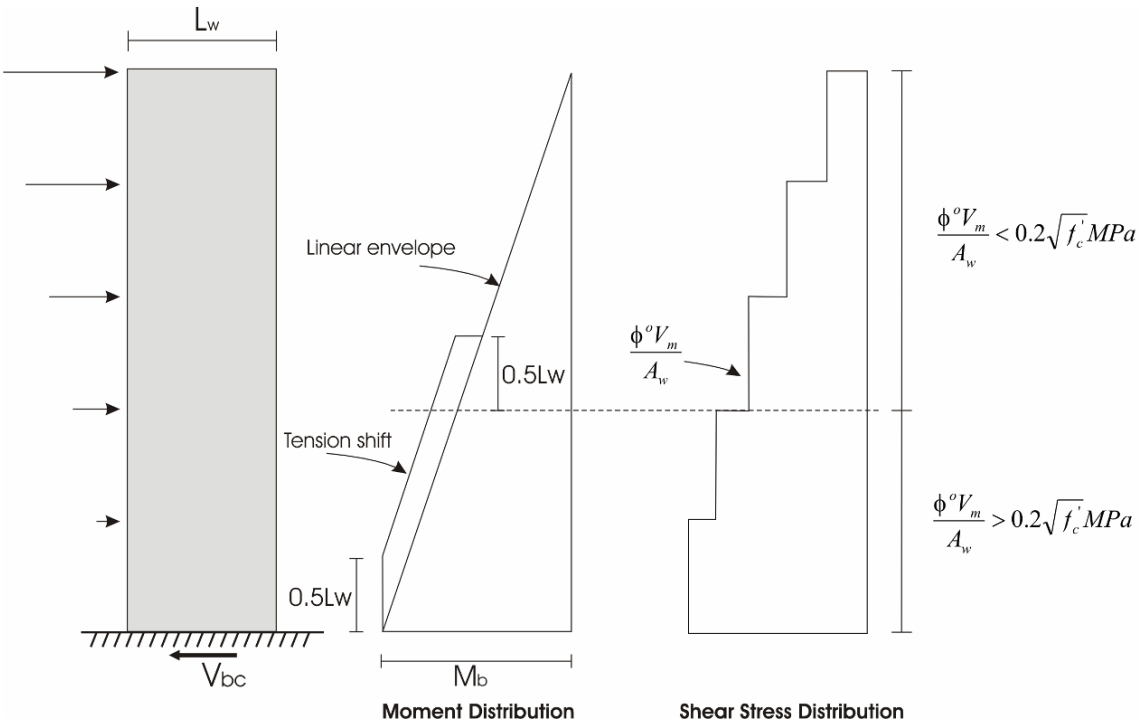

Figure 10-6: Tension shift of the bending moment envelope (modified after Priestley, 1995)

Flexural and shear capacity envelopes for the wall are to be calculated. This involves calculating the flexural and shear capacity of the wall at critical locations, generally this is where curtailment of the reinforcement occurs. The capacity envelopes can be plotted over the demand envelopes to see if the flexural or shear capacity is exceeded. The assumption that the critical section occurs at the base of the wall section can then be validated. When calculating the moment capacity of the wall section at various points up the height of the wall, it is important to consider the reduction in axial load (Paulay and Priestley, 1992). The section capacity is typically quite sensitive to changes in axial load due to structural walls typically having a low axial load ratio. When you consider the M-N interaction diagram for a section with a low axial load ratio the moment capacity can vary substantially with a small variation in axial load.

10.3.4 Alternative Failure Mechanisms

To ensure that the structural wall under assessment conforms to the assumption that a flexural hinge develops and the principles of capacity design, the hierarchy of strength of the critical section needs to be checked. This involves determining if the shear strength and sliding shear capacity are greater than the force required for the flexural over strength to develop. The typical failure modes exhibited by structural walls are shown in **Figure 10-7**. The flexural capacity of the wall should be assessed according to the strain limits specified in Section 10.3.1 and multiplied by 1.25 to account for over strength. The flexural capacity can be expressed in terms of a base shear demand to allow comparison to the shear strength and sliding shear capacity.

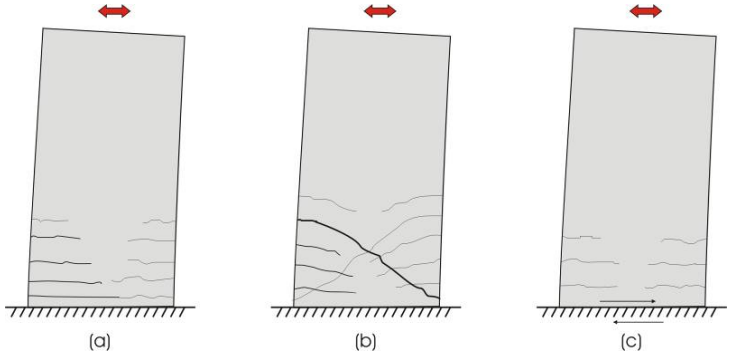

Figure 10-7: Typical failure modes observed in structural walls, (a) flexural; (b) Shear; (c) Sliding shear

When determining the flexural capacity of structural walls it is important to assess whether the reinforcement details are sufficient to allow the full section capacity to develop. This is particularly important for pre-1970's structural walls, which were likely reinforced with plain round bars. Common deficiencies in the reinforcement details, which could inhibit the development of the full section capacity, include inadequate lap splice lengths, which mean that the capacity of the lap splice could govern the section capacity (full bar capacity not achieved). Also inadequate transverse reinforcement in the potential plastic hinge zone can inhibit the development of the flexural strength through insufficient confinement, the inability to prevent buckling of the reinforcement and being unable to adequately clamp the lap splice region (Paulay and Priestley, 1992). There is currently no accurate method available to asses the capacity of lap splices using plain round reinforcement. Therefore, a level of judgment has to be made on the adequacy of the detailing to allow the full flexural strength to develop.

The shear strength capacity of the wall has to be assessed to ensure that it exceeds the shear demand accounting for over strength actions. Code calculation methods offer very conservative estimates of the shear capacity, which are sufficient for design purposes. However for assessment purposes more detailed calculations of the shear capacity are appropriate, as they provide a much better estimate of the true shear capacity. Shear versus ductility models, as provided in the NZSEE guidelines (NZSEE, 2005) or the modified UCSD (Kowalsky and Priestley, 2000) approach are appropriate for assessing the shear capacity of structural walls. These models provide a shear strength envelope that reduces as the ductility demand increases. When assessing the shear capacity of a wall, a low strength reduction factor should be applied as the dynamic amplification due to higher modes has been ignored, a value such as 0.75 is suggested (Priestley, 1995).

If the shear demand is determined to be close to the shear capacity of the wall, a force versus displacement model which accounts for a reduction in stiffness due to the development of shear cracking should be used. An example of such a model is Miranda model (Miranda et al., 2005), which was developed to reduce the conservatism associated with the assessment of reinforced concrete columns with potential for shear failure. The Miranda model, shown in **Figure 10-8** is to be used in combination with a shear versus ductility capacity envelope and provides a more accurate estimate of the displacement and force at which shear failure will occur, than if only flexural cracking had been accounted for. **Figure 10-8** (a) shows the components of the force versus displacement response, when shear cracking is accounted for and a shear capacity envelop is used. Also shown is an idealised flexural force verse displacement response, it can be seen that when this is used the predicted displacement at shear failure will be substantially lower and the predicted strength is likely to be moderately higher. **Figure 10-8** (b) compares an experimental result and predicted strength envelopes, with and without accounting for the effects of shear cracking. It can be seen that the inclusion of shear cracking substantially improves the predictions. The behaviour of a wall (with a shear dominated inelastic mechanism) from the experimental part of this research was predicted using the Miranda model. A comparison of the experimental and predicted response can be found in Chapter 5.

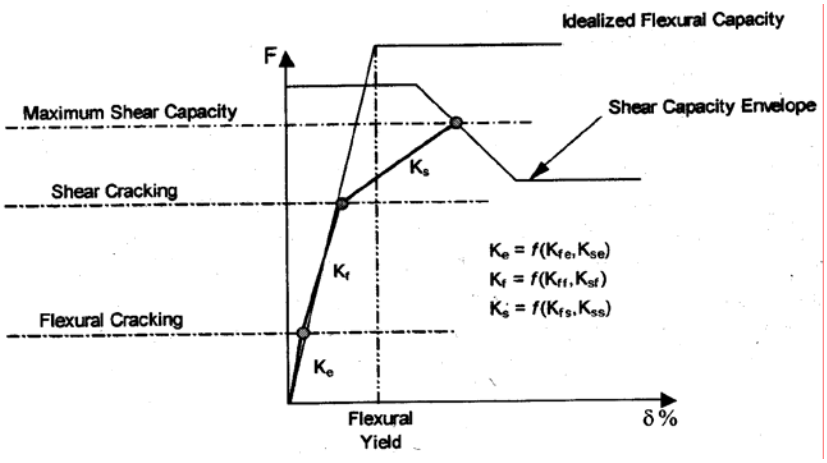

(a)

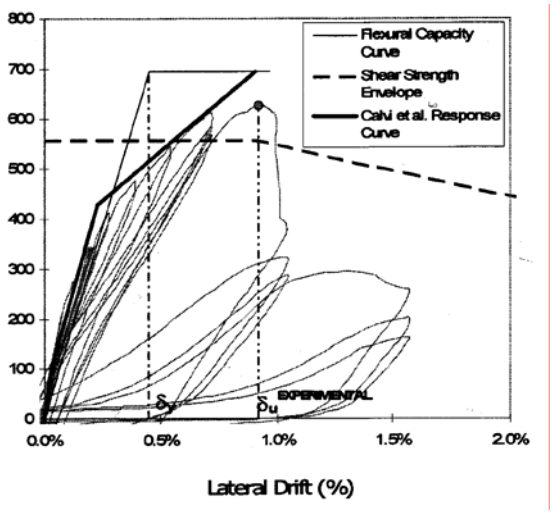

(b)

Figure 10-8: Incorporation of a reduction in stiffness due to shear cracking, in the force versus displacement response (Miranda et al., 2005).

When assessing the shear capacity of pre-1970's structural walls in New Zealand it is important to consider the detailing of the transverse reinforcement. It is common for the shear reinforcement to be anchored by 90 degree bends in the cover concrete at the end of the wall (Priestley, 1995). If spalling of the cover concrete occurs or the shear reinforcement is highly stressed, it is possible that the full shear strength will not be able to develop before the shear reinforcement anchorage fails. It is therefore appropriate to use low strength reduction factors or conservative design code shear strength equations in situations where this type of reinforcement detailing is present.

The sliding shear capacity at the base of a wall can be critical for wall dominated by flexure (Paulay and Priestley, 1992). A flexural crack along the wall to foundation interface or a construction joint can lead to a sliding plane where shear transfer relies on aggregate interlock. The shear transfer relies on a coefficient of friction, force transverse to the sliding plane provided by the axial load and a clamping force generated in the reinforcement. The sliding shear capacity can be calculated using Equation 10-14 (Paulay and Priestley, 1992).

$$V_u = \phi\mu\left(A_{vf}\, f_y + P_u\right) \qquad \textbf{Equation 10-14}$$

Where: ϕ = strength reduction factor (typically 0.85)

μ = friction coefficient

A_{vf} = area of longitudinal reinforcement crossing the sliding plane

f_y = reinforcing yield stress

P_u = axial load

Suggested values for the friction coefficient are typically based on the level of surface roughening provided at a construction joint. A friction coefficient of $\mu = 0.7$ is suggested when no attempt to deliberately roughen the surface has been made (Paulay and Priestley, 1992). When assessing the sliding shear capacity of a wall it will be impossible to determine the level of roughening that has taken place, therefore it would be best to conservatively assume that $\mu = 0.7$.

Once the flexural, shear and sliding shear capacity has been calculated the hierarchy of strength of the critical section can then be determined. If the hierarchy of strength is not governed by the flexural capacity, the displacement capacity and base shear capacity should be adjusted accordingly.

10.3.5 Equivalent Viscous Damping

To calculate the displacement demand on a structural wall an estimate of the equivalent viscous damping is required. The percentage of equivalent viscous damping is required to select a displacement spectrum of the corresponding level of damping. The level of equivalent viscous damping developed depends on the level of ductility a section reaches during its response. The NZSEE guidelines (NZSEE, 2005) provide an estimate for the percentage equivalent viscous damping provided by a well detailed monolithic structural wall based on previous research (Pekcan, 1999) (see **Figure 10-9**). Alternatively the equation shown in

Figure 10-9 can be used (Priestley, 2003). The percentage equivalent viscous damping provided by a poorly detailed existing wall may be considerably less than the estimates provided for a well detailed wall and shown in **Figure 10-9**.

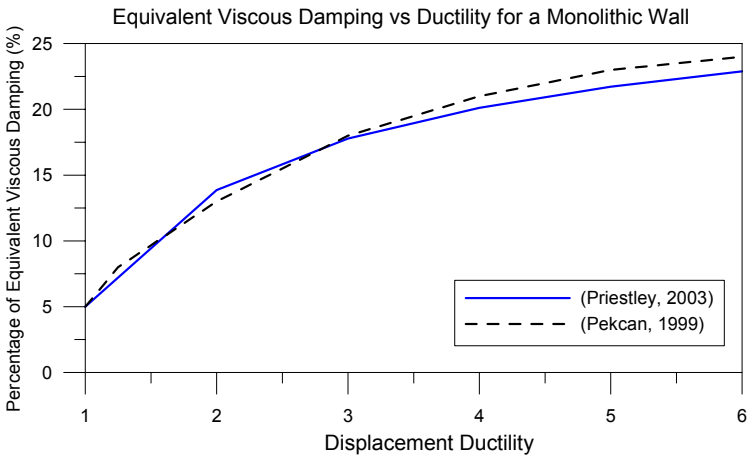

$$\xi_d = 5 + 95\left(\frac{1-\mu^{-0.5}}{\pi}\right)\%$$

(Priestley, 2003)

Figure 10-9: Equivalent viscous damping versus ductility for a well detailed reinforced concrete wall.

10.4 Displacement Based Retrofit Design

If the displacement capacity is determined to be less that the displacement demand, when displacement based assessment is performed, retrofit will be required. The required base shear capacity of the retrofitted wall, (to ensure the displacement demand is within the acceptable limits) can be determined using a displacement based design procedure. The displacement based retrofit design procedure is outlined in **Figure 10-10**. Once the required base shear capacity of the retrofitted wall has been determined a retrofit solution can be designed. When the retrofit design has been completed a displacement based assessment procedure should be performed as a check to make sure the retrofit solution meets the requirements.

When calculating the required base shear capacity of the retrofit solution it is important that appropriate assumptions are made for the type of retrofit solution implemented. The displacement based design procedure can be used for retrofit solutions involving selective weakening or other conventional retrofit techniques. Of particular importance when considering a selective weakening retrofit solution is the level of equivalent viscous damping. A selective weakening solution, which involves introducing a controlled rocking behaviour will have a significantly lower percentage of equivalent viscous damping than a conventional

monolithic wall. The design procedure may require iteration to find an appropriate capacity versus demand balance.

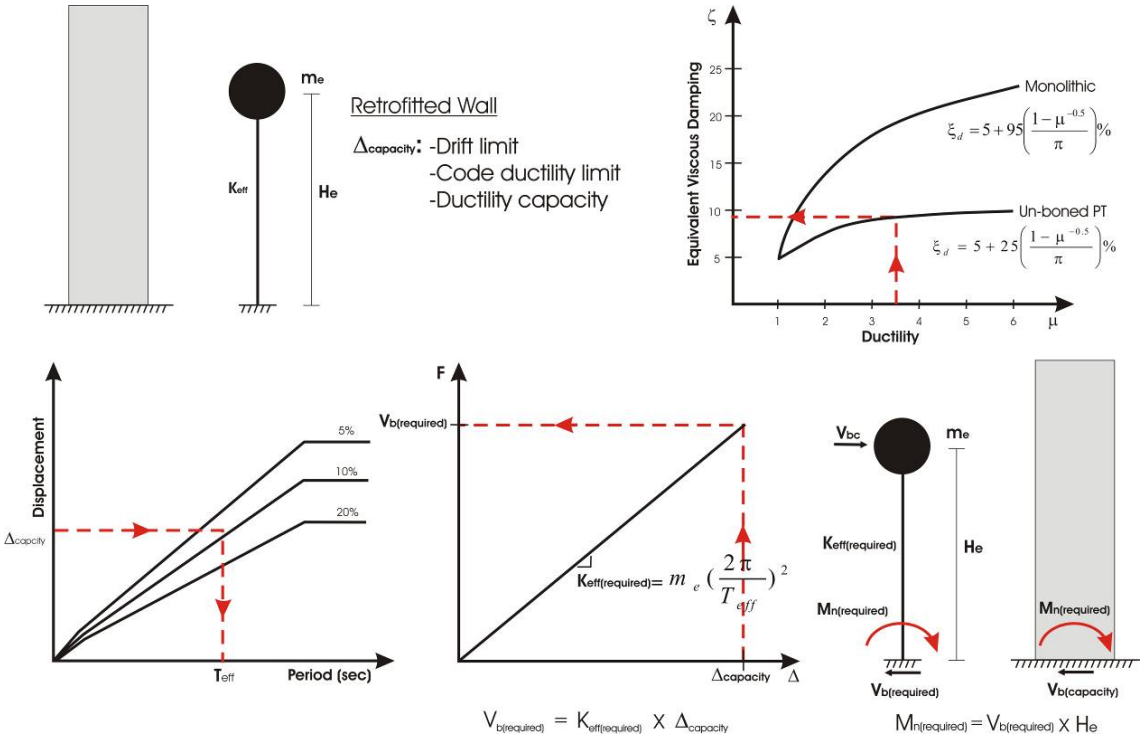

Figure 10-10: Displacement Based Retrofit Design (modified after Priestley, 2003).

10.5 Summary

A review and discussion of the NZSEE (NZSEE, 2005) displacement based assessment procedure for reinforced concrete structural walls was performed. Procedures to determine the properties of the SDOF substitute structure where introduced and the assumptions made regarding the plastic hinge length were discussed. Procedures to use to determine the critical section and to check the assumption that a flexural plastic hinge forms were also discussed. Particular emphasis was given to the assessment of pre-1970's New Zealand structural walls. A displacement based design procedure to determine the required base shear capacity of the retrofitted wall was briefly discussed.

Examples of the displacement based assessment procedure and the displacement based design of a selective weakening retrofit solution are provided in Appendix A.

References:

Chapman, H.E., [1991], "Seismic Retrofitting of Highway Bridges", Bulletin of New Zealand Society for Earthquake Engineering, 24(2): 186-201.

Kowalsky, M.J. and Priestley, M.J.N. [2000] "Improved Analytical Model for Shear Strength of Circular Reinforced Concrete Columns in Seismic Regions" ACI Structural Journal Vol. 97, 2000, No. 3, pp. 388-396.

Miranda, P.A., Calvi, G.M., Pinho, R. and Priestley, M.J.N. [2005]. "Displacement-Based Assessment of RC Columns with Limited Shear Resistance". Report No. Rose 2005/04, European School for Advanced Studies in Reduction of Seismic Risk, Pavia.

New Zealand Standard, NZSS 1900**,** Chapter 9.3, [1964], "New Zealand Standard Model Building Bylaw, Design and Construction, Concrete", New Zealand Standards Institute, 60p.

NZSEE. [2005]. "Assessment and Improvement of the Structural Performance of Buildings in Earthquake – Study Group Draft", New Zealand Society of Earthquake Engineering, Prepared for the Department of Building and Housing

Paulay, T., [1998], "Torsional Mechanisms in Ductile Building Systems", Earthquake Engineering and Structural Dynamics, Vol. 27, pp. 1101-1121.

Paulay, T., and Priestley, M.J.N., [1992], "Seismic Design of Reinforced Concrete and Masonry Buildings" John Wiley and Sons, New York, 1992, 744pp.

Pekcan, G., Mander, J.B., Chen, S.S., [1999], "Fundamental Considerations for the Design of Non-linear Viscous Dampers", Earthquake Engineering and Structural Dynamics, 28, pp. 1405-1425.

Priestley, M.J.N. [1995] "Displacement-based Seismic Assessment of Existing Reinforced Concrete Buildings" Proceedings of Pacific Conference on Earthquake Engineering 2:225-44, 1995, Melbourne.

Priestley, M.J.N. [1997] “Displacement-based Seismic Assessment of Reinforced Concrete Buildings”, Journal of Earthquake Engineering, Vol. 1, No. 1, pp. 157-192.

Priestley, M.J.N., [1998], “Displacement-based Approaches to Rational Limit State Design of New Structures”, Keynote address of the 11th European Conference on Earthquake Engineering, Paris, France.

Priestley, M.J.N., and Kowalsky, M.J. [1998] “Aspects of Drift and Ductility Capacity of Cantilever Structural Walls” Bulletin, NZ National Society for Earthquake Engineering, Vol.31, No2, June 1998.

Priestley, M.J.N., [2003], “Myths and Fallacies in Earthquake Engineering, Revisited”, IUSS Press, Pavia, Italy.

Shibata, A. and Sozen, M., [1976], “Substitute Structure Method for Seismic Design of Reinforced Concrete”, Journal of Structural Engineering, American Society of Civil Engineers, Vol.102, No. 12, pp 3548-3566.

SNZ. [1995] Concrete Structures Standard NZS 3101:1995, Volume 1 Code of Practice and Volume 2 Commentary. Standards New Zealand, Wellington.

SNZ. [2006] Concrete Structures Standard NZS 3101:2006, Volume 1 Code of Practice and Volume 2 Commentary. Standards New Zealand, Wellington.

11 Conclusions and Recommendations

11.1 General Overview

The research presented in this thesis was the first stage of an ongoing research project at the University of Canterbury, focusing on developing selective weakening for the seismic retrofit of reinforced concrete buildings. In this contribution the emphasis was on developing selective weakening for the seismic retrofit of reinforced concrete structural walls. Analytical, numerical and experimental investigations were performed to asses the feasibility of selective weakening as a seismic retrofit strategy. A review of relevant literature showed that as far as the author was aware, only preliminary suggestions of a selective weakening type retrofit intervention have been made (FEMA, 1997; FEMA, 2000; NZSEE, 2005), and that no research has been performed on how to implement such solutions.

The concept and aim of selective weakening for seismic retrofit was introduced in Chapter 3. A selection of possible selective weakening retrofit solutions for a poorly performing structural wall were discussed, along with consideration of the demand-capacity balance. Particular emphasis was focused on considering the foundation capacity when designing a retrofit intervention.

A experimental program consisting of four scaled structural walls was used to confirm the possibility/feasibility of using a selective weakening retrofit approach (Chapters 4-8). The four experimental specimens consisted of two benchmark and two retrofitted walls. Quasi-static cyclic uni-directional testing was performed on the experimental specimens, which were 2/3 scale cantilever wall elements which represented the base portion of a structural wall.

In Chapter 9 non-linear time-history analysis was performed on SDOF and MDOF lumped plasticity models representing a prototype wall, to assess the sensitivity of peak and residual drifts to p-delta and strength degradation. Comparison of the behaviour of the SDOF and MDOF models also allowed to sensitivity of the peak base shear to higher mode effects to be monitored. The likely performance of the benchmark and retrofitted wall specimens could also be determined from the analyses.

In Chapter 10 a review and extension of the NZSEE guidelines (NZSEE, 2005) displacement based assessment procedure for structural walls was performed. Information and procedures were compiled to allow for important assumptions made during the procedure to be checked. Particular emphasis was focussed on appropriate assumptions to make when assessing pre-1970's New Zealand structural walls.

11.2 Conclusions

Conclusions drawn from the analytical and experimental investigations performed in this thesis are discussed in the following sections.

11.2.1 Experimental Investigations

Conclusions drawn from the experimental investigations performed in this thesis on two benchmark and two retrofitted cantilever wall specimens (discussed in detail in Chapters 4-8), include:

- The use of selective weakening retrofit techniques in combination with already available retrofit techniques allows a high level of control over the retrofitted behaviour. This makes selective weakening suitable for use in performance based retrofit designs. The high level of control is provided by the ability to reduce the strength/stiffness of the existing wall be severing reinforcement and/or segmenting the wall. The strength/stiffness can also be increased by using existing retrofit solutions (post-tensioning, additional reinforcement or energy dissipaters) in combination with selective weakening techniques.

- Selective weakening retrofit techniques can be used to introduce performance characteristics of new high performance seismic resisting systems (hybrid) to existing structural walls. The characteristics include the ability to introduce a self-centring behaviour and for minimal damage to be observed after a seismic response. These performance characteristics can be achieved by introduction a rocking behaviour by implementing a horizontal cut a foundation level. The implementation of such a solution was shown in retrofit solution adopted for W1R (Chapter 6).

- Selective weakening retrofit techniques can be used to improve the displacement capacity of an existing structural wall and eliminate strength degradation. Comparison of the behaviour of the experimental benchmark and retrofitted specimens showed that strength degradation observed in the benchmarks walls was essentially eliminated when the retrofitted walls were tested to 2.5% drift. The elimination/minimisation of strength degradation can be achieved by avoiding a shear failure, averting the possibility of a lap splice failure and preventing bar buckling and spalling at the toe regions of the wall.

- The retrofit solutions adopted on the experimental walls were used for proof of concept purposes. Therefore the solutions require refinement to improve practicality issues relating to implementing the solutions and the cost-effectiveness of the solutions.

- When implementing a selective weakening retrofit technique on a structural wall the global effects on the retrofitted wall behaviour need to be considered. This includes the need to consider wall-floor diaphragm interaction. Further research is required in this area.

11.2.2 Numerical Investigations

Conclusions drawn from the numerical investigations performed in this thesis on SDOF and MDOF lumped plasticity models representing a prototype wall, include:

- The inclusion of strength degradation in the hysteretic response only resulted in a slight increase in the experienced mean peak drift. The effect of strength degradation can be more pronounced when p-delta effects are also included.

- The inclusion of strength degradation had a variable effect on the observed mean residual drifts.

- The inclusion of p-delta effects resulted in only a minor increase in the observed mean peak drift. The increase was observed to be more substantial when strength degradation was also included.

- The inclusion of p-delta effects resulted in a major increase in the observed mean residual drift.

- The SDOF substitute structure resulted in very similar mean peak drifts and residual drifts as were observed in the MDOF system.

- A substantial increase in the mean peak base shear was observed due to higher mode effects. The increase in base shear was observed to be more substantial as the intensity of the earthquake record increased.

The performance of the benchmark and retrofitted performance of a prototype wall equivalent to W1 (benchmark) and W1R (retrofitted) was assessed in the numerical investigations. The conclusions drawn from these analyses were:

- At lower intensity levels the retrofit solution resulted in slightly increased mean peak drifts.

- At a high intensity level (0.45g (PGA) (Wellington)) the retrofit solution resulted in a moderate reduction in the observed mean peak drift.

- The most significant advantage of the retrofit solution was the elimination of residual drifts.

11.2.3 Assessment of Structural Walls

In Chapter 10 a review and extension of the displacement based assessment procedure for structural walls, which is provided in the NZSEE guidelines (NZSEE, 2005) was performed, the findings are concluded below:

- The displacement based assessment procedure for structural walls which was discussed in Chapter 10 provides a procedure appropriate for converting a MDOF structure into a SDOF substitute structure. This was used to replace the assumption in the NZSEE guidelines of an effective height of $0.67l_w$.

- Procedures and parameters were discussed which are appropriate for checking the assumption that a flexural hinge forms at the base of the wall. This considers the effects of over strength, higher modes and tension shift.

- Appropriate assumptions to make when assessing a pre-1970's New Zealand structural wall were discussed. This includes material properties, strain limits, typical detailing characteristics and plastic hinge length.

- A displacement based retrofit design procedure was discussed. This is simply a displacement based design procedure which is suitable to use to design an appropriate selective weakening retrofit solution for a structural wall.

11.3 Recommended Future Research

During this research project several areas that require future research were highlighted, which include:

- Research is required to investigate and develop selective weakening retrofit techniques for frame structures, as the research in this thesis focussed solely on developing selective weakening for structural walls. Selective weakening retrofit interventions for frame structures could be used to introduce capacity design principles to frame structures by ensuring a strong column and weak beam system. Preliminary suggestions for the use of a selective weakening type retrofit intervention for frame structures can be found in FEMA-273 (FEMA, 1997) and FEMA-356 (FEMA, 2000) documents.

- Further research is required to develop and simplify the selective weakening retrofit solutions that were introduced in this thesis for structural walls. In this research the retrofit solutions that were implemented were used for proof of concept purposes, therefore appropriate measures are required to improve the cost effectiveness and practicality of such solutions.

- Further investigation of the global effects that a selective weakening retrofit intervention (performed on a structural wall) would have on a structure are required. This includes the need to consider issues such as the out-of-plane behaviour and wall-diaphragm interaction.

- A review of typical reinforcement details in pre-1970's New Zealand structural walls showed that it was typical to use a lap splice of 40 bar diameters in length, when using plain round reinforcement. Further research is required to determine if a lap splice of this length is sufficient for the full flexural capacity of the wall to develop. A procedure to assess the performance of a lap splice detail of this type is also required.

- It was highlighted during experimental testing in this research that concrete walls reinforced with plain round bars do not develop a distributed plastic hinge zone, as do concrete walls reinforced with deformed bars. Concrete sections reinforced with plain round bars typically only develop a single crack at the critical plane. When assessing the ductility of a reinforced concrete section the result is quite sensitive to the plastic hinge length used. Current equations used to estimate the plastic hinge length are for sections reinforced with deformed reinforcing bars, the use of these equations can result in an overestimation of the plastic hinge length when considering sections reinforced with plain round bars. This inturn would result in an overestimation of the ductility capacity of a section that is reinforced with plain round bars. Therefore future research is required to determine the sensitivity of the ductility capacity to the plastic hinge length, how significant the overestimation of the ductility is and a method to appropriately estimate the plastic hinge length of a section reinforced with plain round bars.

11.4 Closing Remarks

This thesis set out to investigate the feasibility and develop a selective weakening approach for the seismic retrofit of reinforced concrete structural walls. Through analytical, numerical and experimental investigations it was shown that a selective weakening retrofit approach (when used in combination with already available retrofit techniques) offers a high level of control over the final behaviour/performance and can exhibit some distinct advantages over conventional retrofit techniques. Conventional retrofit techniques generally focus on

upgrading the behaviour (strength/stiffness) which can have negative side effects, such as exceeding the capacity of the foundation. A selective weakening retrofit approach offers the distinct advantages of being able to ensure that the foundation capacity is not exceeded and it is possible to introduce the desirable characteristics of recently developed high performance seismic resisting systems (hybrid) to an existing wall. This includes the ability to introduce a rocking re-centring behaviour which results in minimal damage and no residual displacements after a seismic response. The results of the experimental, numerical and analytical investigations performed in this thesis confirmed the feasibility and viability of using selective weakening retrofit techniques to improve the performance of structural walls.

References:

FEMA-273. [1997]. "NEHRP guidelines for the seismic rehabilitation of buildings". Building Seismic Safety Council (U.S.), Federal Emergency Management Agency

FEMA-356. [2000]. "Pre-Standard and Commentary for the Seismic Rehabilitation of Buildings". Federal Emergency Management Agency. Washington D.C.

NZSEE. [2005]. "Assessment and Improvement of the Structural Performance of Buildings in Earthquake – Study Group Draft", New Zealand Society of Earthquake Engineering, Prepared for the Department of Building and Housing

Appendix A Worked Examples

A.1 Displacement Based Assessment and Retrofit of a Structural Wall

Displacement Based Assessment & Retrofit - EXAMPLE

-This example shows the procedure required to perform a displacement based assessment on a reinforced concrete structural wall. The example follows the procedure that was outlined in chapter 10.0. The wall shown in this example exhibits characteristics that could be considered typical of a pre-1970's New Zealand structural wall. After the assessment a retrofit solution involving selective weakening techniques is designed using a displacement based design procedure.

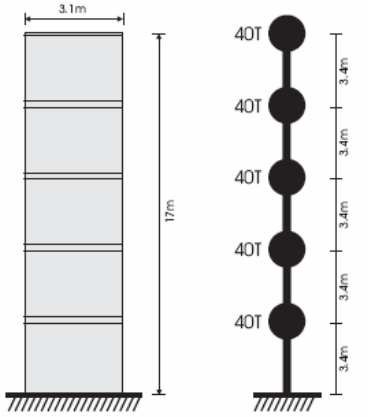

5 Storey, pre-1970's New Zealand Structural Wall

f'c=30MPa fy=300MPa

Axial Load from 75% of Seismic Mass

N*=1500kN

Axial Load Ratio =0.08

- ½" longitudinal reinforcement is curtailed to 3/8" reinforcement just above third floor level

Wall Cross Section

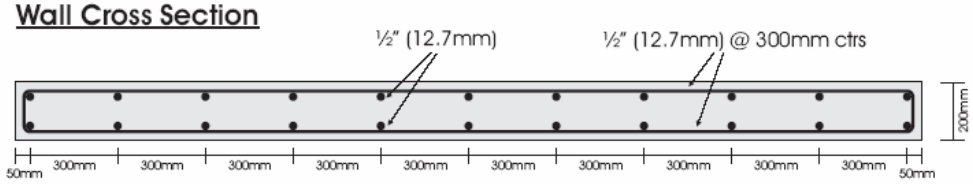

Section Capacity **(Refer Section 10.3.1)**

- Unconfined concrete conditions i.e. ε_c=0.005. Due to large spacing of transverse reinforcement and inadequate detailing (90 degree hooks in cover concrete) to prevent buckling.

Yield Moment & Curvature - Assuming ε_y=0.0015 or ε_c=0.002

M_y=3048 kNm

ϕ_y=0.00072 1/m

-Yield curvature is to be determined from standard section analysis procedures or from an approximate equation, such as equation 10-10.

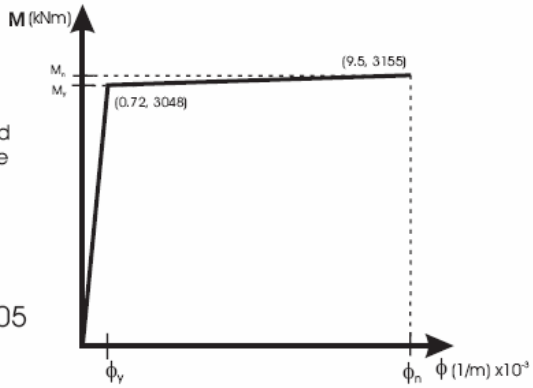

Nominal Moment & Curvature

M_n=3155 kNm - Assuming ε_c=0.005

ϕ_n=0.0095 1/m

Conversion of 5 Storey Wall to an Equivalent SDOF Oscillator

(Refer Section 10.2.2)

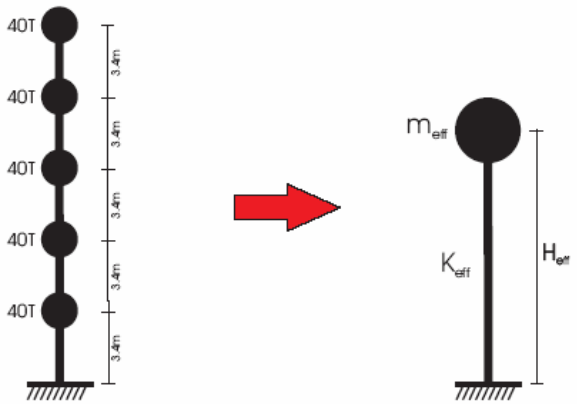

- Assume linear displacement profile up height of wall, with a magnitude of 1.0 at the top of the wall.

$$\Delta_d = \frac{\sum_{i=1}^{n}(m_i\Delta_i^2)}{\sum_{i=1}^{n}(m_i\Delta_i)} = 0.733 \qquad m_e = \frac{\sum_{i=1}^{n}(m_i\Delta_i)}{\Delta_d} = 163.7t \qquad H_e = \frac{\sum_{i=1}^{n}(m_i\Delta_i H_i)}{\sum_{i=1}^{n}(m_i\Delta_i)} = 12.5m$$

Determine the Base Shear Capacity of the 5-Storey Wall

(Refer equation 10-5)

SDOF Substitute Structure

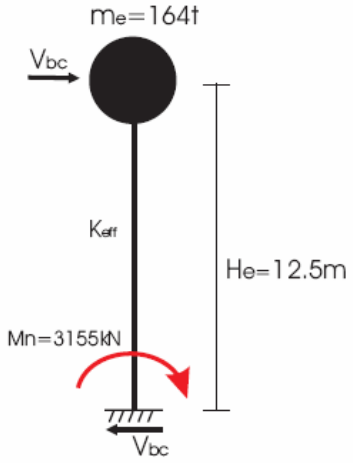

Base Shear Capacity

$$V_{bc} = \frac{M_n}{H_e} = 252kN$$

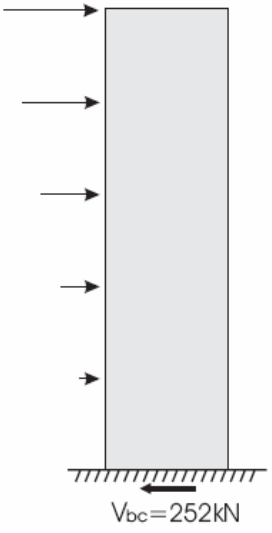

Determine Displacement Capacity of the 5-Storey Wall

(Refer Section 10.3.2)

$L_p = 0.2l_w + 0.03h_n$

(Equation 10-13)

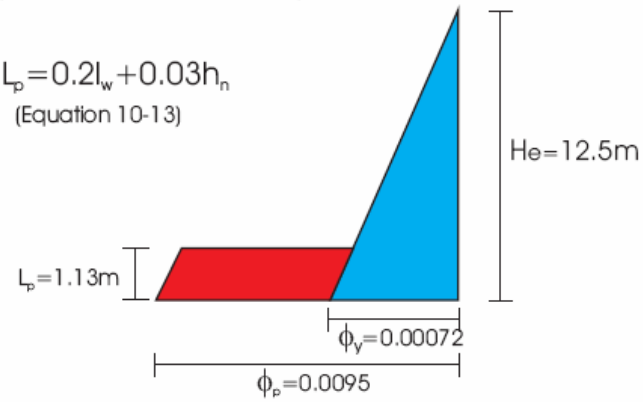

- The plastic hinge length equation used, is for sections that are reinforced with deformed bars. The equation will therefore be likely to over-estimate the plastic hinge length for this wall which is reinforced with plain round bars. This will substantially increase the calculated ductility capacity of the wall. Further research is required to determine the sensitivity and severity of this issue.

Displacement Capacity

$\Delta_y = 0.0375m$

$\Delta_u = 0.118m$

Ductility Capacity

$\mu_\Delta = 3.2$

- Ductility capacity is less than the code specified ductility limit for a structural wall (Typically 5.0). Therefore there is no need to adjust the displacement capacity.

Determine the Effective Stiffness of the SDOF Substitute Structure

(Refer figure 10.1(b) & equation 10-6)

$\Delta_{capacity} = \Delta_u = 0.118m$

$V_{bc} = 252kN$

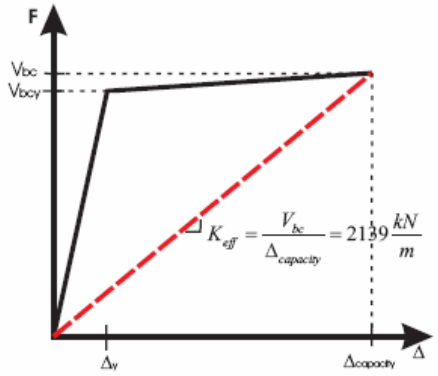

Estimate the Level of Equivalent Viscous Damping

(Refer Section 10.3.5)

Estimate the level of equivalent viscous damping for a displacement ductility of:

$\mu_\Delta = 3.2$

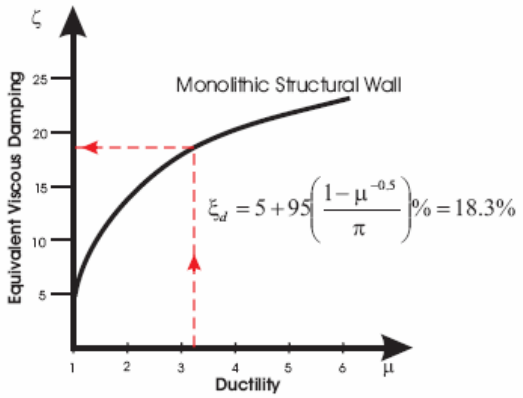

Determine the Effective Period and the Spectral Displacement Demand

(Refer figure 10.1(d) & equation 10-7)

Effective Period

$$T_{eff} = 2\pi\sqrt{\frac{m_e}{k_e}} = 1.73\,\text{sec}$$

Spectral Displacement Demand

- Determine the spectral displacement demand for the SDOF substitute structure

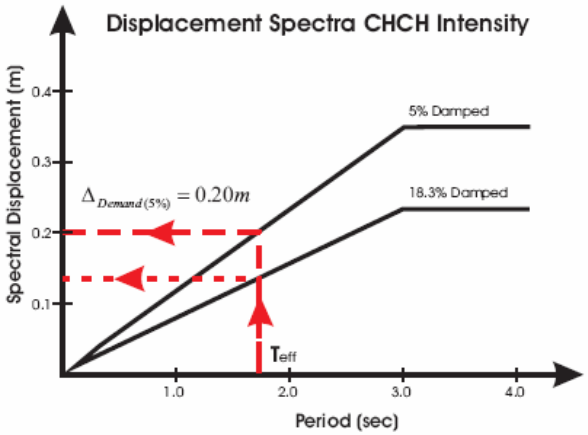

- Method to adjusted displacement demand to account for using a 5% damped spectra

$$\Delta_{Demand(\xi)} = \Delta_{Demand(5\%)}\left(\frac{10}{5+\xi}\right)^{0.5} = 0.131m$$

Compare the Displacement Capacity to the Displacement Demand

$$\Delta_{demand(18.3\%)} = 0.131m > \Delta_{capacity} = 0.118m$$

-Displacement demand is greater than the displacement capacity

Retrofit Will Be Required

Check Assumption that a Flexural Hinge forms at the Base

(Refer Section 10.3.3)

- Check to see if the critical section is at the base of the wall
- Shift BMD to account for higher modes and check if tension shift is required

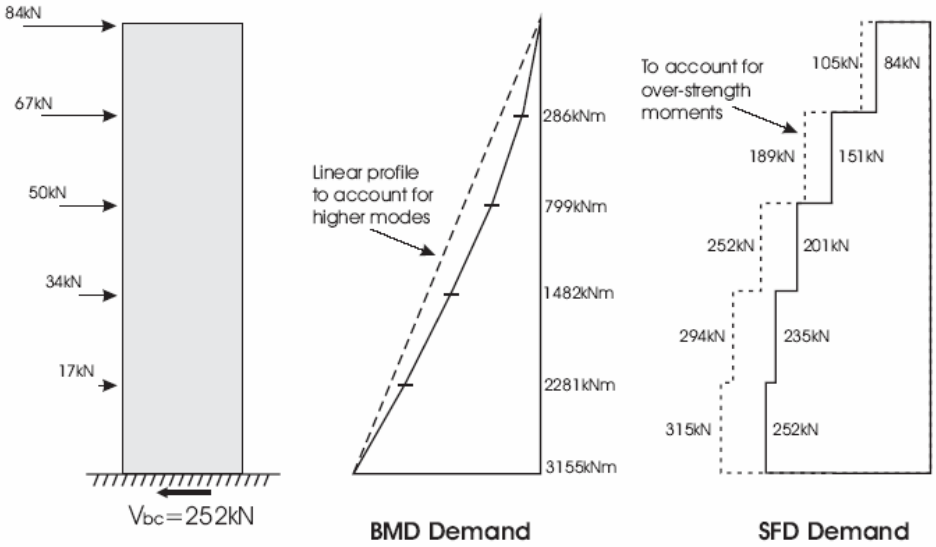

Check shear stress to see if a tension shift is required

$$\frac{\phi^o V}{A_w} \le 0.2\sqrt{f_c'} \quad \Rightarrow \quad \frac{315kN}{3.1m \times 0.2m} \le 0.2\sqrt{30MPa} \quad \Rightarrow \quad 0.5MPa \le 1.1MPa$$

⇒ - Tension shift of the BMD will not be required as shear cracking is unlikely to occur

Check the shear capacity of the wall section

- Shear reinforcement consists of 2-layers of ½"bars at 12" ctrs
- For an initial conservative estimate only account for the reinforcing steel contribution to the shear capacity (i.e. Neglect concrete contribution)

$V_s = A_s f_y (d/s)$ $\quad d \cong 0.8 l_w$

$V_s = (2*127mm^2) \times 300MPa \times (0.8*3.1m/0.3m) = 620kN$

- Peak shear demand from over-strength shear envelope =315kN

620kN ≥ 315kN - Therefore the shear capacity of the wall is sufficient

Check the sliding shear capacity of the wall

$V_{SL} = \phi\mu(A_{vf} f_y + P_u)$ $\quad V_{SL} = 0.85 \times 0.7(11 \times 2 \times 127mm^2 \times 300MPa + 1500kN) = 1141kN$

- The Sliding Shear strength will be sufficient

Check the flexural capacity at appropriate sections

- Flexural capacity needs to be calculated to account for curtailment of reinforcement
- The only curtailment in this example wall is a change from 1/2" to 3/8" longitudinal reinforcement just above the third floor level

Flexural capacity at the base of the wall

Mn = 3155kNm

Flexural capacity above the third floor level

Mn = 1556kNm

- It is important to account for the reduced axial load as you move up the height of the wall

Flexural Capacity Envelope

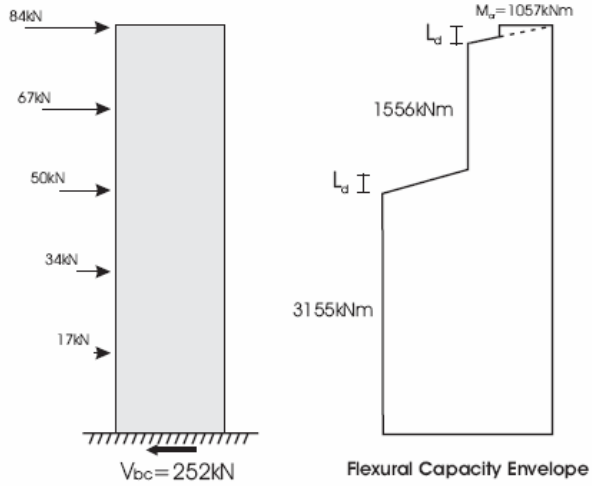

Flexural Capacity Envelope

L_d = 40 bar diameters

- Need to assess whether the lap splice is sufficient for the full flexural capacity to develop
- M_{cr} is the cracking moment

Flexural Capacity Envelope

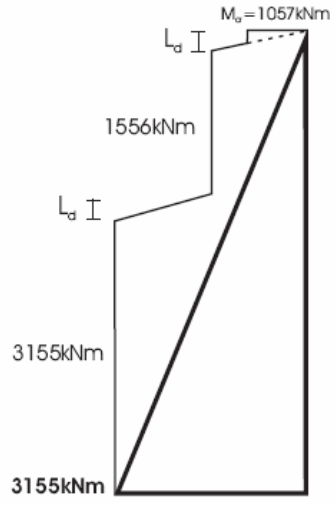

Flexural Capacity vs Flexural Demand

- The flexural capacity up the height of the wall is sufficient to ensure that a plastic hinge forms at the base of the wall.
- The shear strength and sliding shear strength is sufficient to ensure that a flexural hinge forms

Retrofit of the As-built 5-Storey Wall

Retrofit Aim

- Increase the displacement capacity of the wall to satisfy the displacement demand
- Find a solution that does not result in a base shear capacity greater than that of the as-built wall.

Proposed Retrofit Solution

- Use a selective weakening retrofit technique that involves a horizontal cut at foundation level to introduce a rocking re-centring response

- Aim to achieve maximum drift of 2.0%

- A combination of un-bonded post-tensioning and energy dissipation devices may be required to achieve desired behaviour

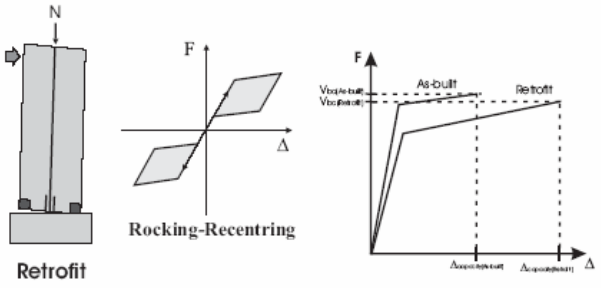

Displacement Based Design of Proposed Retrofit Solution (Refer Section 10.4)

- Use a displacement based design procedure to determine the required base shear capacity for the retrofitted wall

- Ultimate displacement corresponding to 2.0% drift limit $\Delta_u = 0.25m$

Equivalent Viscous Damping

- An estimate of the equivalent viscous damping that will be provided by the retrofitted wall needs to be made, to determine the appropriate displacement spectra to use

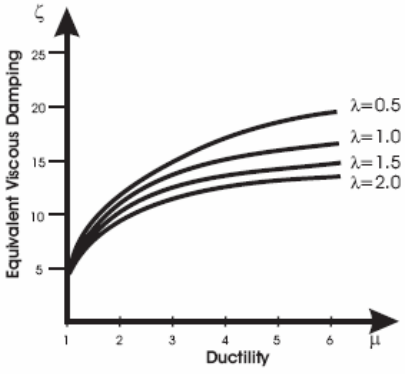

$$\lambda = \frac{M_{PT} + M_{Axial}}{M_{Dissipation}}$$

Equivalent viscous damping for a rocking wall was proportioned from the equation for an un-bonded post-tensioned system & the equation for a monolithic structural wall

- Assume Equivalent Viscous Damping of **12%** for First Estimate

Adjust the Ultimate Design Displacement to for 5% Damped Spectra

- The ultimate design displacement need to be adjusted to account for using a 5% damped spectra

$$\Delta_{Design(5\%)} = \frac{\Delta_{Design(12\%)}}{\left(\frac{10}{5+12}\right)^{0.5}} = 0.326m$$

Determine the Effective Period for the Proposes Retrofit Solution

(Refer figure 10-10)

$$\Delta_{Design(5\%)} = 0.326m$$

$$\Delta_{Design(12\%)} = 0.25m$$

$\Rightarrow$ $T_{eff} = 2.8sec$

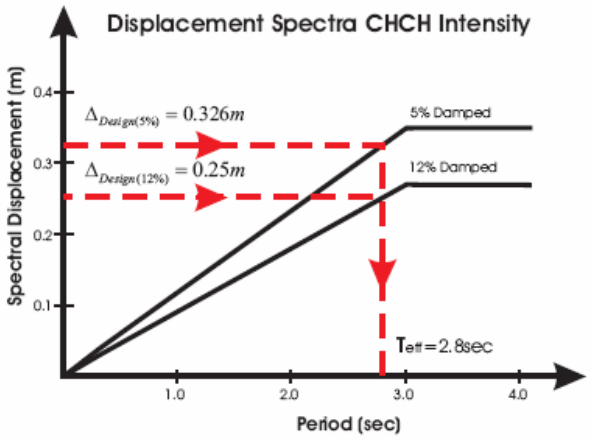

Determine the Required Stiffness & Required Base Shear Capacity

$$K_{eff\,(Required)} = m_e\left(\frac{2\pi}{T_{eff}}\right)^2 = 824\,\frac{kN}{m}$$

$$V_{bc\,(Required)} = K_{eff\,(Required)}\Delta_{Design} = 206kN$$

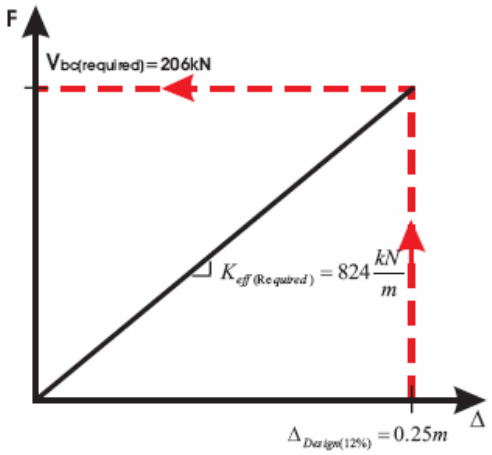

Determine Required Moment Capacity for the Retrofitted Wall

$M_{n(Required)} = V_{bc(Required)}H_e = 2575kNm$

Retrofitted Wall Requires:

$V_{bc} = 206kN$ or $M_n = 2575kNm$

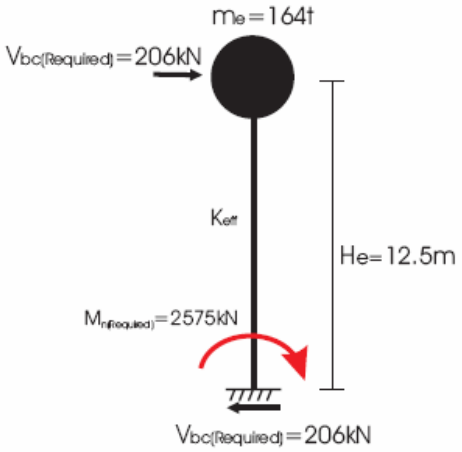

Design Retrofitted Wall Section to Meet the Demand Determined From Displacement Based Design Procedure

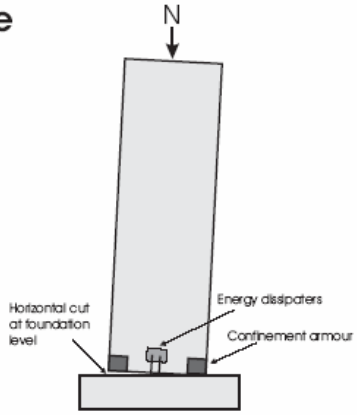

Minimum Required Capacity

$M^* = 2575kNm$

Selective Weakening Retrofit

- Apply horizontal saw cut at foundation level which severs all longitudinal reinforcement
- Rely on axial load to provide re-centring capability
- Use a total of 8-16mm diameter energy dissipaters located symmetrically 100mm each side of the wall centreline
- Need to provide confinement armour at the toe regions of the wall

Section Analysis Results

$M_n = 3060kNm$ ⇒ $V_{bc} = 245kN$

$$\lambda = \frac{M_{PT} + M_{Axial}}{M_{Dissipation}} = \frac{2100kNm}{950kNm} = 2.2$$

Yield drift = 0.40% $\Delta_y = 0.05m$

Ultimate drift = 2.0% $\Delta_u = 0.25m$

$\mu = 5.0$

Required Capacity vs Retrofit Solution Capacity

- The required capacity for the retrofitted wall was determined from the displacement based design procedure performed earlier. The retrofit solution capacity is the section capacity that was determined during the design of the retrofit solution discussed above

Required (DBD)		Retrofit Solution
$M^* = 2575kNm$	$\leq$	$M_n = 3060kNm$
$V_{bc} = 206kN$	$\leq$	$V_{bc} = 245kN$

- Required moment and base shear capacity was determined assuming 12% equivalent viscous damping

Assessment of the Proposed Retrofit Solution

- A displacement based assessment of the proposed retrofit solution will be performed to ensure that the retrofit solution is appropriate

Retrofitted Wall Properties

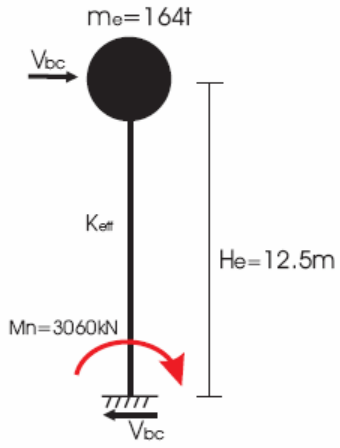

$$V_{bc} = \frac{M_n}{H_e} = 245kN$$

$\mu_\Delta = 5.0$

$\Delta_{capacity} = 0.25m$

$\lambda = 2.2$

Determine the Effective Stiffness and Equivalent Viscous Damping

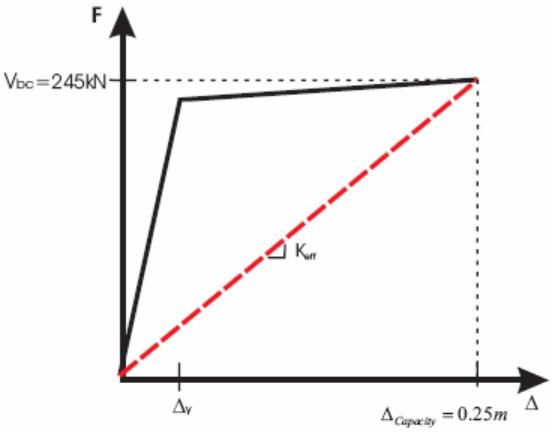

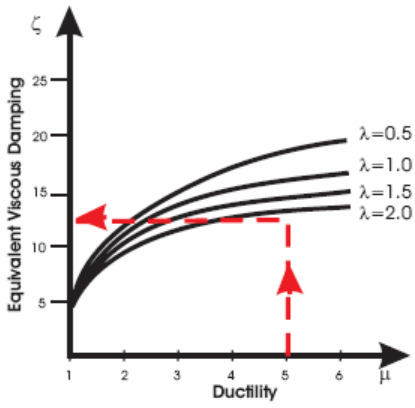

- For $\lambda = 2.2$ and $\mu = 5.0$

$$K_{eff} = \frac{V_{bc}}{\Delta_{capacity}} = 980\frac{kN}{m}$$

$$\xi_d = 0.31\left(5 + 95\left(\frac{1-\mu^{-0.5}}{\pi}\right)\%\right) + 0.69\left(5 + 25\left(\frac{1-\mu^{-0.5}}{\pi}\right)\%\right) = 13.0\%$$

Determine Effective Period

$$T_{eff} = 2\pi\sqrt{\frac{m_e}{k_e}} = 2.60\ \text{sec}$$

Displacement Demand on Retrofitted Wall

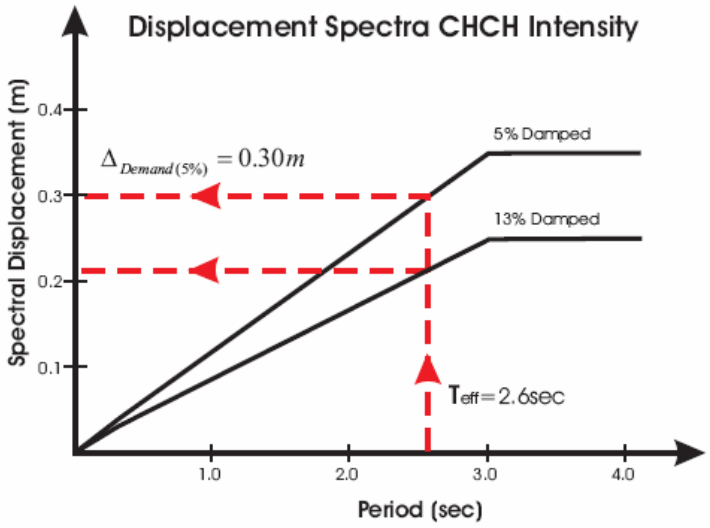

- Adjusted displacement demand to Account for using a 5% damped spectra

$$\Delta_{Demand(\xi)} = \Delta_{Demand(5\%)}\left(\frac{10}{5+\xi}\right)^{0.5} = 0.212m$$

Displacement Demand vs Displacement Capacity

$\Delta_{demand(13\%)} = 0.212m < \Delta_{capacity} = 0.25m$

Retrofit Solution will be Sufficient

- Need to check that other structural and non-strucutral elements within the building can withstand the increased displacement demand.

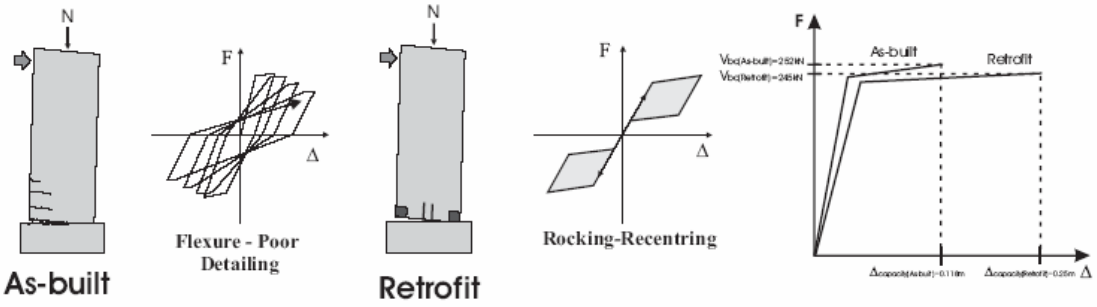

A.2 Displacement Based Assessment and Retrofit of Prototype Wall

Prototype Wall - Displacement Based Assessment

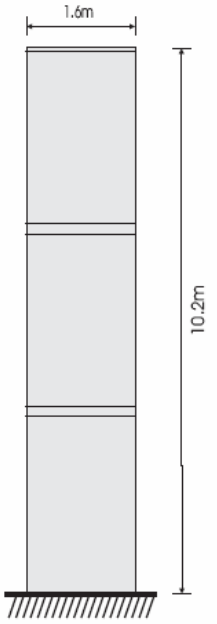

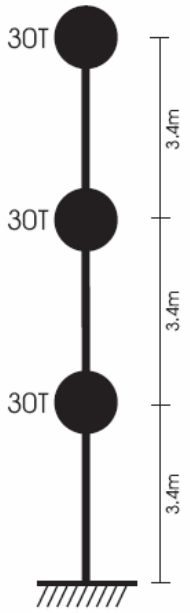

3 Storey, pre-1970's New Zealand Structural Wall

f'c=35MPa

fy=300MPa

Axial Load from 40% of Seismic Mass

N*=380kN

Axial Load Ratio =0.035

Wall Cross Section

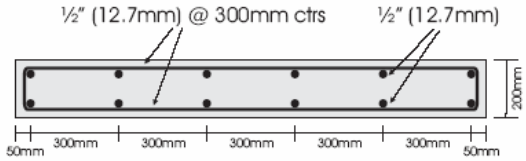

Section Capacity

- Unconfined concrete conditions i.e. ε_c=0.005. Due to large spacing of transverse reinforcement and inadequate detailing (90 degree hooks in cover concrete) to prevent buckling.

Yield Moment & Curvature

M_y=535 kNm - Assuming ε_y=0.0015 or ε_c=0.002

ϕ_y=0.0011 1/m

Nominal Moment & Curvature

M_n=622 kNm - Assuming ε_c=0.005

ϕ_n=0.0205 1/m

Conversion of 3 Storey Wall to an Equivalent SDOF Oscillator

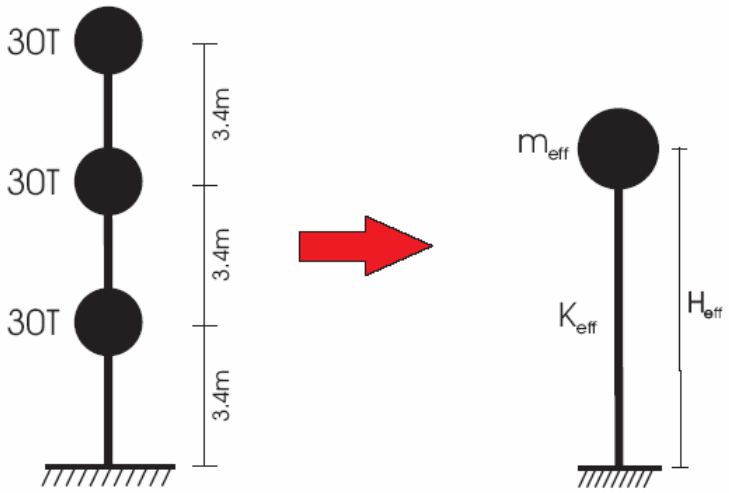

- Assume linear displacement profile up height of wall

$$\Delta_d = \frac{\sum_{i=1}^{n}(m_i\Delta_i^2)}{\sum_{i=1}^{n}(m_i\Delta_i)} = 0.78 \qquad m_e = \frac{\sum_{i=1}^{n}(m_i\Delta_i)}{\Delta_d} = 77t \qquad H_e = \frac{\sum_{i=1}^{n}(m_i\Delta_i H_i)}{\sum_{i=1}^{n}(m_i\Delta_i)} = 7.95m$$

Displacement Based Assessment of the 3 Storey Prototype Wall

Base Shear Capacity

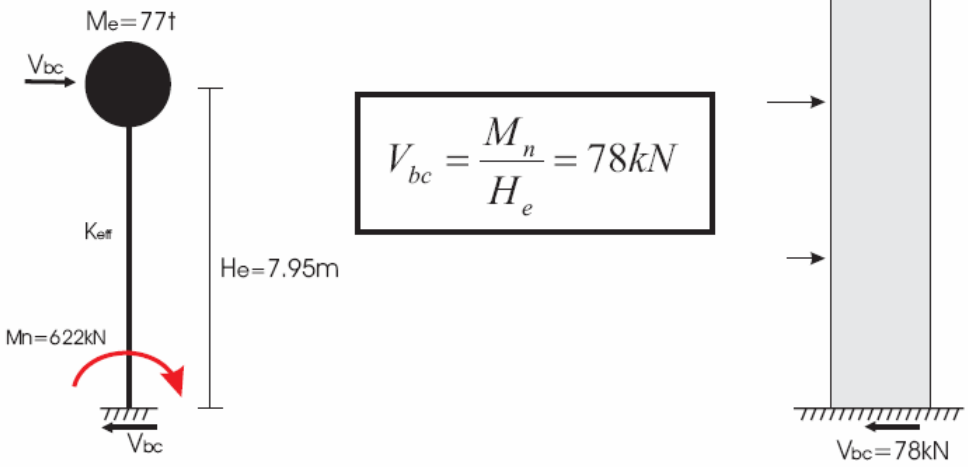

$$V_{bc} = \frac{M_n}{H_e} = 78kN$$

Displacement Based Assessment of the 3 Storey Prototype Wall (Cont'd)

Displacement Capacity

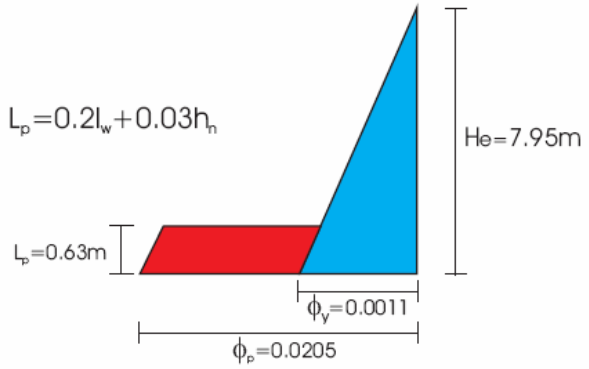

Δ_y=0.023m

Δ_u=0.116m

μ_Δ=5.1

Ductility Limit

- Code limit ductility for structural wall μ_Δ=5.0 ⇒ Δ_u=0.115m

Effective Stiffness

$\Delta_{capacity}=\Delta_u=0.115m$

V_{bc}=78kN

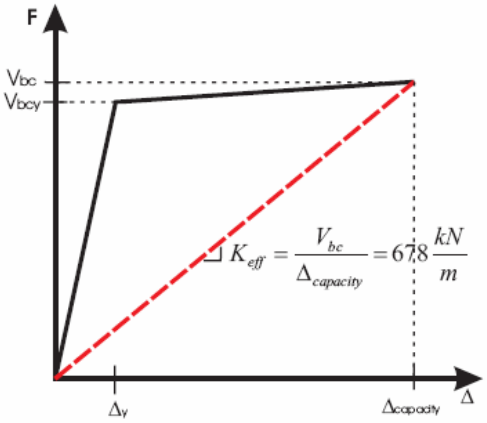

Level of Equivalent Viscous Damping

μ_Δ=5.0

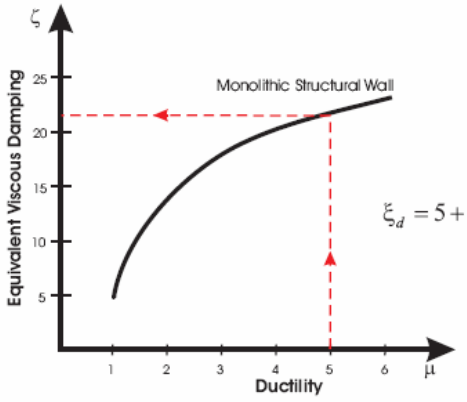

$$\xi_d = 5+95\left(\frac{1-\mu^{-0.5}}{\pi}\right)\% = 21.7\%$$

Displacement Based Assessment of the 3 Storey Prototype Wall (Cont'd)

Effective Period & Spectral Displacement Demand

$$T_{eff} = 2\pi\sqrt{\frac{m_e}{k_e}} = 2.1\,\text{sec}$$

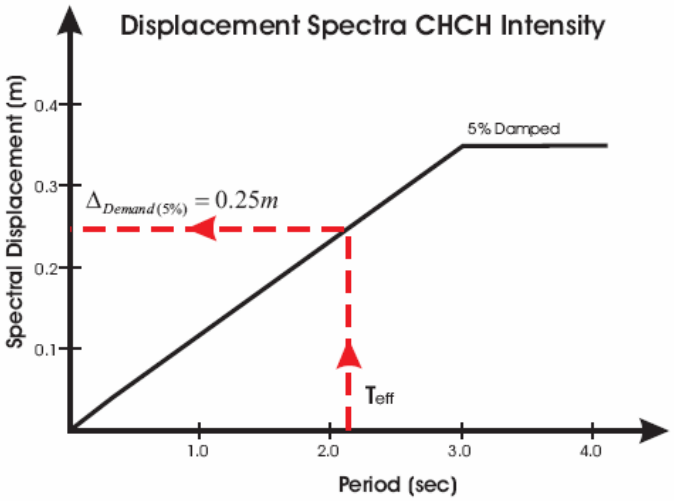

- Adjusted displacement Demand to Account for using a 5% damped spectra

$$\Delta_{Demand(\xi)} = \Delta_{Demand(5\%)}\left(\frac{10}{5+\xi}\right)^{0.5} = 0.153m$$

Displacement Demand vs Displacement Capacity

$$\Delta_{demand(18.3\%)} = 0.153m > \Delta_{capacity} = 0.115m$$

Retrofit Will Be Required

Selective Weakening Retrofit of the 3 Storey Prototype Wall

-Selective weakening retrofit involving a horizontal cut at foundation level to allow wall to rock

-A combination of unbonded post-tensioning and energy dissipation devices will be used to achieve desired behaviour

-Aim to achieve maximum drift of 2.5% and satisfy code requirements

Displacement Capacity

-Ultimate displacement corresponding to 2.5% drift limit

$$\Delta_u = 0.199m$$

Equivalent Viscous Damping

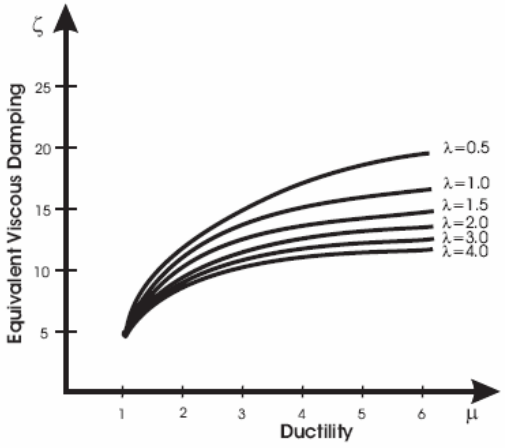

$$\lambda = \frac{M_{PT} + M_{Axial}}{M_{Dissipation}}$$

Equivalent Viscous Damping For Hybrid Wall Proportioned from Equation for Unbonded Post-tensioning Equation & Equation for Monolithic Structural Wall

- Assume Equivalent Viscous Damping of **12%** for First Estimate

Displacement Adjustment

- Displacement demand is adjusted to account for using a 5% damped displacement spectra

$$\Delta_{Demand(5\%)} = \frac{\Delta_{Demand(12\%)}}{\left(\frac{10}{5+12}\right)^{0.5}} = 0.259m$$

Selective Weakening Retrofit of the 3 Storey Prototype Wall (Cont'd)

Effective Period

$$\Delta_{Demand(5\%)} = 0.259m$$

$T_{eff} = 2.8sec$

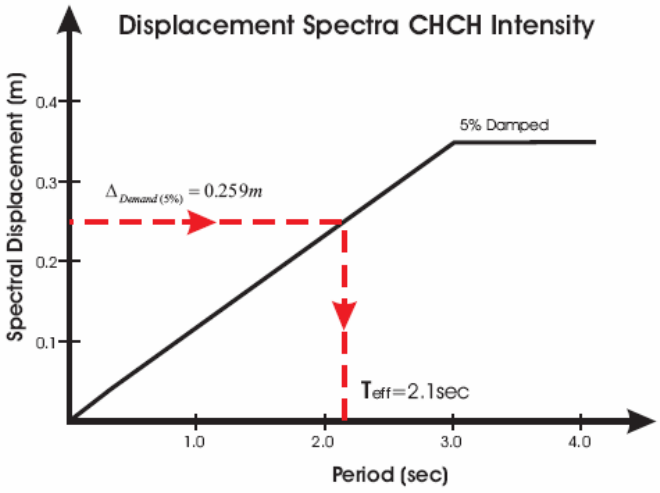

Required Effective Stiffness & Base Shear Capacity

$$K_{eff\,(Required)} = m_e\left(\frac{2\pi}{T_{eff}}\right)^2 = 689\,\frac{kN}{m}$$

$$V_{bc(Required)} = K_{eff\,(Required)}\Delta_{Capacity} = 137kN$$

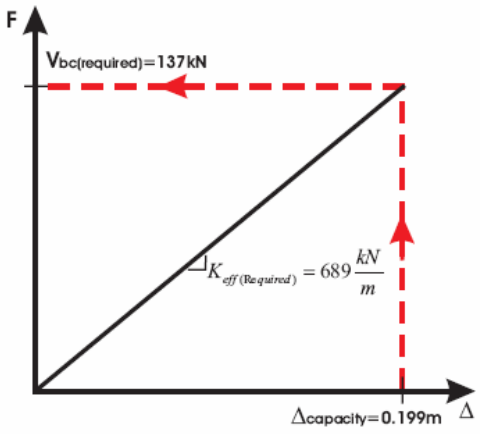

Required Moment Capacity

$M_{n(Required)} = V_{bc(Required)}H_e = 1089kN$

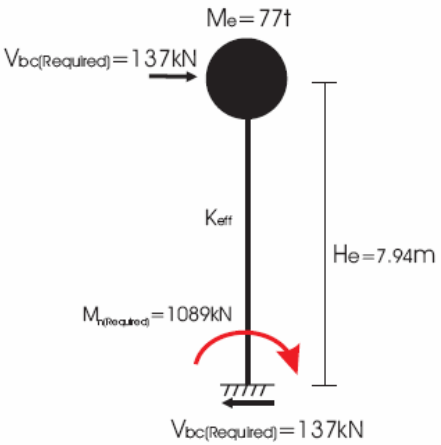

Retrofitted Wall Requires:

$V_{bc} = 137kN$ or $M_n = 1089kNm$

Selective Weakening Retrofit of the 3 Storey Prototype Wall (Cont'd)

- Horizontal saw cut at foundation level severing all longitudinal reinforcement
- Eight seven wire unbonded post-tensioning tendons with an 5m unbonded length
- Initial post-tensioning of 45kN per tendon,
- 4 16mm diameter energy dissipaters located symmetrically 50mm each side of wall centreline

Section Analysis Results

$M_n = 1110kNm$ ⇒ $V_{bc} = 140kN$

$$\lambda = \frac{M_{PT} + M_{Axial}}{M_{Dissipation}} = \frac{1780kNm}{1223kNm} = 1.5$$

Yield drift = 0.33% $\Delta_y = 0.041m$

Ultimate drift = 2.0% $\Delta_u = 0.199m$

$\mu = 6.0$

Retrofitted Wall Capacity vs Required Capacity

Retrofit		Required
$M_n = 1110kNm$	$\geq$	$M_n = 1089kNm$
$V_{bc} = 140kN$	$\geq$	$V_{bc} = 137kN$

- Required moment and base shear capacity was determined assuming 12% equivalent viscous damping, need to check retrofit suitability with adjusted equivalent viscous damping

Selective Weakening Retrofit Check

Retrofitted Wall Capacity

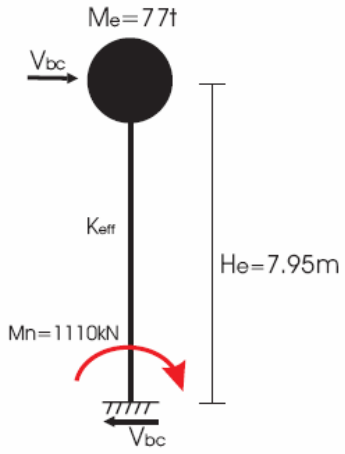

$$V_{bc} = \frac{M_n}{H_e} = 140kN$$

Yield drift=0.33% Δ_y=0.041m

Ultimate drift=2.0% Δ_u=0.199m

μ=6.0

λ=4.0

Equivalent Viscous Damping

- Equivalent viscous damping determined from experimental response at 2.5% drift

$$\xi_{EXP(2.5\%drift)} = 14\%$$

Effective Stiffness

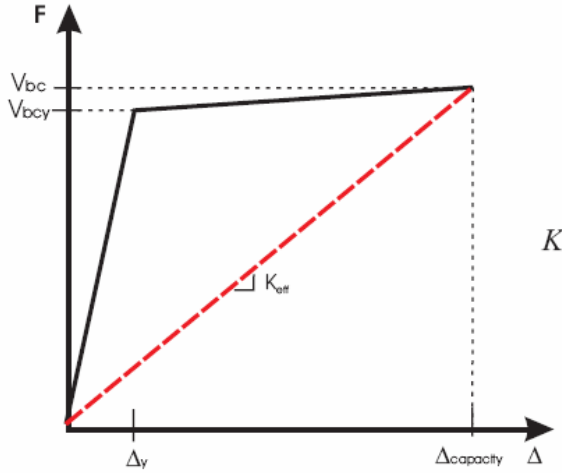

$$K_{eff} = \frac{V_{bc}}{\Delta_{capacity}} = 704\frac{kN}{m}$$

Effective Period

$$T_{eff} = 2\pi\sqrt{\frac{m_e}{k_e}} = 2.1\text{sec}$$

Selective Weakening Retrofit Check (Cont'd)

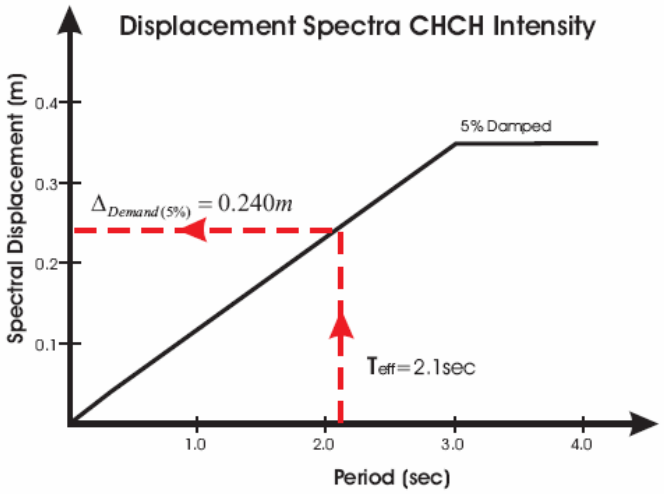

- Adjusted displacement demand to Account for using a 5% damped spectra

$$\Delta_{Demand(\xi)} = \Delta_{Demand(5\%)}\left(\frac{10}{5+\xi}\right)^{0.5} = 0.174m$$

Displacement Demand vs Displacement Capacity

$$\Delta_{demand(14\%)} = 0.174m < \Delta_{capacity} = 0.199m$$

Retrofit Solution will be Sufficient

Appendix B Photo Report

B.1 Photos at each Drift Cycle

B.1.1 W1 – Photo Report

-0.2% drift

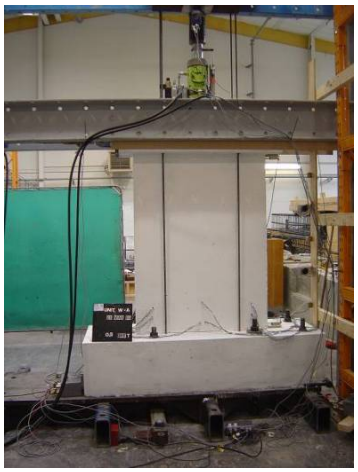

0.2% drift

-0.3% drift

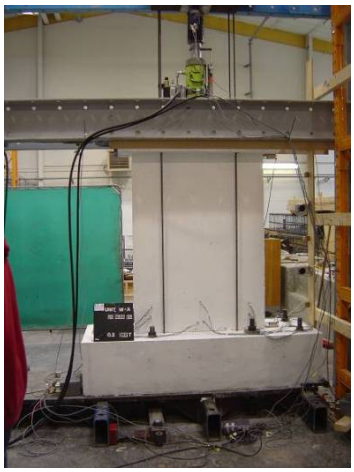

0.3% drift

-0.5% drift

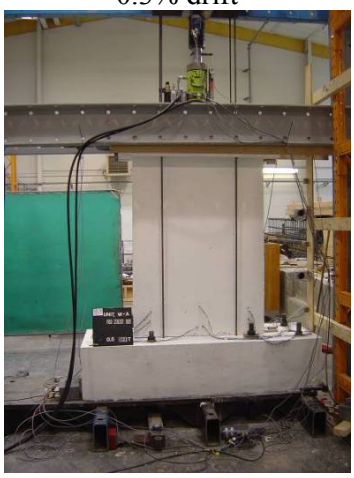

0.5% drift

W1 – Photo Report

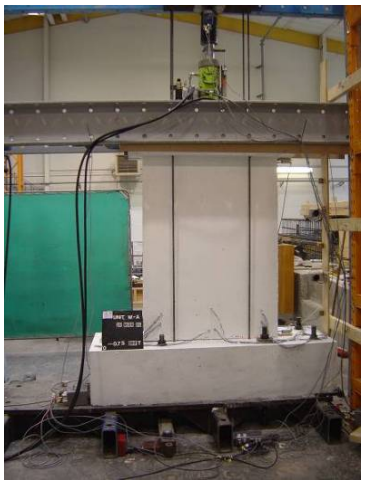

-0.75% drift

0.75% drift

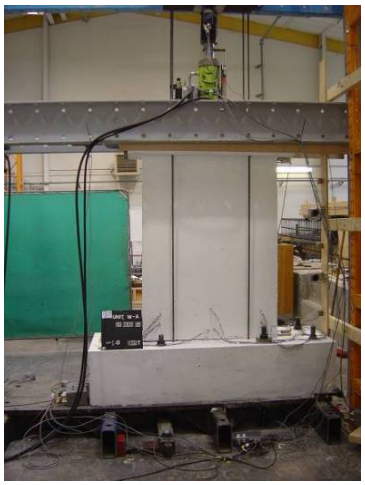

-1.0% drift

1.0% drift

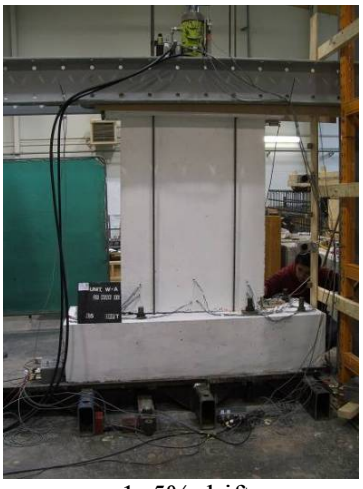

-1. 5% drift

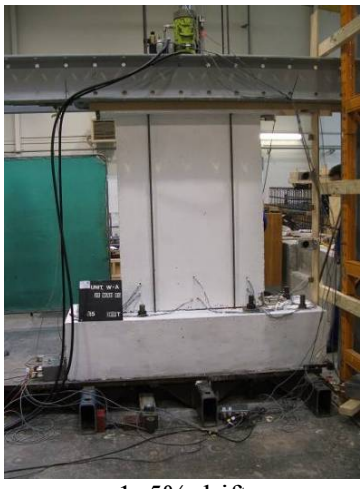

1. 5% drift

W1 – Photo Report

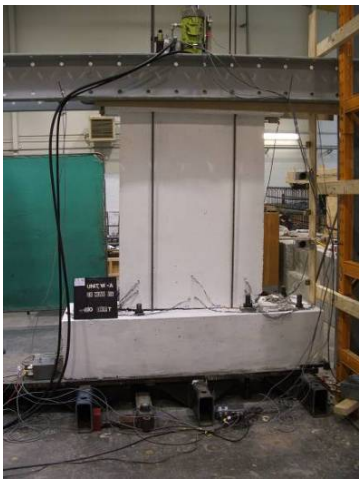

-2. 0% drift

2. 0% drift

-2. 5% drift

2. 5% drift

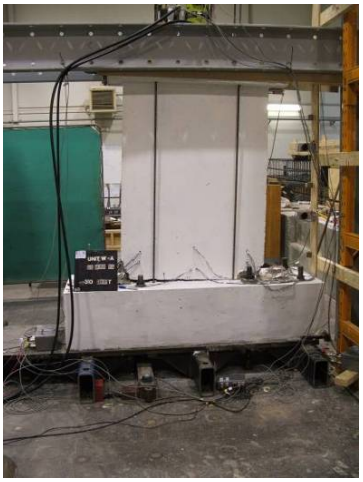

-3. 0% drift

3. 0% drift

B.1.2 W2 – Photo Report

-0.1% drift

0.1% drift

-0.2% drift

0.2% drift

-0.3% drift

0.3% drift

W2 – Photo Report

-0.5% drift

0.5% drift

-0.75% drift

0.75% drift

-1.0% drift

1.0% drift

W2 – Photo Report

-1.5% drift

1.5% drift

-2.0% drift

2.0% drift

-2.5% drift (1st cycle)

2.5% drift (1st cycle)

B.1.3 W3 – Photo Report

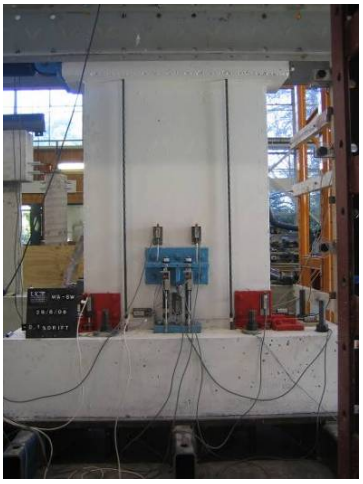

-0.1% drift

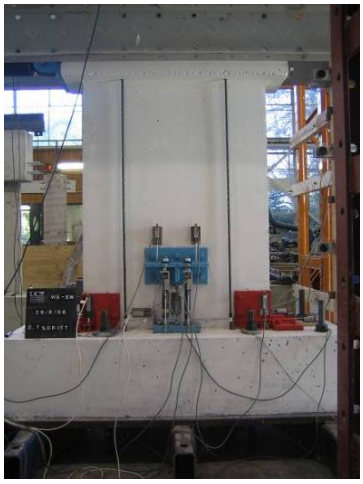

0.1% drift

-0.2% drift

0.2% drift

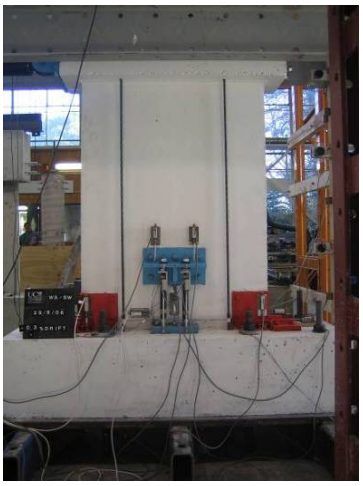

-0.3% drift

0.3% drift

W1R– Photo Report

-0.5% drift

0.5% drift

-0.75% drift

0.75% drift

-1.0% drift

1.0% drift

W1R– Photo Report

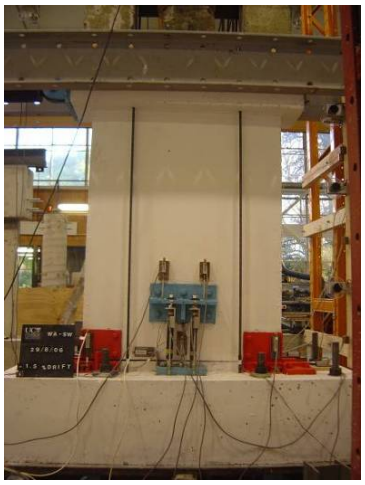

-1.5% drift

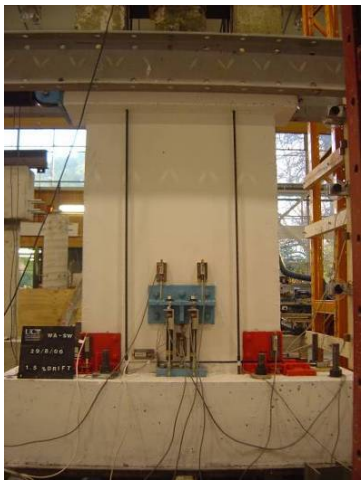

1.5% drift

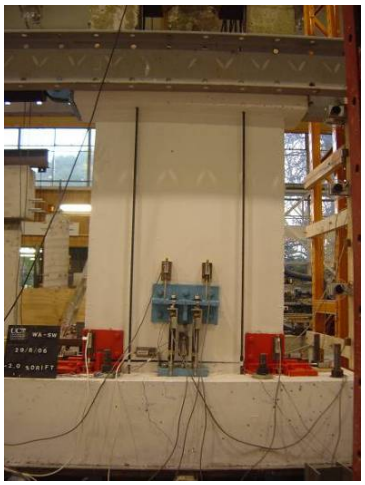

-2.0% drift

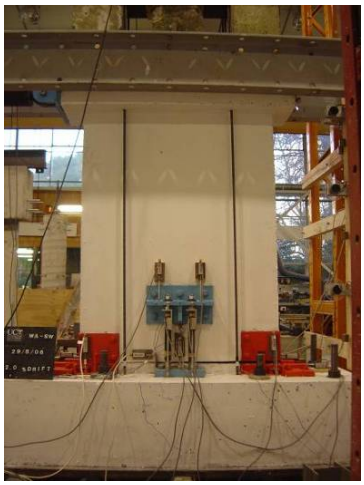

2.0% drift

-2.5% drift

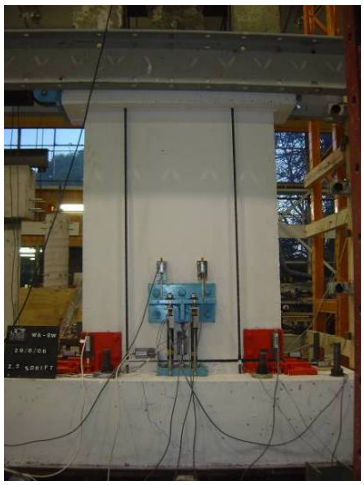

2.5% drift

B.1.4 W2R– Photo Report

-0.1% drift

0.1% drift

-0.2% drift

0.2% drift

-0.3% drift

0.3% drift

W2R– Photo Report

-0.5% drift

0.5% drift

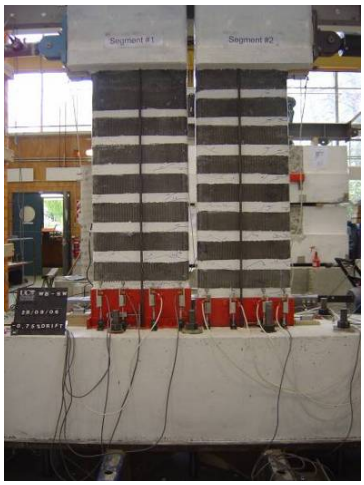

-0.75% drift

0.75% drift

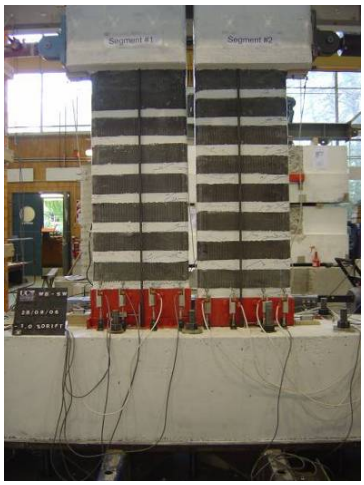

-1.0% drift

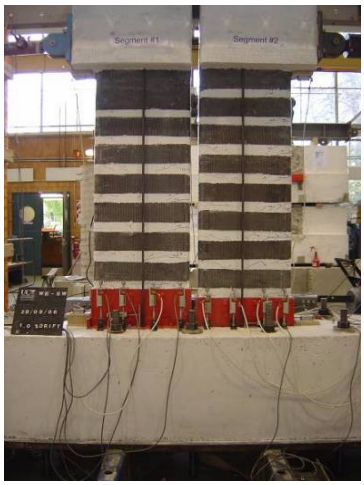

1.0% drift

W2R– Photo Report

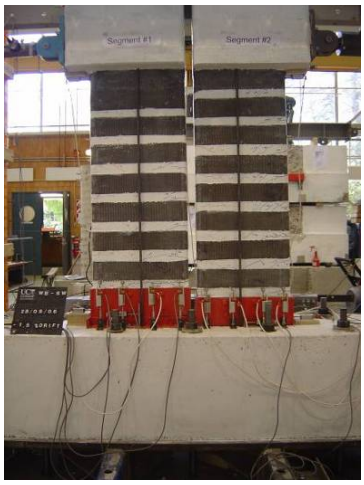

-1.5% drift

1.5% drift

-2.0% drift

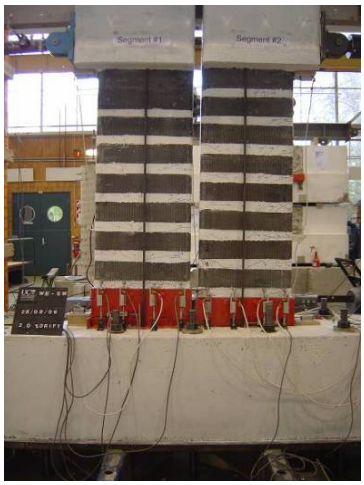

2.0% drift

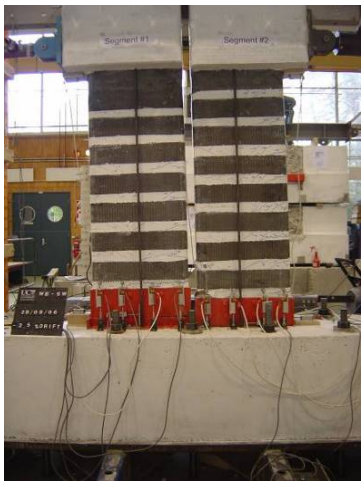

-2.5% drift

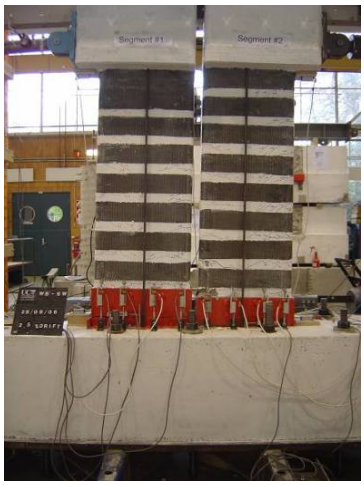

2.5% drift

B.2 Construction Photos

B.2.1 W1 and W1R- Construction

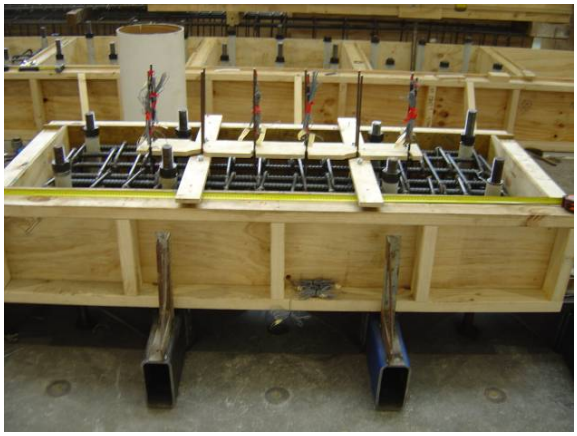

Foundation reinforcing cage

Lap splice starter bars protruding from foundation block

Wall and loading beam reinforcing cage

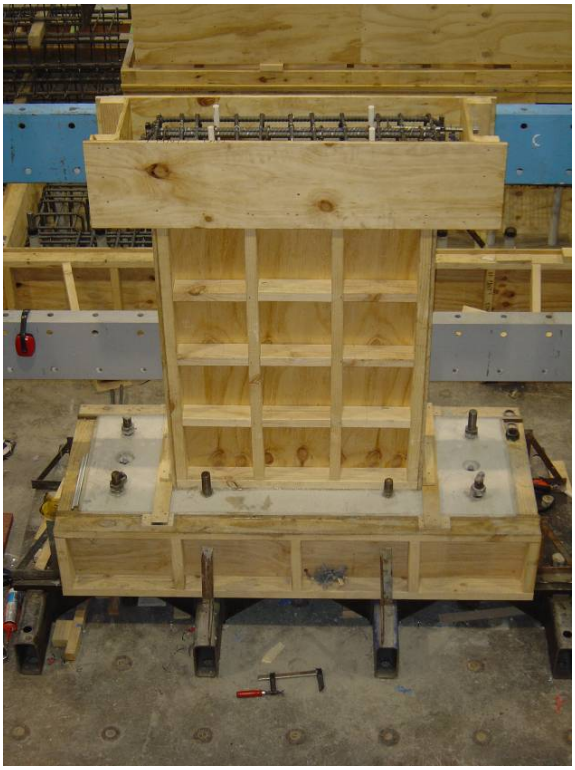

Wall and Loading beam formwork

Wall painted white and awaiting testing

B.2.2 W2 and W2R- Construction

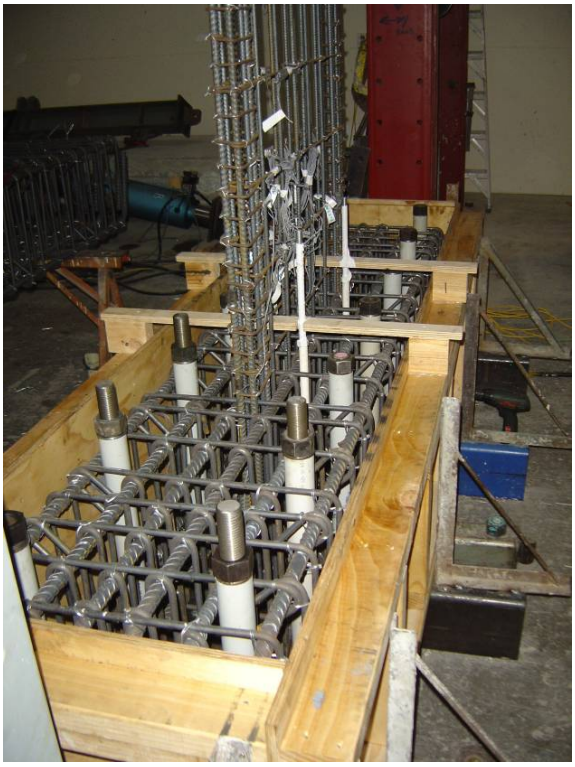

Foundation reinforcement with longitudinal reinforcement protruding

Wall and Loading beam reinforcement

Wall after form work has been stripped

Wall being lifted into place

B.3 Miscellaneous Photos

B.3.1 W1 - Miscellaneous

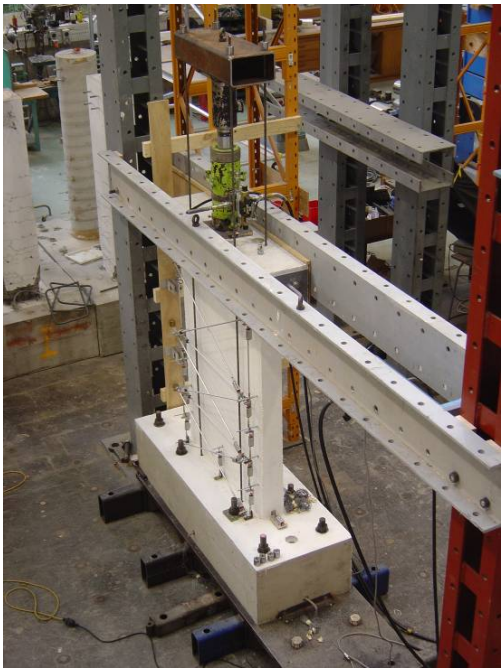

W1 test set-up

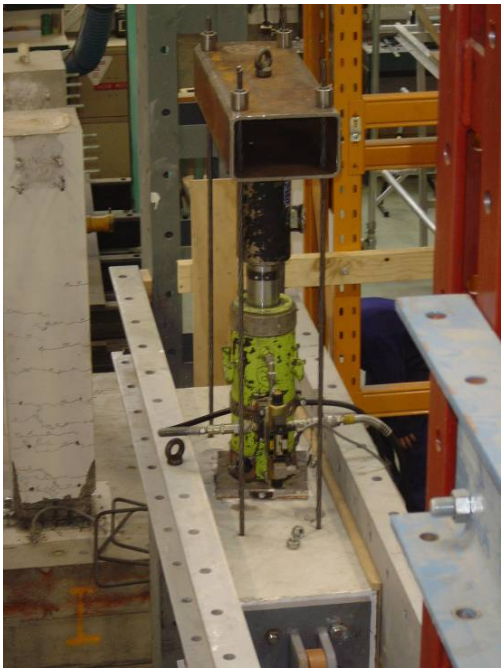

W1 post-tensioning system to apply a constant axial load

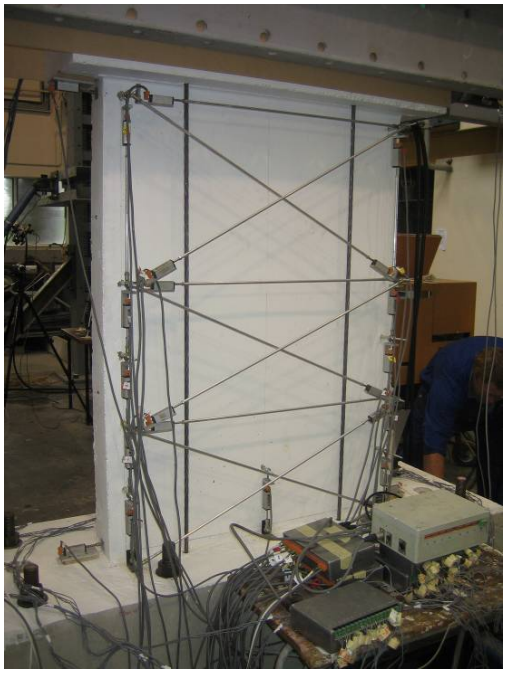

W1 Linear potentiometer arrangement

Buckling and rupture of longitudinal reinforcement at ends of the wall

B.3.2 W2 - Miscellaneous

W2 test set-up

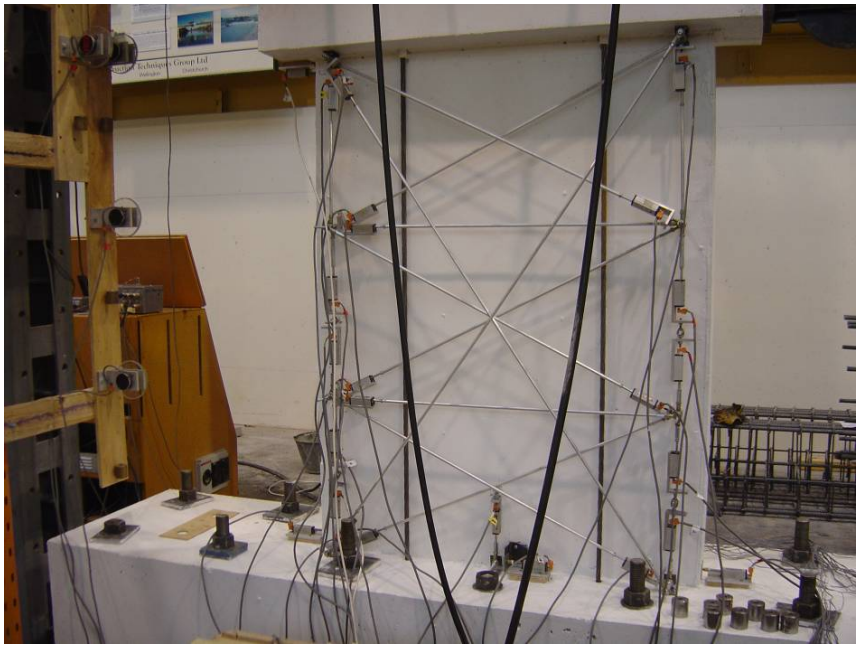

W2 potentiometer arrangement

B.3.3 W1R- Miscellaneous

Horizontal cutting of W1R in progress

Corner confinement armour and shear key

Dissipater mounts and dissipaters

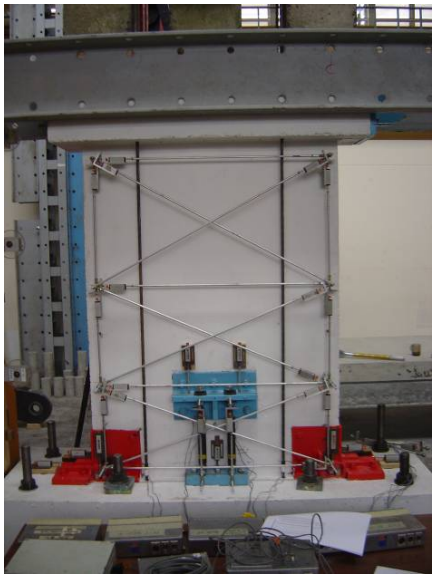

Linear potentiometer layout for W1R

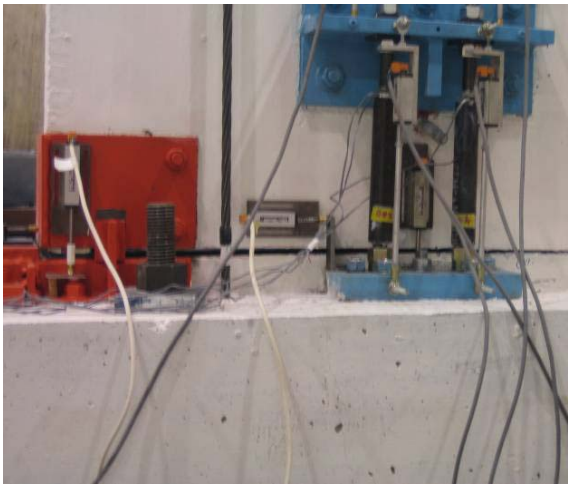

Gap opening due to lateral loading of W1R

Cyclic testing of an energy dissipater

B.3.4 W2R- Miscellaneous

Vertical cutting of W2R

W2R vertically segmented and with rounded corners awaiting FRP wrapping

FRP wrapping in progress

Finished FRP wrapping

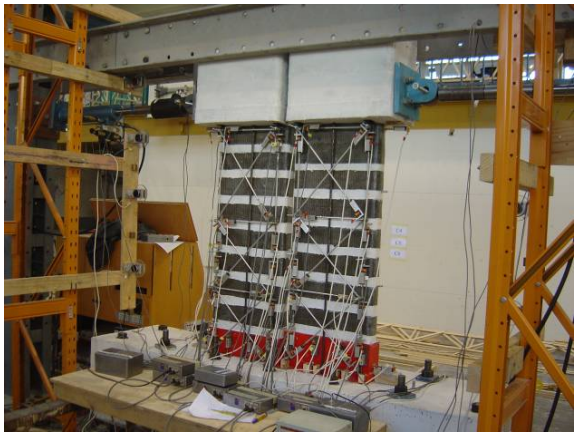

W2R potentiometer layout

W2R test set-up

W2Ra, minor crushing above confinement armour

W2Rb, substantial crushing above confinement armour and first FRP band

Appendix C Calculations and Construction Drawings

C.1 Prototype Development

Prototype Wall Development

- A prototype building was developed using to use in this research project
- The building exhibited typical characteristic of a pre-1970's New Zealand structural wall building (including reinforcement details and seismic provisions)

Prototype Building Layout

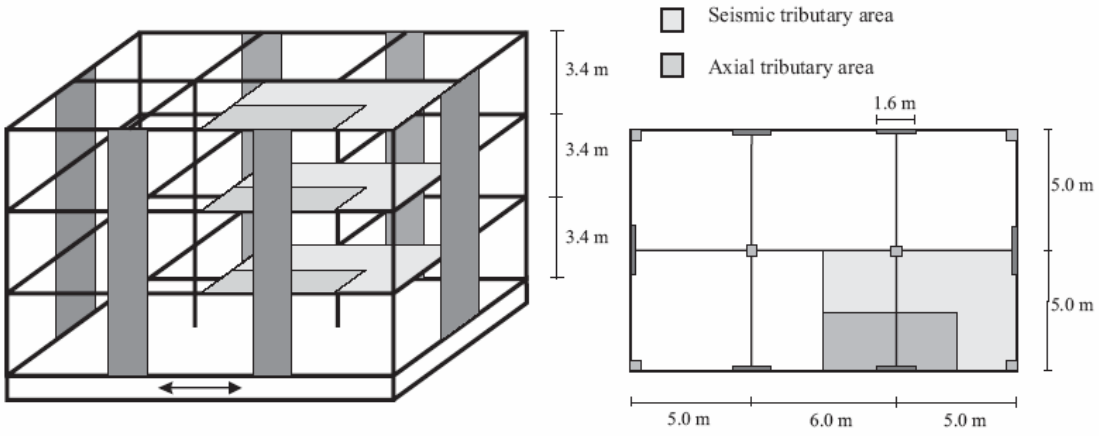

- 7.5kPa per floor (including 1kPa seismic live load)

Prototype Wall

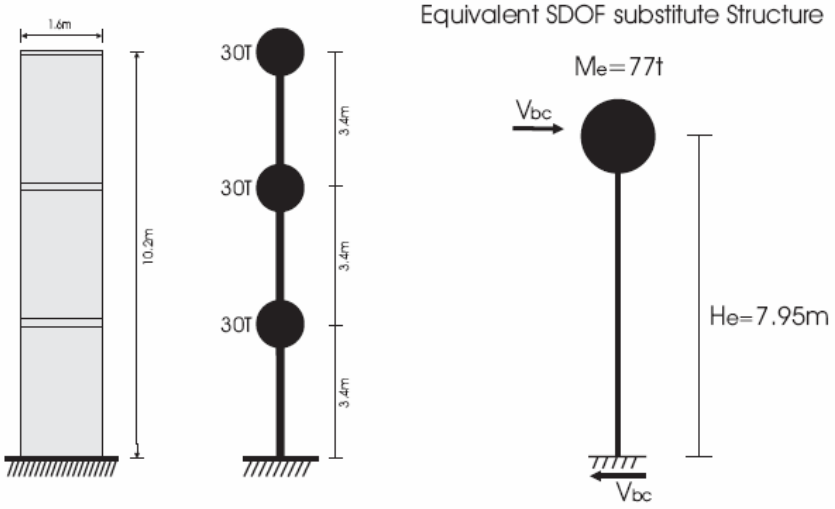

Seismic Loading - As per pre-1970's New Zealand Design Provisions

- Inverted triangular distribution with a seismic coefficient of 0.12 at the top

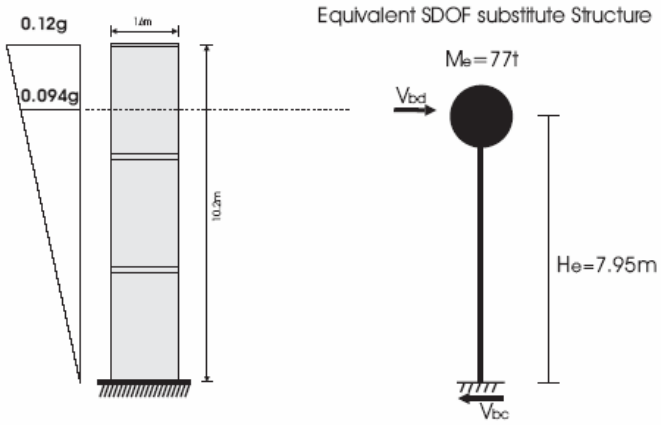

V_{bd} = 77t*0.094*9.81=71kN

Moment Demand

M*=71kN*7.95m=564kNm

Length of Prototype Wall

- Length of prototype wall determined by using typical pre-1970's New Zealand reinforcement details (which are typically independent of wall length) and varying the length until the moment demand was satisfied.
- Typical longitudinal reinforcement consists of 2-layers of ½" bars (12.7mm) at 1 foot (300mm) centres

Required wall length was determined to be 1.6m (see figure below)

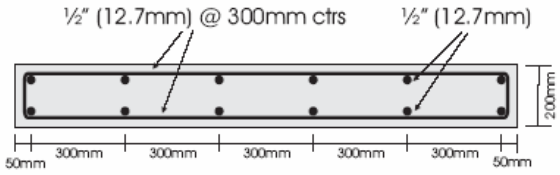

Mn=622kNm

C.2 Similitude Scaling

Similitude Scaling – Assuming Constant Density

Scale factor = λ

Parameter	Prototype	Experiment	Scale Factor
Density (kg/m^3)	ρ_p	$\rho_t=\rho_p$	1.0
Stress (kN/m^2)	σ_p	$\sigma_t=\sigma_p$	1.0
Length (m)	L_p	$L_t=\lambda L_p$	λ
Area (m^2)	A_p	$A_t=\lambda^2 A_p$	λ^2
Force (kN)	F_p	$F_t=\lambda^2 F_p$	λ^2
Moment (kN/m)	M_p	$M_t=\lambda^3 M_p$	λ^3
Mass (kg)	m_p	$M_t=\lambda^3 m_p$	λ^3
Acceleration (m/s^2)	a_p	$a_t=1/\lambda a_p$	$1/\lambda$
Time (s)	T_p	$T_t=\lambda T_p$	λ

C.3 Design Calculations W1

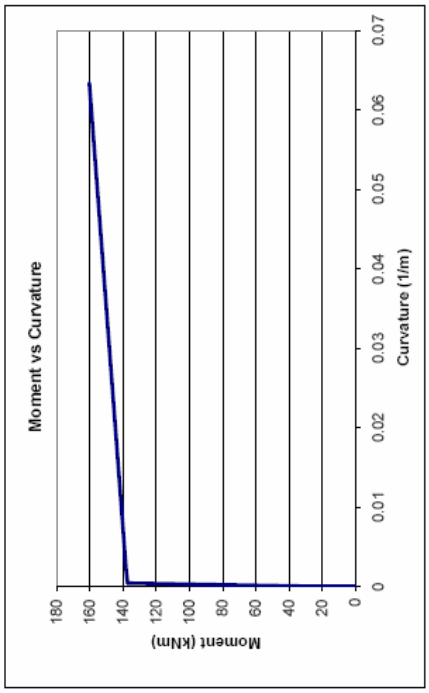

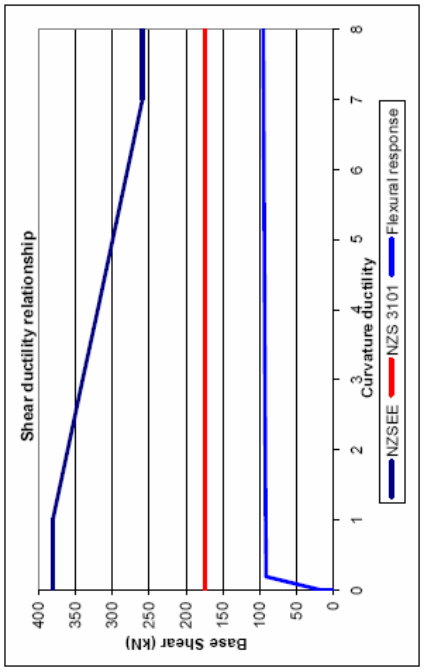

Capacity summary

Decompression

M_{nl}	26.0	kNm
ϕ_{nl}	0.00000007	1/m

Cracking point

M_{cr}	137.1	kNm
ϕ_{cr}	0.00037968	1/m

Yield

M_y	138.1	kNm
ϕ_y	0.00198667	1/m

Ultimate

M_u	160.3	kNm
ϕ_u	0.06340362	1/m

Shear capacity

NZS 3101	174	kN

Revised Priestley model (ACI 2000)

Ductility	Vn
0	381
1	381
2	361
3	340
4	320
5	300
6	279
7	259
8	259

Axial load

N	150	kN
ratio	0.030	

Reinforcement

Longitudinal	fy	300	MPa
	dia	8	mm
	spacing	190	mm
	ratio	0.00423	
Transverse	fy	300	MPa
	dia	6	mm
	spacing	190	mm
	ratio	0.00238	

Wall dimensions

Height	1.5	m
Length	1.04	m
Thickness	0.125	m
H/L aspect	1.44	

Convert moment curvature to force-ductility

Force	Curvature ductility
0	0.00000
17	0.00004
91	0.19112
92	1.00000
107	31.91448

C.4 Design Calculations W2

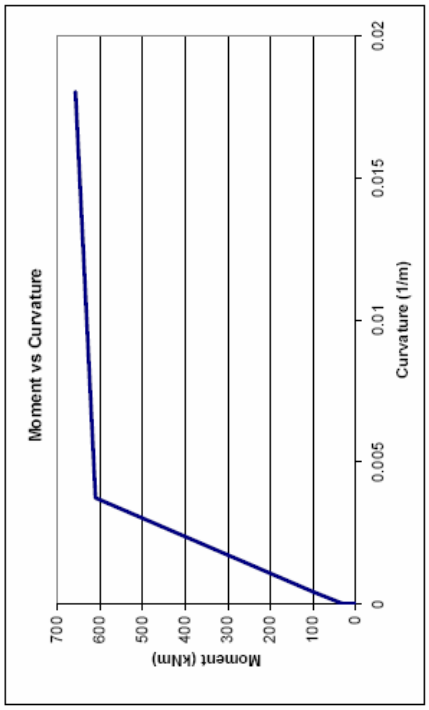

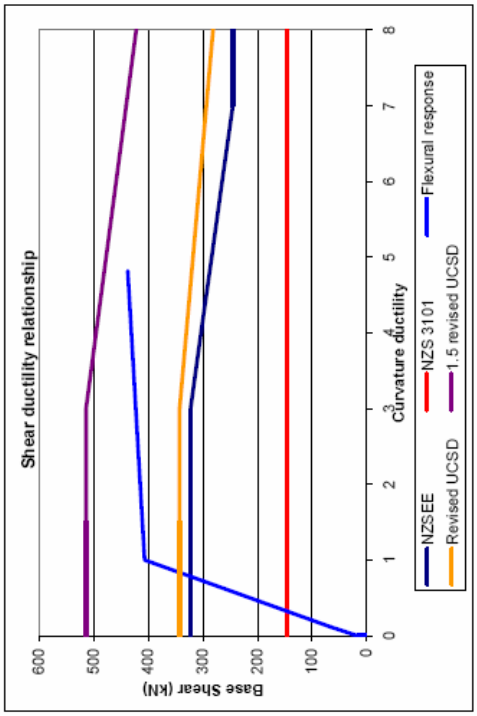

Capacity summary

Decompression

M_{nl}	26.0	kNm
ϕ_{nl}	0.00000011	1/m

Cracking point

M_{cr}	96.6	kNm
ϕ_{cr}	0.00042093	1/m

Yield

M_y	610.5	kNm
ϕ_y	0.00374082	1/m

Ultimate

M_u	657.1	kNm
ϕ_u	0.01802458	1/m

Shear capacity

NZS 3101	146	kN

NZSEE Shear ductility model

Ductility	Vn
0	323
1	323
2	323
3	323
4	304
5	284
6	265
7	245
8	245

Revised UCSD

Alpha	1.5
Beta	1

Axial load

N	150	kN
ratio	0.060	

Reinforcement

Longitudinal			
	fy	540	MPa
	dia	12	mm
	spacing	35	mm
	ratio	0.02879	

Transverse			
	fy	337	MPa
	dia	6	mm
	spacing	200	mm
	ratio	0.00293	

Wall dimensions

Height	1.5	m
Length	1.04	m
Thickness	0.1	m
H/L aspect	1.44	

Convert moment curvature to force-ductility

Force	Curvature ductility
0	0.00000
17	0.00003
64	0.11252
407	1.00000
438	4.81835

C.5 Stress in un-bonded post-tensioning tendons at nominal flexural capacity

Empirical equation for calculating the stress in un-bonded post tensioning tendons at the nominal flexural strength (as per Park, et al., 2002) .

$$f_{ps} = f_{se} + 70 + \frac{f_c^{'}}{100\rho_p}$$

Park, R., Restrepo, J. and Cooke, N., [2002], "Prestressed Concrete – Notes for Statically Determinate Structural Members". Department of Civil Engineering, University of Canterbury, Christchurch.

C.6 Calculation of Equivalent Viscous Damping

Hysteretic damping was represented by equivalent viscous damping. The definition of equivalent viscous damping is explained in **Figure 0-1**. The percentage of equivalent viscous damping was calculated on the second cycle to each drift level to ensure a stabilized force versus displacement response (Priestley, 2003). An additional 5% was added to the hysteretic damping to account for elastic damping.

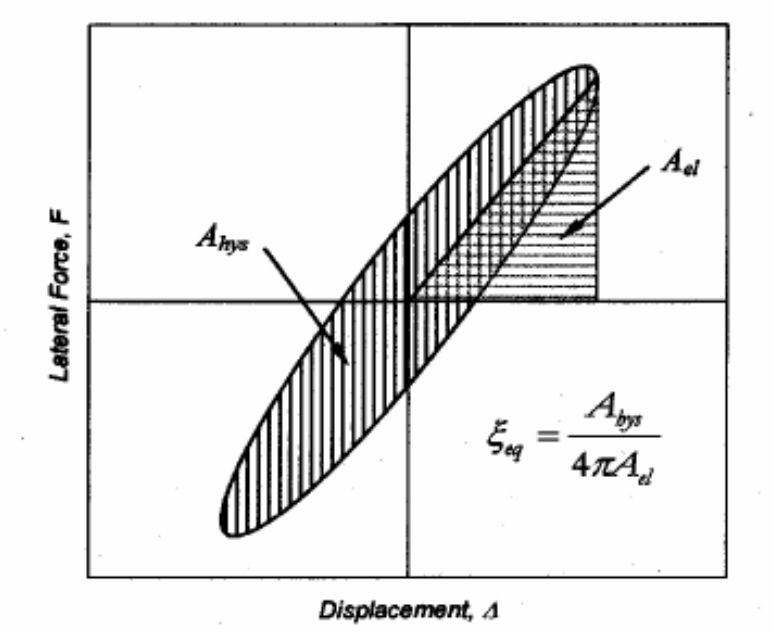

Figure 0-1: Definition of equivalent viscous damping (Miranda et al., 2005).

Estimate of the equivalent viscous damping provided be a hybrid wall

The level of equivalent viscous damping provided by a hybrid wall depends on the ratio between the post-tensioning + axial moment contribution and the dissipater moment (see equation 1).

$$\lambda = \frac{M_{PT} + M_{Axial}}{M_{Dissipation}} \qquad \text{(equation 1)}$$

The equivalent viscous damping can be estimated by combining two equations (Priestley, 20030, the first is for a monolithic reinforced concrete wall and the second is for an un-bonded post-tensioned wall. Equation 2 shows the combination of the two equations.

$$\xi_d = \alpha\left(5 + 95\left(\frac{1-\mu^{-0.5}}{\pi}\right)\%\right) + \beta\left(5 + 25\left(\frac{1-\mu^{-0.5}}{\pi}\right)\%\right) \qquad \text{(equation 2)}$$

An α and β factor are required to determine the relative proportions of the monolithic wall equation and the post-tensioned wall equation to use. Values for a typical range are listed in table 1.

Table 1: typical values for α and β

λ	**α**	**β**
1.0	0.5	0.5
1.5	0.4	0.6
2.0	0.33	0.67
3.0	0.25	0.75

Example equivalent viscous damping versus ductility curves are shown in figure 1.

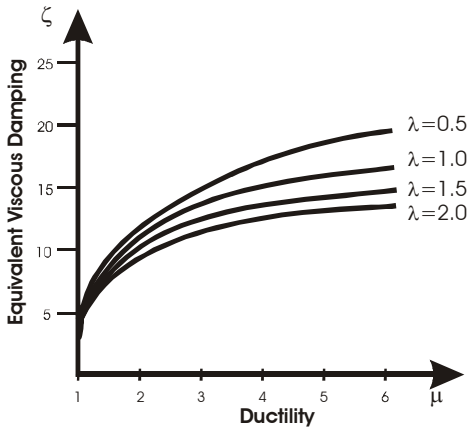

Figure 1: estimate of equivalent viscous damping for a hybrid wall

References:

Miranda, P.A., Calvi, G.M., Pinho, R. and Priestley, M.J.N. [2005]. "Displacement-Based Assessment of RC Columns with Limited Shear Resistance". Report No. Rose 2005/04, European School for Advanced Studies in Reduction of Seismic Risk, Pavia.

Priestley, M.J.N., [2003], Myths and Fallacies in Earthquake Engineering, Revisited, IUSS Press, Pavia, Italy.

C.7 FRP Design for W2R

The retrofit solution for W2R involved vertically segmenting the wall, which severed all the transverse reinforcement. Bands of FRP, acting as external stirrups were used to reinstate the shear capacity. The as-built wall and the wall after being vertically segmented are shown in figure 1.

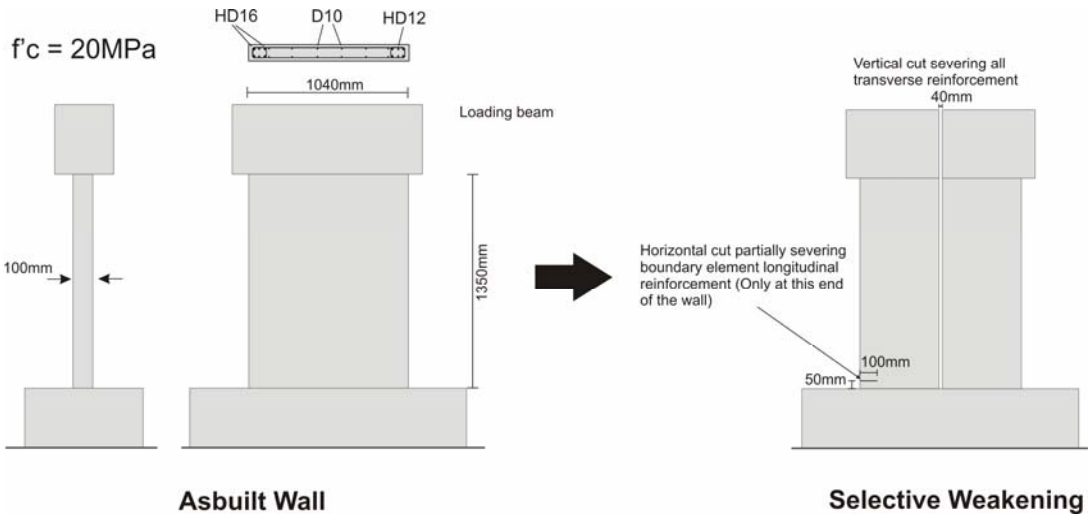

Figure 1: Wall dimensions and vertical segmenting

Section Capacity

The maximum segment capacity was calculated and shown in figure 2.

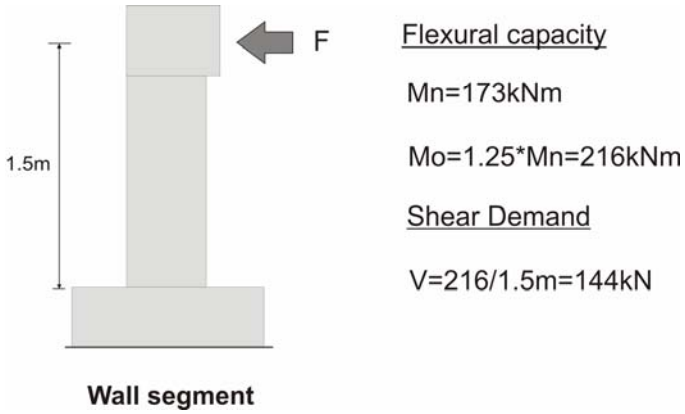

Figure 2: Maximum segment capacity

FRP Design

- FRP is to be used to reinstate the shear capacity as all the transverse reinforcement has been severed
- Assume that the FRP acts as external stirrups and provides the full shear capacity
- Designed following the FRP shear design recommendations found in fib bulletin 14 (Externally bonded FRP reinforcement for RC structures)

FRP Shear Contribution

An equation that can be used to calculate the shear strength contribution provided by FRP bands is shown in equation 1 (fib, 2001).

$$V_{fd} = 0.9\varepsilon_{fd,e} E_{fu} \rho_f b_w d(\cot\theta + \cot\alpha)\sin\alpha \qquad \text{(equation 1)}$$

Where: $\varepsilon_{fd,e}$ = design value of effective FRP strain

b_w = minimum thickness of cross section

d = effective depth of cross section

ρ_f = FRP reinforcement ratio

E_{fu} = elastic modulus of FRP

FRP Details

- Use 100mm wide strips at 50mm spacing up the height of the wall
- Use Sikawrap 100G (glass fibre)

FRP Properties – Sikawrap 100G

Fibre strength = 2300MPa

Fibre stiffness = 76GPa

Fabric thickness = 0.358mm

FRP Design using Sikawrap 100G

Calculate shear capacity using equation 1.

$\varepsilon_{fd,e}$ = 0.006 (proposed maximum strain (fib, 2001)

E_{fu} = 76GPa

$\rho_f = (2t_f/b_w)/(b_f/s_f)$

Where: t_f = fabric thickness = 0.358mm

b_w = minimum cross section thickness = 100mm

b_f = FRP strip width = 100mm

s_f = strip spacing = 50mm

d = 500mm

$\theta = 45^o$

$\alpha = 90^{o}$

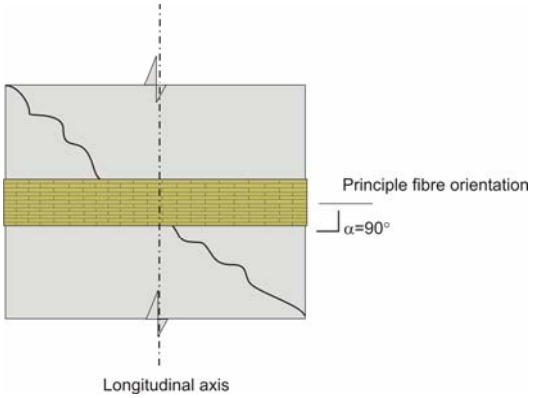

Figure 3: Principle fibre orientation

$V_{fd} = 293kN$ which is greater than the shear demand of 144kN

- therefore 100mm strips of Sikawrap 100G at 50mm spacing will be sufficient
- The FRP solution is shown in figure 4

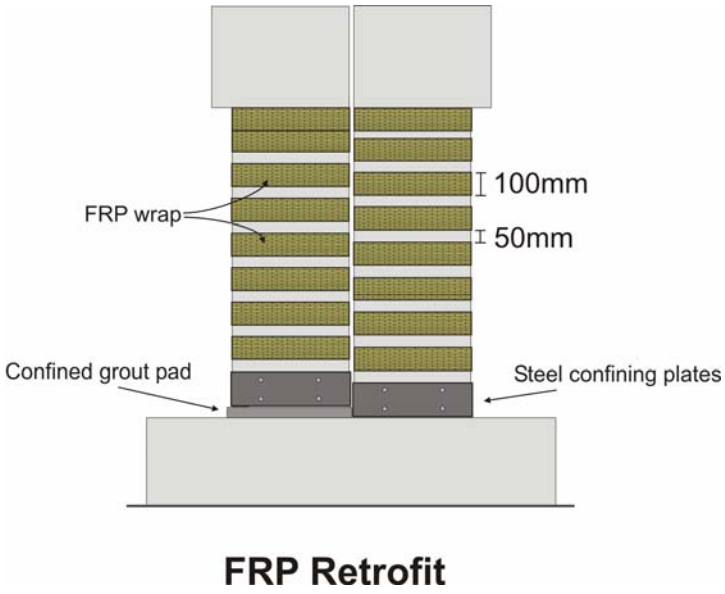

Figure 4: FRP used to provide shear capacity

C.8 Calculating Plastic Hinge Length from Experimental Results

Determining plastic hinge length from experimental data

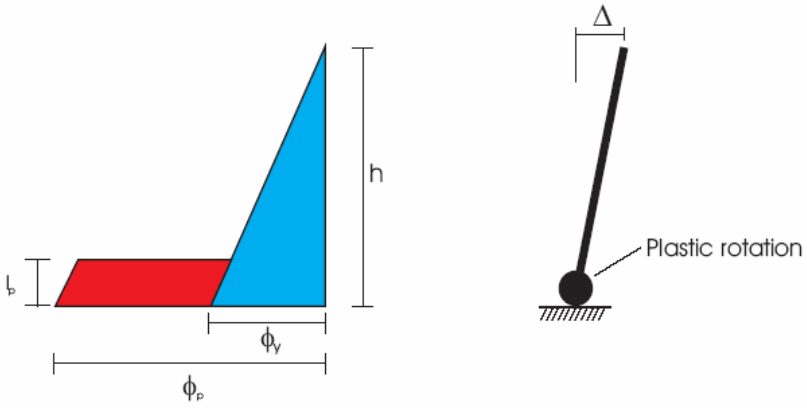

Displacement at top of cantilever

$$\Delta = \phi_y \times \frac{h^2}{3} + (\phi_p - \phi_y) \times l_p \times \left(h - \frac{l_p}{2}\right) \qquad \text{(Equation 1)}$$

Back-calculating plastic hinge length from experimental results

- equation 1 can be rearranged into a quadratic that can be solved to find the plastic hinge length

$$l_p^2 - 3 \times l_p + \frac{\left(\Delta - \phi_y \times \frac{h^2}{3}\right)}{(\phi_p - \phi_y)} = 0 \qquad \text{(Equation 2)}$$

- yield curvature determined from potentiometer data, by determining yield point from strain gauges on the longitudinal reinforcement

- plastic curvature determined from potentiometer data at the displacement at which the equivalent plastic hinge length is to be determined

C.9 Construction Drawings

C.9.1 W1

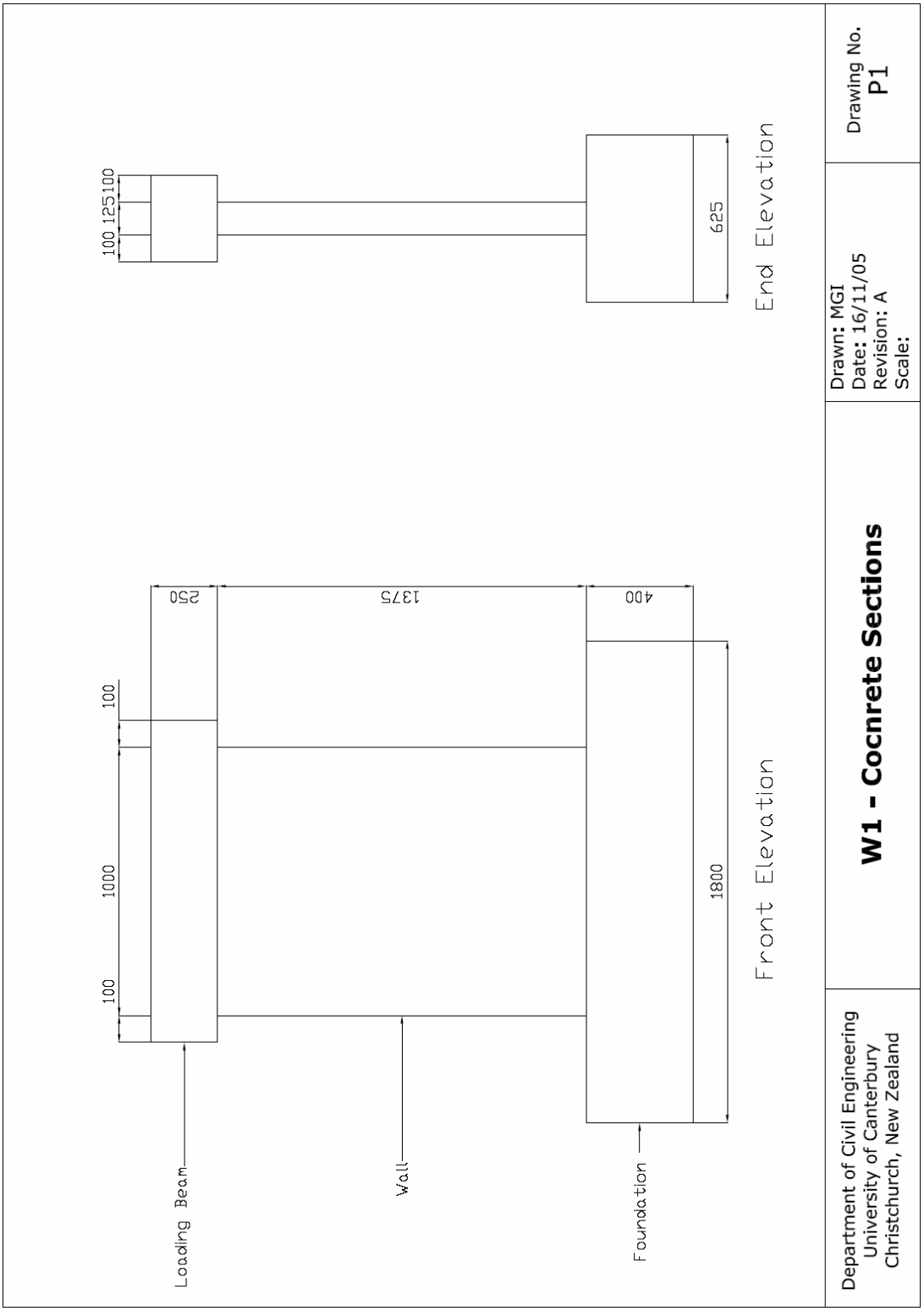

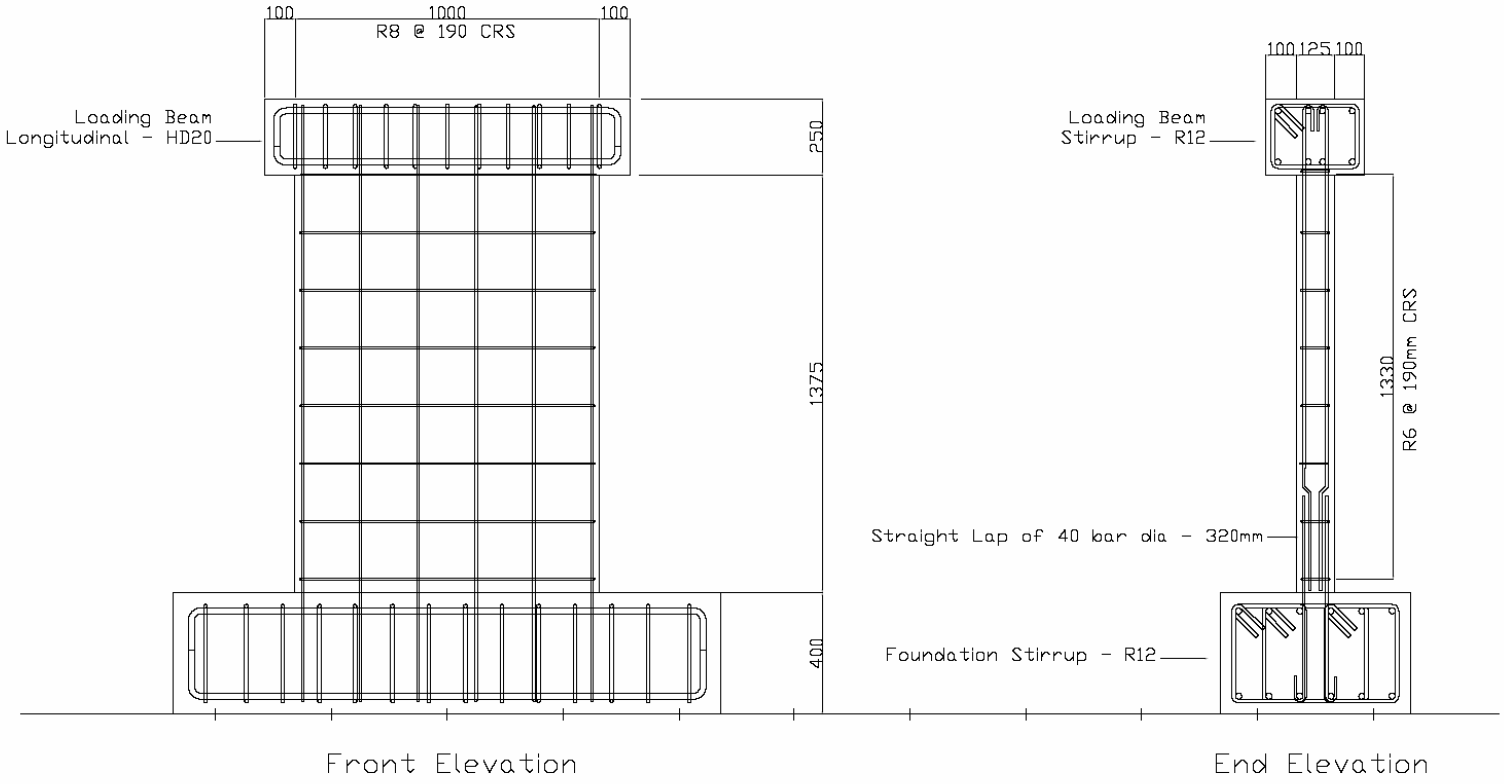

Department of Civil Engineering University of Canterbury Christchurch, New Zealand	**W1 Reinforcement Details**	Drawn: MGI Date: 16/11/05 Revision: A Scale:	Drawing No. P2

Section A-A Loading beam

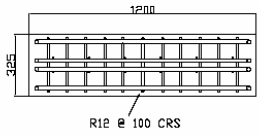

Section B-B Wall section

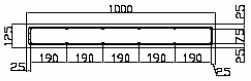

Section C-C Foundation Beam

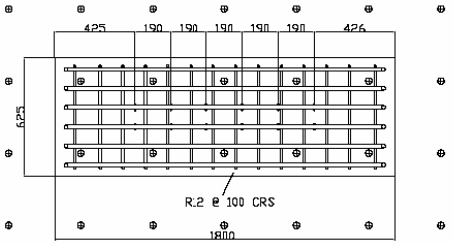

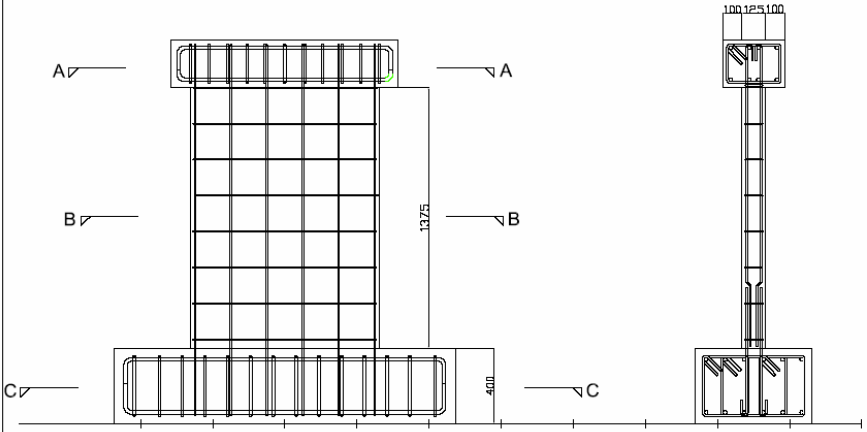

Wall Reinforcement

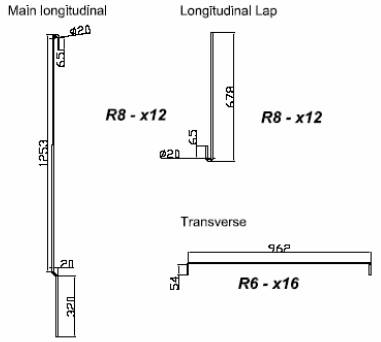

Loading beam reinforcement

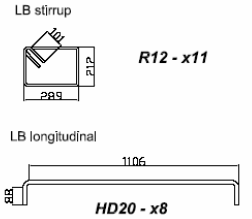

Foundation Reinforcement

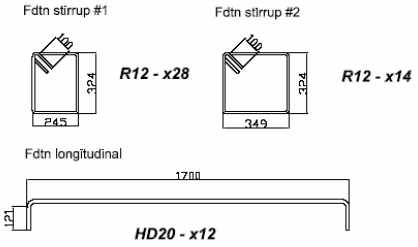

Department of Civil Engineering University of Canterbury Christchurch, New Zealand	**W1 Reinforcement Details**	Drawn: MGI Date: 16/11/05 Revision: A Scale:	Drawing No. P3

C.9.2 W2

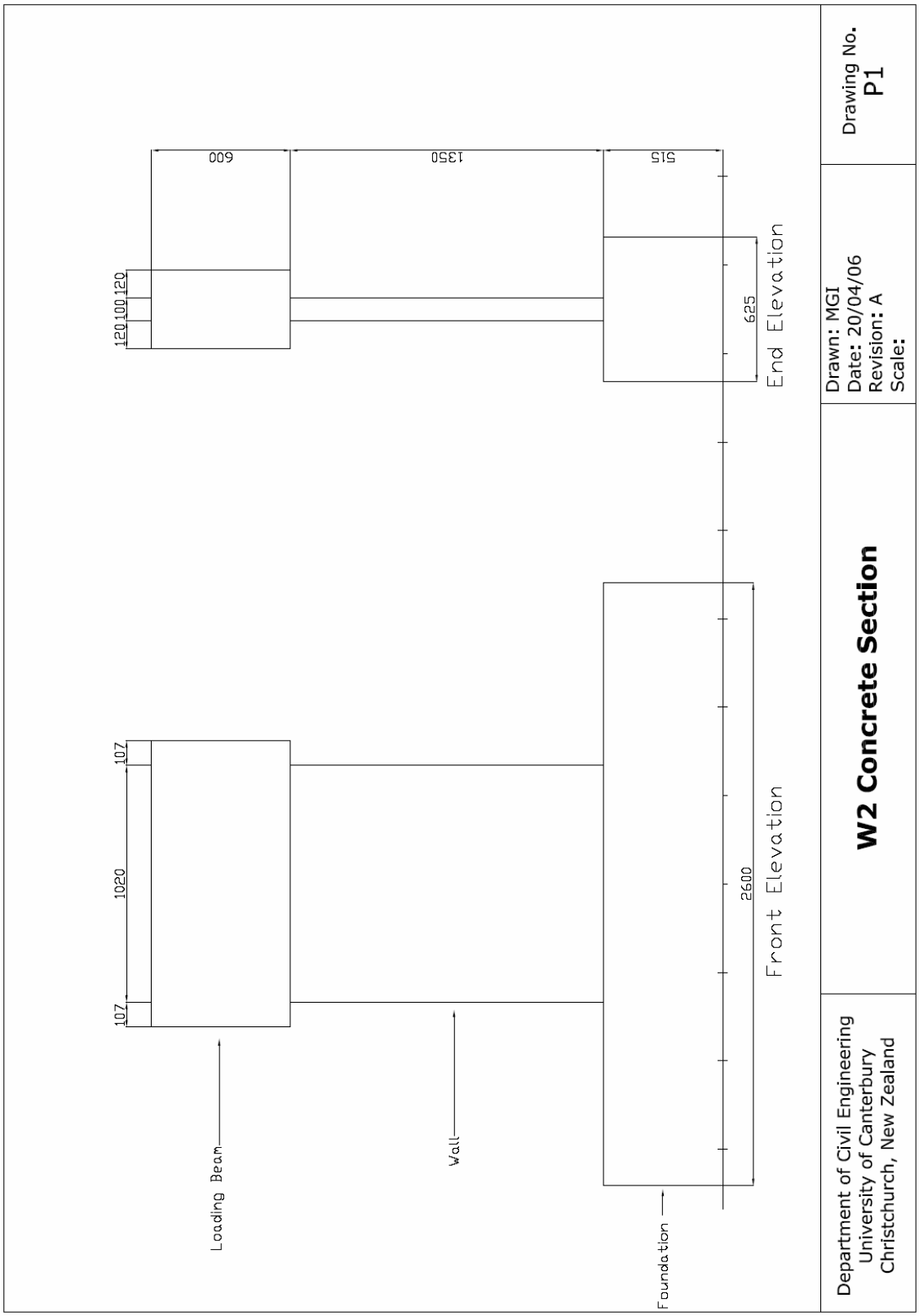
600
1350
515
120
100
120
625
End Elevation
107
1020
107
2600
Front Elevation
Loading Beam
Wall
Foundation
W2 Concrete Section
Department of Civil Engineering
University of Canterbury
Christchurch, New Zealand
Drawn: MGI
Date: 20/04/06
Revision: A
Scale:
Drawing No.
P1

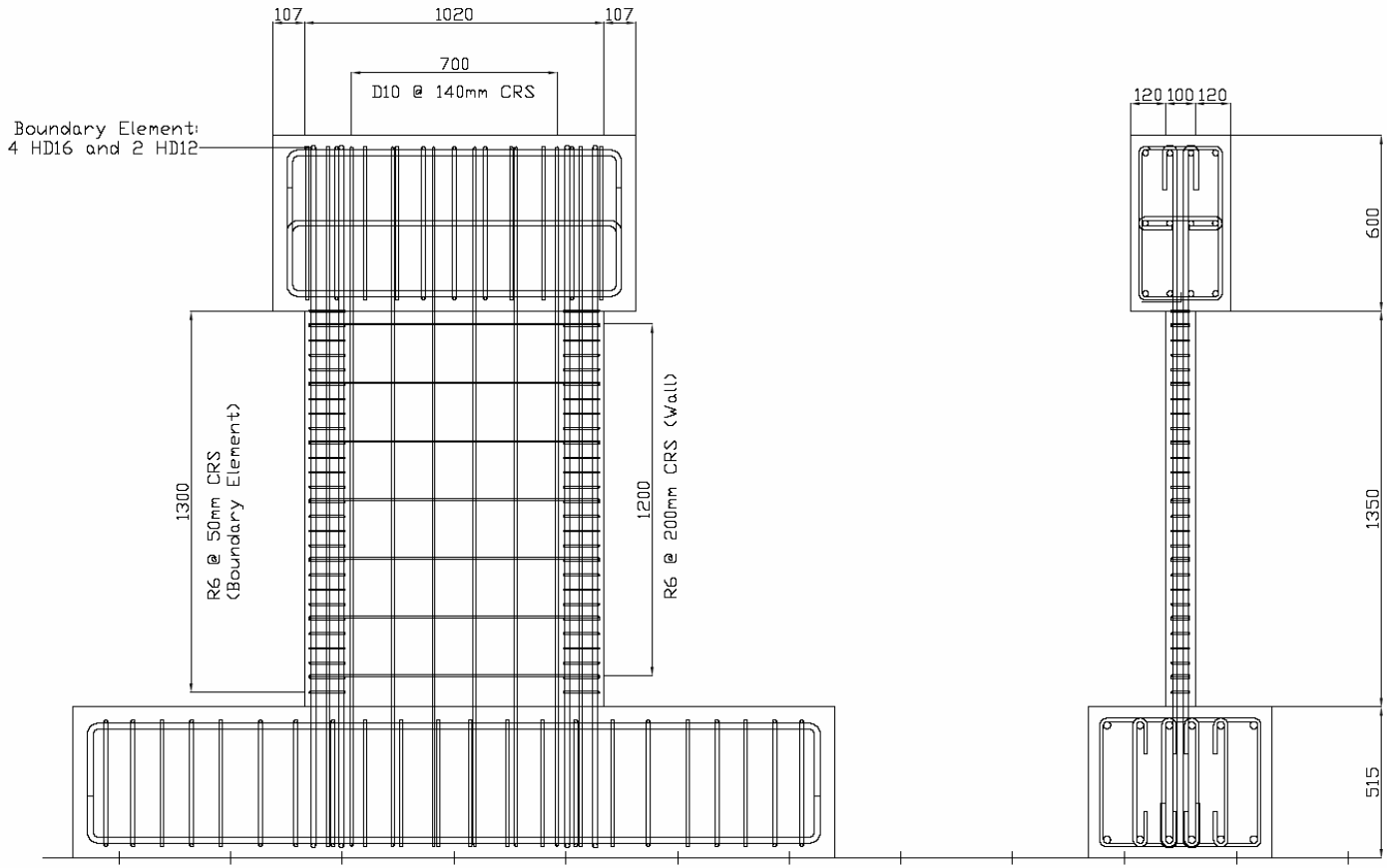

Department of Civil Engineering University of Canterbury Christchurch, New Zealand	**W2 Reinforcement Details**	Drawn: MGI Date: 20/04/06 Revision: A Scale:	Drawing No. P2

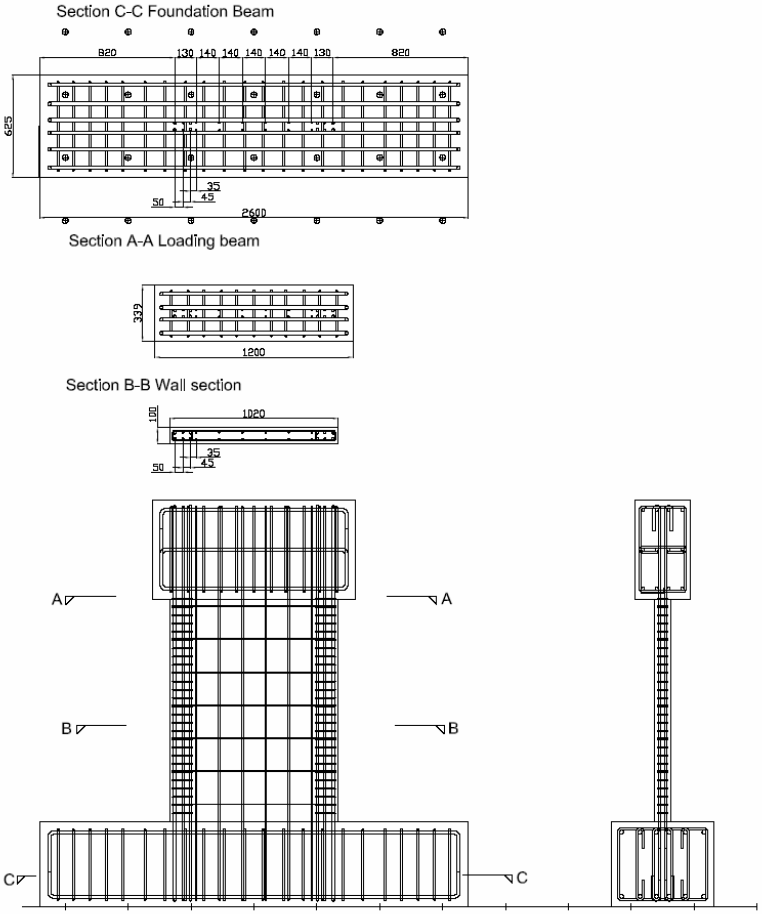

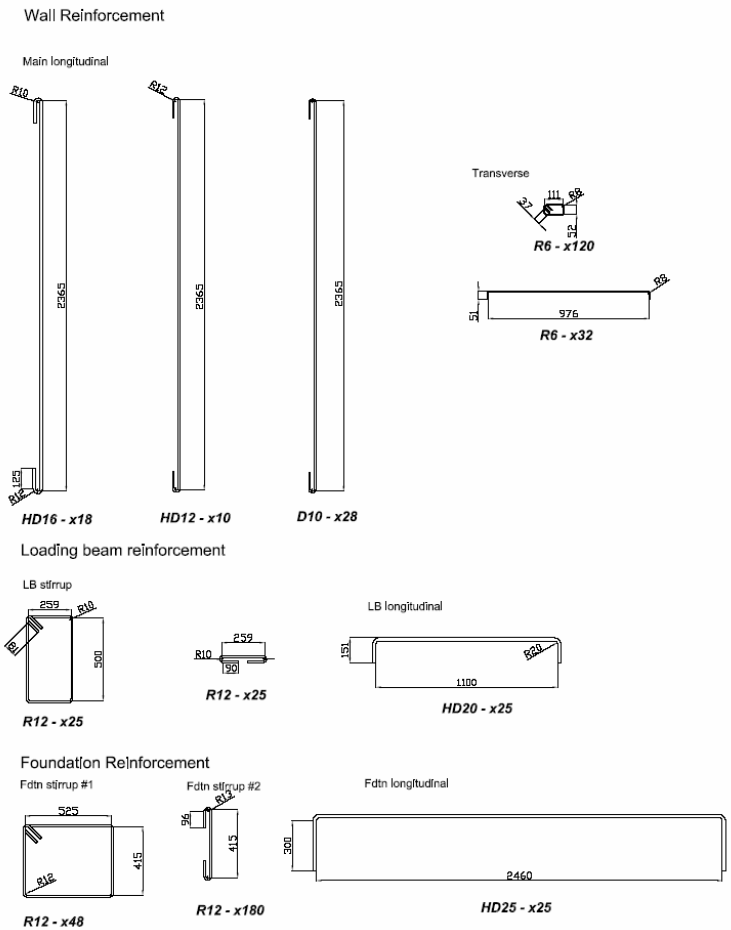

Department of Civil Engineering University of Canterbury Christchurch, New Zealand	**W2 Rebar Details**	Drawn: MGI Date: 20/04/06 Revision: A Scale:	Drawing No. P3

C.9.3 W1R

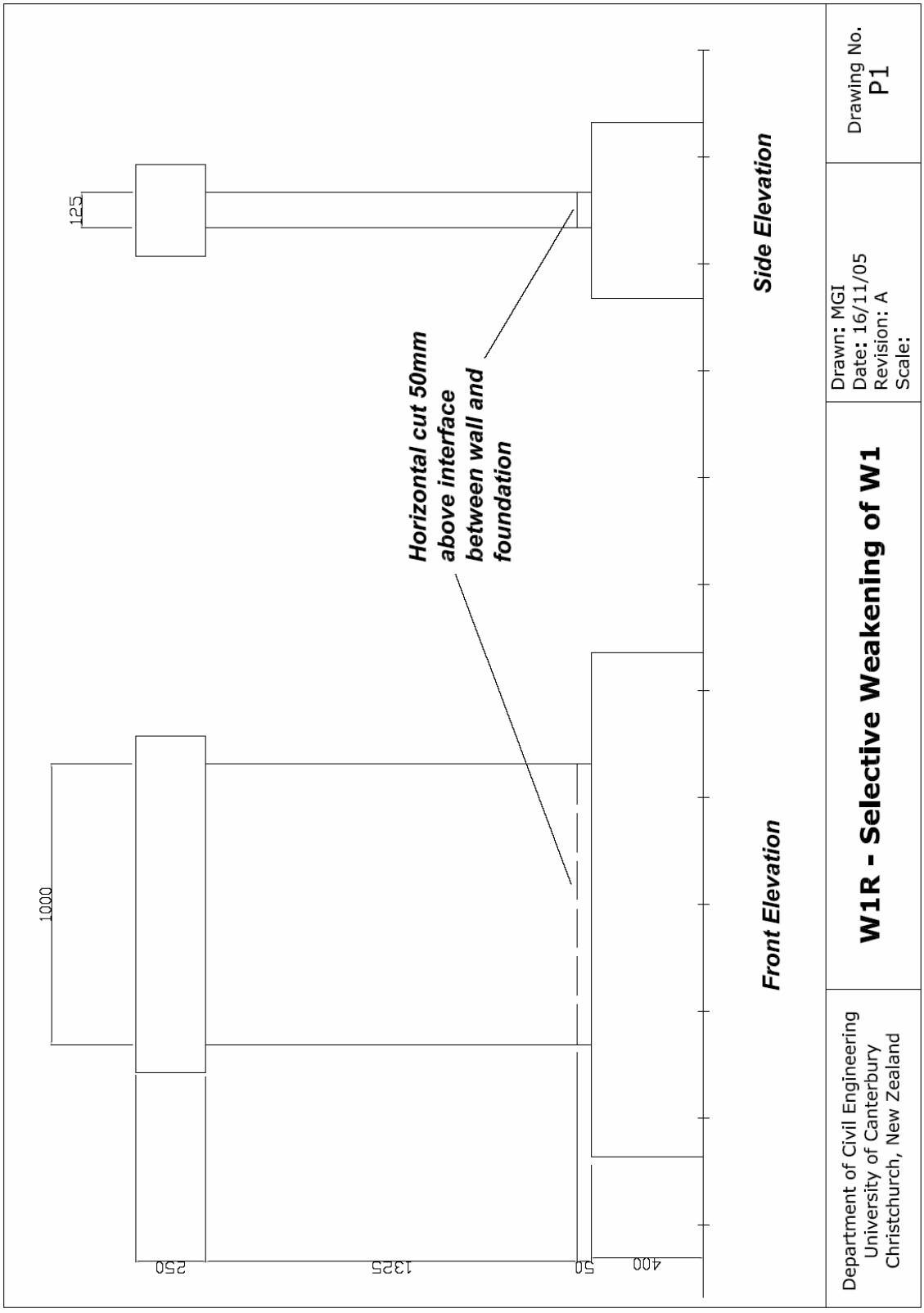
Horizontal cut 50mm above interface between wall and foundation
Side Elevation
Front Elevation
125
1000
250
1325
50
400
W1R - Selective Weakening of W1
Department of Civil Engineering
University of Canterbury
Christchurch, New Zealand
Drawn: MGI
Date: 16/11/05
Revision: A
Scale:
Drawing No.
P1

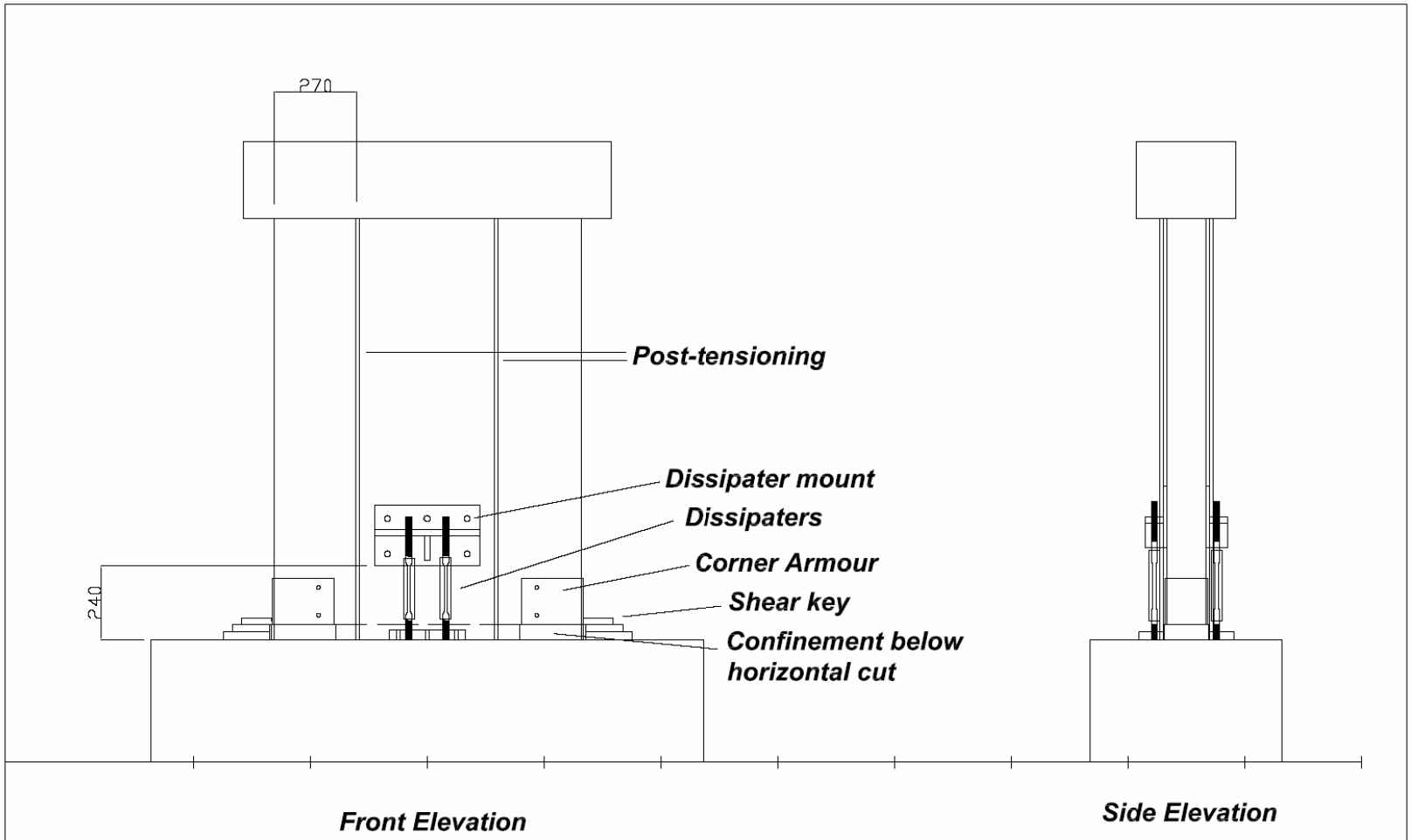

Department of Civil Engineering University of Canterbury Christchurch, New Zealand	**W1R-Retrofit Configuration**	Drawn: MGI Date: 16/11/05 Revision: A Scale:	Drawing No. P2

Foundation Dissipater Mounts

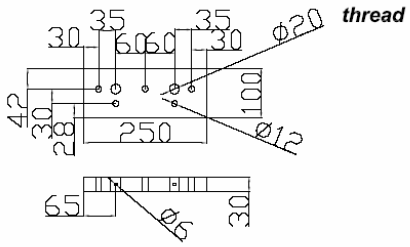

Shear Key

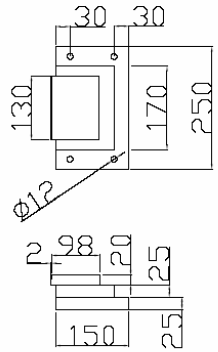

Corner Armour

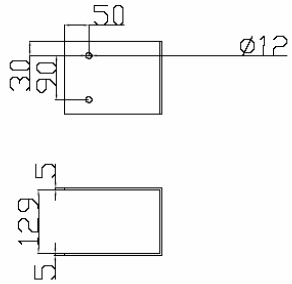

Wall Dissipater Mounts

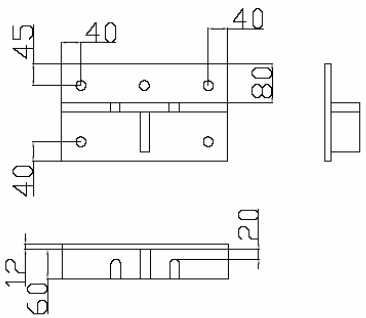

Dissipaters

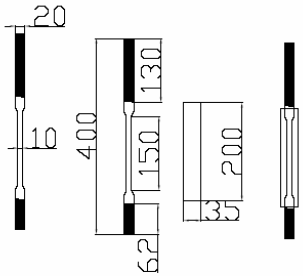

Department of Civil Engineering University of Canterbury Christchurch, New Zealand	**W1R-Retrofit Components**	Drawn: MGI Date: 16/11/05 Revision: A Scale:	Drawing No. P3

C.9.4 W2R

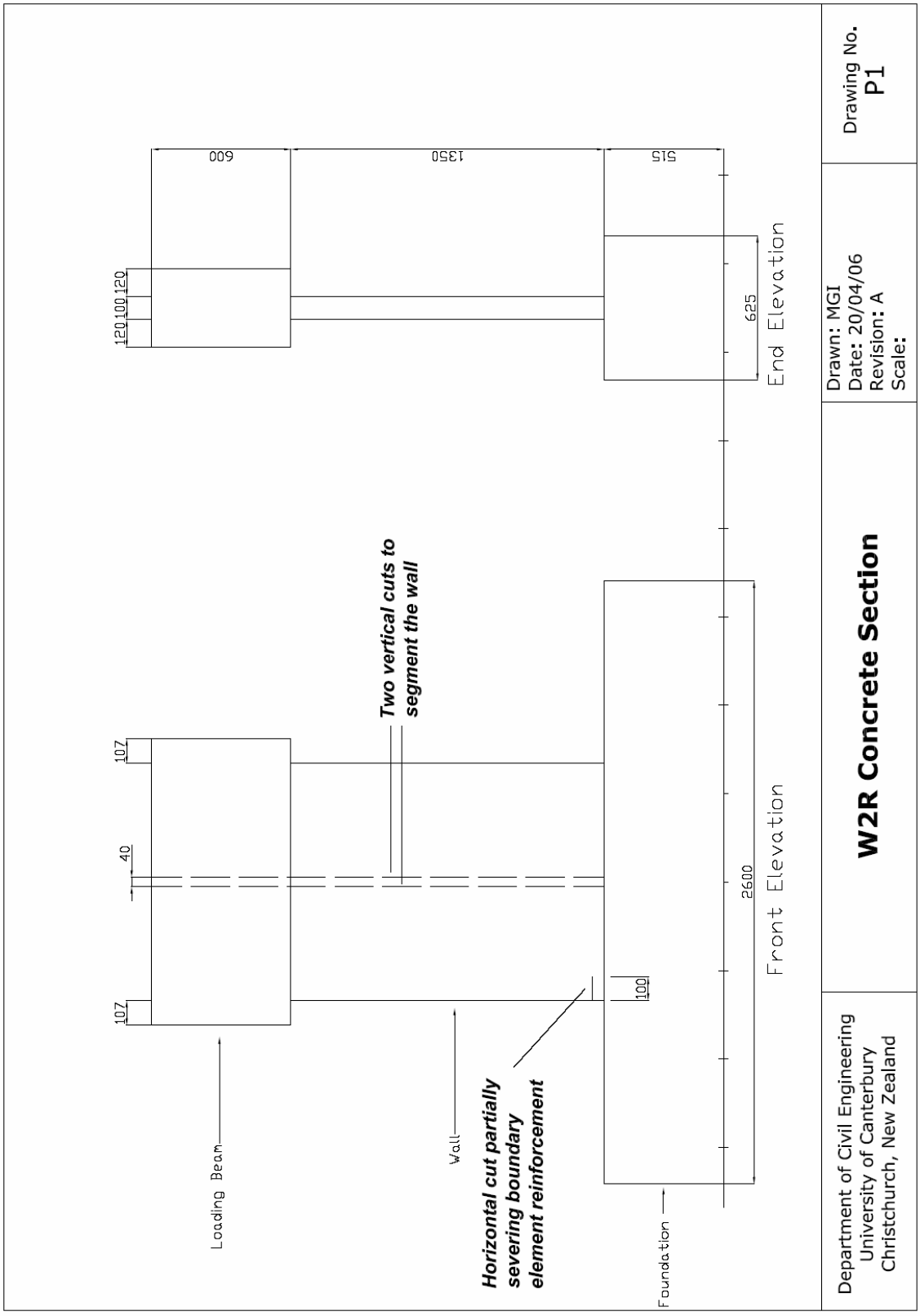
W2R Concrete Section
Department of Civil Engineering
University of Canterbury
Christchurch, New Zealand
Drawn: MGI
Date: 20/04/06
Revision: A
Scale:
Drawing No.
P1
End Elevation
600
1350
515
120
100
120
625
Front Elevation
107
40
107
2600
100
Two vertical cuts to segment the wall
Horizontal cut partially severing boundary element reinforcement
Loading Beam
Wall
Foundation

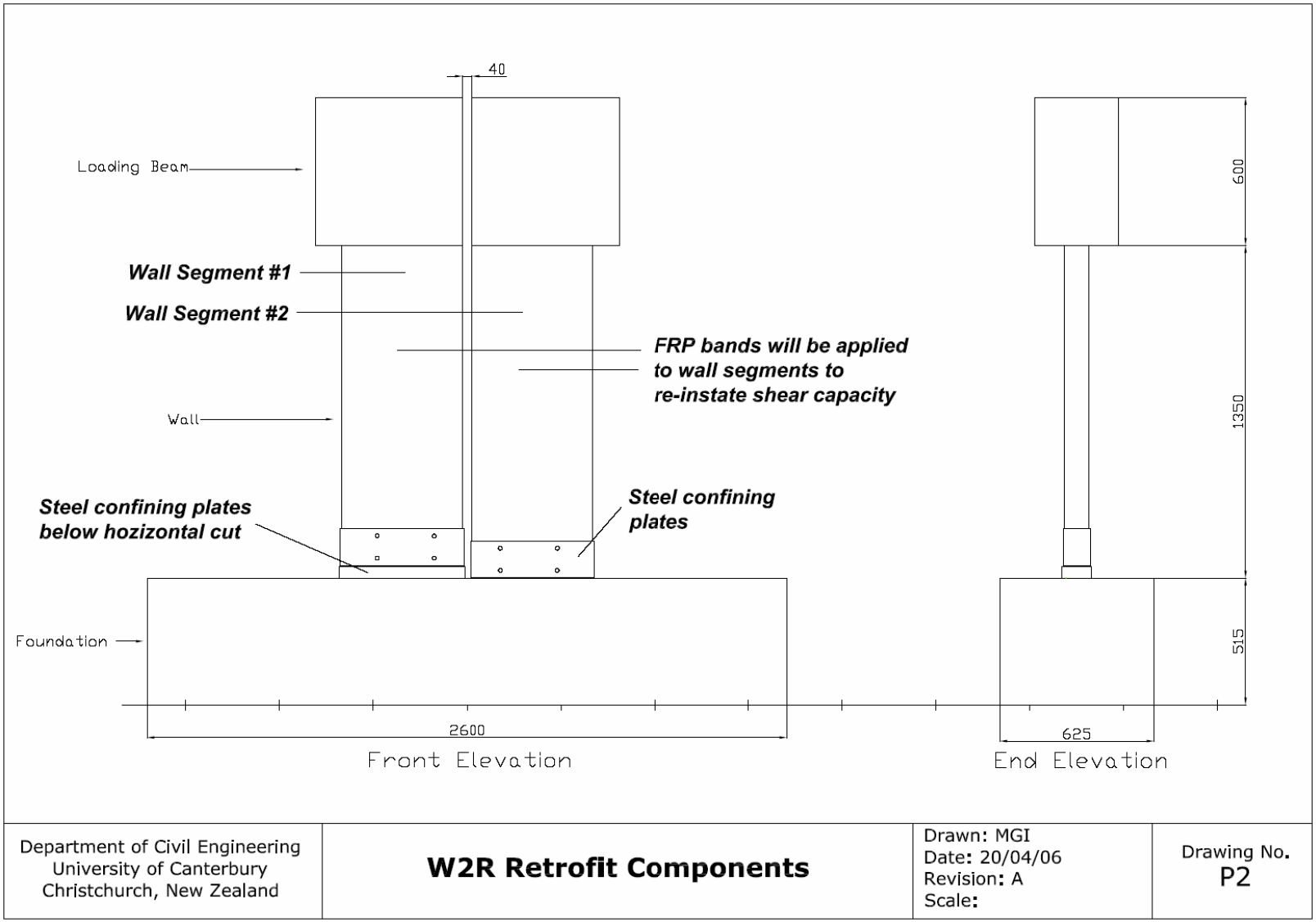

Department of Civil Engineering University of Canterbury Christchurch, New Zealand	**W2R Retrofit Components**	Drawn: MGI Date: 20/04/06 Revision: A Scale:	Drawing No. P2

Appendix D Numerical Analysis Information

D.1 Scaled Earthquake Record Spectra

Scaled earthquake spectra compared to the target spectrum (PGA of 0.14g)

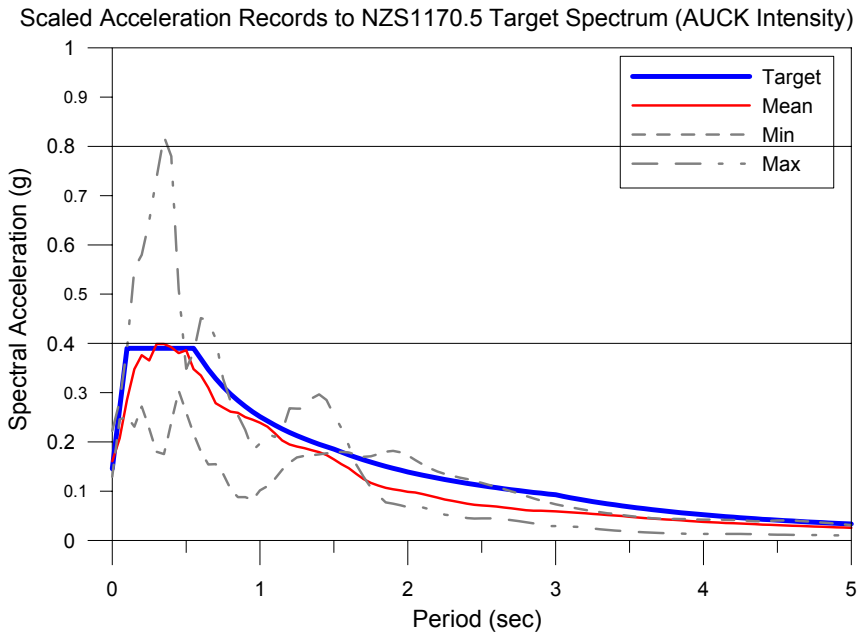

Scaled earthquake spectra compared to the target spectrum (PGA of 0.21g)

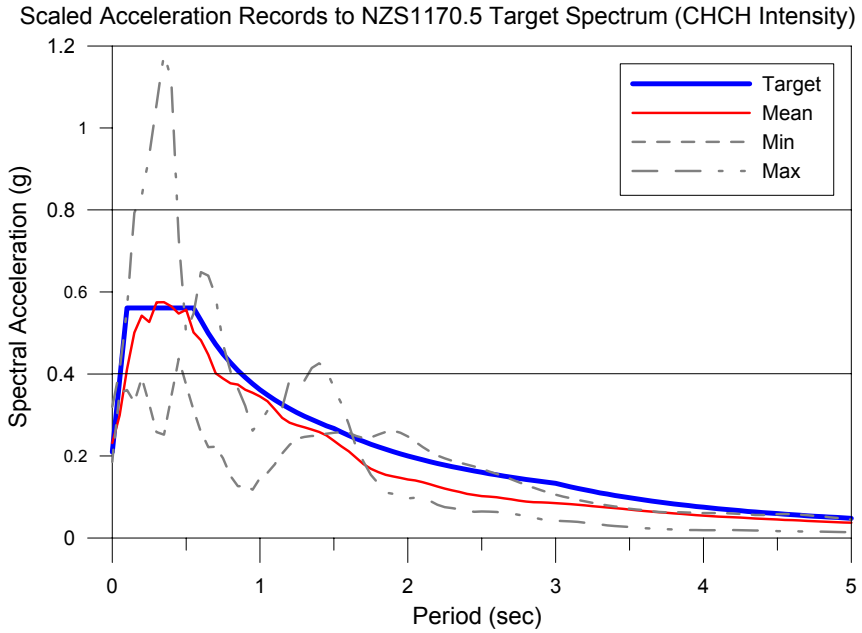

Scaled earthquake spectra compared to the target spectrum (PGA of 0.45g)

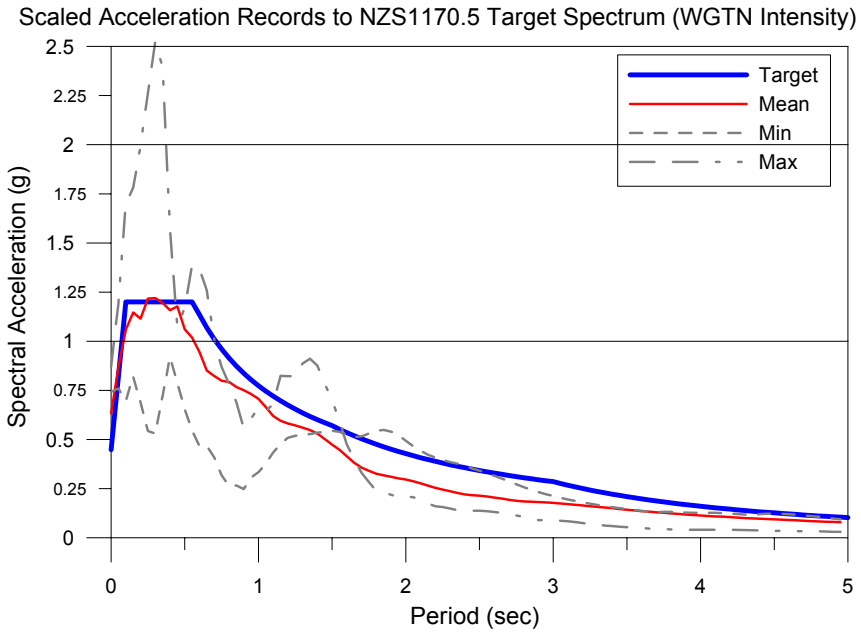

D.2 Example Ruaumoko Input Files

D.2.1 W1 Takeda Calibration – No Strength Degradation

```
                  Takeda-W1 Calibration-No Strength Degradation
W1 Model - Push vs Pull Analysis
* Monolithic pre-1970's Structural wall
* Lumped Platicity - modified Takeda Hystersis
* No Strength Degradation


8 0 1 0 0 -1 1 0 0
3 2 2 3 1 3 9.81 0 0 0.0050 500 1.0
20 20 20 1 3 10 0.7 0.1
5 5 0.00

NODES 1
  1 0.0  0.0    1 1 1  0 0 0 0
  2 0.0  0.0    0 0 0  0 0 0 0
  3 0.0  1.5    0 0 0 -1 0 0 0       !node at which displacement is applied


Elements 1
! N  Sect  I  J  i  j  output
  1  1     1  2  1 2
  2  2     2  3  2 3


PROPS 1
 1 SPRING                   !Rotational spring representing inelatic action
   1 4 0 0 9999999 9999999 112000 0 0 0
   9999 -9999 9999 -9999 167 -167
   0.05 0.2 1.0 1                          !Hystersis parameters


2 FRAME                             ! Elastic frame element representing wall
  1 0 0 0 0 0
  2.5E7 1.04E7 0.1275 0.0 0.0111 0 0 0


WEIGHTS 0
! n  wx
  1 0
  2 0
  3 0


LOADS
! n  Fx   Fy    Mz
  2  0    0     0
  3  0    0     0


EQUAKE load-regime-fixed.txt      ! Experimental displacement loading regime
3     1      .002     1.0    -1      0.     0.     1.
```

D.2.2 W1 Takeda Calibration – Cyclic Strength Degradation

```
                          Takeda-W1 Calibration-Cyclic SD
W1 Model - Push vs Pull Analysis
* Monolithic pre-1970's Structural wall
* Lumped Platicity - modified Takeda Hystersis
* Strength Degradation based on the number of load cycles

8 0 1 0 0 -1 1 0 0
3 2 2 3 1 3 9.81 0 0 0.0050 500 1.0
20 20 20 1 3 10 0.7 0.1
5 5 0.00

NODES 1
  1 0.0  0.0    1 1 1  0 0 0 0
  2 0.0  0.0    0 0 0  0 0 0 0
  3 0.0  1.5    0 0 0 -1 0 0 0        !node at which displacement is applied


Elements 1
! N  Sect  I  J  i  j  output
  1  1     1  2  1 2
  2  2     2  3  2 3


PROPS 1
 1 SPRING                     !Rotational spring representing inelatic action

   1 4 2 0 9999999 9999999 112000 0 0 0
   9999 -9999 9999 -9999 167 -167
   10 22 0.5                              !Strength degradation parameters
   0.05 0.2 1.0 1                         !Hystersis parameters


2 FRAME
  1 0 0 0 0 0                          ! Elastic frame element representing wall
  2.5E7 1.04E7 0.1275 0.0 0.0111 0 0 0


WEIGHTS 0
! n  wx
  1 0
  2 0
  3 0


LOADS
! n  Fx   Fy    Mz
  2  0    0     0
  3  0    0     0


EQUAKE load-regime-fixed.txt       ! Experimental displacement loading regime
3     1      .002     1.0    -1      0.     0.     1.
```

D.2.3 W1 Pampanin Calibration – No Strength Degradation

```
                Pampanin-W1 Calibration-No Strength Degradation
W1 Model - Push vs Pull Analysis
* Monolithic pre-1970's Structural wall
* Lumped Platicity - Pampanin Hystersis
* No Strength Degradation


8 0 1 0 0 -1 1 0 0
3 2 2 3 1 3 9.81 0 0 0.0050 500 1.0
20 20 20 1 3 10 0.7 0.1
5 5 0.00

NODES 1
  1 0.0  0.0    1 1 1  0 0 0 0
  2 0.0  0.0    0 0 0  0 0 0 0
  3 0.0  1.5    0 0 0 -1 0 0 0           !node at which displacement is applied


Elements 1
! N  Sect  I  J  i  j  output
  1  1     1  2  1 2
  2  2     2  3  2 3

PROPS 1
 1 SPRING                        ! Rotational spring representing inelatic action
   1 44 0 0 9999999 9999999 112000 0 0 0
   99999 -99999 99999 -99999 167 -167
   2 1.5 1.0 -0.6 0.8 50 -0.05          ! Hystersis parameters
   2 1.5 1.0 -0.6 0.8 50 -0.05
   2 1.5 1.0 -0.6 0.8 50 -0.05

2 FRAME                                ! Elastic frame element representing wall
  1 0 0 0 0 0
  2.5E7 1.04E7 0.1275 0.0 0.0111 0 0 0


WEIGHTS 0
! n  wx
  1 0
  2 0
  3 0


LOADS
! n  Fx   Fy    Mz
  2  0    0     0
  3  0    0     0


EQUAKE load-regime-fixed.txt         ! Experimental displacement loading regime
3     1      .002     1.0    -1      0.     0.     1.
```

D.2.4 W1 Pampanin Calibration – Max Ductility Strength Degradation

```
                    Pampanon-W1 Calibration - Max Ductility SD
W1 Model - Push vs Pull Analysis
* Monolithic pre-1970's Structural wall
* Lumped Plaicity - Pampanin Hystersis
* Max Ductility Based Strength Degradation


8 0 1 0 0 -1 1 0 0
3 2 2 3 1 3 9.81 0 0 0.0050 500 1.0
20 20 20 1 3 10 0.7 0.1
5 5 0.00

NODES 1
  1 0.0  0.0    1 1 1  0 0 0 0
  2 0.0  0.0    0 0 0  0 0 0 0
  3 0.0  1.5    0 0 0 -1 0 0 0       !node at which displacement is applied


Elements 1
! N  Sect  I  J  i  j  output
  1  1     1  2  1 2
  2  2     2  3  2 3

PROPS 1
 1 SPRING                    ! Rotational spring representing inelatic action
   1 44 3 0 9999999 9999999 112000 0 0 0
   99999 -99999 99999 -99999 167 -167
   8 24 0.5                              ! Strength degradation parameters
   2 1.5 1.0 -0.6 0.8 50 -0.05           ! Hystersis parameters
   2 1.5 1.0 -0.6 0.8 50 -0.05
   2 1.5 1.0 -0.6 0.8 50 -0.05

2 FRAME                               ! Elastic frame element representing wall
  1 0 0 0 0 0
  2.5E7 1.04E7 0.1275 0.0 0.0111 0 0 0


WEIGHTS 0
! n  wx
  1 0
  2 0
  3 0



LOADS
! n  Fx   Fy    Mz
  2  0    0     0
  3  0    0     0


EQUAKE load-regime-fixed.txt      ! Experimental displacement loading regime
3     1      .002     1.0    -1      0.     0.     1.
```

D.2.5 W1R – Bilinear Elastic and Elasto-plastic Calibration

```
                W1R Calibration-Bilinear Elastic+Elasto-plastic
W1R Model - Push vs Pull Analysis
* Hybrid wall
* Lumped Platicity - two springs in parallel
* Bilinear elastic & Elasto-plastic
*


8 0 1 0 0 -1 1 0 0
3 3 3 3 1 3 9.81 0 0 0.0050 500 1.0
20 20 20 1 3 10 0.7 0.1
5 5 0.00

NODES 1
  1 0.0  0.0    1 1 1  0 0 0 0
  2 0.0  0.0    0 0 0  0 0 0 0
  3 0.0  1.5    0 0 0 -1 0 0 0        !node at which displacement is applied


Elements 1
! N  Sect  I  J  i  j  output
  1  1     1  2  1 2
  2  2     1  2  1 2
  3  3     2  3  2 3

PROPS 1
 1 SPRING                    ! Rotational spring representing PT contribution
   1 15 0 0 9999999 9999999 140000 0.0 0.0 0.04
   9999 -9999 9999 -9999 70 -70


 2 SPRING           ! Rotational spring representing dissipater contribution
   1 2 0 0 9999999 9999999 30000 0 0 0.0
   9999 -9999 9999 -9999 70 -70


 3 FRAME                              ! Elastic frame element representing wall
  1 0 0 0 0 0
  2.5E7 1.04E7 0.1275 0.0 0.0111 0 0 0


WEIGHTS 0
! n  wx
  1 0
  2 0
  3 0


LOADS
! n  Fx   Fy    Mz
  2  0    0     0
  3  0    0     0


EQUAKE load-regime-fixed.txt       ! Experimental displacement loading regime
3     1      .002     1.0    -1      0.     0.     1.
```

D.2.6 SDOF As-built Prototype – Time History Analysis

```
                              SDOF-Prototype-Asbuilt

Asbuilt Prototype - modified Takeda Hysteresis
* Equivalent SDOF system representing prototype wall
* Time History - 16 scaled earthquake records
* Elastic beam element with inelatic rotational spring
* No strength degradation
*
*
*

2 0 1 0 4 0 2 0 0
3 2 2 3 1 0 9.81 0.0 0.0 0.0050 100 1.0
20 20 20 1 3 10 0.7 0.1
5 5 0.00
1 5.0

NODES 1
  1 0.0  0.0    1 1 1  0 0 0 0
  2 0.0  0.0    0 0 0  0 0 0 0
  3 0.0  7.94   0 0 0  0 0 0 0     Effective height of equivalent SDOF system


Elements 1
! N  Sect  I  J  i  j  output
  1  1     1  2  1 2
  2  2     2  3  2 3

PROPS 1
1 SPRING
   1 4 0 0 9999999 9999999 447916 0 0 0.00  ! Inelastic rotational spring
   9999 -9999 9999 -9999 667 -667
   0.05 0.2 1.0 1.0                         ! Hysteresis parameters


2 FRAME                                  ! Elastic frame element representing wall
  1 0 0 0 0 0
  2.5E7 1.04E7 0.32 0.0 0.0683 0 0 0


WEIGHTS 0
! n  wx
  1 0
  2 0
  3 754                                 ! Effective mass of equivalent SDOF system


LOADS
! n  Fx   Fy    Mz
  2  0    0     0
  3  0   -378   0                            ! Axial load



EQUAKE
3     1      .002     1.0    -1      0.     0.     1.
```

D.2.7 SDOF Retrofitted Prototype – Time History Analysis

```
                          SDOF-Prototype-Retrofitted

Retrofitted Prototype
* Bilinear elastic and Elasto-plastic hysteresis rules
* Equivalent SDOF system representing prototype wall
* Time History - 16 scaled earthquake records
* Elastic beam element with inelatic rotational spring
* No strength degradation
*
*
*

2 0 1 0 4 0 2 0 0
3 3 3 3 1 0 9.81 0.0 0.0 0.0050 100 1.0
20 20 20 1 3 10 0.7 0.1
5 5 0.00
1 5.0

NODES 1
  1 0.0  0.0    1 1 1  0 0 0 0
  2 0.0  0.0    0 0 0  0 0 0 0
  3 0.0  7.94   0 0 0  0 0 0 0    ! Effective height of equivalent SDOF system


Elements 1
! N  Sect  I  J  i  j  output
  1  1     1  2  1 2
  2  2     1  2  1 2
  3  3     2  3  2 3

PROPS 1
1 SPRING
   1 15 0 0 9999999 9999999 560000 0.0 0.0 0.042 ! Inelastic rotational spring
   9999 -9999 9999 -9999 260 -260                ! representing post-tensioning

2 SPRING
   1 2 0 0 9999999 9999999 120000 0 0 0.0    ! Inelastic rotational spring
   9999 -9999 9999 -9999 230 -230            ! representing energy dissipaters


3 FRAME                                ! Elastic frame element representing wall
  1 0 0 0 0 0
  2.5E7 1.04E7 0.32 0.0 0.0683 0 0 0


WEIGHTS 0
! n  wx
  1 0
  2 0
  3 754                              ! Effective mass of equivalent SDOF system


LOADS
! n  Fx   Fy    Mz
  2  0    0     0
  3  0   -378   0                   ! Axial load



EQUAKE
3     1      .002     1.0    -1      0.     0.     1.
```

D.2.8 MDOF As-built Prototype – Time History Analysis

```
                              MDOF-Prototype-Asbuilt

Asbuilt Prototype - modified Takeda Hysteresis
* MDOF system representing prototype wall
* Time History - 16 scaled earthquake records
* Elastic beam element with inelastic rotational spring
* No strength degradation

2 0 1 0 4 0 2 0 0
5 4 2 3 2 0 9.81 0.0 0.0 0.0050 100 1.0
20 20 20 1 3 10 0.7 0.1
5 5 0.00
1 5.0 3 5.0                              ! 5% damping of the first and third modes

NODES 1
  1 0.0  0.0    1 1 1  0 0 0 0
  2 0.0  0.0    0 0 0  0 0 0 0
  3 0.0  3.4    0 0 0  0 0 0 0           ! First floor
  4 0.0  6.8    0 0 0  0 0 0 0           ! Second floor
  5 0.0  10.2   0 0 0  0 0 0 0           ! Third floor

Elements 1
! N  Sect  I  J  i  j  output
  1  1     1  2  1 2
  2  2     2  3  2 3
  3  2     3  4  3 4
  4  2     4  5  4 5

PROPS 1
1 SPRING
   1 4 0 0 9999999 9999999 447916 0 0 0.00 ! Inelastic rotational spring
   9999 -9999 9999 -9999 667 -667
   0.05 0.2 1.0 1.0                        ! Hysteresis parameters


2 FRAME                                   ! Elastic frame element representing wall
  1 0 0 0 0 0
  2.5E7 1.04E7 0.32 0.0 0.0683 0 0 0


WEIGHTS 0
! n  wx
  1 0
  2 0
  3 294                                   ! First floor mass
  4 294                                   ! Second floor mass
  5 294                                   ! Third floor mass

LOADS
! n  Fx   Fy    Mz
  2  0    0     0
  3  0   -126   0                        ! Axial load
  4  0   -126   0
  5  0   -126   0

EQUAKE
3     1      .002     1.0    -1      0.     0.     1.
```

D.2.9 MDOF Retrofitted Prototype – Time History Analysis

```
                          MDOF-Prototype-Retrofitted

Retrofitted Prototype - MDOF Model
* Bilinear elastic and Elasto-plastic hysteresis rules
* MDOF model representing prototype wall
* Time History - 16 scaled earthquake records
* Elastic beam element with inelatic rotational spring
* No strength degradation


2 0 1 0 4 0 0 0 0
5 5 3 3 2 0 9.81 0.0 0.0 0.0050 100 1.0
20 20 20 1 3 10 0.7 0.1
5 5 0.00
1 5.0 3 5.0                            ! 5% damping of the first and third mode

NODES 1
  1 0.0  0.0    1 1 1  0 0 0 0
  2 0.0  0.0    0 0 0  0 0 0 0
  3 0.0  3.4    0 0 0  0 0 0 0        ! First floor
  4 0.0  6.8    0 0 0  0 0 0 0        ! Second floor
  5 0.0  10.2   0 0 0  0 0 0 0        ! Third floor

Elements 1
! N  Sect  I  J  i  j  output
  1  1     1  2  1 2
  2  2     1  2  1 2
  3  3     2  3  2 3
  4  3     3  4  3 4
  5  3     4  5  4 5

PROPS 1
1 SPRING
   1 15 0 0 9999999 9999999 560000 0.0 0.0 0.042 ! Inelastic rotational spring
   9999 -9999 9999 -9999 260 -260                ! representing post-tensionin

2 SPRING
   1 2 0 0 9999999 9999999 120000 0 0 0.0     ! Inelastic rotational spring
   9999 -9999 9999 -9999 230 -230             ! representing energy dissipater


3 FRAME                                ! Elastic frame element representing wal
  1 0 0 0 0 0
  2.5E7 1.04E7 0.32 0.0 0.0683 0 0 0

WEIGHTS 0
! n  wx
  1 0
  2 0
  3 294                               ! First floor mass
  4 294                               ! Second floor mass
  5 294                               ! Third floor mass

LOADS
! n  Fx   Fy    Mz
  2  0    0     0
  3  0   -126   0                     ! Axial load
  4  0   -126   0
  5  0   -126   0

EQUAKE
3     1      .002     1.0    -1      0.     0.     1.
```